Modelling Hypothalamic Control of Growth Hormone Release and Spike Firing in Oxytocin Cells

Duncan James MacGregor

October 2002

Revised May 2003

Supervisor Prof. Gareth Leng

A dissertation submitted to the University of Edinburgh for the degree of Doctor of Philosophy

School of Biomedical and Clinical Laboratory Sciences

University Of Edinburgh

Declaration

This dissertation is not substantially the same as any I have submitted for a degree, or diploma, or any other qualification at any other university. It is the result of my own work, and except where specifically stated, includes nothing which is the outcome of work done in collaboration.

Duncan MacGregor

June 2003

Table of Contents

Chapter 3 – The Hypothalamic Model

Chapter 4 – Experimenting with the Model

Chapter 5 – Modelling Spike Firing in Oxytocin Cells

Acknowledgements

First and foremost I'd like to thank my supervisor Professor Gareth Leng for his brilliant guidance, help and encouragement throughout this PhD, and especially for his fine editorial skills that have taught me so much in writing this thesis (and his patience on my more teenage occasions). Prof. Leng has been my ideal mentor, giving me a great project to work on, and then having the confidence to allow me to pursue my own path. I hope that in the results that trust has paid off. Most importantly though, Gareth has taught me a way of thinking, of looking at and understanding things with the right balance of care and adventure that I hope I can continue to develop in the future.

Great thanks also go to David Brown, my second supervisor at the University of Cambridge's Babraham Institute, and since departed to the Civil Service. His guidance was invaluable in learning to bridge the worlds of practical biology and theory, and in understanding the previous theoretical work on the GH system. He's also a thoroughly decent chap and excellent host, plying visits to Cambridge with copious cups of tea and wonderful food. I'd also like to thank Dr. Chris Williams of our neighbouring School of Informatics, and my old undergraduate home, for his supervision and excellent guidance with the mathematical background to the oxytocin work. I look forward to continuing the association. One of my greatest debts is owed to Professor David Willshaw, who supervised my undergraduate honours project (unsupervised neural net pattern recognition, based on work of David Marr), my first taste of real research work, before putting me in touch with Professor Leng, leading to everything that has come since, and ending up as my internal examiner.

I have been very fortunate to work alongside many fine people in the Medical School's Laboratory of Neuroendocrinology. In particular I'd like to thank Dr. Mike Ludwig for the use of his oxytocin cell recordings, and his patient help in turning me into a proper biologist. Thanks also go to Dr. Louise Johnston and Dr. Colin Brown for guidance with the GH and oxytocin systems, and to all the members of the lab who I've quizzed at various stages. I've also received great friendship and support from my fellow students, particularly Arleta Marganiec, my fellow wielder of

numbers among the experimentalists and Ekkasit Kumarnsit, for bringing humour to our stuffy room of intensely stared at glowing screens.

I must also thank my unseen sponsors, Merck Research Laboratories, for their foresight to fund basic research with no direct clinical or financial application. I do hope that this modelling work will eventually help to develop treatments, and if that involves expensive drugs, some part of the profits from which in turn fund further research, then please look kindly on the poorer nations of the world while you fleece the rich ones.

Beyond the University I've had many great friends in Edinburgh, and the city as a whole has been a privilege to live in, with its great parks, clubs, cinemas, places you can sneak into that you're not really supposed to, and drinking establishments. My greatest source of sanity and just generally healthy running about in the countryside has been the Dirty Weekenders, the University of Edinburgh's conservation volunteers, who have provided many great days of constructive mischief making. Too many fine individuals to mention individually. My second greatest distraction has been the Forest Café (soon to be formally 'The Forest Collective'), our highly successful local attempt to fly in the face of rampant capitalism, providing good, cheap food and drink in order to fund and support local culture, in the form of art (painting, writing, music, film, everything), education and environmental work. Thanks to Matthew Cheney, Chris Palmer, Jack Richold, James Picardo (who was particularly great in the last months of thesisdom), Dan Gorman, Ryan Van Winkle (yes, really), Ellie Maxwell and everyone for being great friends and co-conspirators. Also special thanks to Mr. William Watson, who alongside being a friend (a Scot, in Edinburgh, no less) has a lifelong ambition to be mentioned in a PhD thesis's acknowledgements section. Lastly, thanks to Ian Copley (head red-man, friend, dirty weekender, and fellow gig goer) all red-men past and present, all my friends, co-performers and organisers of the Beltane Fire Society (www.beltane.org) that has seen me run about Carlton Hill (and various other places) wearing little else but body paint.

Mum and Dad, I thank first of all, for making it all possible in the first place and in fulfilling the resultant responsibilities, just being really great parents. Their

encouragement and support really helped keep me going through the dark days of the thesis. They've given me my keen eye and perfectionism which has so elegantly and obstinately served my pursuit of knowledge, my wide view of the world, and my favourite thing of all, my sense of humour, some of which I hope still manages to lurk in this serious document. Then there's the girls, Amber, Fenella and Ellie, who've shared my moods, bed clothes and affections over the course of this PhD, who will always hold my warmest thoughts. Although I would have to say that in my case charming young ladies are something which a PhD is completed despite, rather than making any useful contribution. Feel I have to say, but not necessarily believe, and possibly continue to internally debate for all eternity, for such things reside in the part of the mind which shall continue to elude investigation, if not for ever, for a long time to come.

Finally my two greatest friends; Nick Holdstock, writer, co-appreciator of music, film, random late night wandering and the perils of charming young ladies and Dr. Jonathan Butt, co-appreciator of fine whisky, fine food, film, philosophy, and that lonely world that bridges and melds art and science. Our unholy trinity was brought together by the class of 1998 MSc Neuroscience course. Nicholas left science to pursue truth (I wouldn't dare to say absolute) in the world of writing and travel. Jon accompanied me on the adventure of further scientific study, the two of us finishing just weeks apart, and being an invaluable friend in the dark final days of a broken heart (those charming young ladies) and a mountain of figures and writing. Don't start a relationship you might care about during your thesis. Just be friends, and be patient.

Duncan MacGregor, June 2003

Forever reachable (I should think) at duncan@theforest.org.uk

Abstract

This work contains two modelling projects, studying the neuroendocrine systems of the hypothalamus, with a view to deriving general principles of neural function.

Growth hormone (GH) is released from the pituitary in a pulsatile pattern under the control of two hypothalamic peptides, growth hormone releasing hormone (GHRH) and somatostatin. Pulses of GHRH trigger pulses of GH but the overall pattern of GH release appears to be controlled in a permissive manner by somatostatin, which inhibits pituitary GH release. The hypothalamic sites of release for GHRH and somatostatin have been identified but we have been unable to observe the endogenous patterns of peptide release or electrical activity in these neurons.

To understand the hypothalamic network which controls GHRH and somatostatin we need to use less direct lines of approach. There is a lot of behavioural level evidence about how GH release is affected by removing these hormones or applying them artificially. At the electrophysiological level we have some knowledge about how the GHRH neurons respond to artificial stimuli and we have anatomical and histological evidence about what substances and connections affect the behaviour of the GHRH and somatostatin neurons. The goal of this project was to gather this evidence, to try and build a model of the hypothalamic network which controls these hormones and use it to derive further clues about how this system might work.

A model has successfully been built, which is able to reproduce the patterns of GH release observed in male and female rats. The model has been used to investigate the system's behaviour and also compared with behavioural experiments in the real system, suggesting new lines of experimental investigation.

In previous work a model of oxytocin cell firing was developed based on the classic leaky integrate and fire model with the addition of a hyperpolarising afterpotential (HAP). The model was successfully used to explain the unusual linear increase in firing activity in response to increased input stimulation, demonstrating the apparently counter intuitive idea that this could be achieved by giving an equal amount of excitatory and inhibitory input pulses. It was also successfully fitted to real data by comparing firing rates and the inter-spike interval (ISI) histograms generated with the model and from experimental recordings. However, recent novel

analysis work has demonstrated a correlation between spike intervals such that a longer inter-spike interval is more likely to be proceeded by a shorter interval and vice-versa indicating that there is some other behavioural component which is capable of remembering previous activity. One candidate for this is the after-hyperpolarisation (AHP) which is much smaller in magnitude than the HAP but lasts much longer, beyond the range of a single spike. The model data generated with just the HAP showed no such correlation but adding the AHP to the model successfully reproduced the spike interval correlation.

Fitting on the basis of ISI histograms takes no account of behavioural properties which are observed over a longer time course and so a new parameter fitting mechanism has been developed which takes account of the relation between successive spike intervals. This is able to retrieve parameters values for the AHP's magnitude and time course as well as the level of afferent input activity, from a cell recording. If the system can be tuned to produce sufficiently accurate values then it will provide a powerful tool for tool for measuring otherwise inaccessible properties of neurons and their firing patterns.

In future work, it should be possible to use this model to study recordings from GHRH neurons and perhaps discover more about their firing properties.

Chapter 1

Introduction

1.1 Introduction

Much of the information communicated between cells and systems in the brain, and the body, is represented not by amplitude, but by the pattern of activity. This has always been the more obviously useful and robust alternative, but it also requires that we attribute memory to very low-level components of the brain, in order to produce and interpret these patterns.

One part of the brain that exhibits very definite temporally patterned activity is the neuroendocrine system. This system forms the brain's interface to much of the body's internal systems and its function is essential to many fundamental processes, particularly development and reproduction. It also has the advantage of producing an easily accessible and relatively simple output, in the form of hormone release into the bloodstream. We know that for several hormones, including growth hormone (GH), a pulsatile pattern of release is optimal for their actions within the body. In male rats, as in humans and many other animals, GH is released in large pulses every three hours. A pattern of large pulses rather than continuous release allows a maximal response to the hormone without desensitising the target receptors, and the pattern of mixed high and low activity may also be used to instruct different systems, with some responding to high and some low activity. These patterns are triggered by neurons, but they operate on a timescale of hours, far longer than the milliseconds over which action potentials fire. We need to understand how processes which operate at very different speeds can integrate with each other and what the dynamics of such interactions might be.

In order to understand such systems, an important approach is to gather the experimental evidence and attempt to model the system. This provides a structure in which to formalise existing knowledge and test theories on how the system functions as a whole. This thesis attempts to model the GH release system, with the objective of reproducing the behaviour of the real system, and predicting and aiding the interpretation of experimental data.

1.2 The Project

The goal of this project is to try and further understand the mechanisms controlling GH release by using the knowledge derived from experiments to build a mathematical model of the system. By implementing this set of static mathematical equations on a computer we can give life to the artificial system and observe its behaviour. If we have based it on what lower level mechanistic knowledge we have of the real system and can show that it is able to accurately reproduce higher level, such as the endogenous release profiles, then it may be able to predict properties of the real system which we have not been able to observe and be able to simulate experiments, as well as providing a possible solution to how the parts of the system function as a whole.

The project follows on from previous PhD work of Elinor Stephens who constructed a model of GH release at the pituitary. By constructing a model of the hypothalamic systems and then adding it on to the pituitary model we will be able to construct a model of the whole growth hormone release system.

1.2.1 Objectives

The primary objective of the project was to produce a model of the hypothalamic network controlling GH release. The first part of this, which formed the research review presented below, involved an investigation of evidence in the literature that might be used to build the model. The second stage was to re-implement the pituitary model. (chapter 2). It was also used for new experiments, testing plausible patterns of GHRH and somatostatin release in preparation for developing the hypothalamic components. This produced a specification for the model in terms of what was available to build it from and what its output had it to be, and formed the basis for the design stage (chapter 3) where a basic model of the complete system was developed. The final part of the model's development (the first part of chapter 4) was experimentation, testing new components, based on less definite experimental

evidence, in the attempt to more closely reproduce the real system and suggest further real experiments.

The second objective was to be able to accurately reproduce real experiments by fitting the model to real data. To do this the values used in the model had to be scaled to fit real units, particularly blood GH concentration. The parameters used in the equations were refined so that the model could reproduce real GH output as accurately as possible. If we had been unable to reproduce data by scaling and refinement then this would have suggested that there was something wrong with the model and its design would have needed to be changed. However, it was successful, and for the final part of the work with the GH system, the second part of chapter 4, the model was used to recreate and extend *in-vivo* experiments, particularly those which test the system by adding exogenous substances. This was an important further test of the model, but it also allowed further interpretation of the original experimental results.

1.2.2 The Research Review

The research evidence divides into three levels of examination; behavioural, electrophysiological, and neuroanatomical. Behavioural results describe the system being examined as a whole, measuring the pattern of GH release during normal function, and in response to administration and blocking of the main substances which appear to control GH; GHRH, somatostatin, and GH itself. These give important clues about how GH is controlled, and establish the output and behaviour which the model must reproduce. GH release is triggered by pulses of GHRH, under the control of somatostatin, which blocks this action. The long period of low GH release, observed particularly in male rats, appears to be controlled by a prolonged release of somatostatin, which is somehow triggered or charged by the GH pulse feeding back to the central systems. GH may also feed back to modulate the form of GHRH release.

The second level is the electrophysiological results. Normal GHRH neuronal activity is blocked by the anaesthetic required to record from these cells, but we do have recordings from the GHRH neurons indicating inhibition of their remaining low level activity in response to stimulation at the periventricular somatostatin neurons. The somatostatin neurons are spread in a thin layer near the third ventricle, making the more accurate electrode placement required for recording too difficult. GH release in response to electrical GHRH stimulation is also measured, indicating a highly non-linear relation where release is dependent on the number of stimulation pulses.

The lowest level, the neuroanatomical, examines the histological and chemical evidence, looking at the connections that might exist in the system, based on anatomical tracing and correlating substances which are released by and effect the involved cells. There is a lot of circumstantial evidence for many substances which effect GH release, the interpretation of which is complicated by the interaction between GHRH and somatostatin, which appear to have reciprocal connections within the hypothalamus. The two better defined substances are galanin, which appears to mediate an inhibitory GHRH-somatostatin connection, and NPY which may mediate GH feedback on GHRH and somatostatin. However, there is also evidence for direct GH-somatostatin feedback.

Together the results provide enough to put together an idea of how the system functions as a whole (presented in chapter 3) and to give a functional description of the system's components.

1.3 GH Release System Research

Growth hormone (GH) is released in a pulsatile pattern (Tannenbaum and Martin 1976) by the somatotroph cells of the anterior pituitary. In the male rat, as in humans, GH release is highly pulsatile. In female rat it is less so, but the pulsatile pattern of release is always an important feature, and one of the main goals of GH research is to precisely define and understand the generation of this pattern.

Many factors influence GH release, but the two most important substances are growth hormone releasing hormone (GHRH) (Guillemin *et al* 1982) and somatostatin, which are released from the hypothalamus and act directly at the pituitary. At the simplest level, GHRH excites GH release and somatostatin inhibits release, but the two also interact in the hypothalamus, and may be modulated by GH itself, complicating their apparent effects. GHRH also acts at the pituitary to increase GH content in the somatotrophs (Barinaga *et al* 1983) by triggering GH synthesis.

Building a model requires an understanding of the system at a functional level, and so the research review concentrates on higher level, behavioural, experiments which examine the system's response to modulation of the substances which directly control GH release. Lower level experimental evidence, such as electrophysiology and anatomy, is examined in order to understand how these substances themselves are controlled.

1.3.1 Profiling GH Release and the Controlling Factors

In-vivo behavioural experiments test the complete system. The results provide detailed evidence on the endogenous pattern of GH release and how this is controlled by GHRH and somatostatin. This information will suggest how the model should work and also provide functional criteria to test the model against.

Pulsatile GH Release

In 1985 Clark et al administered varied patterns of GH to hypophysectomized rats and observed their growth response (Clark *et al* 1985). The optimum pattern of GH to promote growth is 3-hourly pulses, similar to endogenous GH release observed in male rats. Administering the same total dose in less frequent pulses produced a much smaller growth response. Continuous infusion of GH initially produces a similar or

even slightly greater response than the 3-h pulses, but after 5 or 6 days the response to continuous infusion declined, whereas pulsatile administration continued to be effective. This suggested that the peripheral GH receptors become desensitised when continuously exposed to GH. The 3-h pulses of GH provide the frequent exposure required for a good growth response while avoiding long term desensitisation.

GH Release in Response to GHRH

In 1982 Wehrenberg et al developed an antibody to GHRH and, using this to block GHRH in male rats, showed that GH release can be completely abolished with a sufficient dose (Wehrenberg *et al* 1982). With a smaller dose, pulses of GH release remained, but with reduced amplitude. The involvement of somatostatin was ruled out by showing the same result with the addition of somatostatin antiserum. In a follow-up paper (Wehrenberg *et al* 1983) the same group examined the response to artificially administered GHRH. They used antibodies to block endogenous somatostatin and GHRH in conscious male rats. The GHRH antibody was specific to the rat version, and so they could administer the newly- identified human GHRH and measure the GH response. Each injection of GHRH elicited a large increase in blood GH concentration which quickly fell back to basal level. They administered successive injections of GHRH at 1 and 3-h intervals and showed no consistent change in GH response amplitude, although the results do show some variation in GH response. They also showed larger amplitude pulses of GH with higher concentrations of GHRH up to a maximal level.

These results established that GH release is triggered by GHRH in a dose-dependent manner. The next stage was to search for the endogenous GHRH pattern by comparing the response to administered GHRH to normal GH release. The highly episodic endogenous rhythm of GH in male rats makes it difficult to interpret the responses to administered substances without first blocking all hypothalamic control. This problem was tackled by Clark and Robinson (Clark and Robinson 1985b) by moving to female rats, which have a more continuous endogenous GH

release pattern (Eden 1979) and consequently slower growth. GH release in female rats does show some peaks, but these are irregular, more frequent, and smaller than in males, with a higher basal concentration. Clark and Robinson administered human GHRH to normal female rats over 12 days either as a continuous infusion or in 3-h pulses and measured blood GH concentrations and daily weight gain. Rats treated with a pulsatile pattern of GHRH showed a pattern of GH release very similar to the endogenous pattern in male rats, and showed a significant increase in growth compared with rats treated with a continuous infusion or saline-treated controls. There was no evidence of endogenous secretion between the artificially-induced GH pulses, and the rats appeared to become entrained into the new pattern, responding uniformly to each GHRH pulse. This suggests that, as well as stimulating GH release from the pituitary, exogenous GHRH was, directly or indirectly, affecting the hypothalamic systems that control GH release.

The Move Towards Somatostatin Pattern Control

Ferland et al (Ferland *et al* 1976) had shown that the low basal secretion between pulses in males can be increased by using antibodies to block somatostatin. This suggested that somatostatin could be responsible for the low inter-pulse GH release levels while GHRH triggers the GH pulses, when not inhibited by somatostatin. This somatostatin control explained the variable responses to GHRH in male rats and it appeared that the different patterns of endogenous GH release seen in male and female rats were due to different patterns of somatostatin release.

Clark and Robinson (Clark and Robinson 1985c) made a detailed comparison between GH release responses to GHRH in conscious male and female rats. In the first experiment they tested the GH response to a single injection of human GHRH. GH was measured before and after the injection of GHRH to give a temporal profile of release. The responses in males and females showed a similar shape, a rapid increase in blood GH, peaking 3 to 5 min after injection, followed by a uniform decline back to a basal level. However, the GH responses in males varied much more

than in females, with some rats almost failing to respond, and some producing large GH peaks, similar to endogenous GH pulses. None of the females failed to respond, and all produced smaller, less variable GH peaks.

A second experiment tested the GH responses to multiple injections of GHRH at varied intervals. At 3-h intervals, rats were given four injections. Only the responses to the third and fourth injections were recorded. All rats showed a strong, uniform response to these injections with no evidence of GH release between the two pulses. Female rats showed smaller amplitude peaks but their GH levels decayed back to the same low basal levels as the males. The rats again appeared to become entrained into the new patterns of release, and there was even evidence of a rise in GH level in anticipation of the later injections. Performing the same experiment with injections at 90-min intervals, the differences between males and females became more apparent. Females produced fairly uniform GH pulses in response to each injection, but the males only responded to every second GHRH injection, maintaining a pattern of 3-h pulses. Some rats responded to the first and third injections and some to the second and fourth, dividing into two groups 90 min out of phase. At 40-min intervals, females produced larger peaks after the first injection but continued to respond to each injection. Males only produced a large GH peak in response to every third or fourth injection, although they sometimes produced a smaller response to a consecutive injection before failing to respond for the next two or three.

The results show a refractory period in the ability to respond to GHRH in males. GHRH has to be continuously infused for as long as 24h before significantly depleting pituitary GH content (Wehrenberg *et al* 1986), and so this is unlikely to be due to a lack of GH available for release, supported by the fact that females continue to respond to frequent injections of GHRH and males respond to two injections in rapid succession. It appears that the refractory period in the male may be due to a cyclic pattern of endogenous somatostatin release controlling the periods when the pituitary responds to GHRH. In the female, somatostatin appears to be released in a more continuous pattern, at a level somewhere in-between the peaks and troughs of the male pattern so that GHRH is never completely blocked, but does not produce as strong a response as in the male.

Until this time it had been thought that the 3h endogenous GH pulses were likely due to a corresponding pattern of GHRH release from the hypothalamus, but it was becoming clear that pulse frequency was controlled by somatostatin rather than GHRH. Even if it had been the case that GHRH controlled the pattern, it would have merely moved the problem of pulse generation away from GH to GHRH. The other interesting result from this work was that the pattern of response, particularly in males, can become entrained. The paper made an early suggestion that GH itself may be involved in some feedback mechanism.

Detailed Profiling of GH Release

The first study to produce a detailed profile of GH release in male rats (Clark *et al* 1986) used a new system for the automated repetitive micro-sampling of blood. The system could also simultaneously inject or infuse substances into the rat, and the first results included experiments administering GHRH and somatostatin to male rats.

The first experiment infused GH into anaesthetised female rats and simultaneously measured blood GH. The blood GH level rises quickly and then slows to reach a plateau during infusion before rapidly falling back to zero. Endogenous GH release is blocked in anaesthetised rats. The next experiment, in conscious male rats, sampled GH every 12 min for 44 h. This showed the 3h pulses of GH, with amplitude and frequency maintained throughout the sample period, and no sign of any relation to periods of light and darkness. Many pulses consist of two peaks, often reaching as high as 1μg/ml.

The final experiment re-examined the effect on the pattern of GH release of a series of GHRH injections. Male rats were given four 3h injections of GHRH, and GH release was measured throughout the injections and for 12h afterwards. After the first or second injection, the GH responses became entrained, responding to each GHRH injection with a large, single-peaked, GH pulse, and low release between pulses. The GH release pattern after the GHRH injections stopped is described as variable and disorganised, but there still appears to be some trace of the trained 3-

hourly pattern, although with smaller, less well-defined pulses, and a gradual degeneration. GH release eventually returned to its natural pattern after many hours.

In a follow-up paper Clark et al (Clark *et al* 1987) produced detailed profiles of GH release in female rats. If somatostatin secretion in females is less variable, then the GH release profile should more closely match the pattern of endogenous GHRH release. Female rats were monitored for up to five days, with blood samples taken every 12 min. GH release was found to be much more pulsatile than previously observed, with many large peaks, in some rats similar in size to those seen in males. These large pulses were more closely studied by sampling at 4 min intervals. The higher resolution showed that the large peaks rose more slowly than those in males, taking as long as 25 min to reach the peak level. The pulses were quite different from those seen in response to single injections of GHRH, which peak within 3-5 min and are much smaller. These slowly increasing pulses seem likely to be the result of a longer episode of GHRH secretion or a succession of GHRH pulses.

The frequency and amplitude of the pulses was variable, with no apparent regular pattern like that observed in male rats. Release did however seem to vary between more and less active periods, and they suggested that this could be related to the light-dark cycle. Further experiments tried to establish this, but the variation between animals leaves the results rather unconvincing. Longer experiments in which the rats were monitored for five days were particularly concerned with the possible relation of GH release activity to the oestrous cycle, but no connection was found. The final experiment compared normal females with ovariectomised rats. Ovariectomised rats showed larger peaks of GH and multiple peak bursts similar to those in males. They also more clearly show a distinction between night and day activity with a more feminine continuous release pattern during light hours.

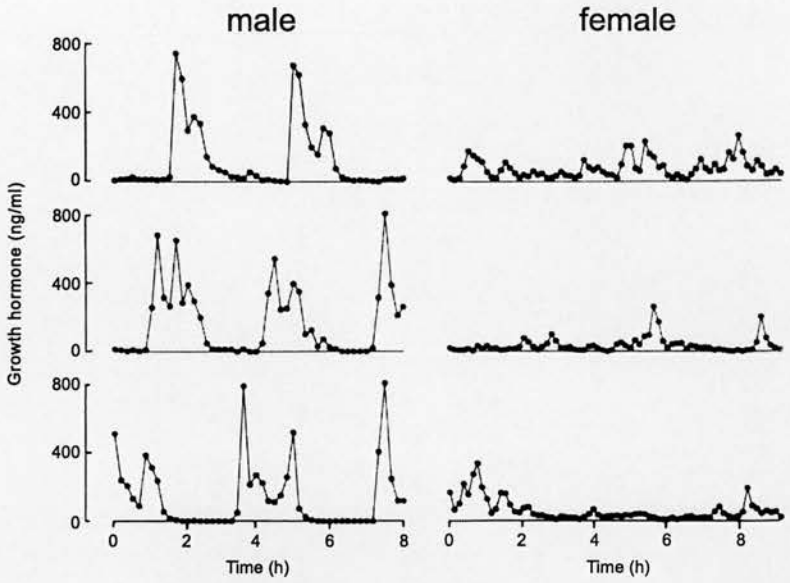

Figure 1.1 : Typical male and female rat GH release profiles. The males show large regular bursts of GH release, consisting of two or three large peaks and very low basal release. The females show smaller, less regular pulses with higher levels of basal release to make up a more continuous overall pattern of release. They tend to show larger pulses during darkness hours.

Exogenous Somatostatin and GH Release

The paper introducing the new sampling system (Clark *et al* 1986) also showed some of the first data on the effect of exogenous somatostatin on GH release. GH release was measured in conscious male rats before, during and after infusion of somatostatin, at two different doses. At the lower dose, endogenous GH pulses remained, but with reduced amplitude. At the higher dose GH bursts were almost completely abolished. However, when somatostatin was withdrawn there was a large "rebound" release of GH. The rebound was blocked with GHRH antiserum showing that it also required GHRH secretion.

It was now clear that the overall pattern of GH release was controlled by somatostatin rather than GHRH. GHRH stimulates individual bursts of GH release, but only under the permissive control of somatostatin. Thus, somatostatin must be low during GH pulses, and high between.

Clark and Robinson (Clark and Robinson 1987) experimented with different patterns of exogenous somatostatin in female rats. In the first experiment, rats were given a continuous infusion of somatostatin at 5 and 50 μg/h. Similar to the males, GH pulses were partially blocked at the lower dose, and almost completely abolished with the high dose infusion. However, as soon as the infusion was stopped there was a large rebound release of GH, and at the higher dose rate the rebound GH pulse was larger and showed multiple peaks, similar to endogenous male GH pulses. Somatostatin has a very short half life in blood (Schoemaker *et al* 1998) and its inhibitory effect is very short-lived once infusion is withdrawn.

It had been suggested, based on the comparison between male and female responses to GHRH pulses, that somatostatin may be released in a sinusoidal pattern in males. This was tested by infusing the female rats with somatostatin in such a pattern with a 3h period similar to the cycle in males. This did produce 3-hourly peaks of GH release, but they were longer than the endogenous male pulses and of lower amplitude, waves of GH release rather than short bursts. The final pattern of somatostatin administration used square wave infusions interrupted in a repeated pattern of 150 min on, 30 min off and was repeated at dose rates of 5 and 25μg/h. GH release was suppressed during the somatostatin infusion, with large rebound peaks of GH release occurring during the interruptions, particularly with the higher dose. Repeating this cycle of somatostatin administration produced a pattern of GH release very similar to the endogenous male GH profile.

To measure the effects of these patterns on growth, the experiments were repeated for longer periods, continuing the somatostatin infusion for 10 days, along with a control group receiving only saline. The continuous pattern of somatostatin reduced bone growth. It had no effect on body weight, but this is difficult to interpret since food intake was increased. The rats treated with the interrupted pattern of somatostatin showed normal bone growth, with an increased rate of weight gain despite normal food intake. The interrupted pattern was further tested by varying the length of the interruption, stopping infusion for 10, 30 and 90 min with rates adjusted to give the same total dose. This showed weight gain inversely proportional to the length of the interval. In addition, both the continuous and interrupted patterns of

somatostatin resulted in increased pituitary GH content over the saline-treated rats and this may have contributed to the large rebound release. Somatostatin does not block GH synthesis at the pituitary.

These results suggest that somatostatin may not only be responsible for the periods of low GH release but may also trigger the bursts of GH release through a rebound mechanism.

Hypothalamic Control of GH Rebound Release

A small rebound GH release in response to somatostatin withdrawal can be observed with pituitary preparations *in-vitro*, but this is much smaller than the rebound observed *in-vivo*, suggesting an active hypothalamic component rather than just the removal of its inhibitory influence. Preliminary results of Clark and Robinson showed that the rebound is also absent in anaesthetised rats, hinting at the involvement of GHRH, which is blocked by anaesthesia.

They went on to further investigate this rebound release (Clark *et al* 1988a). In the first experiment, male rats were continuously infused with somatostatin for 4h. One group of animals was injected with a sub-anaesthetic dose of urethane 1h before the end of the infusion. The control rats showed the normal large, multiple peak GH rebound release, but the rebound release was greatly reduced in urethane-treated rats, supporting the idea of hypothalamic involvement. The second experiment used the 150 min on, 30 min off, square wave pattern of somatostatin infusion. The infusion pattern was repeated for 12 h and during the third infusion the rats were given an injection of either control rabbit serum or anti-GHRH serum. The control rats continued to produce a large rebound GH release after each infusion of somatostatin but the rebound was greatly reduced in rats treated with GHRH antiserum. This was tested further by varying the dose of antiserum and showed a dose dependency relating the reduction in rebound magnitude to the level of GHRH block.

This was good evidence that the somatostatin-induced rebound release involved hypothalamic release of GHRH, but it still left the question of whether GHRH

release was being directly triggered by the sudden removal of somatostatin or whether the exogenous somatostatin was suppressing endogenous somatostatin so that GHRH could act when it was removed. Either way, the mechanism would have to involve the suppression of endogenous somatostatin to allow such a large GH release as observed in the rebound. There had already been a suggestion from work with an *in-vitro* hypothalamic preparation that somatostatin could act centrally to inhibit its own release (Peterfreund and Vale 1984) and work showing that central administration of somatostatin paradoxically stimulates GH release (Lumpkin *et al* 1981).

GH Auto-feedback

GH auto-feedback was originally demonstrated by (Krulich and McCann 1966) who showed that GH administration could reduce pituitary GH content in rats, and it had since been shown to suppress the amplitude of GH pulses in conscious male rats (Tannenbaum 1980) whether given i.v. or i.c.v. However, the mechanism of GH feedback was unclear. GH did not appear to act at the pituitary (Richman *et al* 1981), suggesting a hypothalamic site of action, either increasing somatostatin release or inhibiting GHRH release, or even both, to inhibit its own secretion.

Clark et al (Clark *et al* 1988b) investigated the effects of exogenous GH. Blood GH was sampled for 160min in female rats before giving a 6h infusion of human GH. The normal pattern of endogenous GH release was strongly suppressed during the GH infusion. At a low dose, GH release gradually recovered after strong initial suppression, and at a higher dose there was very little release during the entire infusion. When the exogenous GH stopped, there was no sudden rebound release but the normal pattern did recover within an hour or so. In male rats, the lower dose had little effect on the large endogenous pulses of GH, but at the higher dose GH release was suppressed, although most rats managed one GH pulse after the beginning of the infusion.

To test the mechanism, female rats were given injections of GHRH at 40min intervals before, during and after the GH infusion. The rats produced large pulses of GH release throughout the infusion of human GH, continuing afterwards with little sign of any suppression even at the larger dose of GH. By contrast, infusion of somatostatin blocked the responses to GHRH.

Clark et al (Clark *et al* 1988a) stimulated rebound GH release in male rats by infusing somatostatin with 30min interruptions every 3h. They also added GH to the third or fourth infusion and showed that this greatly reduced the amplitude of the following GH rebound release. Other results had suggested that the rebound was mediated by GHRH release and so this further supported the conclusion that GH feedback inhibits GHRH rather than stimulating somatostatin.

The results give further evidence in support of a GH feedback loop, that it can inhibit its own release, and at concentrations similar to those seen at peaks in endogenous release. However the mechanism was still unclear. The results in females contradict other results suggesting that GH stimulates somatostatin release, since the rats were still able to release GH in response to injections of GHRH. Indeed, the results here would suggest that GH suppresses its own release by inhibiting hypothalamic GHRH release. However, it would not necessarily be the same in males. The more pulsatile pattern of release in the male rats could be related to differences in the GH feedback mechanism.

Carlsson et al (Carlsson *et al* 1990) extended the experiment, comparing the response to injections of GHRH during an infusion of GH, in male and female rats. A control experiment gave male rats injections of GHRH at 45 min intervals, before, during and after a 6h infusion of saline. This showed their normal pattern of 3-hourly responsiveness to the GHRH injections. This was repeated in males and females with an infusion of human GH. The female rats produced a GH pulse in response to each GHRH injection, but during the infusion, each of the male rats produced only one large GH pulse. The spacing relation of the single pulses to those before and after the infusion, and comparison with the saline controls, suggested that the male rats were still following a pattern of intermittent responsiveness to GHRH, although with a prolonged refractory period during the GH infusion. Unfortunately the 6h GH

infusions were not long enough for any of the male rats to show a second GH pulse during the infusion, and demonstrate that the intermittent pattern of GH release was still in place. However, the results show that GH has more of an inhibitory effect than could come from just inhibition of GHRH release, suggesting an increase in somatostatin release. A similar experiment without the GHRH injections (Clark *et al* 1988b) showed a single large pulse after the start of the GH infusion in males. This was ascribed to a delayed onset of the GH-induced inhibition, suggesting that the mechanism of GH feedback may involve a long delay.

GH Control of the Endogenous Rhythm

The possibility that there was also some GH-induced somatostatin release in females was tested by repeating the experiment with lower doses of GHRH. However, the female rats still showed large GH pulses in response to each injection. Together these results indicate that the effect of GH feedback in rats varies strongly between the sexes. GH appears to stimulate the release of somatostatin in males and inhibit GHRH release in females. The stimulation of somatostatin, only in males, makes GH an ideal candidate for an endogenous feedback mechanism.

The effect of GH on a more purely endogenous rhythm was tested by Carlsson and Jansson (Carlsson and Jansson 1990). In their first experiment male rats were given 3-h injections of human GH while blood GH was sampled at 10 min intervals. The response to the first injection varied depending on how recently the rat had produced an endogenous GH pulse. Those which had recently released GH pulse showed little response to the first injection, but the other rats produced large GH pulses. After the second GH injection all of the rats produced a pulse of GH release. This continued, with all the rats producing synchronised 3-h pulses of GH release, with no endogenous pulses between the injections. The results even show that GH levels were already increasing before the injections. Injections were continued at 3-h intervals for 24h. When sampling was resumed in the morning, the rats were still producing GH pulses in synchronisation with the GH injections, but pulse amplitude

had fallen to about half the size of those seen earlier in the experiment. This fall in amplitude may have been due to excessive stimulation of somatostatin or inhibition of GHRH, or desensitisation to GH. The combined dose of exogenous and endogenous GH would certainly be higher than normally experienced by the system. After 24h the phase of the GH injections was completely shifted by giving the next injection after only 1.5h and then continuing at 3h intervals. This resulted in almost complete suppression of the GH release pulses. However, there was only one more injection after the phase shift, which one rat did respond to with a GH pulse. The rats may have eventually synchronised with the phase shifted pattern if the injections had continued for longer.

In the second experiment the GH injections were given at 1.5h intervals, at half the dose to maintain the same total dose. Most of the rats produced a large GH pulse in response to the first injection, but unlike the 3h pattern, they failed to synchronise with the following 1.5h injections. They continued to produce pulses of GH release, but at longer intervals than the endogenous male pattern and with gradually decreasing amplitude.

The synchronisation of GH release with the 3h injections provides good evidence that GH could function as the feedback trigger for the endogenous male pattern. GH must somehow be able to trigger a long suppression of GH release, probably by stimulating a prolonged release of somatostatin. This role for GH is further supported by the out of phase 1.5h injection appearing to extend the suppression period.

1.3.2 Hypothalamic Structures and Substances

Lower level experiments, examining the anatomy and behaviour of components within the hypothalamus, are used to define the mechanisms controlling GHRH and somatostatin release. This will identify and define the functional properties of the components that can be used to build the hypothalamic model.

GHRH and Somatostatin Neurons

Hypothalamic peptides which act at the anterior pituitary are released by neuronal cells which project to the median eminence. Here the peptides are released close to the portal blood supply which carries them to the pituitary. Using a technique where axonal release is blocked in order to collect the product synthesised within cell bodies, and then applying a GHRH immunoreactive test, a large population of GHRH releasing cells was identified in the arcuate nucleus of the hypothalamus (Jacobowitz *et al* 1983) mostly in the ventrolateral region (Sawchenko *et al* 1985). The number of cells was found to be in the region of 1500 on each side of the brain. However, destroying the arcuate nucleus did not completely eliminate GHRH immunoreactivity (Daikoku *et al* 1986) and several much smaller populations of GHRH-containing cells were found in the parvocellular portion of the paraventricular nucleus, the ventromedial nucleus and in the dorsomedial nucleus. These are very small populations, however, of around 50 cells and are not thought to project to the median eminence (Wiegand and Price 1980).

The earliest attempts to investigate somatostatin distribution, in the mid 1970's, used amino acid extraction techniques (Brownstein *et al* 1975). The highest concentration was found in the median eminence but it was also detected in the preoptic area, cortex, septum, thalamus and in the mid brain. Subsequent immunoreactivity experiments in the mid 1980's also found somatostatin in many other areas of the brain. However, the somatostatin found in the median eminence is localised in nerve terminals (Pelletier *et al* 1974) and the peptide is also found in neuronal cell bodies in the periventricular/anterior region of the hypothalamus (Alpert *et al* 1976). Electrical stimulation of the preoptic/anterior hypothalamic area inhibits GH release (Martin et al 1978.) and also causes an increase in the somatostatin levels found in portal blood (Chihara *et al* 1979). Selective lesions of the periventricular area cause a reduction in the levels of somatostatin found in the median eminence (Critchlow *et al* 1981). Together, these results suggest that somatostatin released from the median eminence originates in cells bodies in the periventricular nucleus of the preoptic/anterior area of the hypothalamus. A small

population of somatostatin-containing neurons has also been found in the arcuate nucleus (Kawano *et al* 1982) but there is no evidence that these cells project to the median eminence. However, they are well positioned to act on the nearby GHRH neurons.

These two groups of cells, the GHRH-releasing neurons in the arcuate nucleus, and the somatostatin neurons in the periventricular nucleus form the major hypothalamic control sites for GH release, but there are likely to be other groups of local cells or inputs from other parts of the brain which influence these two groups, perhaps to coordinate their actions, mediate GH feedback or to provide some other pattern generation input.

Other Structures and Substances

Apart from GHRH and somatostatin, many other substances have been identified which affect GH release, neurotransmitters including dopamine, adrenaline, serotonin, acetylcholine and GABA, as well as hypothalamic or circulating peptides such as Substance P, neurotensin, opioids, bombesin, galanin, ghrelin, leptin and NPY. It is unlikely that all of these play an important role in controlling GH release under normal conditions. Some of them probably play some sort of modulatory role to cope with special conditions such as stress or hunger. Many of these substances are likely to originate in the same cells, since many neurons are capable of releasing a variety of transmitters and peptides. Two substances for which there is particularly good evidence for a role in normal function are adrenaline and galanin.

The central adrenergic systems appear to play an important role in the control of pulsatile GH secretion. Administration of the centrally acting α_2-adrenoreceptor agonist clonidine increases GH release in rats whereas non-centrally acting agonists do not have this effect (Day and Willoughby 1980), suggesting that the adrenoreceptor influence is taking place within the CNS. Spontaneous (Arnold and Fernstrom 1980) and clonidine-induced (Durand *et al* 1977) GH release is blocked by the selective α_2-adrenoreceptor antagonist yohimbine and spontaneous release is

also suppressed by adrenaline synthesis inhibitors (Terry *et al* 1982) which indicates an adrenergic rather than noradrenergic endogenous agonist. It is likely that the adrenergic agonist acts on GHRH release, since GH secretion following clonidine is blocked by GHRH antisera (Miki *et al* 1984) but not somatostatin antisera (Krulich *et al* 1982).

Galanin is present in GHRH containing cells which project to the median eminence (Niimi *et al* 1990) acts to increase GH release. This action is blocked by GHRH antisera (Murakami et al 1988.) and it has been suggested, based on human studies, that galanin acts to inhibit somatostatin release (Loche *et al* 1990). This is supported by the detection of galanin receptor mRNA in somatostatin, but not GHRH, neurons (Chan *et al* 1996). The level of GH increase in response to galanin is higher in woman than men, and is proportional to oestrogen levels (Giustina *et al* 1993). Blocking endogenous galanin in male rats significantly disrupts the normal GH release pattern (Maiter *et al* 1990). Pulse amplitude is severely reduced and pulse frequency is increased. The evidence together suggests that galanin may mediate an inhibitory connection from GHRH to somatostatin.

Neuropeptide Y (NPY) appears to be involved in the negative feedback from GH at the hypothalamus. GH receptors are expressed on NPY neurons in the arcuate nucleus (Kamegai *et al* 1996). NPY has been shown to stimulate somatostatin release (Rettori *et al* 1990). Fos expression in response to GH has been detected in conjunction with somatostatin mRNA in the arcuate and periventicular nucleus (Minami *et al* 1992). Activation in the periventricular nucleus was only observed after a 40min delay. In further study, the Fos expressing cells were matched with somatostatin and NPY containing cells, but not GHRH (Kamegai *et al* 1994). Synaptic connections between NPY neurons and periventricular somatostatin neurons have been detected (Hisano *et al* 1990). Note that these results are all in male rats. The evidence suggests that NPY may act to mediate stimulatory GH feedback to the periventricular somatostatin neurons.

Gathering Evidence

Trying to judge the relative importance of these substances by examining their potency is difficult because the only output which can be accurately measured is GH release which many of them control indirectly through GHRH or somatostatin. To cut down the complexity we must consider them in terms of functions rather than specific substances.

The main source of control from outside the hypothalamus and pituitary appears to be the adrenergic input, and this may be a good candidate for providing a basic rhythm for the GHRH neurons, perhaps in a similar fashion to LH release system which has a noradrenergic input. However, the apparent significance of adrenergic inputs can be misleading. Many systems initially cease to function when this input is removed but then after some time recover their activity, and they often only seem to require the existence of the input rather than a specific input pattern, suggesting a permissive role for the adrenergic input rather than any specific functional control.

The current mathematical model of GH release at the pituitary uses just GHRH and somatostatin as its inputs and it is desirable to maintain this simplification, at least initially. This leaves just the substances and structures which act in the hypothalamus to consider. Dopamine does appear to be one of the key players in the hypothalamus. There is good evidence that GHRH neurons contain tyrosine hydroxylase (TH), which often indicates dopamine synthesis. Dopamine acts at the somatostatin neurons in the periventricular nucleus, suggesting that dopamine may mediate an excitatory link from the GHRH to somatostatin neurons. GABA seems to mediate an inhibitory connection to the GHRH neurons, and the possible GHRH release site suggests an auto-inhibitory mechanism. Neurotensin appears to play a similar role to dopamine, released from the GHRH neurons and exerting a stimulatory influence on the somatostatin neurons. However, the action of galanin, providing an inhibitory link from GHRH to somatostatin, is supported by less circumstantial evidence.

Ghrelin, the recently discovered endogenous version of the artificial secretagogues, such as GHRP, has a potent stimulatory effect on GH release.

However, this appears to be specifically related to feeding and weight control and may not play a role in normal GH release.

GHRH and Somatostatin Interaction

There is evidence that somatostatin neurons may form direct synapses with the GHRH cell bodies. Fibres containing somatostatin innervate GHRH neurons in the arcuate nucleus (Daikoku *et al* 1988), although the origin of the fibres is unclear. Somatostatin receptors have been detected in a sub-population of arcuate neurons (Epelbaum *et al* 1989) and some of these have been identified as GHRH neurons (McCarthy *et al* 1992). Subsets of GHRH neurons express mRNA for somatostatin receptor subtypes, sst1 and sst2 (Tannenbaum *et al* 1998). The density of arcuate sst1 receptors detected is 2-3 fold greater in male rats than in female rats (Zhang *et al* 1999). The sst1 receptor subtype has also been detected in periventricular somatostatin neurons (Helboe *et al* 1998). Selectively blocking these receptors shows that sst1, but not sst2 is essential to normal GH release in male rats (Lanneau *et al* 2000). Blocking sst1 reduces GH pulse amplitude, without any large disturbance to pulse frequency. Closer examination of the 15-min sampled GH profile, however, suggests that blocking sst2 does produce more clearly defined individual peaks within the GH pulse. In mice, knocking out the sst2 receptor stops pre-administered GH blocking the arcuate nucleus Fos response to GH or GH secretagogues (Zheng *et al* 1997), suggesting that sst2 receptors mediate inhibitory GH-GHRH feedback.

The main uncertainty is the source of somatostatin acting at these receptors. It is possible that the somatostatin cells in the arcuate nucleus act as inter-neurons mediating a link to the GHRH neurons. However, neuro-anatomical tract studies have found projections from the periventricular to the arcuate nucleus (Toth and Palkovits 1998), leaving the possibility of periventricular somatostatin neurons innervating the GHRH neurons. A small proportion of arcuate GHRH neurons also appear to contact periventricular neurons (Fodor *et al* 1994).

It is likely that some of the substances identified earlier are involved in mediating interaction between the two main groups of neurons. Galanin may mediate an inhibitory link from GHRH neurons to somatostatin neurons. There is also evidence that opioid neurons may mediate a connection from somatostatin to GHRH neurons. Opioids have been shown to increase GH release through an excitatory action on GHRH neurons (Miki *et al* 1984) and there is anatomical evidence of connections between periventricular somatostatin neurons and opioid neurons.

GH Feedback

NPY neurons in the arcuate nucleus appear to mediate stimulatory GH feedback to the periventicular somatostatin cells. However, GH receptors are also found on periventricular somatostatin neurons and GH appears to act directly at somatostatin cells as well as through NPY. Most of the low level results unfortunately come from just male rats. There has been argument over whether GH acts by inhibiting GHRH or stimulating somatostatin release and suggestion that this may vary across gender. GH induces Fos expression in arcuate somatostatin and NPY neurons (above) and GH receptors have been detected in arcuate neurons (Minami *et al* 1993). Comparison with arcuate somatostatin and GHRH cell distribution is so far inconclusive but they have been colocalized with NPY neurons. The arcuate NPY neurons appear to innervate periventricular somatostatin neurons and they may also connect to the arcuate somatostatin neurons to mediate inhibitory GH-GHRH feedback.

How GH might get into the central system is still a mystery. Large peptides of this type are not normally expected to be able to cross the blood-brain barrier.

Sexual Dimorphism

Rats show a particularly strong sexual variation in GH release. Behavioural results suggest in particular that the effect of GH feedback varies between male and female rats. In the arcuate nucleus, GHRH mRNA expression is approximately 2-3 times higher in the male (Maiter *et al* 1991). Somatostatin mRNA expression in the periventricular nucleus is also greater in male rats (Chowenbreed *et al* 1989). There is not thought to be any difference in the number of somatostatin neurons, and the assumption is that the greater levels of somatostatin mRNA expression in the males indicate higher levels of synthesis and release activity in the somatostatin neurons. Periventicular somatostatin peptide content is higher in males (Murray *et al* 1999a).

The sex differences are believed to mainly influenced by gonadal factors, particularly testosterone and oestrogen. Testosterone acts through androgen receptors on the somatostatin neurons to maintain somatostatin mRNA expression (Argente *et al* 1990). Expression of the receptors themselves is sexually dimorphic (Herbison 1995). Oestrogen acts to feminize baseline GH and pulse frequency in male rats (Painson *et al* 1992) but its site of action is less well determined. Sexually differentiated oestrogen receptors are found in conjunction with somatostatin in the bed nucleus of the stria terminalis but not in the periventricular nucleus (Herbison and Theodosis 1993).

1.3.3 Electrophysiological Evidence

So far we have mainly considered evidence from experiments designed to detect the existence and effects of substances when administered to the hypothalamus. The trouble with the interpretation of such results, is that, in the CNS, there are many systems within close proximity, which can make it difficult to draw certain conclusions. Similar substances perform many different roles and their existence and even apparent effects on a structure are not sufficient to conclude endogenous involvement in the system being studied. With electrophysiological experiments we

are taking a step back to a higher level view of activity. Stimulating one structure and showing an effect at another doesn't give as much detail about the mechanism but it does provide more certainty that we have discovered a real connection involved in the system's function.

Unfortunately electrophysiological investigation of the hypothalamic systems involved in the control of GH release suffers the major drawback that arcuate GHRH neuron activity is blocked by anaesthesia. In addition, it has never been possible to record from the periventricular somatostatin neurons because of their anatomical layout, spread in a thin layer beside the third ventricle. However, this does still leave two lines of approach; stimulation of the arcuate GHRH neurons, and concurrent stimulation of the periventricular nucleus and recording from the GHRH neurons. It is possible to stimulate but not record from the periventicular nucleus because stimulation does not require such accurate electrode placement.

Stimulating the Arcuate Nucleus

The first of these approaches was used by Dickson et al (Dickson *et al* 1993) to investigate the effect of different patterns of stimulation of the arcuate nucleus on GH release. The idea of testing different patterns of stimulation, with varying frequency and duration, came partly from a comparison with hypothalamic oxytocin and vasopressin neurons, which have quite different optimal patterns of stimulation with relation to the release response. Oxytocin neurons appear to be more dependent on frequency of stimulation, whereas vasopressin neurons depend more on duration. In a review paper Robinson (Robinson 1991) suggested that the varied patterns of GH release across male and female might be comparable to the respective pulsatile and phasic patterns of release seen in oxytocin and vasopressin neurons.

In the experiments blood GH was measured before and after a pattern of electrical pulses delivered to the arcuate nucleus of anaesthetised male rats. A 50Hz (5s on / 7s off) pattern of pulses applied for 5min was used to test whether direct stimulation could elicit a GH release response. GH was measured 5 and 10min after stimulation

and showed a large release, comparable to endogenous pulses in conscious male rats. For comparison, each rat was given an injection of GHRH at the end of the experiment which showed a very similar GH release. The effect of stimulation frequency was investigated by using three protocols; 10Hz (continuous), 20Hz (5s on / 5s off) and 50Hz (2s on / 8s off), each giving the same total number of pulses, but at different frequencies, and repeated for 2min. All three protocols produced a GH release, but smaller than the large response in the first experiment and with no significant difference between the three. The next experiment tested the effect of the number of stimulation pulses, using three 50Hz protocols with an increasing number of pulses; (2s on / 8s off), (3s on / 7s off) and (4s on / 6s off). This time there was a significant difference in the GH responses. The first protocol produced a small pulse of GH release, the second produced a much larger response, and the third produced a response comparable with endogenous GH pulses. The proportional increase in GH release was much greater than the increase in the number of pulses, suggesting a non-linear relation between neuronal GHRH stimulation and pituitary GH release. This was tested by comparison with the dose of injected GHRH required to produce the same GH responses. However, doubling the dose of GHRH did not nearly produce as great an increase in GH release as doubling the number of electrical pulses, suggesting that the non-linear relation is at the level of the GHRH neurons.

These results clearly show that GH release can be elicited by direct stimulation of the arcuate nucleus and since GHRH neurons make up a large proportion of the cell population in this area it is likely to equate with their stimulation. The fact that this works under anaesthesia also indicates that the loss of spontaneous release must be due to suppression of these cells' excitatory inputs rather than their ability to respond. The GH release in response to the optimal stimulation pattern was of a similar profile and magnitude to that elicited by a maximal dose i.v. injection of GHRH and it seems fairly certain that stimulation does cause a release of GHRH. However, any of the other substances such as galanin, which have been colocalized with GHRH, could also be contributing to GH release response, possibly by inhibiting somatostatin release.

Stimulating the Periventicular Nucleus

Anatomical and pharmacological work had suggested that there was a connection from the periventricular somatostatin neurons to the arcuate GHRH neurons and it was also believed that the rebound release following somatostatin withdrawal was mediated by some hypothalamic mechanism involving the release of GHRH. Okada et al (Okada *et al* 1991) had shown that GH rebound release could be elicited by directly stimulating the periventricular nucleus. If this was part of the endogenous system then it would have to involve some link between the somatostatin and GHRH neurons. Dickson et al (Dickson *et al* 1994) proceeded to investigate this by attempting to concurrently stimulate the periventricular somatostatin neurons and record from the arcuate GHRH neurons in anaesthetised male rats.

To identify possible GHRH neurons, cells were tested for projection to the median eminence using antidromic identification. A total of 53 arcuate neurons were identified in this way and classed as the AD group. Most of these cells were spontaneously active, but with a mean firing rate of less than 2Hz. Another comparison group of 29 cells was identified which did not project to the median eminence and showed bursting type spontaneous activity. These cells had a similar mean inter-spike interval (ISI) to the AD cells but a much shorter modal ISI, reflecting the burst type activity. Cells which didn't fit either group were rejected for use in the rest of the experiment.

Each cell left in the two groups was tested for its response to 5min of periventricular stimulation at 10Hz. Out of all the cells tested 54% were inhibited during stimulation, and 15% were excited, while the rest showed no response. There was no significant difference between the two groups, although a slightly larger proportion (64%) of the AD cells were inhibited during stimulation. Recording from the arcuate cells continued after the end of the periventricular stimulation in order to test for a rebound response. Out of the AD cells which were inhibited during stimulation, 40% showed a rebound hyperactivation, with a firing rate significantly higher than before periventricular stimulation. However, the same response was found in 27% of the bursting group which were inhibited. A further attempt to

separate the two groups was made by testing their response to stimulation of the basolateral amygdala. Stimulation in this area has previously been shown to cause the release of GH without releasing other pituitary hormones and is thought to act by stimulating GHRH neurons. Of the AD cells, 57% were excited by stimulation of the basolateral amygdala but there was still no significant difference to the proportion which responded from the bursting group.

These results give strong evidence for an inhibitory connection from the periventricular nucleus to neurons in the arcuate nucleus, and it is likely that many of these arcuate neurons which project to the median eminence contain GHRH. The strong rebound activation, including some of those which were excited or unresponsive during stimulation of the periventricular nucleus, is also good evidence that this may be the hypothalamic mechanism which mediates the GH rebound release in response to somatostatin, and detecting such a mechanism at this level gives further suggestion that it may be part of the endogenous system. Despite testing with several criteria, the bursting cells continued to show similar responses to the antidromically identified neurons and it is quite possible that these represent a population of interneurons which are connected to the GHRH neurons.

1.4 Methods

The experimental system for this project is a set of differential equations implemented as computer software. This produces a graphical display of the model's output and allows the model's parameters to be immediately adjusted. It also includes several other features for examining the output graphs, such as measuring the time between two points.

Equations

Differential equations are equations which, instead of giving some static absolute value, define how a value changes with time, or some other progressive measure. The simplest example is speed, which is the differential measure which tells us how distance changes with time. In the model, we represent the static state of a system using a set of variables which represent values such as blood GH concentration, somatostatin concentration or lower level properties such as a measure of the number of free pituitary GHRH receptors. Each equation defines how an individual variable changes, often using previous values of that variable and other variables in the system. The equations will also include parameters, values which do not change while the model is running, but which can be changed to alter the behaviour of the equations and consequently the whole system to some lesser or greater degree. Parameters can often be related to values such as the strength of a synaptic connection or may belong to more obscure mathematical constructions.

Computer Implementation

The current version of the model program is coded in C++ and runs on a Windows based PC. The user interface code makes use of the Microsoft Foundation Classes (MFC). The original version of the model program was developed in C, but it was decided that recoding it in C++ would make it easier to adapt and maintain in the future.

The program displays each of the model variables as a graph against time, and allows all of the model parameters to be adjusted and the model instantly rerun. The previous model software, used to develop the pituitary model was an old Fortran program implemented on a UNIX system. Parameters had to be changed by editing a text file and the whole program had to be rerun. Displaying the results involved typing text commands and it became a lengthy process. Making the program easier to use has made it much easier to experiment with the model and visualise the results.

In addition to learning the techniques necessary for creating the user interface, it was necessary to learn how to accurately implement differential equations in a computer program. Differential equations theoretically model analogue values to an infinite degree of accuracy and so any computer implementation is always an approximation. The method which the model program currently uses is the Runge-Kutta algorithm. This runs fairly quickly and is sufficiently accurate for the type of equations and time scale used in the model.

Chapter 2

The Pituitary Model

2.1 Introduction

This chapter describes the pituitary GH system and the model developed by the PhD work of Elinor Stephens. The model was chosen from several alternative designs based on alternative interpretations of the experimental data on the pathways by which GHRH and somatostatin control GH release. It was based on data from *in-vitro* experiments in the pituitary and successfully fitted to quantitative *in-vitro* data. As new work for this project, the model has been reproduced and used to experiment with alternative formulations of possible GHRH and somatostatin input patterns, in an attempt to work back from what we know about GH release to a more refined set of possible input patterns from the hypothalamus.

2.2 The Pituitary GH System

The pituitary is essentially a factory which synthesizes and releases hormones under the control of the hypothalamus. The posterior pituitary forms a delivery system which releases the two peptide hormones oxytocin and vasopressin which are synthesized in the hypothalamus and directly transported to the pituitary by axonal connections, for release into the bloodstream. The anterior pituitary is a more complex system which manufactures and releases the larger protein hormones. Hormone synthesis and release at the anterior pituitary is controlled by hypothalamic peptides which are released by the terminals of hypothalamic neurons at the median eminence into the portal blood supply, which carries them to the pituitary. This form of transport means that the pituitary cells receive single combined signals from each peptide rather than many pulses from the thousands of hypothalamic neurons.

Growth hormone is synthesized and released by anterior pituitary cells called somatotrophs. These receive two major signals from the hypothalamus, GH releasing hormone (GHRH) which stimulates release and synthesis of GH and somatostatin which inhibits the release-triggering action of GHRH to block GH release. Several other substances act at the pituitary to affect GH release, but usually by modulating

the actions of GHRH and somatostatin. One exception is the synthetic peptide, growth hormone releasing peptide (GHRP) which also stimulates GH release, behaving in a similar manner to GHRH.

2.2.1 The Response to GHRH

GHRH triggers an almost immediate release of GH into the bloodstream in a dose-dependent manner up to a maximal level. The somatotroph stores synthesized GH, and it is this stored GH which is preferentially released in response to GHRH rather than newly-synthesized GH. If the pituitary is exposed to a prolonged infusion or very frequent pulses of GHRH then the response will desensitise, recovering with time after the exposure to GHRH. With desensitisation, the GH release response to GHRH gradually falls to a level which remains above basal pituitary GH release. The mechanism of desensitisation is still a matter of research. Prolonged exposure to GHRH *in-vitro* or *in-vivo* results in a depletion of pituitary GH stores but this takes a long time, at high doses, and is insufficient to explain the relatively short term effect which is observed. What is also likely to play a role, and is perhaps the major factor, is some type of receptor desensitisation, or down-regulation in the pathway between receptor and release, and various possibilities for this mechanism form the variations in the design for the pituitary model.

In addition to triggering release, GHRH also stimulates the synthesis of GH, an action which is not blocked by somatostatin, so while the release action may sometimes be inhibited, GHRH will continue to stimulate the synthesis and subsequent storage of GH at the pituitary. This action is triggered by the same receptors on the somatotrophs but acts through a pathway which somewhere diverges from the release pathway. The synthesis action is also much slower than the relatively immediate release response.

2.2.2 Cellular Mechanisms of the GHRH Response

The release component of the GHRH response appears to act by triggering an influx of calcium which causes the exocytosis of stored GH vesicles. GHRH binds to a G-protein linked membrane receptor which activates adenylate cyclase and causes a rapid, but transient, increase in cyclic adenosine monophosphate (cAMP). This triggers the rise in intracellular calcium, mainly by opening voltage activated L-type calcium channels, but also by causing release from intracellular calcium stores. Release from intracellular stores is insufficient to cause exocytosis alone but may regulate genesis and docking of secretory vesicles (Blondel *et al* 1995). The rise in intracellular calcium is also thought to inhibit adenylate cyclase activity, causing a temporary de-activation of the G-protein receptor triggered calcium influx and limiting the release response to GHRH. However this process acts on a timescale of seconds and is not a candidate for the desensitisation mechanism. Desensitisation to GHRH *in-vitro* takes about 20min and so possible mechanisms must be capable of acting on this timescale. There is also a lack of cross-desensitisation between GHRH and GHRP, which further reduces the possibilities, particularly suggesting something in the triggering pathway rather than depletion of GH stores, unless GHRH and GHRP trigger release from separate stores, which seems unlikely. The best candidates for the desensitisation mechanism are receptor down-regulation, down-regulation of the second messenger pathway, and depletion of readily releasable GH stores.

GHRH receptor down-regulation has been shown to take place, acting over a period of hours. All G-protein linked receptors undergo desensitisation after receptor binding as part of the activation process. Many other similar types of G-protein linked receptors, such as the LHRH and GH receptors, are internalised after binding, a process which appears to be necessary for recycling the receptor, and the GHRH receptors may undergo a similar process. An alternative mechanism for receptor desensitisation may be decoupling of the activation process, removing the ability of the G-protein to activate adenylate cyclase.

There is no doubt that the stores of GH can be depleted and that this will result in a reduced release response to GHRH, but this is probably not the main mechanism behind the relatively fast desensitisation which is observed. The fast onset, recovery and magnitude of desensitisation all suggest a mechanism which is closer to switching off the release response rather than something that is being gradually used up, such as the stored GH. However, this possibility can be refined by considering the process by which the stored GH-containing vesicles are transferred from the cell's storage compartments to the cell surface, where the vesicles can fuse and release GH. It is thought that the vesicles do not move freely within the cell, but are transported by a network of microtubules. This limits the amount of GH which is close to the cell surface and ready for fast release, giving the idea of a readily releasable store, which may be used up and replenished more quickly than the cell's main store of GH. This provides a possible mechanism, but again it would require that GHRH and GHRP access, at least partially, separate pools of releasable GH.

There is also evidence that desensitisation may take place at the stage of the second messenger pathway which triggers the cAMP response. The cAMP response to GHRH stimulation in rat pituitary cells exposed to a chronic infusion of GHRH is reduced but the same cells continue to release GH in response to cAMP stimulators or artificial replacements (Ceda and Hoffman 1985). This would be consistent with the independent desensitisation between and GHRH and GHRP since their activation pathways are less likely to be shared.

2.2.3 The Actions of Somatostatin

Somatostatin acts quickly at the somatotrophs to inhibit basal GH release and block the release-triggering action of GHRH, but not the effect of GHRH on GH synthesis. Somatostatin effectively controls the pattern of GH release by exerting permissive control over the release action of GHRH. In addition, somatostatin appears to act to reverse the desensitisation to GHRH, and this may be more than just another effect of its blocking action. Treatment with somatostatin following exposure to GHRH

increases the rate of recovery from desensitisation, suggesting that it may actively reverse desensitisation. Somatostatin treatment before exposure to GHRH also has a 'priming' effect, increasing the response to a subsequent exposure to GHRH (Dickerman *et al* 1993).

If a large dose of somatostatin is used to block release from the pituitary, then it will be followed by a rebound release of GH which does not require GHRH, although a pulse of GHRH coinciding with somatostatin withdrawal will produce a much larger rebound pulse of GH. A longer suppression with somatostatin, up to 20 min, will produce a larger rebound response. This rebound action is probably related to the other actions of somatostatin, either because it inhibits GH release while synthesis continues, allowing the releasable store to build up, or by its ability to reverse desensitisation, increasing the GH release second messenger pathway responsiveness.

2.2.4 Cellular Mechanisms of Somatostatin Action

There are several different G-protein linked receptors for somatostatin on the somatotrophs. One of these inhibits the action of adenylate cyclase and the others are believed to regulate ion channels and exocytosis. Somatostatin acts to inhibit adenylate cyclase, and this is likely to be one of the ways it blocks the action of GHRH. This results in a reduction in cAMP, but only partially. The effect of GHRH on GH synthesis is also mediated by cAMP and it is probable that there are at least two independent cAMP mediated pathways activated by GHRH. Somatostatin only appears to block one of these. However, somatostatin also blocks the release pathway beyond cAMP activation. When somatostatin is administered with a cAMP analogue, the inhibition of GH release remains, even with the elevated cAMP levels. This may be due to one of the somatostatin receptors working on ion channels. One of the somatostatin receptors acts to increase potassium conductance, thereby hyperpolarizing the cell and preventing the influx of calcium, which is required for exocytosis. This also blocks the release-triggering action of GHRP.

2.3 Developing the Model

Taking first of all a top-down approach, the first stage in modelling is to outline what is known about the target system in functional terms. This will form both a basis for the model, and a target, a set of goals which the model must meet. However, there may be several possible explanations for each of these functional components, and if the model is to be based on a simplified representation of the biological components which are responsible for each functional component of the system, rather than just replicating their high level behaviour, then the choice of the biological basis will affect the properties of the component. In fact, modelling comes into its own at this stage, providing a formal system in which to test alternative ideas as to how an observed behaviour may arise. The model representation should be as simple as possible, but in modelling a system at this level, it is important to maintain a representation which relates to the biology, in order not to miss hidden properties, and to be able to relate conclusions back to the real system.

2.3.1 The Functional Pituitary GH System

These are the functional components as outlined in Elinor's thesis :

i) GHRH stimulates GH release in a dose-dependent manner

In-vitro, exposing GH cells to varying doses of GHRH for a fixed duration produces GH release according to a classic sigmoidal dose-response relationship with the logarithm of the GHRH dose. The magnitude of the response also varies with the duration of exposure. In response to a single pulse of GHRH, cells produce a single pulse of GH which varies in magnitude with the duration and magnitude of the GHRH pulse. The same relationship is observed *in vivo* in the female rat when given injections of GHRH, but not in the male rat, where the GH response magnitude varies, probably because of periodic high levels of somatostatin.

ii) Dose-dependent desensitisation to GHRH

During an infusion of GHRH, GH cells *in-vitro* initially produce a large GH response, but the rate of release rapidly decreases, following a roughly exponential decline. Responses to succeeding pulses of GHRH depend on the pulse frequency and magnitude. The first pulse will elicit a large pulse of GH, but if a subsequent pulse of GHRH occurs too soon after, it will produce a smaller pulse of GH. Larger GHRH pulses require a longer interval between pulses to get the same GH response.

iii) Somatostatin inhibits GH release in a dose-dependent manner

When somatostatin is also infused, a GHRH infusion produces a GH dose-response curve of the same sigmoidal form but with a reduced magnitude. The response to pulses of GHRH is reduced with somatostatin infusion and the basal level of GH release between pulses is also lower. The inhibitory effect of somatostatin is dose-dependent, and a large enough dose can entirely block any significant GH release.

iv) Somatostatin can prevent desensitisation, and can increase responsiveness to GHRH

Infusing somatostatin between GHRH pulses reduces the time required between each pulse to elicit the same large response, apparently accelerating response recovery. Pre-treatment with somatostatin also increases the GH response to a single pulse of GHRH.

v) Rapid removal of somatostatin cause a GHRH dose-dependent rebound release of GH

When somatostatin infusion is terminated, for a short period GH release increases to a level above that which occurred prior to somatostatin treatment before falling back to the basal level. The rebound is larger following a higher dose or longer duration infusion of somatostatin. The rebound is much larger however if accompanied by a pulse of GHRH. If GHRH is infused during the somatostatin infusion then the rebound will be smaller indicating that desensitisation to GHRH occurs even while somatostatin is blocking GH release. This concurs with the *in-vivo* results (section 1.2.1) which demonstrated that somatostatin can block spontaneous (endogenous GHRH pulses) and artificial GHRH pulse induced GH release, and that following the end of the somatostatin infusion there is a very large release of GH which can be suppressed by knocking out endogenous GHRH.

vi) Basal GH release

GH cells *in-vitro* produce a constant low level of GH release which is reduced by somatostatin infusion, or by taking away extra-cellular calcium. This suggests that there is constant activity in the calcium-regulated exocytotic pathway and also some constitutive activation of the intracellular pathways which trigger GH release in response to GHRH.

2.3.2 The Underlying Mechanisms

Together, these functional components form the basis and target for the model, but before these can be translated into a form which can be directly modelled, their biological mechanisms must be examined in order to decide exactly how to model them. Most of these components are well-understood processes that can be modelled using standard techniques, but the processes behind the desensitisation to GHRH and

somatostatin's effect on this are uncertain. Elinor's thesis re-examines the possible biological mechanisms for this process and develops several options for proceeding with the modelling.

a) Depletion of readily-releasable reserves

This is based on the idea that there is a complex process required to get from GH synthesis to exocytosis, requiring transport from the synthesis site through a system of microtubules to the readily releasable reserve of docked GH vesicles at the membrane. The nature of such a system means that the store of releasable GH can be rapidly depleted but only replenished more slowly. The main argument against such a mechanism is the lack of cross-desensitisation between GHRH and GHRP. This would require separate pools of releasable GH or even different types of GH cells responding to only GHRH or GHRP and there is no evidence that this is the case. There is some heterogeneity in response between individual somatotrophs, but no apparent separate populations. Ties between release pools and particular receptor types are also unlikely since part of the release pathway involves diffusible second messengers that can not be so precisely targeted. The other option is desensitisation in the second messenger pathway at some stage which is not common to GHRH and GHRP, or receptor down regulation. Rejecting the notion of depletion of a releasable pool will allow the model to treat the supply of GH as essentially unlimited since depletion of the entire GH reserve requires sustained release for a period well beyond the time scale of the model.

b) Desensitisation in second messenger system / down-regulation of GHRH receptor

GHRH and GHRP bind to different receptors and trigger second messenger pathways that remain independent until voltage-gated ion channels trigger calcium entry and exocytosis. The lack of cross-desensitisation indicates that desensitisation occurs independently in the two pathways, prior to where they converge. Elinor's thesis takes this alternative as the way to proceed with the model, although she still

develops a model representation of a releasable pool for comparison. This turns out to produce a form which actually functionally equivalent to the model based on receptor / pathway desensitisation.

2.3.3 The Model Representation

The release pathway is complex, involving several levels of dynamics; receptor binding and recycling, a finite pool of G-proteins, saturable second messenger systems, finite numbers of ion channels and the channel dynamics themselves. However, attempting to model this in its entire complexity, even if successful, will still only understand the system at the same low level. From a bottom-up approach (in complement to the top-down approach described above), the goal of modelling larger parts of the brain should be to reduce the apparent complexity of the system, to understand what it is really doing at a functional level. Much of the low-level complexity in a biological system is necessary to the implementation, but is not representative of function. Many of these dynamics will be compensating against each other, or forming together, to produce what may actually be quite simple dynamics. The reason for examining the system at a low level is to choose the right simplification rather than to reproduce the complexity. With this goal in mind, Elinor's thesis develops several alternative models for this part of the system, based on the Law of Mass Action, the idea that substances and processes can be treated as continually changing concentrations (variables) and rates of reaction (parameters in equations) which define how the concentrations affect each other. The model is intended to work on a timescale of minutes and it ignores processes which are only significant on a much longer timescale, such as cell growth and GH synthesis.

The model itself consists of a set of variables, each representing some substance or the state of some component of the system, and a set of differential equations which describe how these values interact with each other.

The first stage in the process of GHRH triggering GH release is the binding of GHRH to its receptors. The level of binding will be proportional to the product of the

concentration of GHRH (the variable r in the model) and the concentration of free receptors (f in the model). This variable f really represents the ability of the system as a whole to react to GHRH, but the simplest translation back into biological terms is to call it the number of free receptors, since these will likely form the major limit on the response. As GHRH enters the system, and binds to and activates receptors, f declines proportionally. The level of binding and the subsequent activation of second messengers is represented by the variable u. This value is then used as a signal to generate GH release using a sigmoidal relationship. The original design version of the model also uses a third variable w in this part of the system to represent the refractory period in the transition from bound activated receptors, u, back to free receptors, f. This value w could be translated back into some element such as internalised receptors, in the process of being recycled, or the kinetics of ion channels with minimum closed and open times. These three variables are tied together by a principle of conservation s.t. $f + u + w = constant$. As the level of activation, u, increases, f is used up. The level of GH release increases proportionally to u, which then decreases again, increasing w. The cycle is completed as w is depleted to restore f. This means that the system's capacity to respond and trigger GH release is conserved and also limited, ensuring saturation in the GHRH-GH dose-response curve.

Somatostatin inhibits GH release in at least two ways, by activating potassium channels to hyperpolarize the cell and prevent voltage-gated calcium entry and also by inhibiting the increase in adenylate cyclase triggered by G-protein linked GHRH receptors. Both of these processes are essentially limiting the transduction of GHRH triggered activation into GH release and so this inhibition is represented by making the u dependent rate of GH release also inversely, and non-linearly, proportional to the somatostatin level. The non-linear relationship means that there is a maximal level of somatostatin which almost completely blocks GH release. Somatostatin's ability to accelerate the resensitising process is modelled by making the rate of transfer from w to f partly dependent on the somatostatin level.

2.3.4 Modelling Designs

This basic design for the model still leaves the construction of the actual equations and final options about how to implement the functional properties. During the original development of the pituitary model, several versions were produced before settling on a final refined version of the model.

The prototype design version of the model uses six variables; the GHRH level (or concentration), r, the somatostatin level, s, the GHRH-GH release system variables, f, u and w, and the GH level, h. GHRH and somatostatin are modelled by simple equations that contain just an input component, specified from outside the model and a decay component representing clearance in the pituitary bloodstream.

Model 1

The first stage of designing the equations was to develop a function which would give the non-linear relation between the variables u and s and the processes they control, GH release and resensitisation. The following model equations were produced based on a standard modelling form :

$$\Phi(u) = \frac{1}{1+e^{(-u-u_0)/\delta_1}}$$

$$\Phi(s) = \frac{1}{1+e^{(-s-s_0)/\delta_0}}$$

These give a non-linear form (similar to those illustrated in figure 2.1) which is controlled by a threshold parameter, u_0 or s_0 and a rate parameter, δ_0 or δ_1. Most processes where one substance controls another have some sort of threshold, otherwise insignificant levels of a substance would have a disproportionate effect on the model's behaviour. The non-linear increase in activation represents the smaller increase in effect with the same increase in the substance at already high levels. The

equation is scaled to give values between 0 and 1. By changing the steepness parameter the function can produce a gradual increase in activation or act as a sharp switch when the value exceeds the threshold.

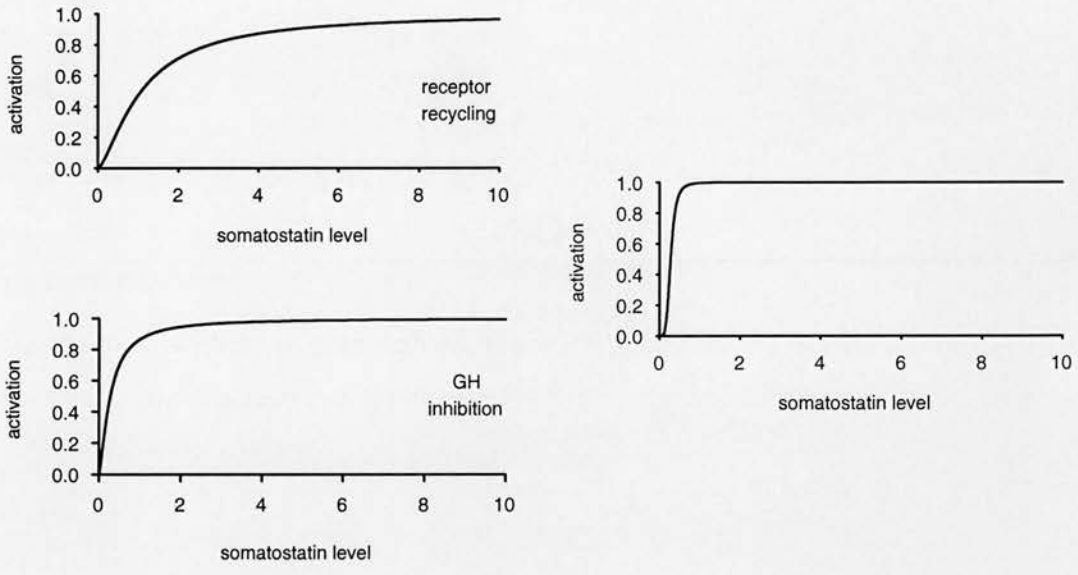

Figure 2.1 : Activation curves for receptor recycling $\Phi_b(s)$ and GH release inhibition $\Phi_r(s)$. These example curves are from the final version of the pituitary model, but use the same form as $\Phi(u)$ and $\Phi(s)$ in the first prototype version. Parameters are $s_0 = 0.029$, $\delta_0 = 0.3$ (top left); $s1 = -0.56$, $\delta_1 = 0.3$ (bottom left). The right hand curve shows the effect of using a smaller δ value to increase the gradient and produce a more switch-like activation, parameters $s1 = -0.56$, $\delta_1 = 0.1$. (Note : These parameters and equations refer to the final version of the model, not the version 1 prototype in this section.)

The activation value $\Phi(u)$ is used for the rate of GH release and the rate of transfer from u to w. The activation value $\Phi(s)$ is used for the transfer from w to f, representing the effect of somatostatin on the recycling process, and also on the transfer from u to w, increasing the rate of u's depletion, to inhibit GH release. This gives the following set of differential equations for the GHRH-GH release system :

$$\frac{df}{dt} = -k_1 rf + (k_2 + k_3\Phi(s))w$$

$$\frac{du}{dt} = k_1 rf - (k_4 + k_5\Phi(s))u - k_6\Phi(u)$$

$$\frac{dw}{dt} = (k_4 + k_5\Phi(s))u - (k_2 + k_3\Phi(s))w + k_6\Phi(u)$$

$$\frac{dh}{dt} = k_9\Phi(u) - k_{10}h$$

At this stage the model (figure 2.2) can be simplified because of the principle of conservation that dictates that $f + u + w = f_T$, where f_T is a constant which defines the maximum potential for activation. This means that only two of these equations are required, and if the equations for u and f are kept then w is defined by $w = f_T - u - f$. The rate parameters are set so that when the somatostatin level is low and u is high then the rate of GH release will be greater than the somatostatin-controlled transfer from u to w. The low level of somatostatin will also mean a slow transfer from w to f so that when GHRH triggers transfer from f to u and subsequent GH release, f will fall causing desensitisation to GHRH. Conversely, when somatostatin is high, u will fall quickly, suppressing GH release, and transfer from w to f will be faster, accelerating resensitisation. GH release itself is modelled simply as the activation due to u, $\sigma(u)$ modified by a rate parameter and a decay component.

This first version of the model was tested by adjusting the parameters to produce a roughly realistic response between input levels of GHRH and somatostatin and GH release. The model produced the desired basic behaviour but not the desired dynamics. The main problem was that u is depleted as fast as it triggers release and so it never gets much above its threshold value, u_0, causing very low levels of GH release. It was also considered at this stage that modelling somatostatin inhibition by increasing the rate of u's depletion was not a good representation of the biological mechanism.

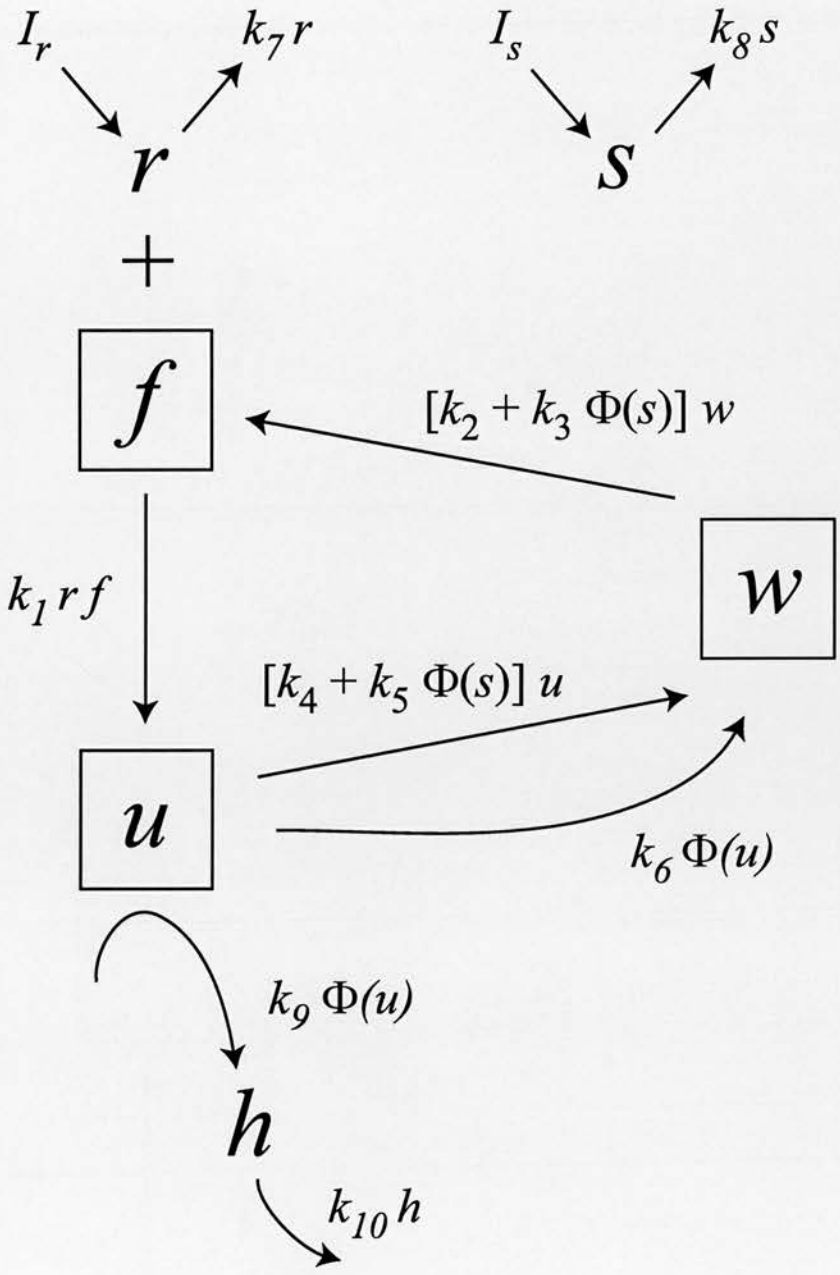

Figure 2.2 : Model prototype 1. Pathway begins with binding of r and f, depleting f and increasing u. Variable u is depleted by two routes, one dependent on somatostatin, and the other proportional to GH release. Release will only occur when u is high enough to defeat depletion due to the somatostatin dependent term, allowing $\Phi(s)$ to control release. The $\Phi(s)$ term in the transfer from w to f allows somatostatin to accelerate resensitisation.

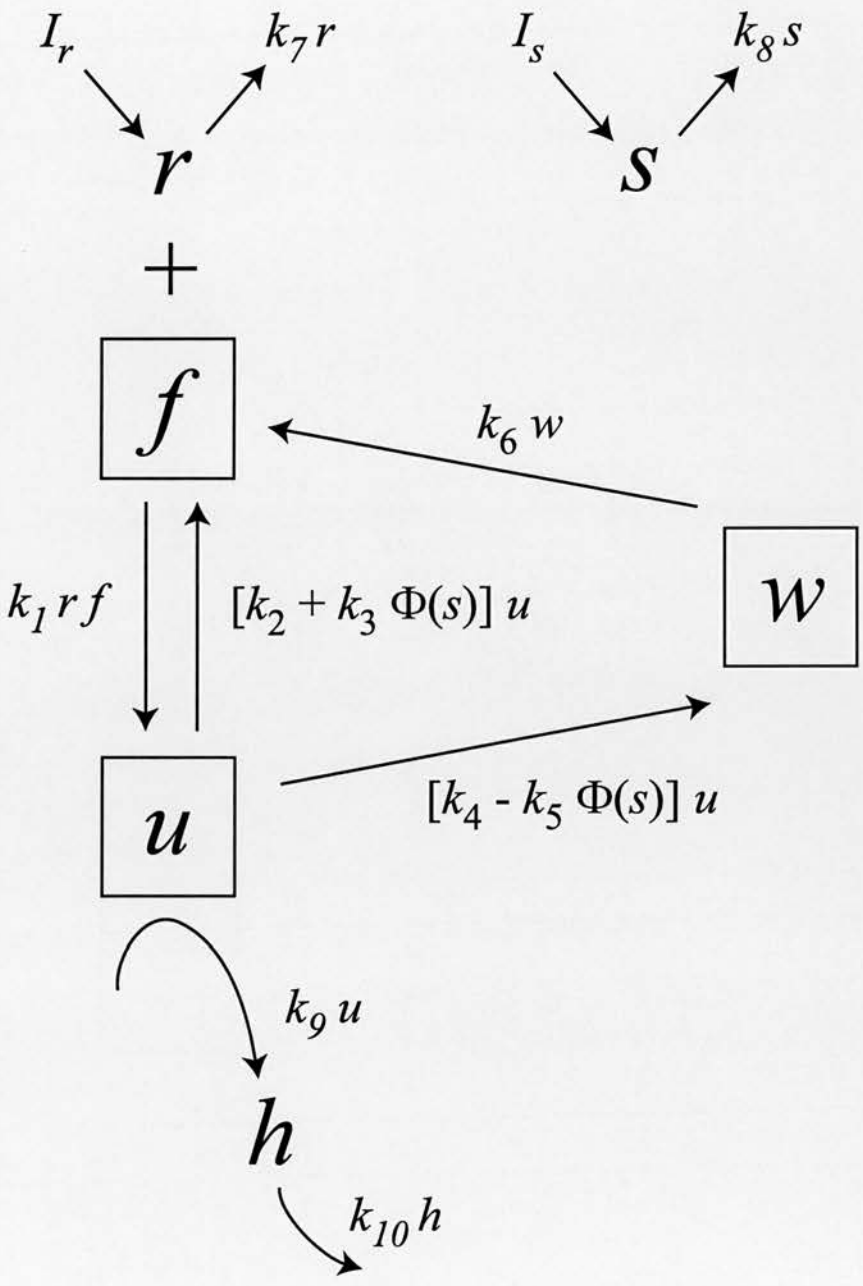

Figure 2.3 : Model prototype 2. Pathway begins with binding of r and f, depleting f and increasing u. There is now a direct somatostatin dependent route back to f. Transfer from u to w is inhibited by somatostatin so that the new direct route is preferred when $\Phi(s)$ is high. Release is directly proportional to u. Model function is similar with $k_5 = 0$ and so this term can be removed, since the k_3 term already accelerates the opposing process.

Model 2

The first change was to shift the somatostatin-controlled resensitisation component so that it transfers directly from u back to f. This gives two pathways, and returning to the biological interpretation, creates two possibilities for a bound GHRH receptor. It could fail to activate the whole pathway, either because of failing to associate with a G-protein or failing to activate adenylate cyclase (which can be inhibited by somatostatin), and end up just being recycled. Alternatively, it successfully triggers the whole release pathway, and follows the path back to f through w. The balance between these two paths is controlled by somatostatin, so that a high level of somatostatin causes more transfer directly back from u to f, causing u's depletion and inhibiting release. The second change in this version of the model is just to get rid of the component that depletes u at the same relative rate to release. The rate of transfer from u to w and u to f, not controlled by somatostatin is then just proportional to u, rather than the release rate. The new equations are given below :

$$\frac{df}{dt} = -k_1 rf + (k_2 + k_3\Phi(s))u + k_6 w$$

$$\frac{du}{dt} = k_1 rf - (k_2 + k_3\Phi(s))u + (k_4 - k_5\Phi(s))u$$

$$\frac{dw}{dt} = (k_4 - k_5\Phi(s))u - k_6 w$$

$$\frac{dh}{dt} = k_9\Phi(u) - k_{10}h$$

In this version somatostatin increases the rate of the immediate recycling route and also decreases the rate of transfer through the full release pathway, controlled by parameter k_5. The model still behaves in the same manner with $k_5 = 0$, taking away

the negative effect of somatostatin on the release pathway, and so it can be simplified by removing this component. The positive somatostatin component, increasing direct receptor recycling, implements inhibition in a less intuitive manner, but also fills the role of accelerating resensitisation, although at the expense of u. However this indeed turned out to be the downfall of this version of the model. No combination of parameter values was able to produce the desired behaviour and it was the clear that the major flaw was transfer from w to f not being dependent on somatostatin. When the level of GHRH is increased and release is triggered, increasing w, then somatostatin has no way to accelerate the restoration of f. Any changes to parameters to allow quicker resensitisation, essentially by limiting the transfer to w, also caused insufficient desensitisation, allowing prolonged high levels of release. The value for u tended to stay near its maximum, requiring the threshold for activation due to u to be set very near this maximum value and to be made very sensitive.

The conclusions after testing this version suggest two solutions to the problem with u's profile. The version of the model here requires the rate of transfer in and out of u to be similar, so the level shows little variation, but what could be measured instead is the rate of flow rather than the actual level. The first suggested way to do this would be to have a time delay in the transfer from u to w, but the software which was being used to implement the model didn't allow such a feature. This would stop u's content being immediately returned to f, enforcing desensitisation but it would do so in quite a rigid fashion, depending on the length of fixed delay rather than the amount of GHRH input. The second suggestion was to differentiate between freshly bound contribution to u and older content of u but again this presented the problem of a fixed arbitrary point, dividing between 'new' and 'old' making the model unable to produce a similar type of response to different lengths of GHRH pulse.

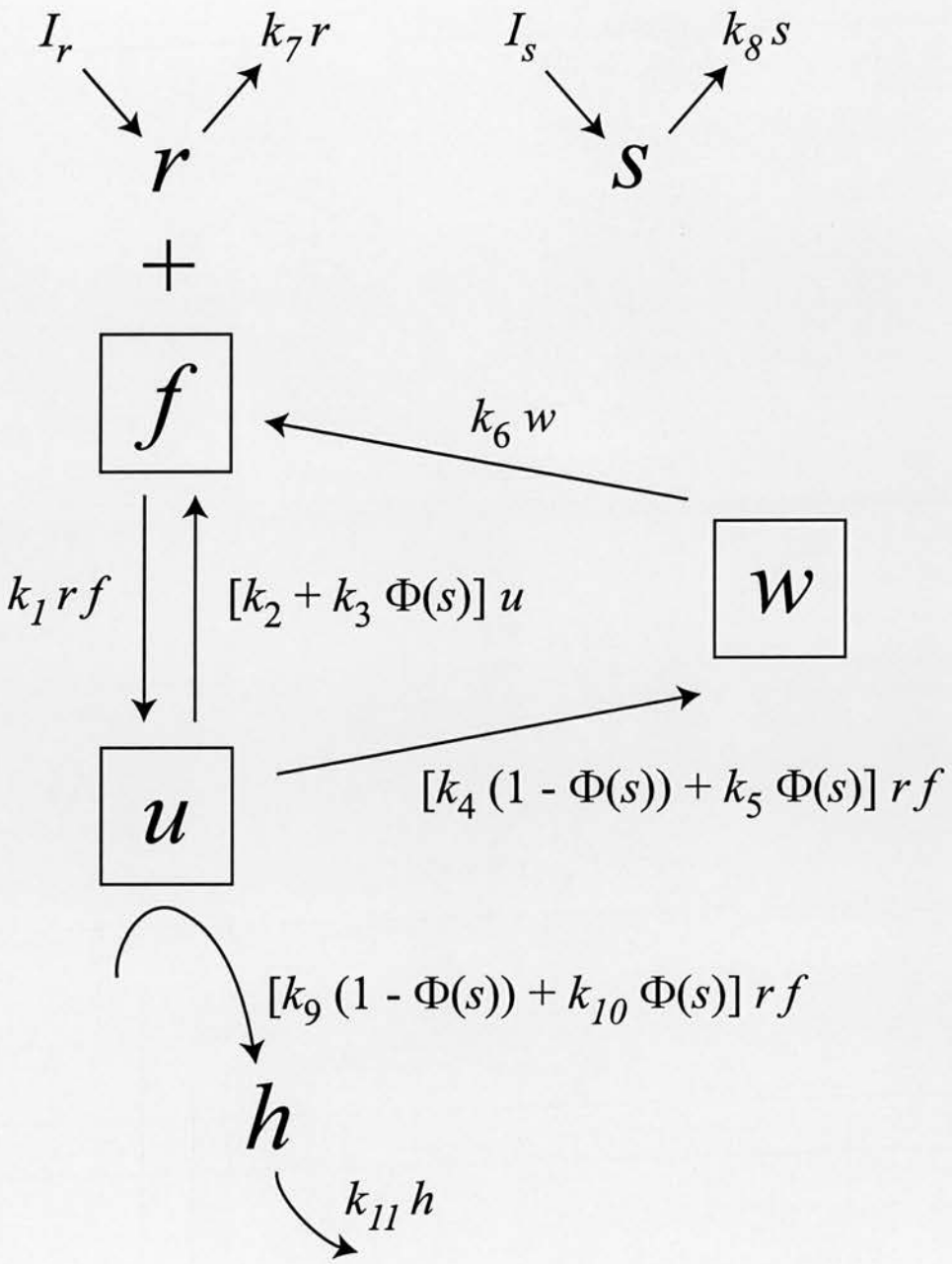

Figure 2.4 : Model prototype 3. Pathway begins with binding of r and f, depleting f and increasing u. Binding is reversible, allowing a direct, partially somatostatin dependent, route from u back to f. The rate of transfer from u to w, and GH release, is now proportional to the rate of binding. The construction with two opposing $\Phi(s)$ terms is intended to force preference for the direct route when $\Phi(s)$ is high but also allow a route for somatostatin dependent resensitisation through w.

Model 3

The third version of the model replaces the transfer from *u* to *w* and also GH release with a construct proportional to the rate of binding (the product of r and f) which has two components, proportional and inversely proportional to somatostatin, balanced by their parameters so that the direct recycling route is preferred in the presence of somatostatin, and the release route otherwise. This allows somatostatin to directly inhibit transfer from *u* to *w* and GH release and uses the rate of u's increase rather than its absolute level. It also matches the rate of release to the transfer between *u* and *w*. These changes gave the set of equations below :

$$\frac{df}{dt} = -k_1 rf + (k_2 + k_3\Phi(s))u + k_6 w$$

$$\frac{du}{dt} = k_1 rf - (k_2 + k_3\Phi(s))u + k_1(1-\Phi(s))rf - k_5\Phi(s)rf$$

$$\frac{dw}{dt} = k_4(1-\Phi(s))rf + k_5\Phi(s))rf - k_6 w$$

$$\frac{dh}{dt} = k_9(1-\Phi(s))rf + k_{10}\Phi(s)rf - k_{11}h$$

To correct the problem of somatostatin-independent resensitisation after GHRH-triggered release an extra reverse connection from *w* to *u* was added, creating a path for somatostatin-controlled transfer back from *w* to *f*, through *u*. After adjusting the parameter values this version of the model was able to successfully produce the desired behaviour, comparable to the real system. With these parameter values, *w* stayed at a very low value, effectively not being used and indicating that it could actually be entirely removed from the model.

2.3.5 The Final Model Design

Working with these prototypes highlighted a particular problem with designing a model in this manner. Although it makes sense intuitively to use variables to represent stages in the process, in the real system there are time delays, so that the components do actually store something for a time and record what is going on. However, with just the differential equations and instantaneous change, the variables tend to stay at either a high or low level, not really giving any representation of their inputs and outputs. The solution to this was to use the rate of increase rather than the variable itself, the main example being using the rate of binding, rf, instead of u. The model can still have components which directly use a variable, but they shouldn't be set up to produce too much concurrent input and output activity. The final version of the model also removes w, effectively just cutting it out of the system. The component u takes over the representation of the desensitised, activated state. The principle of conservation remains, and this means that the model can be further simplified by replacing u with $f_T - f$.

The model's central process is the reversible binding which transforms $r + f$ into u. The bound receptors are continually recycled at a rate proportional to u, with a slow constant component and another faster path controlled by somatostatin. The model still uses the original activation equation for somatostatin, but the one for u has been replaced by the binding rate. GH release triggered by GHRH is composed of two components proportional to rf. One is constant, giving a level of release which isn't blocked by somatostatin and will normally be very small. The other, larger release component is inversely proportional to somatostatin, allowing somatostatin to block release in a dose-dependent manner. The biological interpretation of this final form is that somatostatin blocks GH release at the final stages of the pathway, preventing depolarisation and calcium-dependent exocytosis of GH. In addition to GHRH-triggered release, there is some constitutive activation in the GH release pathway, which produces basal GH release, and is also sensitive to inhibition by somatostatin. To simulate this in the model a small constant, c, is added to the GHRH level, r.

The final problem with the model was that the level of GHRH was being controlled by the reverse link in the transfer from u to f and r. This was causing significant depletion of the GHRH level if somatostatin was increased when GHRH was already high, due to the replenished f, causing more binding with r faster than r was being replenished. In the real system the amount of GHRH is much larger than the number of available receptors and so the GHRH level should never be significantly depleted by binding. This was fixed in the model by just taking away the components of the GHRH equation which modified the level of GHRH with binding and receptor recycling.

The behaviour of this final simplified version of the model is no less complex than prototype version 3, maintaining all the functional properties, along with the improvements, and the model successfully produces all the behaviour from the original specification. The final form of the pituitary model's equations, those used for the further work to go on and develop a model of the complete system, are described in the next section.

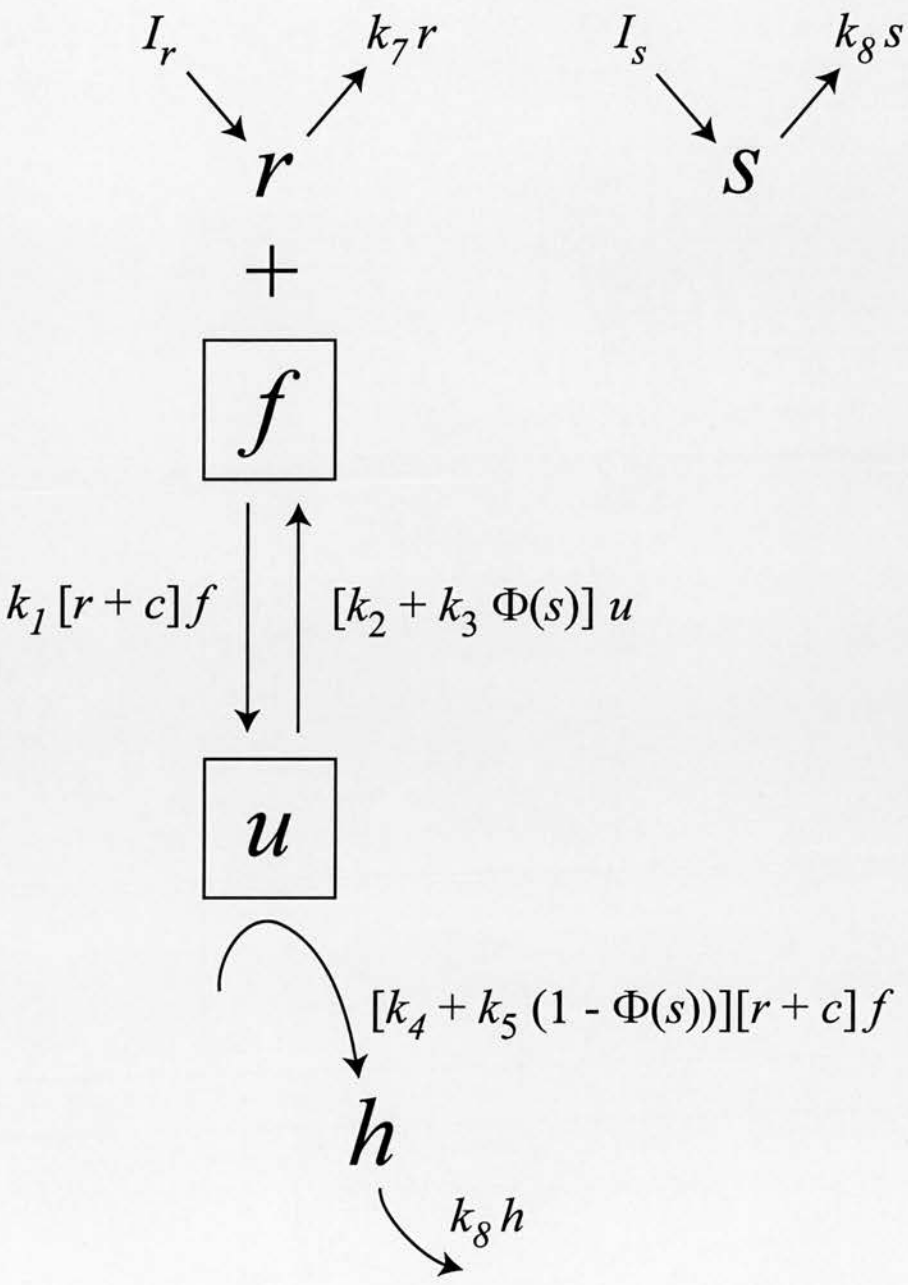

Figure 2.5 : Final pituitary model design. Pathway begins with binding of r and f, depleting f and increasing u, at a rate increased by c to represent constitutive activation. Binding is reversible, transferring from u back to f at a rate accelerated by somatostatin. Release is proportional to the binding rate with a smaller non-somatostatin dependent component (k_4) and a larger component (k_5) inhibited by high somatostatin levels. Conservation between f and u s.t. $f + u = f_T$ allows u to be replaced by $1 - f_T$.

2.4 Fitting to Real Data

In the second part of the previous thesis the model was fitted to real data to calibrate its parameters to give a quantitative, as well as qualitative, match to real data. Two types of *in-vitro* experiment were used to fit the model; perifusion, which measures the model's response to discrete pulses of input substances such as GHRH, and static incubation, which measures the total amount of release in response to long infusions of GHRH and somatostatin, usually to get dose-response relationships.

2.4.1 Perifusion Experiments

In these experiments an *in-vitro* preparation of isolated pituitary cells from male rats was contained in a dish with a constant flow of perifusate, a mixture of the substances used to keep the cells alive and whatever might be released from the cells. At one minute intervals a sample of the perifusate was removed to be assayed for GH in order to produce a temporal profile of the GH response to various substances added to the preparation, particularly GHRH and somatostatin and also GHRP.

To fit the model to the perifusion data, a special formulation of the model's equations was developed which used a reduced number of parameters and could be directly compared with the *in-vitro* experiment's inputs and outputs. This was fitted to the experimental data using non-linear regression and the fitted parameter values were translated back into estimated parameter values for the original model. On the whole good fits were achieved, but for some parameters, particularly those describing the rate of resensitisation, it was not possible to get consistent values across all of the experimental data which was being used. There were also problems due to the limitations of the *in-vitro* preparations, such as leakage of GH due to cell damage, increasing the apparent basal release to a level more significant in relation to the level of release during stimulation than it would be *in-vivo*. The final fitted values however are a good representation of the system. The uncertainty in the

values of some of the parameters is not great enough to have a large effect on the model system's behaviour.

2.4.2 Static Incubation Experiments

These experiments test the response of a preparation of GH cells to an infusion of some substance such as GHRH in order to measure the total amount of GH released in response to a particular concentration of the stimulating substance. The results are used to produce a dose-response curve mapping the GH response to a range of concentrations of GHRH, with and without the presence of somatostatin. This is in contrast to perifusion experiments which record the GH response on a temporal axis.

The dose-response curve for GH in response to GHRH is sigmoidal with the logarithm of the GHRH concentration. The magnitude of the GH response in the *in-vitro* experiment depends on factors such as the number of cells and their condition after cell dispersion, and so the result can only give a relative measure of the range of GH release in response to GHRH, rather than an absolute measure of the maximum level of GH release. For the fitting a specialised formulation of the model was used to match the form of the infusion experiments with a reduced set of parameters, similar to the form used for the perifusion experiments. Experimental data from several different sources was used and the units had to be scaled to a common measure for GH and GHRH. It was possible to get good fits to the data but not with a unique set of parameter values and the only way to get a unique set of parameters values was to fix the parameter describing the rate of resensitisation. Testing the quality of fit over a large range of values for this parameter produced very similar scores, indicating that the infusion experiments don't preserve enough information about the system to determine this parameter. However, it was possible to combine the fitted values from the infusion experiments with the better constrained values from the perifusion data to eventually settle on a fixed set of parameters for the model.

2.4.3 Finalising the Parameters

Once a set of fixed parameters had been derived for the formulation of the model used for fitting, these values were used to produce estimated values for the parameters of the full model (table above). In further work subsequent to the thesis, (Brown et al, unpublished), the parameters were tested with more experimental data and managed to get a good fit with values which were identical or only slightly different to the previously fitted values. This confirmed that the model together with the fitted parameter values is a good qualitative and quantitative representation of the real pituitary GH release system. The quality of the model's fit to the data is also evidence to back up the model's biological basis and the significance of the mechanisms on which it is based. The pituitary model now gives a firm base on which to build and test ideas about the rest of the system, the hypothalamic networks which generate the patterns of GHRH and somatostatin release.

2.5 The Pituitary Model

The first objective of this thesis project was to reproduce Elinor's pituitary model, produce a new software implementation and then to reproduce and extend her results, in the direction of preparation for modelling the hypothalamic systems. This section first presents the equations for the final form of the pituitary model with some description of their function and the parameters which control them. The second part describes the first results using the pituitary model, reproducing those in Elinor's thesis demonstrating the model's simulation of the pituitary GH system's functional properties.

2.5.1 The Pituitary Model Equations

To further simplify the model's equations, the total number of GHRH receptors, previously f_T, has been scaled to 1, replacing the measure of the absolute number of receptors with a proportionate measure. The number of free receptors is represented by the variable f, and this simplification allows the number of bound receptors (previously u) to be just $1-f$, instead of using the separate variable, or $f_T - f$, reducing the number of parameters. The other three variables are r, the GHRH concentration, s, the somatostatin concentration, and h, the GH concentration. Each of these variables has its own differential equation to describe the way it changes with time and in response to other substances in the system, incorporating all the components which increase or decrease the level of that substance. The concentrations of GHRH (r) and somatostatin (s) are modelled by simple equations which represent release rate from the hypothalamus and the rate of clearance in the bloodstream :

$$\frac{dr}{dt} = I_r - k_6 r$$

$$\frac{ds}{dt} = I_s - k_7 s$$

I_r and I_s are parameters which give the respective release rates for GHRH and somatostatin. These function as inputs to the model which can be set to any value and usually follow a pattern defined by an input protocol. The values k_6 and k_7 give the rates of clearance in the blood stream which are modelled as proportional to the current concentration, giving exponential decay, a standard form for modelling clearance.

The effect of somatostatin on the processes of receptor recycling and GH release is modelled by calculating a level of somatostatin activation, $\Phi(s)$ which is a non-linear function of somatostatin concentration :

$$\Phi(s) = \frac{1}{1 + e^{(-\log_{10}(s) - s_0)/\delta_0}}$$

The best way to explain this equation is show what it looks like (figure 2.1). The level of activation varies between 0 and 1. After s reaches a certain value, controlled by s_0, the activation value will increase quickly and then level off at a plateau. The same equation is used for recycling and GH release, but with different threshold and gradient parameters, s_0 and δ_0, and s_1 and δ_1, respectively. The final version of this equation has the modification of using the log of the somatostatin concentration, instead of using it directly. In many biological systems the effect of a substance varies as its log rather than linearly, i.e. at low concentrations a small increase has a large effect, but the same increase at a larger concentration has less effect, and so the base 10 log of s is used instead as just s itself. The adds an extra layer of non-linearity to the activation equation.

The number of free GHRH receptors, f, is modelled by :

$$\frac{df}{dt} = -k_1(r+c)f + (k_2 + k_3\Phi(s))(1-f)$$

The first part of the equation represents the rate of receptor binding, modelled as the product of the number of free receptors (f) and GHRH concentration (r) at rate k_1. This reduces the number of free receptors and so is negative. The extra value, c, is added to the GHRH concentration in order to represent constitutive activation of the release pathway which produces basal release. The second part of the equation represents receptor recycling (resensitisation) which is modelled as the product of the number of bound receptors, (1-f), and the sum of the normal rate, k_2, and the rate due to somatostatin $k_3\Phi(s)$.

The final equation models the system's output, the rate of GH release :

$$\frac{dh}{dt} = [k_4 + k_5(1-\Phi(s))][r+c]f - k_8 h$$

This represents GH release as the product of the rate of receptor binding, $(r + c)f$ and a sum which allows release at rate k_4 independently of somatostatin and extra release

at rate k_5, which is modified by somatostatin activation. Normally k_5 is much larger than k_4 making the somatostatin-blockable component much more significant.

2.5.2 The Model Parameters

The parameters used here are based on those in an unpublished manuscript (Brown et al unpublished). This presented the thesis and carried out some further work, mainly to refine the parameter values and adding improvements such as using the log of somatostatin in the somatostatin activation equation. The model's final set of parameters were generated based on values estimated from real data and by experiments fitting the model to real *in-vitro* experimental data, described later. The only change to the parameters made for developing the hypothalamic model was using a much longer half life for GH, by reducing the value of k_8, so that the model could be matched with *in-vivo* experiments rather than the *in-vitro* experiments used in the previous work. This is a fairly high level model using an abstract representation of the real system and so many of the parameter values cannot be tied to direct equivalent real experimental measures and as such do not use particular units of measure. The default set of parameters is presented in the table below :

Parameter Name	**Description**	**Default Value**
I_r	GHRH release rate	10
I_s	somatostatin release rate	10
k_1	GHRH binding rate	0.1
k_2	receptor recycling rate	0.002
k_3	som controlled recycling rate	0.018
k_4	GH release rate	9
k_5	som controlled GH release rate	71
k_6	GHRH clearance rate	5
k_7	somatostatin clearance rate	5
k_8	GH clearance rate	0.07
c	constitutive activation level	0.01
s_0	recycling som act. threshold	0.029
s_1	GH release som act. threshold	-0.56
δ_0, δ_1	somatostatin activation gradients	0.3

The clearance rate parameters, k_6, k_7 and k_8, are scaled to give half lives in minutes so that the model is scaled to one minute per model time unit. The default values for the release rate parameters, Ir and Is are just arbitrary values chosen to give levels of GHRH and somatostatin at a recognisable level, in the range of 0 to 100 units. Properly scaling these to match the real system is very difficult because of the variations in effective concentrations *in-vitro* and the lack of *in-vivo* measurements. The GHRH binding rate works relative to this arbitrary GHRH level and the proportional 0 to 1 range for f. The two pairs of parameters k_2 and k_3, and k_4 and k_5 are scaled to match the arbitrary somatostatin level but can be compared to each other, both pairs using a small independent rate and a larger somatostatin controlled rate. The constitutive activation parameter, c, is scaled relative to the GHRH level and the somatostatin activation equation parameters, s_0 and s_1, are similarly scaled relative to the somatostatin level. This activation level can never go to a negative value but the negative value for s_1 makes sure that even very low levels of somatostatin have a significant inhibitory effect on GH release.

2.5.3 Input Protocols

The inputs to the model take the form of patterns of GHRH and somatostatin. These are controlled by the release rate parameters, which give the magnitude of the inputs, and protocols which give the timing, describing a series of pulses, or longer periods of switched on release, separated by periods of no release. For GHRH these usually consist of short pulses, simulating the likely endogenous pattern, and somatostatin release usually consists of longer periods of on and off activity, but in the current implementation any square wave pattern can be defined. The form of these protocols is illustrated in the results below (figure 2.8).

2.5.4 First Experiments With the Model

These experiments use the final version of the model with the default parameters taken from the most recent work with the pituitary model, but reproduce the early experiments in Elinor's thesis demonstrating the model's fulfilment of its behavioural requirements in simulating the pituitary GH release system. Before generating these results the new implementation of the model was validated by reproducing the experiments in the thesis with the original parameters and the new version successfully produced identical results, which are not shown here.

Response to GHRH Alone

For the first tests the model was given varied patterns of GHRH input, with no somatostatin input, to test the relationship between GHRH and GH release. The first experiment in figure 2.6a shows the model running with no GHRH input at all. GH quickly climbs to its basal level of release, controlled by c, which then declines very slowly until settling at a steady level. The plot of f shows GHRH sensitivity falling from its initial value of 1 to an equilibrium level at approximately 0.65. If f is set to a lower initial value then it will climb to the same equilibrium level, with GH release slowly climbing in parallel. At this point the level of GH release, which is partly controlled by f, has reached a point where response desensitisation and resensitisation are occurring at the same rate to maintain a steady state in the model, with the GH level at 7 units. Although f mainly represents free GHRH receptors it also measures the system's general ability to respond to release stimulation and so constitutive activation is allowed to reduce f in the same manner as GHRH, although usually at a much smaller magnitude.

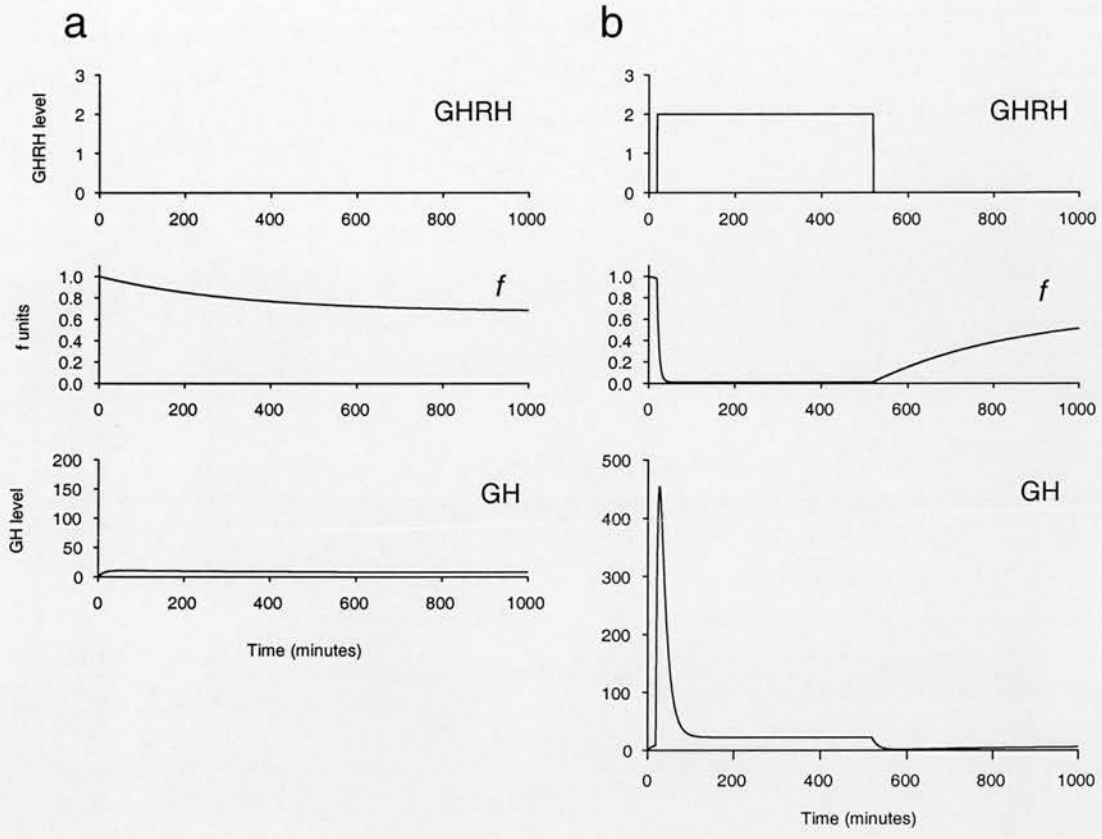

Figure 2.6 : **a**. no GHRH, *f* falls to equilibrium level, low level basal GH release; **b**. GHRH infusion, *f* rapidly depleted then slowly recovers after infusion, large pulse of GH release which falls with rapid desensitisation before settling at minimal level.

The second experiment tests the response to a long constant exposure to GHRH (figure 2.6b), comparable to an infusion. This produces a very large peak of GH release which rapidly declines as the model system becomes desensitised, with *f* falling very quickly to almost 0, maintaining a low level due to the recycling process and sustaining the GH release level at 23 units. When the infusion stops, the GH level drops to almost 0, slowly recovering back to basal level as *f* resensitises.

In the third experiment the model was tested with pulses of GHRH (figure 2.7a). Each pulse produces a corresponding GH pulse, which decline with successive pulses of GHRH as the system desensitises, until reaching a steady response level. With higher frequency pulses of GHRH (figure 2.7b) desensitisation is more rapid and the eventual steady response level is lower. The size of the GH response varies

directly with the height of the GHRH pulse and with the GHRH pulse duration, in an almost indistinguishable manner, partly due to GH's long half life, which masks the difference between effects on pulse height and duration. The GH pulse size is really just sensitive to the total amount of GHRH, at least within a limited time range. Similarly, larger magnitude or longer GHRH pulses cause more rapid desensitisation.

These experiments demonstrated the model's ability to reproduce dose-dependent GH release response and desensitisation to GHRH, and also basal GH release. The next set of experiments tests the model system's behaviour with somatostatin.

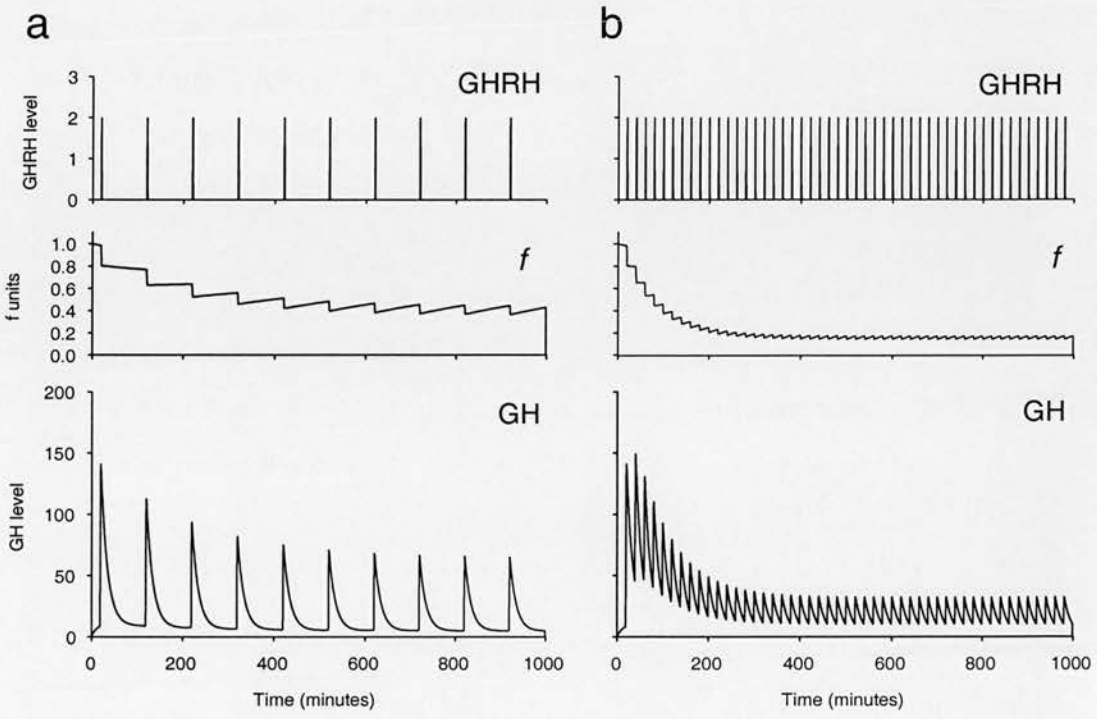

Figure 2.7 : **a**. pulses of GHRH at 100min intervals, *f* reduces with each pulse, with some recovery in the intervals, GH pulses correspond to GHRH with smaller peaks as caused by desensitisation, levelling out at an equilibrium steady response; **b**. pulses of GHRH at 10min intervals, *f* falls more rapidly with less time for recovery in the shorter intervals, corresponding rapid pulses of GH release showing the faster desensitisation to a lower steady response level.

In the first of these tests, the model was given an infusion of somatostatin with no GHRH input (figure 2.8a) to compare with figure 2.6a. Initially, with no somatostatin, GH climbs to its basal release level and then slowly declines as *f* falls

towards its equilibrium, but when somatostatin is added basal GH release is blocked, falling to almost 0. At the same time, somatostatin increases the rate of resensitisation and *f* climbs until it reaches a higher equilibrium level at approximately 0.9 units. When somatostatin is withdrawn again GH rapidly climbs back up to basal level, rising above this in a small rebound, and then slowly declines back to basal level as *f* falls back to its lower equilibrium at 0.65.

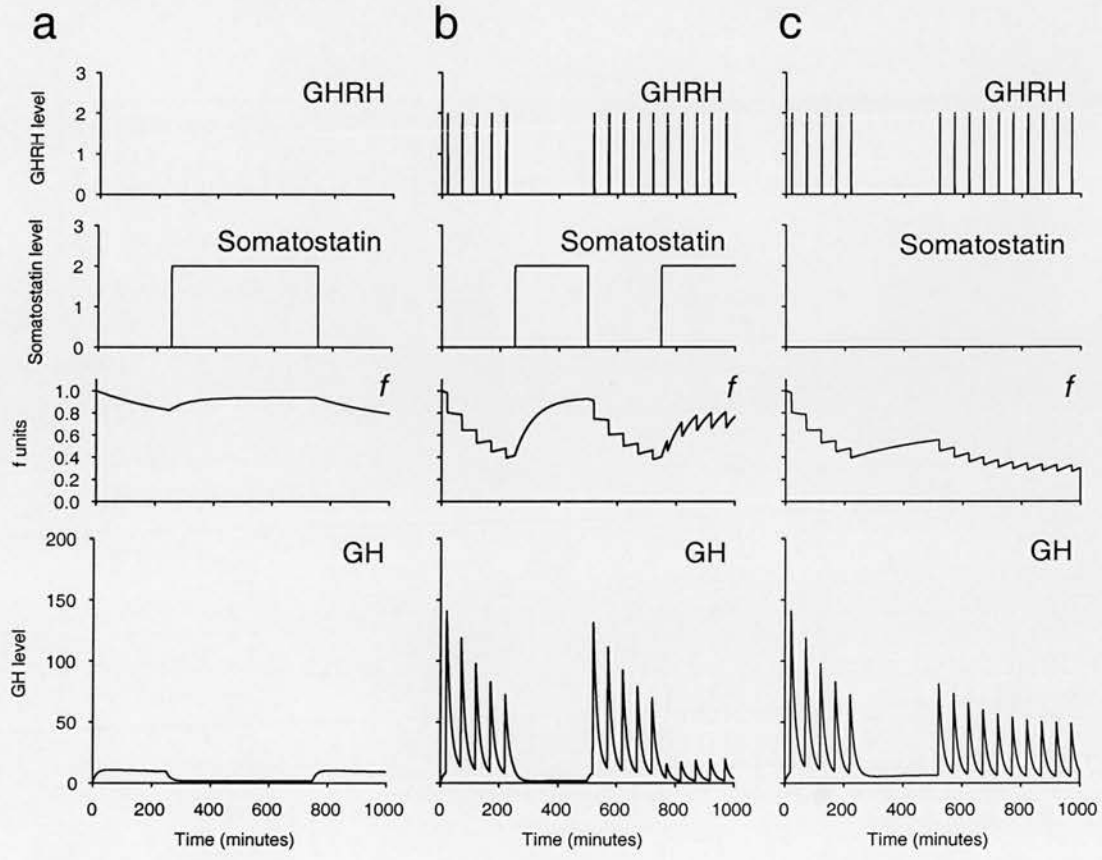

Figure 2.8 : **a**. 500 min infusion of somatostatin, *f* maintained at high level, basal GH release blocked; **b**. mixed pattern of 1 min duration, 50 min interval GHRH pulses and somatostatin infusions 250min off, 250min on repeated, pulses of GHRH without somatostatin produce progressively smaller GH pulses with desensitisation, somatostatin infusion blocks basal GH and accelerates resensitisation, following GHRH produces another large rebound GH response, very small GHRH triggered GH pulse during somatostatin infusion, somatostatin still maintains *f* but at lower level; **c**. same pattern of GHRH as b without somatostatin infusions, first burst of GHRH produces similar large response but recovery during quiet period is much slower producing a smaller GH response to following GHRH pulses

The second experiment with somatostatin mixes GHRH pulses with somatostatin infusions (figure 2.8b). A similar test in figure 2.8c shows for comparison the same pattern of GHRH without any somatostatin. Without any somatostatin, each GHRH pulse produces a corresponding GH pulse, which become smaller as the system desensitises. After a gap in the GHRH pulses there is little recovery in response to the next train of GHRH pulses. However with an infusion of somatostatin between the trains of GHRH pulses, basal GH release is inhibited and the response to the following train of GHRH pulses is much greater. When somatostatin is infused during the train of GHRH pulses the GH response is greatly inhibited, producing very small regular pulses of GH release. Somatostatin also maintains sensitivity to GHRH while it is inhibiting release, even though GHRH continues to trigger desensitisation with the release response inhibited. Reducing the dose of somatostatin reduces the level of inhibition of GH release and also reduces its effect on resensitisation (figure 2.9).

These tests demonstrate the dose-dependent somatostatin inhibition of GH release, its ability to prevent desensitisation and increase responsiveness to GHRH and also the small rebound effect on GH release when somatostatin is rapidly removed. The model has successfully satisfied all the functional criteria in order to reproduce the pituitary GH system. The results demonstrate the competitive roles between GHRH and somatostatin, controlling the level of GH release and the system's ability to respond. Somatostatin is very important in controlling the pituitary GH response, both in making sure that the intended GH pulses are large enough and in enforcing low levels of release between GH bursts.

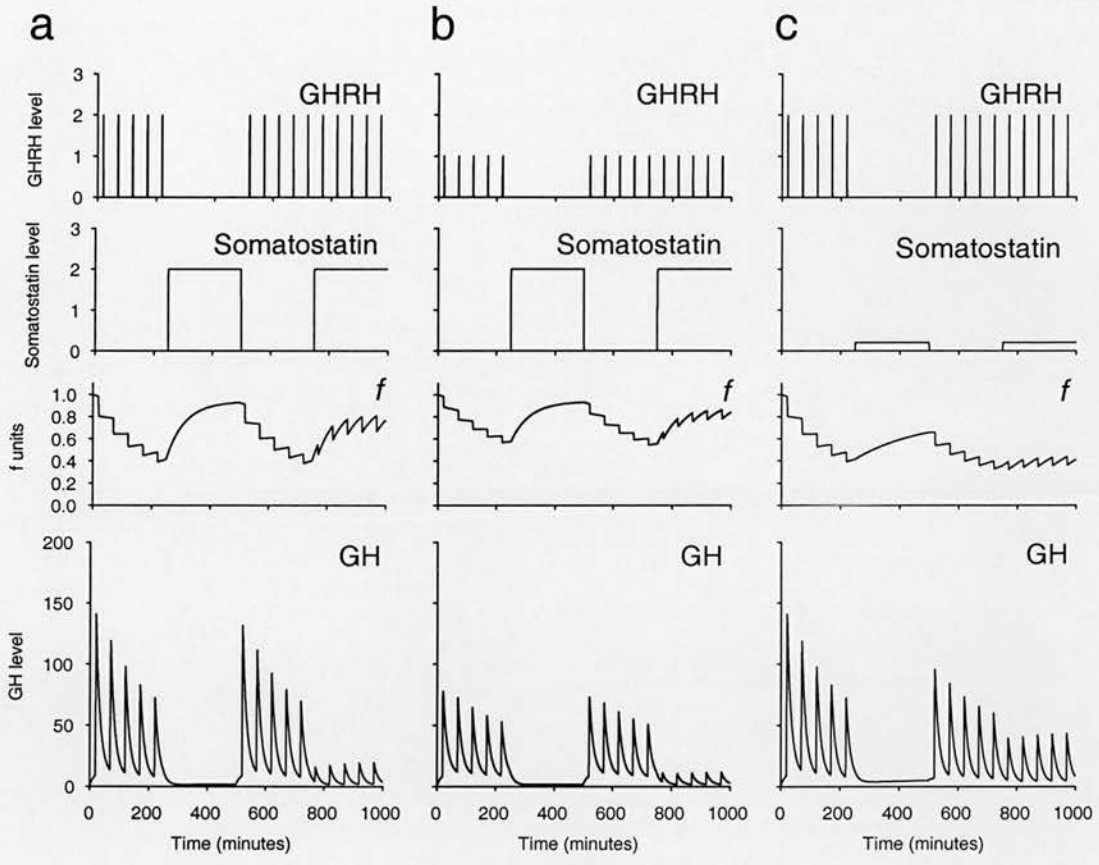

Figure 2.9 : **a**. repeat of figure 2.8b, $I_r = 10$, $I_s = 10$; **b**. reduced GHRH dose, $I_r = 5$, smaller pulses of GH release, f shows less desensitisation; **c**. reduced somatostatin dose, $I_s = 1$, larger pulses of GH release with reduced inhibition of GHRH action, f shows less recovery during somatostatin infusion, lower GH rebound after somatostatin withdrawal.

2.5.5 Scaling the GH Level

Fitting the model to *in-vitro* data was able to scale the model's dynamics, but only in a relative manner, leaving the model's output, GH release following an arbitrary scale. The level of GH release cannot be scaled using *in-vitro* data, because this data itself treats the GH level on a relative scale, with the level of GH release depending on the characteristics of the *in-vitro* preparation, and not matching the *in-vivo* system. However, now that the model has been fitted at a relative level it should be possible to use the results from *in-vivo* experiments to at least roughly scale the

model's GH output to real units comparable with the *in-vivo* experiments. The scaling will always be approximate since the levels of GH release vary between different experiments, and between individual animals. However, it should be good enough to improve the ability to compare the model's output with real data.

The technique for scaling the GH level will be to compare the response to GHRH and the maximal level of GH release, using the pituitary model to simulate *in-vivo* experiments where animals are given injections or infusions GHRH. The GH response is sensitive to the duration of the GHRH pulse and the comparison will be limited by how well the model's input protocols can be compared to injections. The minimum duration for a pulse in the model is 1min and this may be too long to directly compare with an i.v. injection lasting seconds. However, injections are likely to be performed fairly slowly, and a minute possibly is a realistic timescale.

Since the model has already been fitted on a relative scale, it may be sufficient just to compare the maximal level of GH release in response to GH. It should be possible to determine this value for the real system from *in-vivo* experimental data and also with the model. It may also be possible to use this to scale the model's GHRH levels to real units by comparing the dose in infusion experiments which should be easier to match between the model and real data than injections.

Experimental References

The first paper used for fitting (Wehrenberg et al 1983) tests the GH response to varied dose injections of GHRH and also 30min infusions. The maximum GH response was achieved with a 1 nmole (1 μg) dose of GHRH, with GH reaching a peak level of approximately 9μg/ml. With the 30min infusion of GHRH at 0.5nmole/min GH reached a peak level of just under 10μg/ml after 10min before declining back to under 2μg/ml within an hour. A different experiment in (Clark et al 1985) figure 2 produces a similar maximum level for GH release. Here they test the GH response to high dose injection of GHRH in male and female rats, demonstrating the variation in the peak GH response level, probably mainly due to varied

somatostatin levels. The maximum response is the same 9μg/ml. The same paper presents the response to multiple injections of GHRH over a longer timescale and here the peak GH levels are considerably lower, no higher than 4μg/ml. The reason for this is mainly the delay between the injection and the first blood sample, usually 10min, and comparing with figure 2 shows that allowing for the delay, this gives a similar level of release.

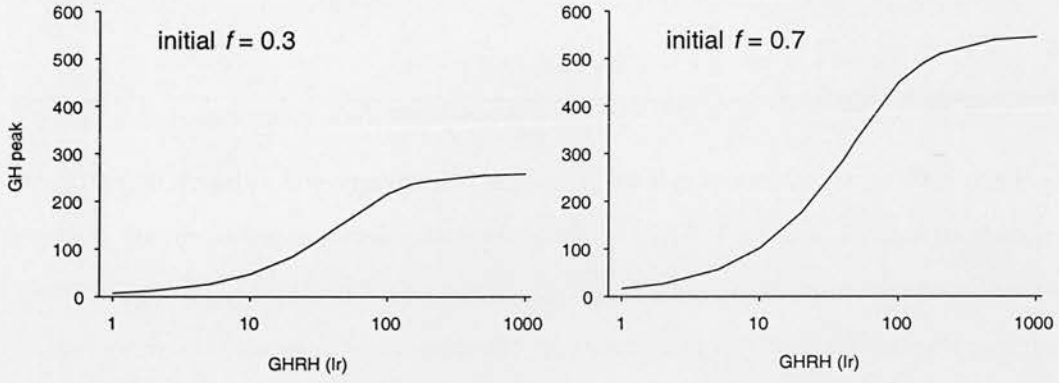

Figure 2.10 : Dose response curves plotting the peak level of model GH release against the base 10 log of the GHRH input rate (I_r). Both curves show the sigmoidal form which matches the GHRH-GH dose-response curve in the real system, but increasing the initial value for f produces a large increase in magnitude.

Comparing with the Model

The model was first used to produce its own GHRH-GH dose-response curve. For the first version of this the peak GH response was measured with 1min GHRH pulses, varying the GHRH release rate, I_r. The first complication which arises is the initial value for f, since this measures the ability to respond to GHRH and will have a large effect on the amount of GH released. To make a comparison, the experiment testing varied dose rates for GHRH was repeated with initial f values 0.3 and 0.7. The resulting dose-response curves are presented in figure 2.10. Peak GH release with initial f = 0.3 was 258 units and with initial f = 0.7 the GH peak was 545 units. This second value for f (0.7) is similar to its equilibrium level during basal GH

release. After a 90min infusion of somatostatin in the model, f can be as high as 0.88, which gives a GH peak at 680 units. Setting f to its maximum value gives an absolute maximum GH response peak of approximately 750 units. With all the values for f, a GHRH release rate of 500 units was sufficient to get close the maximal GH level. Testing the GH response to 30min infusions of GHRH produced the same maximal GH levels and this matches the result in (Wehrenberg *et al* 1983) where the infusion produces a similar GH peak (slightly higher, but within the error range) to the high dose injection.

There is no way to measure f in the real system, but we can assume that the biggest responses to GHRH in the experimental results correspond to a fairly high f, and so the model results with f = 0.7 or 0.88 are probably a better match to the highest responses in the real system. According to the error bars some of the experimental results may have been GH peaks as high as 12μg/ml. Considering this, a rough match between the data and the model could be that 500 model units = 10μg/ml, or 1 model GH unit = 20ng/ml. If the *in-vivo* results indicate an average absolute maximum level of GH release at 10μg/ml then the scale might be 1 model GH unit = 15ng/ml. However, since levels of release vary a great deal between results, and these represent the highest levels detected, for the results in this thesis a scaling of 1 model GH unit = 10ng/ml is used. These results also indicate a match between GHRH levels, comparing I_r with *in-vivo* data, to give 1 model I_r unit = 1ng of GHRH.

2.6 GHRH and Somatostatin Inputs

The first set of proper new experiments with the pituitary model is an attempt to reproduce the endogenous pattern of GH release in the male and female rat by controlling the input protocols for GHRH and somatostatin in the pituitary model. The aim is to discover what sort of patterns of release the hypothalamic network needs to produce based on the assumption that the pituitary model is an accurate representation of the real system. It is likely that there will be several plausible input

patterns, but experiments at this level can at least be used to constrain the target for hypothalamic modelling.

2.6.1 The Target Release Pattern

One of the first points to consider is the basis on which to compare data from the model and the real system. In modelling a whole system at this level it is more important to reproduce the characteristics of the real data rather than exact quantitative details. The exact form of the GH bursts and the magnitude of the pulses varies between experimental subjects and so, together with the relatively low temporal resolution of much of the data, the only definite characteristic is the general form of the release pattern, although closer analysis can still give clues to the functioning of the system and the line between what can be considered a quantitative or a qualitative detail is often blurred.

GH release in the male rat occurs in 3-hourly bursts of several large pulses of GH over roughly 1 to 1.5 h (the period of apparent pulse activity varies in different results). The burst usually consist of around two to four distinct peaks of varying height but of similar duration. Between the bursts there are very low levels of release, often below the threshold of detection. The blood GH concentration in female rats does show some peaks but these are irregular, more frequent, and usually smaller than the distinct pulses seen in males, making up a fairly continuous release of GH in the female with a higher basal concentration. Figure 2.11 gives examples of the typical male and female release patterns.

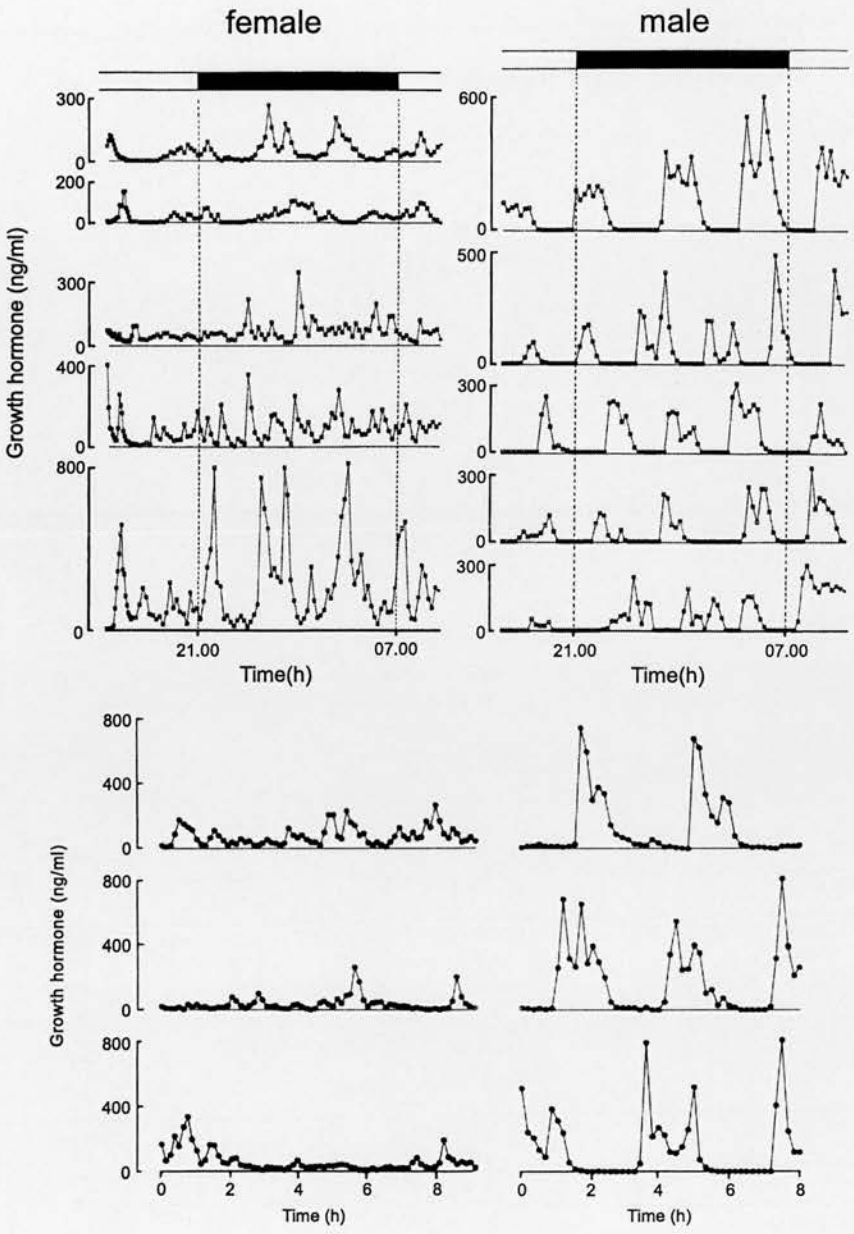

Figure 2.11 : GH release profiles in male and female rats. The top profiles are sampled at 10min intervals. The black bar indicates the period of darkness. The bottom profiles and sampled at 12min intervals. Male rats show a multi-peaked pulse of GH release approximately every 3h. The form of the pulse is irregular but usually shows 2 or 3 distinct peaks, with a tail at the end the pulse where GH is no longer being released, indicating exponential rate blood clearance (half life approx. 10min). Inter-pulse GH levels are very low or undetectable. The female rats show a much less regular pattern of GH release, with no distinct pulses. The profile, however, does show distinct peaks and periods of higher release. Minimum GH levels are higher than the male. The overall effect is a more continuous release of GH compared to the male. *Modified from (Clark et al 1987) and (Clark and Robinson 1988).*

2.6.2 Likely Patterns of Hypothalamic Release

Under the modulation of somatostatin's inhibitory effect, GHRH governs the amplitude of GH pulses, and individual pulses of GH correspond to single pulses of GHRH. Somatostatin is released in long periods of sustained release which disappear during the GH pulses. The periods of somatostatin release also seem to start and stop fairly quickly; experimenting *in-vivo* with an infusion of somatostatin in a sinusoidal pattern did not reproduce the normal pattern of release (Clark and Robinson 1987) and the endogenous somatostatin pattern is thought to be closer to a square wave form. GHRH seems to be released as shorter pulses corresponding to the pulses of GH. The limited evidence that exists, (Plotsky and Vale 1985), suggests that there is less GHRH release during the periods of somatostatin release, and vice versa. The more continuous pattern of GH release in the female is thought to reflect a fairly constant level of somatostatin, at a magnitude somewhere between the highest and lowest level in the male.

2.6.3 Testing Release Patterns with the Pituitary Model

The pituitary model provides a controlled system in which to test these ideas. The first set of experiments tests three possible patterns based on pulses of GHRH and longer bursts of somatostatin, which all generate a pattern of GH release which roughly resembles the male pattern. The first of these uses just pulses of GHRH with no somatostatin (figure 2.12a). This reproduces the basic pattern, but has relatively small pulses of GH compared to basal release, which itself is higher than the almost undetectable level observed in male rats between GH bursts. The second experiment (figure 2.12b) shows the same pattern of GHRH, with continuous somatostatin release between the GHRH pulses. This produces much larger GH pulses as somatostatin primes and resensitises the system between bursts of release, also suppressing basal GH release. In the third experiment (figure 2.12c) the pulses of GHRH are maintained with no quiet periods. This produces the basic pattern of GH

pulses but with small pulses of release between the large pulses, which themselves have smaller GH peaks, with the system not being left to resensitise. The patterns of input in the second experiment produce the most efficient pattern of release for growth and also the one that most closely resembles the real male pattern. This input pattern is taken as the basis for more refined testing.

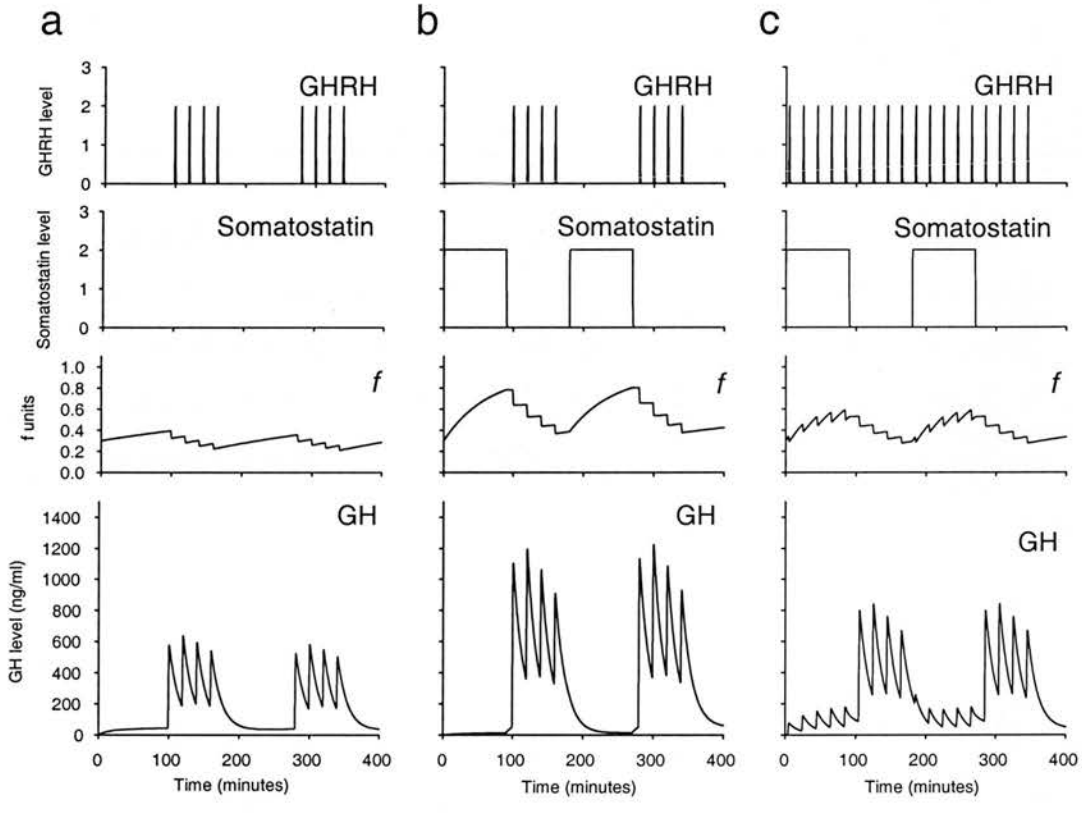

Figure 2.12 : **a**. 1min pulses of GHRH at 20min intervals in 2 bursts of 4 pulses, corresponding 4 peak bursts of GH, with small peaks; **b**. same pattern of GHRH with alternate 90min infusions of somatostatin, *f* is charged up to a higher level, corresponding 4 peak burst of GH with larger peaks, comparable to *in-vivo* release with model units scaled at 1 unit = 10μg/l; **c**. same pattern of somatostatin with continuous GHRH pulses, *f* charges but continues to be depleted by GHRH, 4 peak bursts of GH with some release between bursts.

Testing Varied GHRH Pulses

Some more refined testing can be done to compare the output of the pituitary model with the form of the GH pulse in experimental data, in particular looking at the number of individual peaks and their relative size. The information on the exact form is fairly rough however, due to the rarity of published endogenous release profiles and the limitation of the temporal resolution, determined by the frequency of GH blood sampling. The number of peaks within the GH pulse is also masked by the half life of GH in the bloodstream, which between different results, ranges from 10 to 15 min. GH blood profile data which has been processed through a deconvolution model to remove the effect of the decay rate (approximately reproducing the original release rate) (Hartman *et al* 1991) often shows more peaks than appear in the original data.

Examining GH profiles from male rats (figure 2.11) suggests that the GHRH pulses are frequent enough to trigger another pulse of GH before the previous one has died away. Estimating the duration of the GHRH pulses is difficult because the length of the GH pulse is dominated by its decay rate. Experimentation with the model suggests that a longer GHRH pulse has more effect on the height than on the width of the GH pulse. The number of peaks in real data is usually at least two, but can be three or four, and these may represent a larger number of individual GHRH pulses. Repeating the experiment in figure 2.12b with a longer GH decay rate of 15 min shows less of a fall between the GH pulses but the individual peaks are still more distinct than in real data. However, the model can also be used to simulate the effect of sampling by limiting its temporal resolution, and the same data at a 12 min sampling rate is displayed in figure 2.13a. The GH bursts shows fewer, less distinct peaks and the apparent relative height of the peaks, between the two bursts, is also different, being purely down to the luck of exactly when the sample is taken. In an interesting paradoxical result, increasing the number of GHRH pulses actually reduces the apparent number of GH peaks as demonstrated in figure 2.12b. Adjusting the exact timing of the sample points also has a significant effect on the sampled GH profile (figure 2.13b). These limitations of the sampled data in comparison with the

model suggest that, in the real release profile, there must be reasonable gap (at least as long as the sample period) between the real GH peaks within the pulse, since individual peaks do often appear in the sampled release data. In the model, very frequent GH peaks tend to appear as just a single large peak in the sampled profile (figure 2.13b).

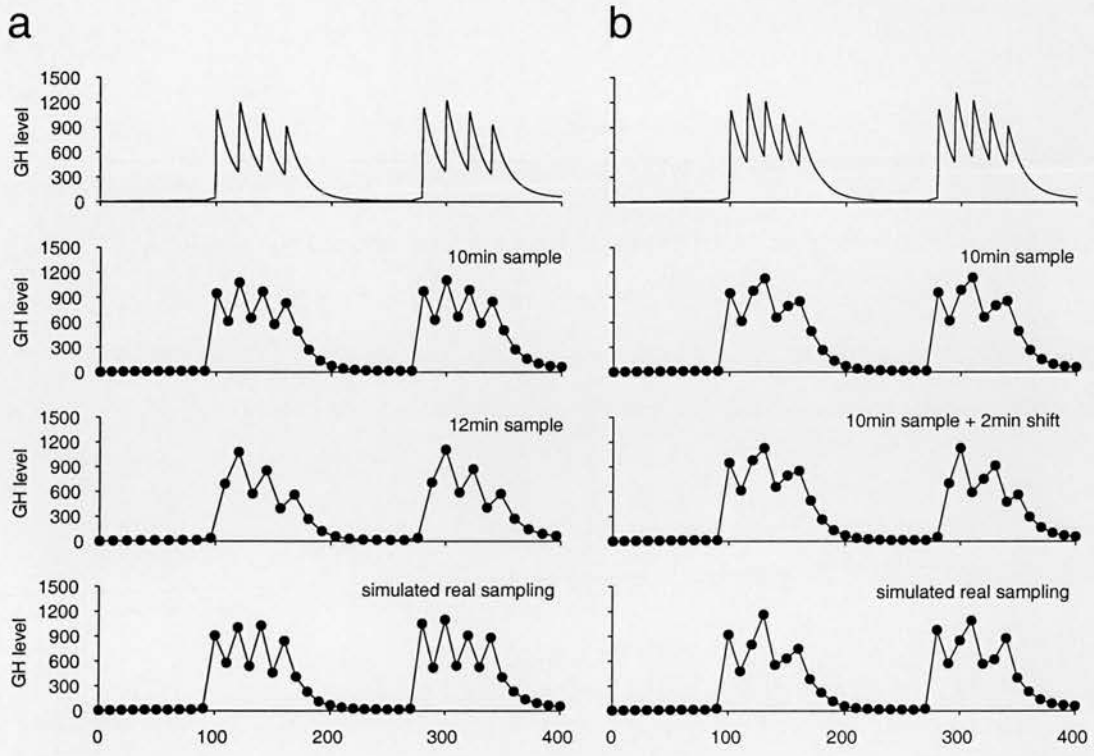

Figure 2.13 : **a**. as figure 2.12b, with 10min, 12min and simulated real sampling (10-min sample with 10% assay error, 30s sample period and random start point), 12min sampling shows loss of peaks in GH burst; **b**. similar to figure 2.12b with 2 bursts of 5 GHRH pulses at 15-min intervals, 10-min sampling shows only 3 peaks, shifting sample timing for second burst by 2 min changes the heights of the peaks, simulated real sampling shows less regular forms for the peaks and varied heights

If the true pulse rate is faster than the sample rate then the sampling won't be able to pick up individual peaks and troughs, merging the peaks together. However, this also depends on the regularity of the pulses, with the effect being more random with less regular spacing, as is likely to exist in the real system, and this was also tested

using the pituitary model by adding the ability to randomly generate the spacing of GHRH input pulses, following a Poisson distribution and controlled by a minimum refractory period. The first test of random GHRH pulses (figure 2.14) performs an equivalent experiment to figure 2.12b. The pattern of GH release is similar to the equivalent test with regular GHRH pulses, but with correspondingly less regular peaks of GH release within the burst, more comparable to the irregular pattern observed in real data (figure 2.11). In figure 2.14 the model was also used to test the effect of random pulse timing on the sampled GH profile. The two bursts of GH pulses are similar but in the sampled data the height and number of pulses varies due to the random pulse timing interacting with the sampling of the data.

Simulating Real Sampled GH Profiles

Comparing the model's normal display of GH output with the sampled version illustrated the dramatic effect that sampling has on the GH release profile. Since this sampled nature is common to all data on real GH release, this becomes a very important factor in interpreting real experiments. Several other factors, as well the actual sample rate, effect the final measured GH profile. The actual assaying of each sample has a fairly high error rate, relative to the GH level in the sample, so that each point has a 10% uncertainty. Samples are also not based on just one discrete time point but are collected over periods of around 30s. The goal here is to extend the model's simulation of sampling to include these additional factors by implementing a more sophisticated version of sampling.

The first stage of this was to implement the 30s sample periods. The model runs at a temporal resolution of 8 points per minute, 7.5s. per point, so a 30s period would use 4 of these points. The method is for each sampled measure to take the average of four model time points. This is then adjusted by a uniform random component of up to 10% of the sample measure, to simulate the error in the assay. Finally, the start point for sampling is randomised, so that this is independent of the GHRH input intervals in the model.

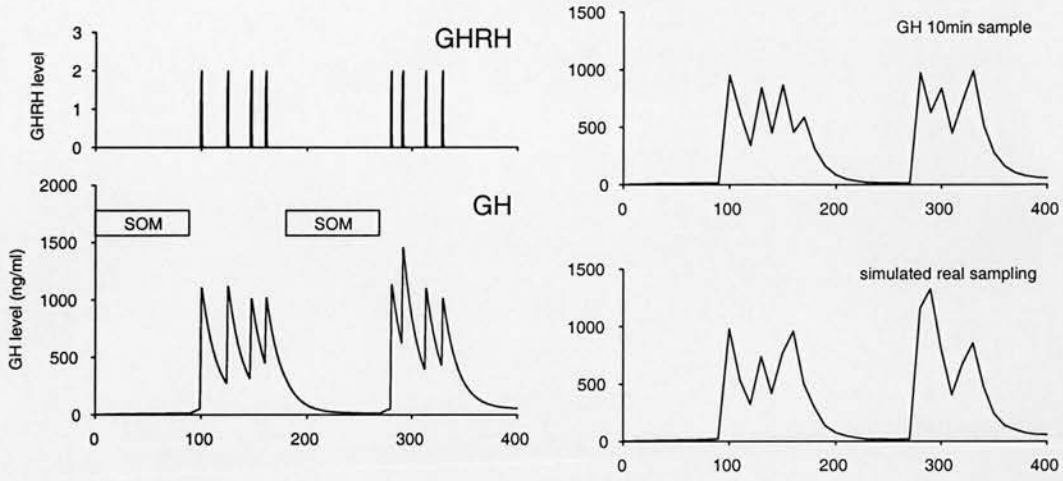

Figure 2.14 : Randomly timed GHRH pulses, with alternating somatostatin infusions, similar to figure 2.12b. GHRH pulses with 10-min mean interval + 10-min refractory period. Graphs on the right show the same GH release data, 10-min samples, simulated real sampling (10-min sample with 10% assay error, 30s sample period and random start point)

Testing these additions to the generation of sampled data shows that none of them has as dramatic an effect as the original addition of basic sampling, but they do work to reduce the regularity in the form of the model's artificial data. In order to test the individual effects each of the new processes was first tested alone, in addition to basic sampling at 5-min intervals. The 30s sample periods had very little effect on the form of the profile, but they did slightly increase the height of the GH peaks, by increasing the influence of the real peaks on the sampled measurements. Adding the 10% errors also had no effect on the general form, but did change the height and form of the individual peaks, making some appear wider or thinner than others, with less regular slopes coming off the peaks. Making the start point for sampling random had a larger effect on the heights of the peaks, although not enough to change their height order. It also sometimes affected the form of the peaks when by chance two sample points were fitted between the highest points. Increasing the sampling interval to 10min reduced the effect of the sampling periods and the randomised sampling time, and also reduced the effect of the 10% error on the shape of the

peaks. This is as expected, since the magnitude of the change in the profile due to the sampling intervals will dominate, having a much larger averaging effect than the 30s sample periods. The sample periods only have a more significant effect on the shape of the pulses when they are made as long as the sample intervals. Figure 2.13 shows the same data used for the previous sampling results, processed with all the new sampling features. The general form of each burst is still similar because they are each generated by regularly spaced GHRH pulses and the sampling is still evenly spaced, even with the random starting point. Figure 2.14 shows the new sampling applied to data produced with randomly timed GHRH pulses. Here, the new sampling features have a more significant effect on the sampled GH profile, changing the number of distinct peaks, and their height order.

Varied Somatostatin Input Patterns

Within the assumptions of the pituitary model, the only alternative to the pulsatile form of the GH burst being controlled by GHRH is a more complex pattern of somatostatin release during the period of high GH release activity. Somatostatin would still need to remain high during the periods of low release in order to create the periods of very low or undetectable release observed in the male rat, but it could conceivably follow a more complex pattern during the GH burst, something closer to the previous pulsatile pattern of GHRH. To test this the model was run with a pulsed pattern of somatostatin alternating with a constant infusion, along with varied patterns of GHRH input. In the first test GHRH is input as a constant infusion during the pulsed phase of somatostatin, illustrated in figure 2.15a. This produces a huge release of GH (note the scale in the figure), much larger than previous experiments with the model, due mainly to the priming by the infusion of somatostatin and the very long exposure to GHRH. Although the GH level isn't scaled to directly compare with real data, *in-vivo* experiments do show a release response to pulse type injections which is on a similar scale to endogenous release, and this very large level observed here in the model is likely to be beyond the range observed in the real

system. Its form with a very large initial pulse followed by much smaller ones also varies from real data where following GH pulses within the burst are often of a similar size to the first one. Therefore although this reproduces the gross level behaviour of GH bursts it is unlikely to be representative of the real system. The sharp peaks of GH release observed in real data cannot be reproduced in the model without using pulsed GHRH input.

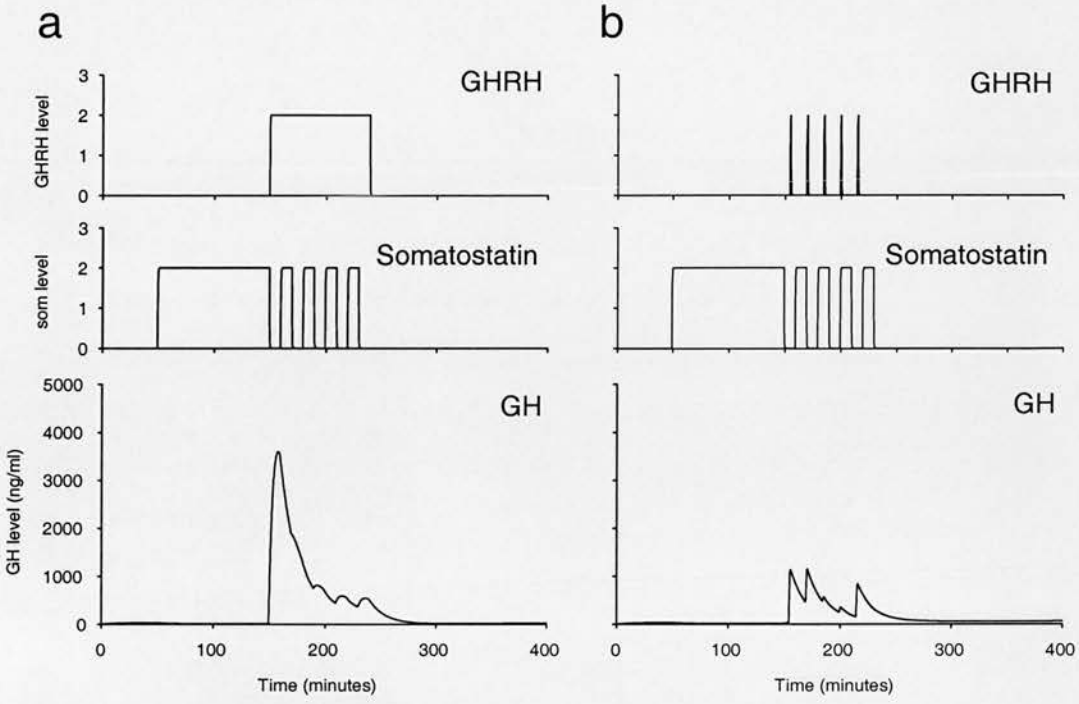

Figure 2.15 : **a**. GHRH infused during a pulsed phase of somatostatin (10min duration, 10-min interval), this produces a very large release of GH, over 4000ng/ml, much larger than GH peaks observed *in-vivo*; **b**. pulses of GHRH (1min duration, 15-min interval) during a similar phase of pulsed somatostatin, this produces a burst of GH release with a much closer resemblance to *in-vivo* data, showing irregular GH pulses which depend on GHRH timing relative to the somatostatin pulses

In the second test GHRH is input as pulses similar to those used in previous experiments. This produces a GH burst, but its form depends heavily on the frequency and timing of the GHRH pulses. If the GHRH pulses are synchronised with the periods of low somatostatin release then they produce regular large pulses of GH but if they correspond with the high periods of somatostatin then the burst

consists of very small GH pulses. Changing the timing of the GHRH pattern so that the pulses do not synchronise with somatostatin (figure 2.15b) produces more interesting, less regular bursts of GH with some GHRH pulses producing GH pulses and some being blocked. The pattern of GH release does appear similar to real data.

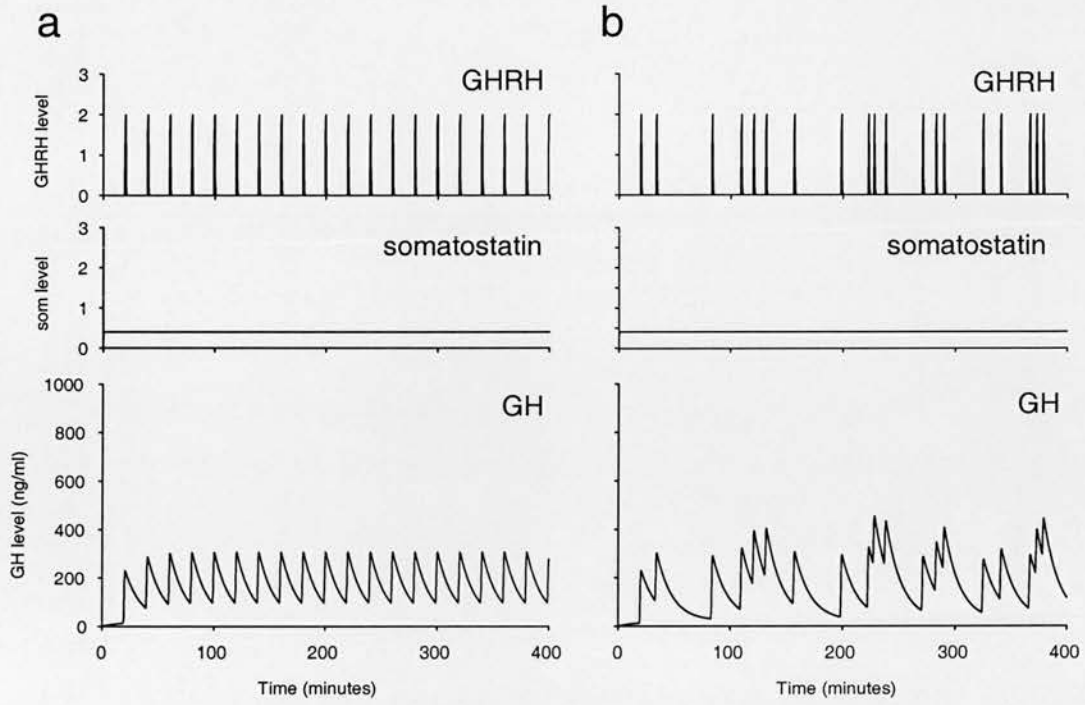

Figure 2.16 : Simulating GH release in the female rat; **a**. pulses of GHRH at regular 20 min intervals during a constant low level infusion of somatostatin ($I_s = 2$); **b**. similar constant low level somatostatin release with randomly timed GHRH pulses, produces a pattern of GH release which resembles release in the female rat, closer pulses of GHRH produce larger GH peaks

Producing the Female Release Pattern

Release in the female rat consists of smaller, less regular pulses of GH forming a more continuous level of GH release with no distinctive periods of completely blocked GH release, as in the male. This is thought to correspond to a more continuous pattern of somatostatin release, at a lower dose than the high points of somatostatin release in the male. To test this in the model, the somatostatin release

rate was reduced to $s_r = 2$ (compared to 10 for the male) and given as a continuous infusion along with pulses of GHRH. Regular pulses of GHRH (figure 2.16a) produce a corresponding pattern of small GH pulses, partially inhibited by the low level release of somatostatin. The difference in pulse height compared with the male is similar to the real data but the pulses are much too regular. Figure 2.16b shows the same test using randomly timed GHRH pulses. This shows a much closer resemblance to the real data, with varied intervals and heights of the GH pulses.

2.7 Conclusions for the Hypothalamic System

Experiments with the pituitary model support the evidence from behavioural experiments suggesting that the pattern of GH bursts is likely to be controlled by an alternating level of somatostatin, with the peaks of GH release triggered by individual pulses of GHRH. Exposing the pituitary model to such a pattern of input produces a GH release profile which closely resembles real data. One of the most important points demonstrated here is that the pattern of release requires GHRH to be suppressed at the pituitary and in the hypothalamus. Using this fitted model, and also from *in-vitro* results, the inhibition by somatostatin at the pituitary is not strong enough to completely block GH release when pulses of GHRH are still being released from the hypothalamus. GHRH release itself must be blocked, and release inhibition at the pituitary is also essential in order to block basal release between the GH bursts. The very low levels between bursts are essential to GH signalling.

The simplest control mechanism for the central blocking of GHRH would be somatostatin itself since it already needs to follow such a pattern, or alternatively some common mechanism which controls the GHRH and somatostatin release patterns. The requirement to synchronise the two, and the unnecessary added complexity makes independent control mechanisms unlikely. Therefore the hypothalamic network probably does involve interaction between the GHRH and somatostatin neurons.

The main alternative presented here to the pattern of alternating infusions of somatostatin and the bursts of GHRH pulses is the more complex pattern of somatostatin controlling the form of the GH burst. This was able to produce a pattern of GH release which looks similar to real data. The main argument against this is that it is a more complex solution requiring more sophisticated central interaction between somatostatin and GHRH. Whether extra complexity is required will depend on how easily and robustly the simpler pattern of release can be generated.

Using randomly timed GHRH pulses has no major effect on the overall pattern of GH bursts but it does produce a GH profile that resembles the less regular patterns of release observed in real data. If the system required a regular pattern of GHRH then this would be more difficult to produce and the system would be less robust. One of the main questions for developing a hypothalamic network will be the source and nature of the mechanism which controls the production of GHRH pulses.

Chapter 3

The Hypothalamic Model

3.1 Introduction

This chapter describes the development of the hypothalamic model. The first stage of this was the specification, defining the output which the new components need to produce, and gathering existing knowledge about the system on which to base the new components The second stage of development was to use the specification, the defined output and what we already know about the system, essentially the pieces which are available to build it from, to come up with a basic design for the system. This basic design was then translated into a mathematical form and taken into the third stage, which consisted of a cycle of implementing, testing and experimenting with the model's design, with the goal of matching the structure and behaviour of the real system. Analysis of the model system's components and its behaviour as a whole can then be used to make predictions for the real system and suggest further experimental work with results predicted by the model.

3.2 The Specification

The outputs of the hypothalamic system are the patterns of GHRH and somatostatin release, and these form the inputs to the pituitary model that goes on to generate GH release. The likely form of these outputs has been developed by examining the results of *in-vivo* behavioural experiments with the real system, and by using the pituitary model to experiment with different patterns of GHRH and somatostatin. Based on the tests which validated its qualitative and quantitative properties, the assumption is to be made that the model is an accurate representation of the pituitary system, and its structure and parameters can be treated as fixed. While this may not be ideal, it is necessary to have the system as well defined and specified, essentially restricted, as possible in order to make the design and testing a tractable process.

The second part is the existing structures and what we know about their behaviour and interaction, similar to the functional components presented for the pituitary

system. Gathering this information was the main goal of the research review in chapter 1 and the information will be summarised here in a form ready for developing the model.

3.2.1 The Model's Output

The model's first desired output is the endogenous pattern of release in the male rat, but it should also be easily adapted to produce the less regular and more continuous pattern of release in the female rat, which is thought to be a similar system, modified by different exposure to sex hormones, particularly oestrogen. Initially, the target outputs for the new hypothalamic components will be the patterns of GHRH and somatostatin release defined during experiments with the pituitary model, short pulses of GHRH and square wave periods of sustained somatostatin release.

The aim is to create a self-contained system which is capable of generating the desired output without any external input which isn't already suggested or defined by existing knowledge about the real system. Defining an external input which contains part of the output pattern effectively just shifts part of the problem away from our system, and fails to provide a complete solution to how the system functions. It may turn out to be the case that some external input is required, but exhaustively attempting to make the system work without any such input will provide better evidence for its existence.

3.2.2 Existing Components

These are the well defined functional and structural components derived from what we already know about the system with a decent degree of certainty :

i) GHRH is released by a group of neurons in the arcuate nucleus

Evidence from *in-vitro* and *in-vivo* experiments indicate that pulses of GH correspond to pulses of GHRH, and so the form of GH release suggests GHRH is released in sharp pulses, lasting a few minutes. Relatively short, sharp pulses must require synchronisation between the GHRH neurons.

ii) Somatostatin is released by a group of neurons in the periventricular nucleus

The true pattern of somatostatin release is also unknown, but periods of high somatostatin release probably match periods of low GH release in the male rat.

iii) Somatostatin has an inhibitory effect on the GHRH neurons

More recent work has focused on the negative effect of somatostatin on GHRH mRNA expression, but the best evidence for this connection is the electophysiological studies. The electrical connection suggests a very direct and fast acting inhibitory effect on GHRH neuronal activity and release.

iv) GH inhibits its own release

Administering GH *in-vivo* has a dramatic inhibitory effect on its own release and on an unusual timescale. The effect takes in the range of an hour to develop, and it takes one to two hours for normal release to recover after the infusion. The properties of the inhibitory effect also vary between male and female rats. In both, an infusion of GH suppresses its own release, but the female rat, unlike the male, continues to respond to injections of GHRH. The male would normally show a more varied response to GHRH injections because of its periods of high somatostatin release, but after administering exogenous GH the period of unresponsiveness is longer than usual. This appears to suggest inhibition of GHRH in the male and female and also prolonged somatostatin release in the male, but interpretation is complicated by the

interactions between GHRH and somatostatin, making it difficult to distinguish direct and indirect effects.

v) GH stimulates the somatostatin neurons

The only evidence for the dynamics of this is what we can extract from the effect of GH on its own release. It appears to be able to trigger a prolonged release of somatostatin, lasting longer than the original pulse of GH. The effect also appears to be delayed and it is thought to take up to an hour between the original GH release and the corresponding increase in somatostatin levels (Chihara *et al* 1981). This suggests an effect on the releasable pool of somatostatin, rather than direct electrical stimulation.

vi) Other connections

There is some evidence for a connection from the GHRH neurons to somatostatin neurons, possibly via some other transmitter. Acetylcholine has been co-localised with GHRH and has an inhibitory effect on somatostatin *in-vitro*, providing a possible inhibitory link. Similar evidence exists with galanin, but similarly circumstantial evidence also suggests an excitatory link mediated by dopamine.

Much of the behavioural evidence also suggests GH acting at the GHRH neurons to inhibit release, particularly in the female rat and probably also in the male. In particular, the large GHRH-dependent rebound observed following somatostatin withdrawal is blocked by GH infusion in the male and female.

The main outside input for which evidence exists is an adrenergic input to the GHRH neurons which appears to be necessary for GHRH release, perhaps providing the electrical activity to stimulate release from the GHRH neurons.

3.3 The Basic Design

For the first stage, the components of the system specified above were laid out together to form a picture of the system (figure 3.1). The main structural components are the GHRH neurons, the somatostatin neurons and the pituitary GH release system. This first design includes the links for which good evidence exists, the inhibitory link from somatostatin to GHRH and the GH feedback link to the somatostatin neurons.

3.3.1 System Function

The next stage was to consider how this system might produce the target output pattern, beginning with the GH release profile in the male rat. Individual pulses of GHRH trigger the individual peaks of GH release. This means that there needs to be something to generate the individual pulses of GHRH, either some periodic inhibitory input or a pulsatile excitatory input. One candidate for this is the adrenergic input. The apparent form of the GHRH pulses, based on the corresponding GH release, suggests that this input should be a series of short pulses.

An alternative mechanism for triggering pulses of GHRH is the somatostatin withdrawal rebound. When somatostatin is infused *in-vivo*, blocking GH release, and then suddenly withdrawn, there is a large rebound release of GH which is triggered at least partly by GHRH release. The mechanism of this rebound is still not understood. One idea is that exogenous somatostatin may inhibit endogenous somatostatin, leaving GHRH unopposed upon its withdrawal (Clark et al 1988), but another idea is that the rapid fall of somatostatin induces GHRH release, suggesting a mechanism which could play a role in normal function. The large rebound release may not play a role in the endogenous system but in the attempt to reduce the use of outside inputs this does provide a possible mechanism for triggering GHRH.

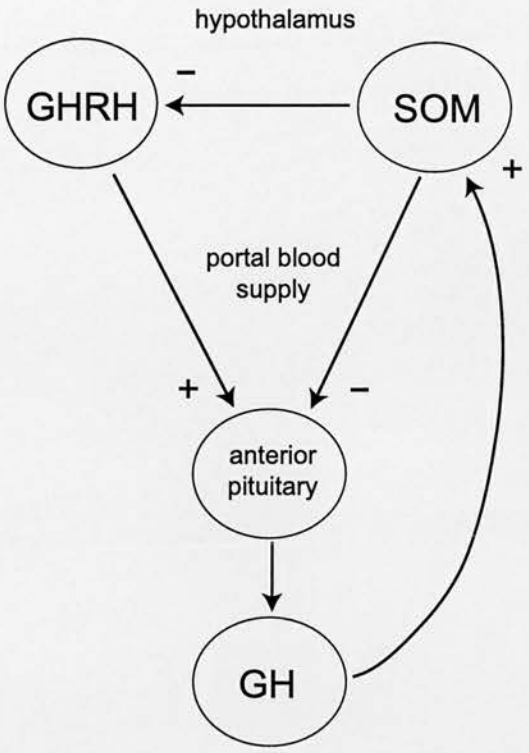

Figure 3.1 : Basic knowledge about the GH release system. This shows all the components and connections for which good evidence already exists and forms a starting point for designing the model.

The overall output repeats in a cycle, and so in the absence of any outside generator producing this pattern, the system needs to have its own cycle. Assuming that somatostatin controls the overall pattern of release, there needs to be a feedback input to somatostatin. The obvious choice for this is GH itself. GHRH release triggers GH release which would then stimulate somatostatin release, which in turn would inhibit GHRH release from the hypothalamus and GH release at the pituitary, switching off the feedback signal. Eventually the somatostatin stimulated by GH would decline and GHRH would once again trigger GH release and repeat the cycle.

3.3.2 Simplifications

This is a model of the system at a functional rather than mechanical level, and major simplifications will be made in representing the system's components. In the pituitary model GHRH and somatostatin are each represented by a single variable which measures the level of the peptide in the system. We are thus assuming that each group of neurons can be treated as single unit. This works for several reasons, the main one being the timescale of the model. The model works on a scale of minutes, whereas neurons work on milliseconds and so activity is averaged out. We know that the neurons do synchronise because this is necessary in any system to produce pulsatile output. The other major reason is the way in which electrical activity is transduced into hormone release. Although individual action potentials trigger individual releases of peptide, the release from individual neurons all diffuses into a common transport channel to the pituitary, and so the GH releasing cells experience overall GHRH or somatostatin activity rather than the actions of single cells.

3.4 Building the Model

Turning the basic design into a working model formed into two generations of model development. The first generation formed a process of learning how best to formalise the types of connections in the system, exploring the properties of the mathematical constructions and refining them to get the system functioning correctly. The second generation, which formed the final basic version of the model, rebuilt the model, using more biologically representative components, such as the Hill equations, to create a more refined model which better matches the quantitative details of the real system.

3.4.1 Mathematical Representation

The state of the system is stored as a set of variables that represent measures such as hormone blood level or number of free receptors, each related to some component of the system. The functions of each component may be broken down into more variables but this will only be done with the aim of reproducing the component's behaviour, rather than just its mechanism. The basic GH model (figure 3.1), has four variables, representing the blood concentrations of GHRH, GH and somatostatin, and the number of free GHRH receptors at the pituitary, variable f from the pituitary model. To maintain the model's simplicity, the same variables for GHRH and somatostatin are used to represent the hypothalamic components and their actions at the pituitary. This makes the assumption that the level of activity in the hypothalamus can be matched directly to the level of peptide released into the portal blood.

Each variable has a corresponding differential equation, and these equations contain parameters which relate to some measure such as a threshold or synaptic strength, or may belong to a more abstract mathematical construction. The model also contains other equations, such as $\Phi(s)$ in the pituitary model, which calculate values such as level of receptor (and associated downstream component) activation.

Hill Equations

A standard form for modelling the effect of one substance on some component of a system is the Hill equation. In the later version of the model, these equations model the actions of peptides on neurons. In general, these equations model the effects of ligand-receptor binding and allow a variable threshold for activation and variable steepness using the Hill coefficient, which measures the degree of cooperativity of the binding. If binding is cooperative, then the binding rate is affected by the current level of bound complex, so if the effect is positive, the binding rate will increase as the level of bound complex increases. If the effect is negative then the binding rate is

reduced. This controls the gradient with which the level of binding increases. These equations give a biologically realistic, but simple, way of getting a measure of activation where there is a substance binding to receptors. The equations produce a value ranging from 0 to 1, with a higher value indicating a higher level of binding, or activation. The general form is given below :

$$activation = \frac{l^n}{l^n + th^n}$$

where l is the level of ligand present, th is the threshold, and n is the Hill coefficient.

Storage Variables

For this model a type of variable has been developed which represents a measure of the ability to release a substance, or 'releasability'. This is deliberately vague because it is intended to represent functional properties rather than a particular mechanism. The real biological substrate could be something like vesicle mobilisation or the number of activatable receptors. The idea is that they allow a substance to charge up the ability to release something without directly triggering its release. They form a 'memory' that allows a substance to trigger an effect which takes place over a longer timescale or at a different time point to when the original trigger substance was experienced. This was originally developed to model rebound effects. The storage variable could be charged up during inhibition while its release was blocked, and then allowed to drain quickly after inhibition to produce a large rebound spike. It has also been used to model the effect of GH on somatostatin, by getting GH to charge up a somatostatin release variable so that the relatively short period of GH pulses can trigger a much longer period of somatostatin release.

Input Protocols

Even fairly complete models of self-contained systems usually need some sort of external input to control them, or at least to provide some driving activity. When the system of equations is run in software, the variables are progressively calculated at discrete time points. Inputs are usually given to the system by perturbing the variables, changing them to a specified value at a specific time point, or they can just be added to existing activity. A whole series of inputs can be defined in order to form a pattern, such as a series of spikes, and this whole pattern of inputs is known as the protocol. Each variable can have its own protocol, but usually only a few of them will be controlled in this way.

3.5 Comparing Model Output to Real Data

In the early stages of developing the model, assessing the model's output will be based more on the qualitative rather than quantitative features of the real data, focussing on reproducing the system's behaviour, and basic features of the release pattern. As development progresses (particularly the second generation version of the model and chapter 4) this will shift towards more exactly matching the quantitative features of the real data. The direct output comparison combines with the goal of designing the model in a manner which fits what we know about the biological systems, it's biological plausibility. The criteria for comparing model output are given below :

- GH pulse cycle duration – approx 180min in male rats
- GH pulse duration – the duration of high GH release in each pulse
- GH pulse height – peak GH release levels within each pulse
- number of GH peaks with each pulse
- inter-pulse GH levels – very low in the male rat
- width of individual GH peaks

The reference data for the normal pattern of real release is shown in figure 2.11. This illustrates GH release in male and female rats at 10min and 12min interval sample rates. There is a large variation in the form of individual GH pulses, and between animals, though most pulses follow the 180min cycle. GH pulse duration is approximately 90min, with a similar period of inter-pulse low GH release. Peak height in this data corresponds to 800ng/ml although other data (not shown) sometimes shows peaks as high as 1200ng/ml. The sampling process tends to underestimate peak GH levels. Inter-pulse GH levels are very low, often zero, although with occasional very small GH peaks. Each GH pulse usually consists of 2 or 3 distinct peaks. The first is often the largest, although not always. Looking at the top male profile in the figure, sometimes there is a large drop between peaks making them very distinct (the third GH pulse) and sometimes the drop is smaller (the first GH pulse) giving a more flat top to the GH pulse. Measuring the width (or duration) of GH peaks is limited by the sample rate, but the one or two sample points within each peak indicate that they are approximately 15 to 20min long.

To make a direct comparison with the real data, the model's GH output is subjected to a similar sampling process. Figure 3.5b shows the first example of model data which resembles the real data. The pulse cycle length matches real data. There are a similar number of GH peaks within each pulse, and the peak height and width is similar to real data. The main variation, which is more difficult to formally quantify, is the more regular form of the model data, with little variation between the shape of each GH pulse, compared to real data. The period of low inter-pulse GH is also slightly shorter in this model data, with GH pulses lasting approximately 100min.

Figure 3.7 shows two sets of model data compared for their match to real GH release data. The second set of data (figure 3.7b) is stated as being a better match because it shows higher GH peaks and also 3 rather than 2 peaks within each GH pulse. It does however have the trade-off of having a shorter inter-pulse low GH period, compared to the better match in figure 3.7a. Such a comparison becomes subjective, depending on which particular set of real data is used for reference, due to the variation within real data.

Figure 4.2 introduces random input pulse timing to better match the variation observed in real data. The gives a better match to real data just by better covering the range of different forms observed in real GH pulses. Figure 4.2c in particular shows a good match to the GH pulses with a small drop between individual peaks.

In the final stages of model refinement the judgement becomes more difficult with more subtle difference between sets of model output. Here various possibilities are presented rather than being definitely compared, such as figure 4.7. The difference here is mainly in the number of peaks within each GH pulse. However, Figure 4.7a shows more distinct peaks than would normally be observed in real data, making 4.7b the better match to real data.

3.6 The First Generation

The pituitary model used four variables each with a corresponding differential equation, three representing the concentrations of GHRH (r), somatostatin (s) and another giving a measure of free pituitary GHRH receptors (f). The hypothalamic model was built onto the pituitary model by adding to and modifying the existing equations.

3.6.1 The Model Equations

The first part of the system to be considered was GHRH. At this stage, the system was considered at a very simple level, not looking at the detail of the GH pulses and their multiple peaks, and the mechanism which seemed capable of triggering the GH pulse was the somatostatin withdrawal rebound. To produce a rebound, a new variable, g, was added to represent the ability of the GHRH neurons to immediately release GHRH, or 'releasability'. This component would charge up to a maximal level, at a rate inversely proportional to the current store, and be depleted as GHRH was released. Inhibition of GHRH release by somatostatin would allow it charge up

to a high level so that sudden removal of the inhibition would produce a large pulse of GHRH release, assuming that there would be some existing level of basic activity which would trigger release with inhibition removed (figure 3.2). The function of g is described by the following equation :

$$\frac{dg}{dt} = l_1(1-g) - l_2 r_{act} g \qquad \text{[e1]}$$

GHRH releasability, or charge, increases at a rate controlled by parameter l_1, relative to the existing charge g, to produce saturation at a maximum value of 1. The value falls at a rate proportional to g controlled GHRH, at a rate by parameter l_2.

The second part of the system to be designed was the somatostatin-GHRH inhibition. A measure of the inhibition (r_{act}) was added to be used with the GHRH equation. This is shown below :

$$r_{act} = \frac{1}{1+\exp[sig_1 \log_{10}(s) - sig_2]}$$

This gives a standard negative sigmoid curve with gradient and threshold controlled by sig_1 and sig_2 respectively. Depending on the gradient, controlled by sig_1, this allows a fairly sudden block of GHRH when somatostatin reaches a high enough level. It also means that there will be little GHRH release until somatostatin falls back below the threshold. The modified GHRH equation, integrating the two new components, takes the form :

$$\frac{dr}{dt} = r_{act}(I_r + l_3 g) - k_6 r$$

This changes the original equation by allowing r_{act} to block the input component and adding an input from g, controlled by the rate parameter l_3. This allows an input based on the charge, g, to increase GHRH release independently of the artificial

input, I_r. Modifying the whole input by r_{act} allows a total block of release, rather than just blocking individual inputs.

Finally, this is the modified somatostatin equation integrating simple GH feedback:

$$\frac{ds}{dt} = I_s - k_7 s + j_2 \Phi(h)$$

The new component $\Phi(h)$ is a measure of activation due to GH, similar to Φ(s) in the pituitary model. It is given by the following equation :

$$\Phi(h) = \frac{1}{1+\exp[-(\log_{10}(h) - h_0)/\delta_h]}$$

This equation is best explained by referring to the illustration for $\Phi(s)$ (figure 2.1). The level of activation varies between 0 and 1. After h reaches a certain value, controlled by h_0, the activation value will increase quickly and then level off at a plateau. The gradient of the change is controlled by δ_h, with a smaller value giving a steeper change. Parameter j_2 scales the activation value from $\Phi(h)$ to give a release level. Figure 3.2 illustrates the complete system.

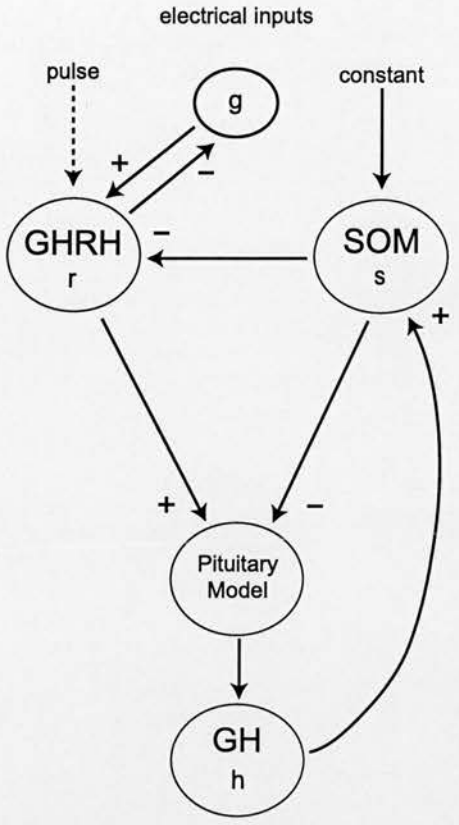

Figure 3.2 : The first generation model. GHRH pulses are triggered by charging a releasable pool (g) which allows a large rebound release of GHRH when somatostatin inhibition is removed. The pool continually charges and is depleted as GHRH is released. Somatostatin release is driven by an excitatory feedback from GH. For this to work, a delay had to be added so that the GH pulse wouldn't immediately inhibit itself. Pulse input was added to GHRH in order to produce multiple peaks with each GH burst, removing the need for the rebound mechanism.

3.6.2 Testing the Model

This version of the model was built by developing the somatostatin-GHRH interaction and rebound, then adding GH feedback. The model program allows artificial input protocols to control GHRH and somatostatin levels in a way that simulates *in-vivo* experiments. This allowed the individual components of the model to be tested in isolation rather than having to work together immediately. The model uses the final version of the pituitary model The only modifications are the

hypothalamic components added to the GHRH and somatostatin equations, and their associated components.

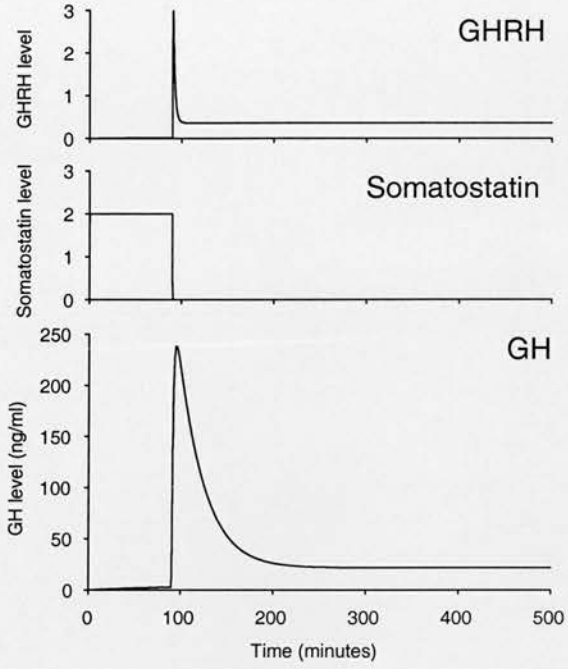

Figure 3.3 : Using somatostatin withdrawal rebound to generate a GHRH pulse. 90min somatostatin infusion allows g to charge while inhibiting GHRH release. Upon withdrawal, GHRH is released, with g rapidly discharging to leave basal level of GHRH release at low level equilibrium (sig_1=20, sig_2=0.1, l_1=0.05, l_2=0.5, l_3=20). The discharge of g at a rate proportional to the remaining pool leaves a tail on the GHRH pulse, prolonging the GH pulse. Peaks in real GH profiles (fig 2.11) tend to be shorter, indicating sharper GHRH pulses.

To test the GHRH rebound and somatostatin-GHRH inhibition mechanism, the model was run with an input pattern of somatostatin defined as two 90min infusions, separated by 90-min. The process began by setting the parameters to values which produced roughly male rat levels of GH release and then went on to vary these values to test their effect on release with the other parameters already set.

The first parameters set were the threshold and gradient for r_{act}, somatostatin's inhibitory control over GHRH. For the rebound to work, somatostatin at its level between GH pulses must almost entirely block GHRH release, and so the threshold

and gradient were set so that r_{act} was close to 0 during the somatostatin infusions. Values sig_1 = 10 and sig_2 = 0.1 were used to give an r_{act} value of 0.06 with high somatostatin. The charge component of GHRH release was switched on and the parameters set so that the 90min somatostatin infusion would be sufficient to charge g to its maximum level, and the rebound pulse produced a large GH pulse (approx 5ng/ml). Initial values were l_1 = 0.05, l_2 = 0.5 and l_3 = 20. The first problem was that the somatostatin-triggered inhibition was insufficient to totally block GHRH release, leading to levels of GH release during the somatostatin infusion higher than those observed in the male rat. To counter this, sig_1 was increased to 20, and this produced a sufficient inhibition of GHRH. The resulting rebound produced a sudden increase in GHRH release which quickly decayed as the releasable store was depleted (figure 3.3).

Increasing l_2, the rate at which GHRH uses up the releasable store, reduced the size of the GHRH release pulse, making it sharper and reducing its height with a corresponding effect on GH release, but did not significantly effect the overall form of the GH profile. In addition to the sharp rebound pulse, the GHRH store mechanism also produced a level of basal GHRH release, due to the constant charging. The level of this was controlled by the balance between l_1 and l_2, with a small value for l_1, relative to l_2, keeping it at a low level.

For further testing the parameters were set to the following values :

Parameter	Value
l_1	0.05
l_2	0.5
l_3	20
sig_1	20
sig_2	0.1

3.6.3 First Conclusions

The combination of somatostatin inhibition of GHRH, and rebound release, worked well but requires a very sharp effect of somatostatin on GHRH, so that the

block works more like a switch, rather than a gradual dose-dependent inhibition. The rebound produces a large, sharp pulse of GHRH which is able to trigger a large GH pulse. However, this system is unable to produce the multiple peaked GH bursts as seen in real experiments. The single peak pulse of GH is also not as sharp as the GH peaks in real data (figure 3.3). In a further test of the rebound mechanism, the artificial somatostatin input was replaced with more realistic, gradually decaying levels of somatostatin. The system was still able to function but the somatostatin-GHRH inhibition had to be made steeper still in order to get a pulse of GHRH release rather than a gradual leakage (not illustrated). A sharp pulse of GHRH is required to get a pulse of GH release, as opposed to a gradual increase and decay in the GH level.

3.6.4 Adding GH Feedback

The next stage was to add GH feedback and remove the artificial control of somatostatin. This was done very simply, by adding a GH component to the somatostatin equation, using an activation function similar to the one used in the pituitary model to represent the effect of somatostatin on GH release and receptor recycling. The activation function uses two parameters controlling its threshold and steepness, h_0 and δ_h. These were given initial values $h_0 = 8$ and $\delta_h = 0.5$, after testing the activation level against typical GH levels. These values give a very sharp change in activation, with a threshold at a GH level of 8 units. This low threshold makes the effect on somatostatin more dependent on the duration of GH release, rather than the level of release, so long as release is above the threshold level. Without the sharp gradient, there is too much somatostatin release during the GH burst caused by basal GH release, and making the threshold too high reduces the period between the GH bursts by making a shorter period of GH release trigger somatostatin.

To produce the first pulse of GH to trigger feedback, the model was tested with an input protocol giving one 90min infusion of somatostatin. With parameter j_2 (controlling GH feedback) still set to 0, this produced a single pulse of GHRH and

corresponding GH release, decaying back to basal level and then remaining there. Increasing j_2 just caused an immediate increase in somatostatin, leading to a smaller GH pulse and a higher level of constant GH release following, as the increased somatostatin level maintained a low level of GHRH release through the rebound mechanism. Higher values for j_2 obliterated the GH pulse leaving just a constant low level release of GH, which reduced in level after j_2 became large enough to cause a sufficient increase in somatostatin to make the inhibitory effect on GHRH more significant than the excitatory effect on the GHRH store.

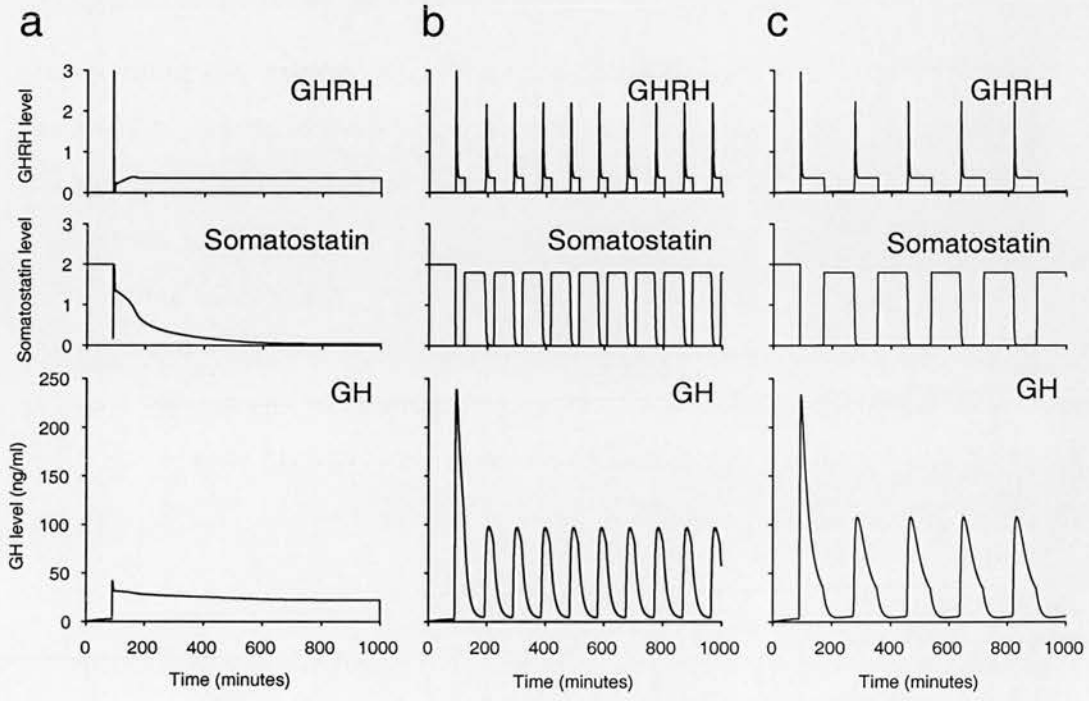

Figure 3.4 : **a**. GHRH rebound combined with GH-somatostatin feedback with no delay, somatostatin infusion followed by withdrawal triggers first GHRH pulse, immediate somatostatin release truncates GH pulse, somatostatin declines and system goes into equilibrium producing low level GH release; **b**. GH-somatostatin feedback with 30min delay, after delay GH triggers somatostatin release which recharges g and triggers another GHRH pulse, and cycles; **c**. as b. with 80min GH feedback delay to produce pulses of GH every 180min, comparable to pulse cycle in the male rat. A 2min delay is sufficient to produce small pulses (not shown) ($j_2 = 10$).

This first version didn't work because as soon as GH levels rose, somatostatin levels increased and blocked most of the GH pulse (figure 3.4a). The feedback was too fast, and so a delay was added by allowing the activation function to use a value for h from an earlier time point. This makes sense, because in the real system it is likely to take some time for GH, which is released peripherally, to feedback to the CNS. The delay was initially set at 30min. This immediately fixed the problem of feedback truncating the peak of the GH pulse. Parameter j_2 was increased until feedback produced a high enough level of somatostatin release to inhibit GHRH release and trigger a rebound pulse. Beginning with the form in figure 3.3, higher values gradually reduced the length of the single GH pulse as the delayed GH triggered somatostatin release inhibited the long GHRH maintained tail. Between j_2 = 8 and j_2 = 9 pulses of GH began to appear, as the somatostatin level became high enough to allow GHRH releasability to charge. Pulses continued in a regular pattern, following a cycle lasting 95 min (figure 3.4a). Increasing the delay to 80 min produced longer pulses of GH and a cycle lasting 180 min, comparable the GH profile in male rats (figure 3.4c).

For the first time, the model was able to produce regular pulses of GH without any outside input, just a single GHRH pulse (or somatostatin infusion) to start the cycle. After one or two pulses the model settled into a regular pattern of GH release, not dependent on the original triggering input. The only parameters which had a significant effect on GH pulse frequency were h_0 (the GH-somatostatin feedback threshold) and the delay value for h. A longer delay or lower threshold reduced GH pulse frequency. Pulse amplitude was affected by the r_{act} parameters, sig_1 and sig_2 and also δ_h. When somatostatin inhibition of GHRH is less steep (a smaller value for sig_1), the pulse amplitude is reduced until pulses are completely lost.

In male rats there is a high level of variation in GH pulse amplitude between animals, but they all show the same regular pattern of 3-hourly GH pulses. This suggests, that as with the model, the effect of GH on somatostatin is more dependent on the duration of release, rather than the absolute amount.

3.6.5 Adding an Input to GHRH

The final change to this version of the model was to alter the GHRH equation so that GHRH release requires GHRH available for release, and another input. This would allow a more complex pattern of GHRH release rather than just single rebound pulses. It is also a good biological model; the charge (releasability) variable could represent the amount of GHRH ready for release and the input could be electrical activity, both of which are required. This is the new version of the GHRH equation :

$$\frac{dr}{dt} = r_{act}(I_r g) - k_6 r$$

The positive component is now the product of GHRH charge (g) and input activity (I_r). GHRH input protocols were used to provide the input component, consisting of a train of short pulses, similar to the artificial GHRH input used with the pituitary model. The pulses were each of 1min duration with 15min intervals. All the other parameters were left at the values set previously, including a delay of 80min. There was no effect on the overall pattern of GH pulses, with the length of the pulses and the quiet period between them remaining the same, but the input pulses now produced multiple peaks within the GH pulses and made them look much more like real pulses of GH release (figure 3.5a). This further supports the idea that there is another component involved in generating the pattern of GHRH pulses, perhaps a further interaction with somatostatin or GH or an outside pulse generator such as an adrenergic input.

Adding input pulses removed the need for a GHRH rebound pulse, and removing the rebound component made very little difference to the form of the GH pulses (figure 3.5b). Using the rebound form of the GHRH equation summed with artificial input produces GH bursts with a much higher peak at the start of the pulse, combining the effect of the rebound with regular input. However, following the principle of keeping the model as simple as possible, it was decided to remove the rebound mechanism at this stage. On its own it is insufficient to produce a pattern of

GHRH of the form required to match real data and combined with a pattern of GHRH stimulation it makes no significant contribution to the model's function.

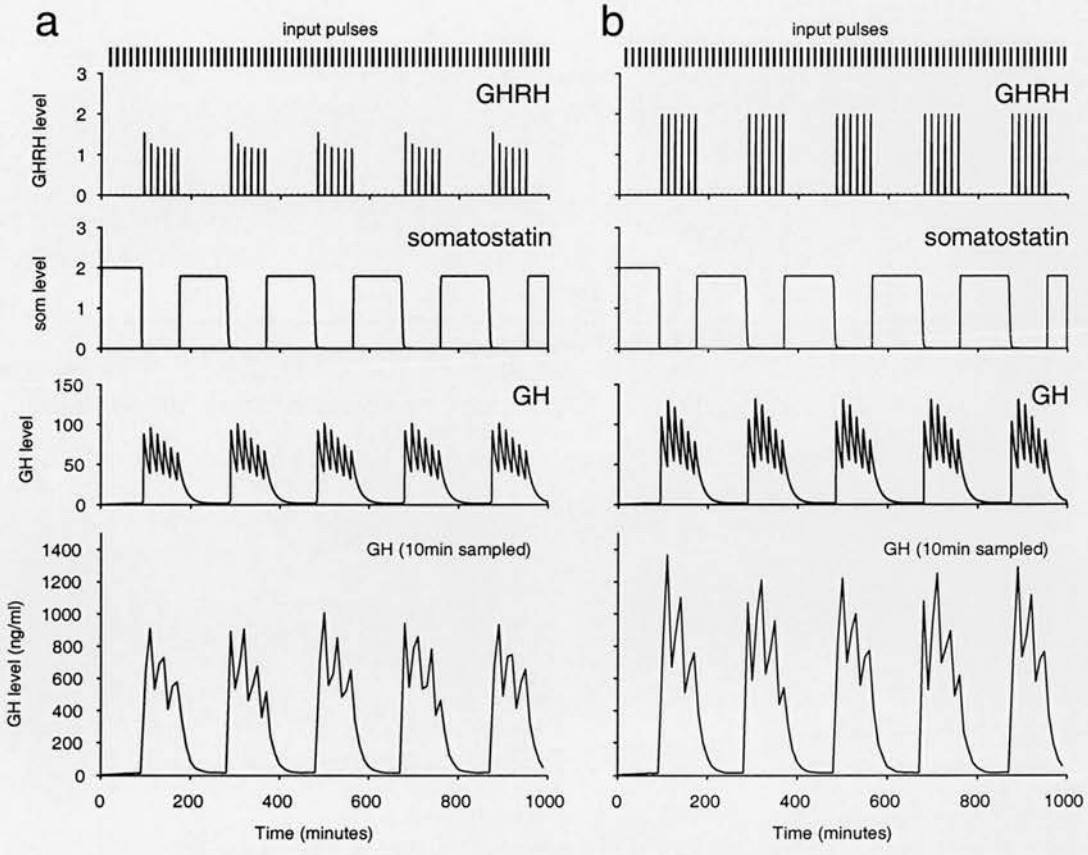

Figure 3.5 : initial 90min somatostatin infusion; **a**. 1min duration, 15min interval, input pulses trigger release from GHRH releasable pool (*g*), corresponding multi-peak pulses of GH release; **b**. GHRH release directly defined as 1min duration, 15min interval pulses, produces similar multi-peaked GH pulses; bottom traces show GH release scaled at 1model unit = 10 ng/ml, sampled at 10min intervals, with 10% error, 30s sample period and random start point, sampled GH profile often shows first peak as largest when this is not the case in unsampled data.

3.6.6 Conclusions

Although this version of the model did work, in that it was able to produce the basic pattern of GH pulses, the relations between somatostatin and GHRH and

between GH and somatostatin were rather unrealistic, using switch-like activation curves, although it is possible that a sequence of non-linear relations in the biological system could produce an overall switch-like relation. The GH pulse patterns also showed a shorter quiet period than seen in the real male release pattern, and a long delay was required to produce a pattern of GH pulses following the same timescale as the male rat. The next stage was to go on to develop more biologically plausible interactions and attempt to more accurately reproduce the real pulse patterns.

3.7 The Second Generation

The first change to the model was to replace r_{act} and $\Phi(h)$ with Hill equations to model the hypothalamic effects of somatostatin and GH. Like the old equations, these give a value that ranges from 0 to 1, with a higher value indicating a higher level of binding, or activation. This is the new equation for r_{act} :

$$r_{act} = 1 - \frac{s^{n_1}}{s^{n_1} + th_1^{n_1}}$$

The parameter th_1 gives the threshold for activation (really the level for half maximal receptor binding, but with a reasonably steep coefficient it essentially forms a threshold) and n_1 is the Hill coefficient giving the steepness with which the level of binding increases. The Hill equation is subtracted from 1 since it is being used for inhibition. The binding of somatostatin in the hypothalamus is thought to be highly cooperative (Wagner *et al* 1998) and so n_1 = 4. The new simplified equation for GHRH, removing the releasability component, is given below :

$$\frac{dr}{dt} = r_{act} I_r - k_6 r$$

Figure 3.6 shows the model's output at this stage, the first generation with the GHRH releasability component removed and the original r_{act} replaced with the new Hill

equation version, using parameters $n_1 = 4$ and $th_1 = 1$. The changes so far make no major difference to the model's behaviour, but use a more biologically plausible representation of somatostatin's inhibitory effect on GHRH.

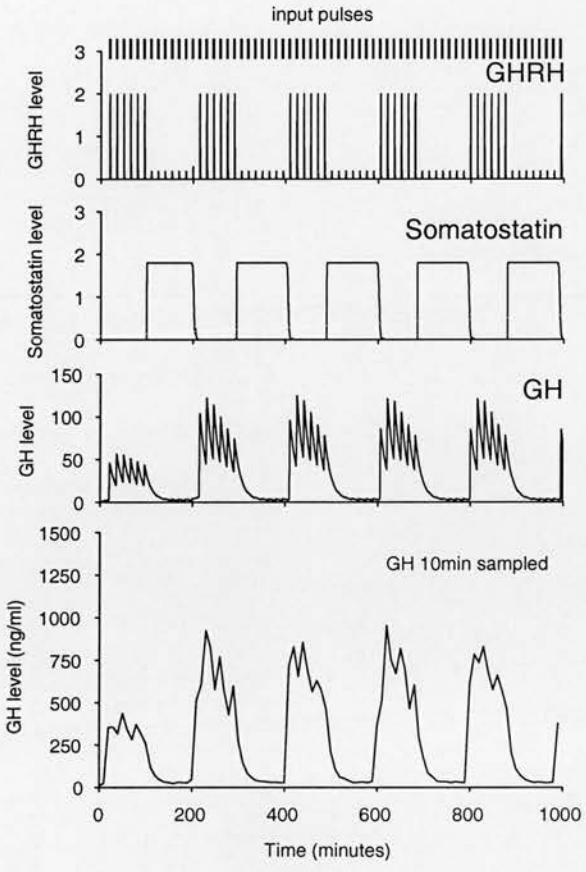

Figure 3.6 : The first generation model with Hill equation somatostatin-GHRH inhibition, 15min interval input pulses. The first GH pulse shows smaller peaks because of no previous somatostatin release to charge pituitary GHRH sensitivity (*f*). The reduced gradient of the somatostatin-GHRH inhibition leaves small pulses of GHRH and corresponding GH during periods of high somatostatin. Model behaviour is otherwise unchanged. The small inter-pulse GH peaks do not show in the sampled data.

The equation for GH activation acting on somatostatin, previously Φ(h), has been renamed h_{act} :

$$h_{act} = \frac{h^{n_2}}{h^{n_2} + th_2{}^{n_2}}$$

This has a similar form to the new r_{act} equation, with the threshold parameter th_2, and the Hill coefficient n_2. The behaviour of these two equations is not radically different to the old versions but they are more robust, in that they are less sensitive to the parameter values, and don't require such extreme values to work well. They also more closely represent the biological mechanisms and are known to give a good fit to the activation profile in ligand-receptor binding. The main difference in behaviour from a basic sigmoid equation is that the gradient of the Hill equation depends on the threshold as well as the coefficient. As the threshold increases, the level of activation increases more slowly, unlike the basic sigmoid where increasing the threshold just shifts the curve without changing its shape.

The second stage in advancing the model was to develop a more sophisticated connection between GH and somatostatin. A new charge (releasability) variable, s_r, was added for somatostatin. The idea was to develop a mechanism that would allow GH to trigger a prolonged period of somatostatin release, potentially longer than the actual period of GH release, without having to use very long delays. Instead of directly affecting somatostatin release, GH charges up somatostatin releasability.

The new equation for s_r is :

$$\frac{ds_r}{dt} = s_{r1}h_{act} - s_{r2}I_s s_r$$

Somatostatin releasability increases at a rate proportional to GH receptor activation (h_{act}) controlled by the parameter s_{r1}. The level of charge decreases with somatostatin release at a rate controlled by s_{r2}. The difference from the equivalent equation for GHRH (e1, page 95) is that the charge and discharge rates are not proportional to the current level of charge. Relative rates give a non-linear rate of change relative to peptide release, which is unlikely to be the case in the real system. A more linearly varying charge variable also makes it easier to achieve the sharp changes in release, such as sudden pulses, which are required by the model. The new component was

integrated into the somatostatin equation by making the release rate the product of s_r and input activity (I_s) to give the new equation below :

$$\frac{ds}{dt} = I_s s_r - k_7 s$$

This form allows the decoupling of the direct connection between GH and somatostatin release, allowing GH to charge up the store, which is turned into somatostatin release at a rate not directly dependent on GH release activity. Release is split into two components, the availability of the substance and the triggering electrical signal, which for somatostatin is defined as a constant level of activity so that it releases as soon s_r is charged. Using the constant level could allow the model to be further simplified, with just a constant instead of the input activity, but maintaining the use of the input protocol will allow more flexibility for later experimentation.

3.7.1 Testing the New Model

The input protocols were set up to give regular 1min pulses of input to GHRH at 15min intervals and constant stimulation to somatostatin. The GHRH pulses were sufficient to trigger the first GH pulse. The GH feedback delay was initially set at 30 min. The two parameters for h_{act} were set at n_2 = 2 and th_2 = 20. Setting a lower threshold allowed too much somatostatin release with low levels of GH, resulting in very small GH peaks. Increasing the threshold had a direct effect on GH pulse amplitude, reducing the somatostatin level during the GH pulse and increasing the size of the GHRH pulses. The remaining parameters to be tested were s_{r1} and s_{r2}, controlling the rates of charge and discharge of the somatostatin store. To set these the model was initially run with hypothalamic control of somatostatin disabled, so that somatostatin was purely controlled by the input protocols, set up to give a normal pattern of GH release. The two values were likely to act relatively to each other and so s_{r1} was given an initial value of just 1, since this appeared to produce a

reasonably scaled level of charge. The value, s_{r2} was then adjusted so that the level of charge from one pulse of GH would gradually fall back to 0 with somatostatin release between the GH pulses. This gave a value of 0.005 and these two values were set for testing the full model.

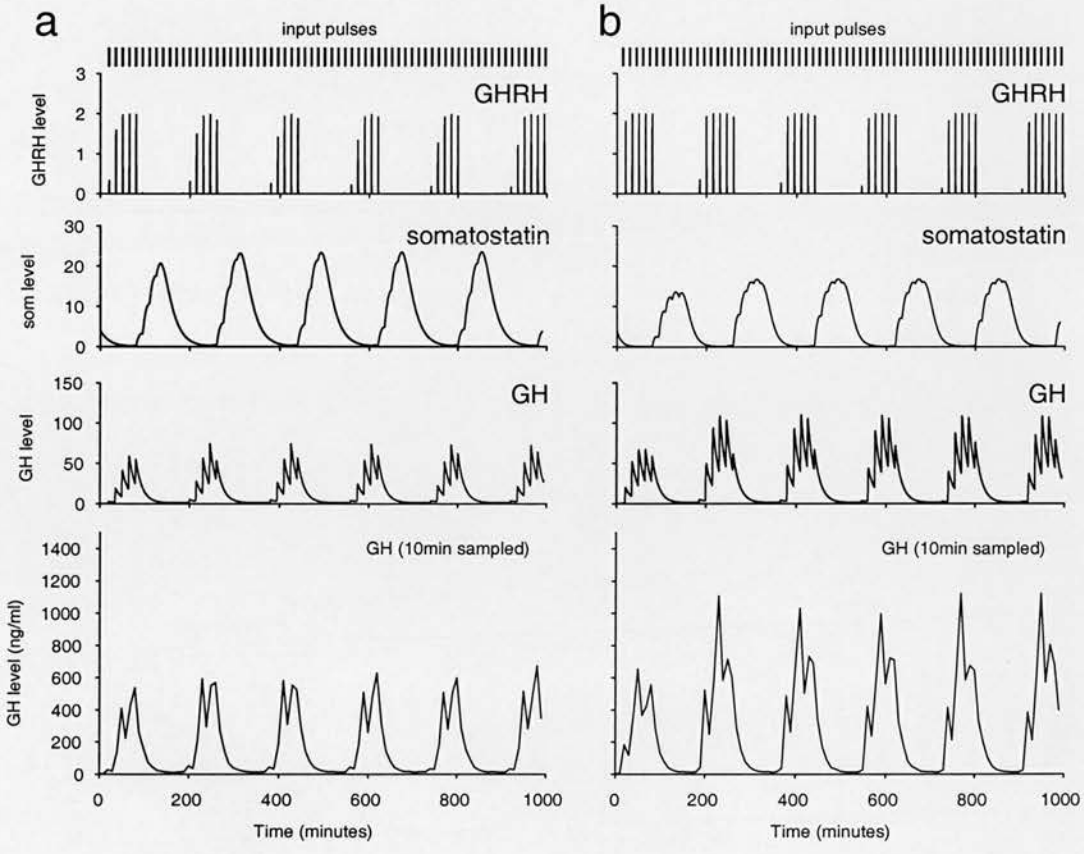

Figure 3.7 : **a**. Full second generation model. GH release triggers charging of somatostatin store (s_r), constant activation releases somatostatin at rate proportional to s_r, gradual decline in somatostatin produces smaller GHRH pulses and corresponding GH peaks at start of GH pulse, less obvious in the sampled data. Note the larger scale somatostatin axis compared to previous figures. (n_2=2, th_2=20, delay=45, s_{r1}=1, s_{r2}=0.005), pulse cycle = 185min; **b**. parameters adjusted to better match real data and give squarer somatostatin release by increasing s_{r2} (n_2=2, th_2=30, delay=60, s_{r1}=1, s_{r2}=0.01), pulse cycle = 180min.

The full version of the model was immediately able to produce pulses of GH release (figure 3.7a). GH pulse cycle length was 150min. The GH pulses were fairly

small in height and so th_2 was increased to 30 to return them to an amplitude more comparable with real data. This slightly reduced the cycle length to 145min. Increasing the GH feedback delay to 45min gave a cycle length of 185min, matching the GH pulse cycle in the male rat, and with a much shorter delay than was required with the first version of the model. Somatostatin release now had a more wave like form, climbing steeply in response to each GH pulse in the previous burst and then falling more gradually until low enough to allow GHRH pulses to trigger the next burst of GH release. The gradual fall in somatostatin resulted in smaller pulses of GH at the start of the burst, with the GHRH pulse still partially inhibited. This could be improved by increasing n_1, and increasing the sharpness of somatostatin's inhibitory effect on GHRH. Increasing the threshold, th_1, actually made the effect worse, probably since it would also reduce the sharpness of the activation curve. Another way to return somatostatin to more sudden changes in level, giving a squarer wave form, was to increase the rate of s_r discharge, s_{r2}. Increasing this to 0.01 gave a much steeper fall in somatostatin and produced much bigger GH peaks but at the cost of reducing the cycle length, to give a cycle of 150 min with a 45 min GH feedback delay. Getting back to a 180 min cycle length required a GH feedback delay of 60 min (figure 3.7b). This produced a pattern of GH release which appeared a good match to the release profile in male rats (figure 2.11).

Controlling the Somatostatin Release rate

The main problem with the new mechanism is the direct relation between the level of somatostatin release and the amount stored. In simple systems, if all the releasable store is stimulated then the release rate will be directly proportional to the amount stored, but this is very wasteful, releasing somatostatin at a rate far higher than is required to inhibit GHRH and GH at the pituitary. A better mechanism might be to limit the release rate to a maximum. To do this a new activation component, Hill equation sr_{act}, was added to the somatostatin equation so that the release rate was

limited to a value from 0 to 1, determined by the level of activity, I_s and the somatostatin store, s_r, and scaled by I_s. The new equation is given below :

$$sr_{act} = \frac{(I_s s_r)^{n_3}}{(I_s s_r)^{n_3} + th_3{}^{n_3}}$$

This was integrated into the equations for somatostatin and s_r by replacing the direct use of s_r, as shown below :

$$\frac{ds}{dt} = I_s sr_{act} - k_7 s$$

$$\frac{ds_r}{dt} = s_{r1} h_{act} - s_{r2} I_s sr_{act}$$

Parameters th_3 and n_3 were set to give release with any level of s_r and a steep switch between the maximum and zero release when s_r is drained. A typical result is illustrated in figure 3.8a. Adding this mechanism further decouples the length of the GH pulse from the delay between them and creates sharper changes in somatostatin release, giving a squarer wave form. This reduces the problem of gradual change in the somatostatin level causing smaller pulses of GH at the start of the burst. The length of the delay between GH bursts becomes much more dependent on the rate of s_r charge and discharge, allowing a longer pulse cycle length with a smaller GH feedback delay.

Setting a Maximum For the Somatostatin Store

A simpler way of limiting the amount of somatostatin, and one that should increase the biological plausibility of the mechanism, is to put a maximum on s_r. This was implemented by limiting the rate at which GH can increase the amount of charge, using the following new equation for s_r :

$$\frac{ds_r}{dt} = s_{r1} h_{act} ((sr_{\max} - s_r) / sr_{\max}) - s_{r2} I_s s_r$$

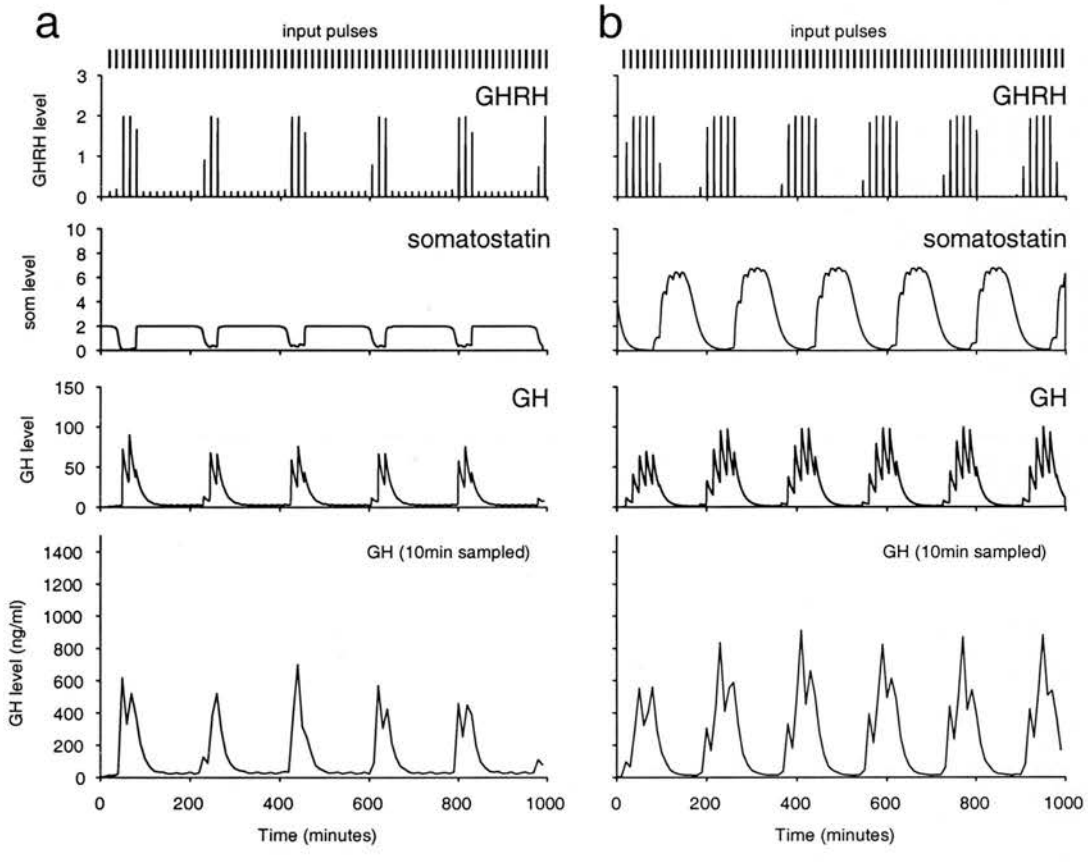

Figure 3.8 : **a**. Decoupling somatostatin release rate from sr using Hill equation to limit release. This makes the period of high somatostatin much more dependent on s_{r1} and s_{r2} and less dependent on the length of the GH pulse, allowing long pulse cycles without using a larger feedback delay, it also causes higher somatostatin release during the pulse period, reducing GH pulse height (s_{r1}=1, s_{r2}=0.005, n_3=2, th_3=1, delay=30), pulse cycle = 190min. **b**. Similar to figure 3.7b, with s_r limited to a maximum level, note the smaller scale for somatostatin, limit reduces somatostatin release and produces squarer wave form (n_2=2, th_2=30, delay=60, s_{r1}=1, s_{r2}=0.008, sr_{max}=5), pulse cycle = 180min.

The new component limits s_r to a maximum value defined by the parameter, sr_{max}. It makes the charge rate proportional to the difference between the current charge and the maximum. This reduces somatostatin output to levels sufficient to provide maximal inhibition of GHRH without releasing larger quantities than is necessary (figure 3.8b). It also forces the pattern of somatostatin into a squarer wave form by

cutting off the large peak. The maximum level of somatostatin release matches the value specified by sr_{max}, in a similar manner to parameter j_2 in the first version of the model. Reducing somatostatin release slightly reduces the length of the quiet period between GH pulses, but otherwise the GH release pattern is unaffected. The reduction in cycle length can be compensated by reducing the rate of s_r discharge, s_{r2}. With $sr_{max} = 5$, the cycle length can be returned to 180 min by reducing s_{r2} to 0.008 (from the previous value of 0.01), very slightly reducing the height of the GH peaks.

3.7.2 Conclusions

The new version of the model was able to produce a pulsatile pattern of GH release, and using ligand-receptor activation relationships, more closely based on biological mechanisms. Using the more sophisticated GH-somatostatin feedback mechanism allows the model to reproduce the long period of GH release inhibition without having to use such a long absolute delay, and also suggests a possible mechanism to be tested in the real system. Adding the extra layer of complexity, with the activation equation controlling the somatostatin release rate, essentially returns the model's behaviour to the state before using the somatostatin store, with a square wave pattern of somatostatin release. The difference is that the period of high somatostatin release is now controlled more by the charge and discharge parameters rather than the GH feedback delay. The main argument against this new system is that it requires a more complex system in the hypothalamus. However, examining real data also suggests that the period of high somatostatin release is closely related to the length of the GH burst, suggesting that there is a close causal relation between the two, unlike in this new mechanism. Using the releasability component allows the model to produce a pattern of GH release which matches the real data using a shorter, and probably more realistic, GH feedback delay, and so for the final version of the basic model it was decided to compromise, and keep the somatostatin releasability component, limited to a maximum level, but without the extra activation component, sr_{act}. The model is of course maintained in a manner which allows the

switching of these components for later experiments if further results cast doubt on the decisions made at this stage. The idea of dividing somatostatin release into releasability and input activity has worked well and suggests work for real experiments, perhaps *in-vitro* work investigating the effect of GH on somatostatin cells to find out if GH pre-treatment increases release in response to an electrical stimulus. Little is known of the real mechanism by which GH increases hypothalamic somatostatin release.

Whether the model really needs the more complex GH feedback mechanism depends on interpretation of the delay. The GH pulse in data from male rats usually lasts at least an hour, and so the delay between GH release and increased somatostatin release must be at least 60min. However, the question is of how this delay is made up. It seems unlikely that the 60min or more can be just the amount of time it takes GH to reach the periventricular neurons. It is more likely that there is some more complex mechanism which delays the response between GH reaching the periventricular nucleus, and somatostatin release.

The final basic version of the model is illustrated in figure 3.9. The final set of parameters is given in the table below :

Parameter	Value
s_{r1}	1
s_{r2}	0.008
$sr_{\max}$	5
n_1	4
th_1	1
n_2	2
th_2	30
delay	60

The two essential hypothalamic components are the somatostatin-GHRH inhibition and the GH-somatostatin feedback. Together these allow sudden changes in GH release and create a cycle which generates a pulsatile pattern of release. There is good evidence that these exist in the real system, but no detail on the dynamics of the interactions, giving any information on timing, thresholds, or response curves for the interaction of these substances. To model them, parameters have been chosen by

trying to stay within a biologically plausible range and by comparing the model's output with real data. The other component which had to be added to the model was a pulsed input to the GHRH neurons, in order to produce the multiple peaks within the GH burst. Evidence from the real system gives two possibilities for the source of such an input, an adrenergic input, similar to that used in the LH Model (Brown *et al* 1994) or a feedback connection from GH to the GHRH neurons. These two sources suggest input with quite different properties, one driven by the model and the other following a pattern unrelated to the release pattern. Testing these is left to the next chapter.

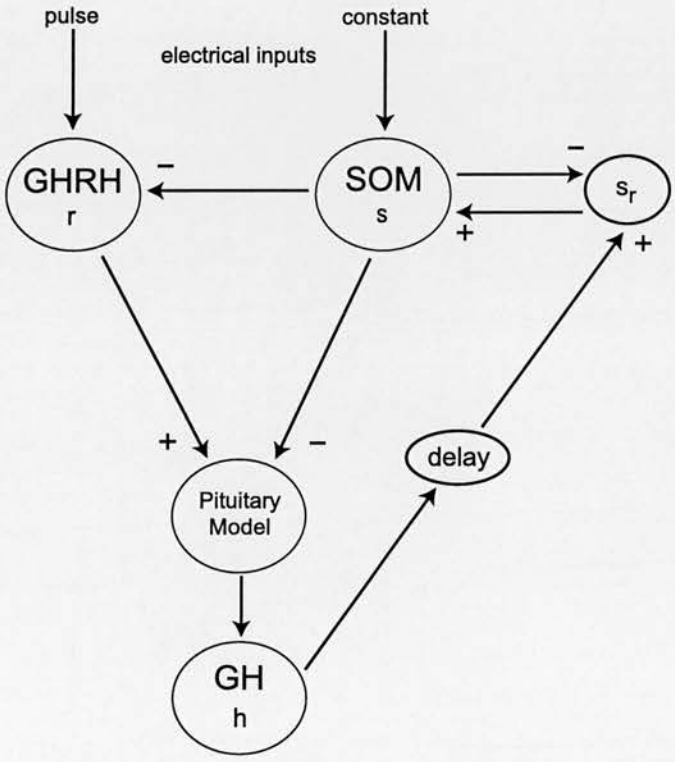

Figure 3.9 : Final version of the basic model. Somatostatin inhibits GHRH and GH release. GH feeds back with a delay to charge the pool of releasable somatostatin. A GH pulse causes high level somatostatin release which continues until s_r is drained and somatostatin allows GHRH release again, triggering another GH pulse.

The basic version of the model produces an output profile which closely resembles GH release in the male rat and provides a base on which to experiment with other components which may exist in the real system, with the aim of getting a more exact fit to the real data and making the system more robust. The system should also be capable of reproducing *in-vivo* experiments, and can perhaps aid their interpretation. Another important test of the system will be the ability to reproduce the female pattern of GH release. This will need to be combined with adding a random component to the GHRH input activity and so this is left to the next chapter, although initial tests during the model's development have suggested that the current version should be capable of this with little modification, as required by the original specification.

Chapter 4

Experimenting with the Model

4.1 Introduction

This chapter takes the basic version of the full GH system model and uses it as a base with which to experiment with the system, testing the effect of new components and using the model to simulate *in-vivo* experiments. The aim here is to further refine the model, to get a closer fit to real data and also to begin doing genuine experimentation, testing less well defined knowledge and identifying new ways in which to explore the real system.

The first part of this chapter investigates the GHRH input pulses which were added in order to produce the multiple peaks within the GH burst. The aim will be to define what criteria these need to fulfil in order to match the peaks observed in real data. It will be desirable to have the specification of this external input as loose as possible, in order to avoid this input being used to drive the model's output pattern. It will be essential to this analysis to use the sampled version of the model's GH output, since the pattern of GH release can appear quite different when the temporal resolution is reduced. If the model is to reproduce the quantitative as well as qualitative features of real GH release then the only fair way to compare them is using the simulation of how GH is measured in real experiments.

The first change to the model will be to make the timing of GHRH input pulses random, in a similar manner to experiments with the pituitary model. A further development of this will be to attempt to reproduce the less regular pattern of release observed in the female rat. The entirely new components which will be tested with the model are those suggested by experimental data, which may play a role in the normal system. Testing these will indicate what sort of functional role they could play and on the basis of this, how likely they are to exist in the real system.

Using the model to simulate existing *in-vivo* experiments will be a further important test of how well the model represents the real system. If the model is able to reproduce the real experimental data then it should provide a useful tool to be able to add to the interpretation of these results. It will be possible, under the assumption that the model is an accurate representation of the system, to explain the mechanism behind the system's response to experimental intervention.

4.2 GHRH Input Activity

The aim here is to test the nature of the external GHRH input by experimenting with how much it can be varied in the model and still produce a pattern of GH release which resembles real data. The first part of this will be to experiment with the frequency of the input pulses. The current 15 min intervals are very long compared to what might be expected from some general non patterned driving input. Most electrical signals in the brain are of a much higher frequency and, assuming that there is an outside electrical input to the GHRH neurons (and this would seem likely to be the case since blocking possible inputs blocks out GH release) then it is unlikely to follow such a regular form, or such a slow rate. The second part of the testing will add a random factor to the input pattern intervals. However, before attempting either of these the next important step is to examine the sampled form of GH output with the full version of the model.

4.2.1 The Sampled GH Profile

The sampled profiles here use the extended sampling process developed in chapter 2, including 30s. sample periods and 10% proportional error in each sample measure, to simulate the measuring of the GH profile in real experiments. Sampling has the effect of reducing the number of peaks which appear in each GH burst and also effects the size and shape of the GH peaks. Applying sampling to the model's GH output produces a profile which much more closely resembles real data. The main differences between real GH bursts and the un-sampled model profile are the sharpness and frequency of individual peaks, and the smaller peaks of GH release which appear in the model, but not in real data. Running the model data through the sampling process hides the smaller peaks, reduces the number of peaks and makes them less sharp, producing a profile very similar to the real data. Figure 3.8 shows the model data along with a sampled version (15min GHRH pulse intervals). In real data, the GH profile is the only evidence for the form of GHRH release and the effect

of sampling complicates the interpretation. There are likely to be more individual GHRH pulses than the number of individual GH peaks which appear. The next goal with the model is to test what range of GHRH pulse frequencies could be responsible for the sampled profile which appears.

4.2.2 Varied GHRH Pulse Frequencies

For these tests the basic version of the GH system model was used with the parameters specified at the end of chapter 3, varying the GHRH pulse frequency by controlling the input activity specified by the input protocol. The simulated sampling uses 10min sample intervals, in common with typical real data. The pulse interval was gradually increased (reducing the frequency) beginning with just a 1min interval between the 1min duration GHRH input pulses, each triggering a corresponding GHRH pulse during the periods of low somatostatin. Similar experiments with the pituitary model have already suggested that the interval needs to be quite long in order to get individual peaks because of the 10min half life of GH in the bloodstream.

For GHRH pulse intervals of up to 10min, nothing but very small individual peaks appear in the sampled (10min sample intervals) GH burst (figure 4.1a). This is as expected, given the sample interval. At 12min GHRH intervals, well defined two peaks bursts begin to appear (figure 4.1b), and then at 14min intervals some of the bursts show three peaks, beginning to more closely resemble real data. When the pulse interval increases to 18min, 4 peak sampled bursts appear (figure 4.1c) and the number of peaks stays at 4 until the interval increases to 21min and it falls back to three, as the number of peaks in the un-sampled GH profile reduces, falling to two peaks after the interval increases to 31min.

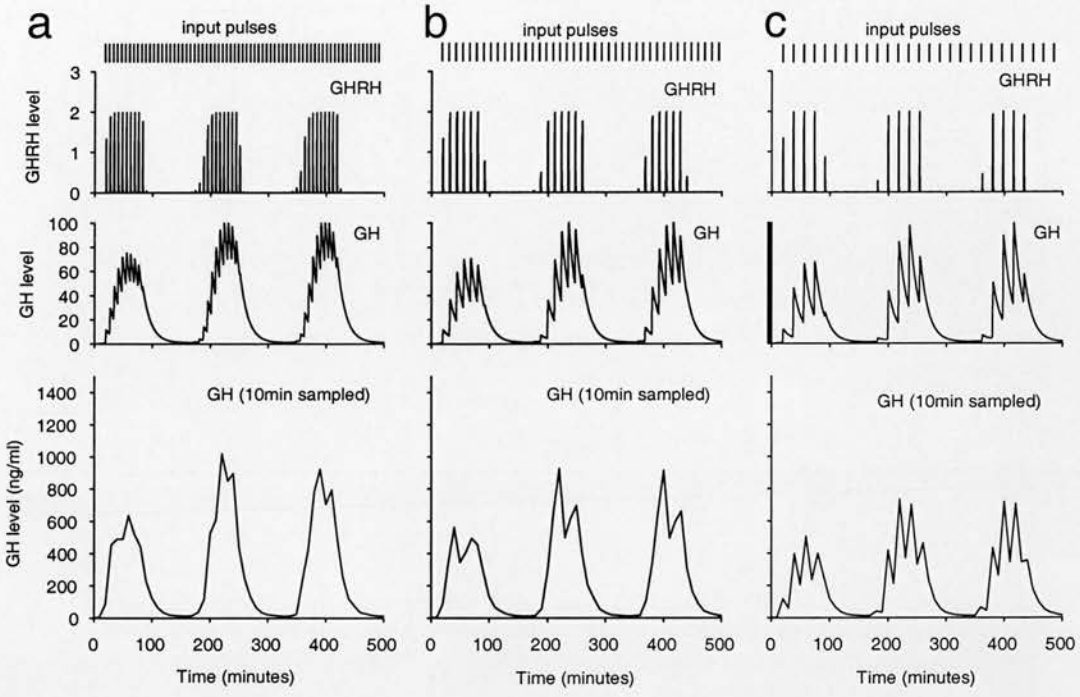

Figure 4.1 : Varied GHRH input pulse intervals and sampled profile; **a**. 7min pulse intervals, only small peaks within sampled GH pulse; **b**. 12min pulse intervals, 2 distinct peaks within sampled GH pulse; **c**. 18min pulse intervals, 4 distinct peaks within sampled GH pulse, now matches unsampled data, larger input pulse interval also creates smaller chance for sampling to detect peak height in unsampled data, producing smaller peaks in sampled profile.

Two competing processes cause this climb and then fall in the number of peaks appearing in the sampled profile. In the first place the number of peaks increases as the intervals become big enough for the samples to pick up more individual peaks. At the same time the number of peaks in the un-sampled profile decreases, in line with the reduced number of GHRH pulses. When the interval becomes big enough for sampling to pick up all the peaks the falling number of GHRH pulses takes over control of the number of peaks appearing in the sampled profile. Real GH profiles using 10min samples (figure 2.11) show two or three distinct peaks in each GH burst. On the basis of the current model, this suggests that the interval between GHRH pulses is likely to be in the range of 15 to 30 minutes.

4.2.3 Random GHRH Pulse Intervals

Although the basic model is able to match the general form of the GH bursts in real data, including the number of peaks, the length of the burst and the quiet period, the form of the model's output is too regular to exactly match real data, where the spacing of bursts, their duration and the number and height of peaks varies. It is also an important test of the model's robustness that it should still be able produce the pulsatile pattern of GH release without depending on a regular form for the input activity.

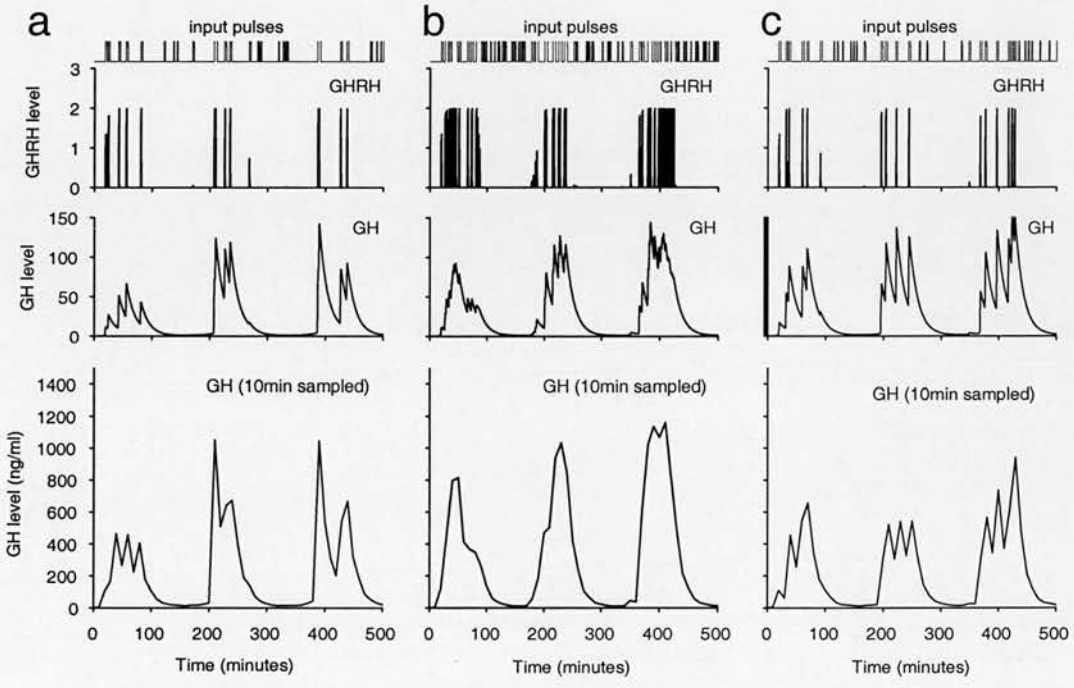

Figure 4.2 : Random input pulse intervals; **a**. 15min mean interval, sampled pulses show 2 or 3 distinct peaks; **b**. 5min mean interval, sampled pulses show no distinct individual peaks; c. 10min mean interval + 5min refractory period, sampled pulses show 2 or 3 distinct peaks, also shows truncated peaks which show a similar form to real data (figure 2.11).

To do this the model software's control of the input protocols was adapted so that so that instead of specifying a fixed interval between each input pulse, the interval

could be specified as a random component defined by a mean and a fixed refractory component (which can be zero). The random component is generated using the Poisson distribution, the standard form for randomly timing an individual event. The model was set up using the final set of parameters for the basic model, defined in the table at the end of chapter 3. With these parameter values and GHRH input pulses of 1min duration at 15min intervals, the model produced a regular pattern of pulsatile release matching the general form of the GH profile in male rats (figure 2.11).

For the first test the mean interval length was set to 15min, matching the previous regular protocol, with no refractory period (figure 4.2a). The first important result is that the pattern of 3h bursts of GH release was maintained. There was some variation in the time between bursts, ranging from 170min to 190min, but the general form showed little change. With the randomly timed GHRH pulses, each GH pulse had a different form, with peaks varying in height and numbers, sometimes three peaks and sometimes just one large single peak, very similar to some of those observed in the real release profiles. The random GHRH pulses also reduced the number of GH pulses with smaller GH peaks at the start of the pulse, which are usually not observed in the real data.

Experiments continued by varying the mean interval length. Using a short mean interval of 5min showed similar problems to the short interval tested with regular pulses. The sampled GH bursts tended to show only one large peak (figure 4.2b). The random spacing did reduce this problem, with a few pulses showing three small (very little drop between) peaks. Increasing the mean interval increased the number of pulses with two or three peaks, although the variation observed between interval lengths was less well defined than with the regular intervals. Pulses continued to resemble the form of real data with mean pulse intervals as high as 50min, although increasing the mean interval over 30min tended to produce some occasional pulses with very small peaks. Adding a refractory period produced better results at lower mean pulse intervals, taking away the very short intervals causing larger single peaks in the sampled profile. Using a 10min mean interval with a 5min refractory period produced a good match to real data (figure 4.2c). One particular feature which is observed in the real data profiles, particularly the 12min sampled figure, is square

tops to some of the sampled bursts, which appear to be truncated peaks. In the sampled model data these tended to be observed more commonly with lower mean pulse intervals, of 10min or 15min.

The model has proved that it does not need a regular pattern of GHRH input in order to produce regular bursts of GH. Using the random pulses the model now produces a match to real data as close as can be judged given the resolution of real data. The form of the sampled model bursts provide a good match to those observed in real profiles, and using the estimated scaling of 1 model GH unit to 10ng/ml of real GH, the height of the pulse gives a good match to real data where pulses are observed as high as 1200ng/ml. The model demonstrates that the sampled peaks are likely to be smaller than the true peak levels of GH release, with sampling in the model producing as much as a 40% reduction in the height of GH peaks. Random pulse timing extends the range of mean pulse intervals which can produce the number of peaks observed in real data but still suggests a similar range to that predicted with regular GHRH pulses, perhaps 10 to 30min.

4.3 The GH Profile in the Female Rat

The pattern of GH release in the female rat is much less regular than the male, losing the well defined 3h pulses. The levels of release never drop as low as the periods between pulses in the male and GH peaks tend to be lower, although data from some female animals does show peaks with heights comparable to those observed in males. The pulses of GH observed in the sampled female profiles appear to follow a similar frequency to those observed in the male bursts, and it is thought that the underlying pattern of GHRH activity is similar, with the sexually differentiated patterns being produced by varied patterns of somatostatin release. Evidence suggests that the sex steroids testosterone and oestrogen affect the control of somatostatin, perhaps modulating the effect of GH feedback. The model can be used to test this, by using the parameters controlling the somatostatin store and GH feedback to attempt to reproduce the female pattern of release. However, earlier

experimentation during the development of the model also suggested an alternative point at which the effect of somatostatin could be varied between the sexes. Varying the inhibitory effect of somatostatin on the GHRH neurons can produce a pattern of release similar to the female, and so this will also be tested here.

The testing here was done using the standard set of parameters, with randomly timed GHRH input, using a mean pulse interval of 15min added to a 5min refractory period.

4.3.1 Varying GH Feedback Activation

The first parameter tested was $th2$, the Hill equation threshold for GH feedback. Reducing this value makes the GH peaks smaller and lengthens the GH burst cycle but maintains the regular pattern of bursts. Increasing its value has the corresponding opposite effect, increasing the height of GH peaks and shortening the cycle length, but also maintains the regular male pattern of release. The effect of changing the Hill coefficient, n_2, was similar. Reducing the value made the GH pulses much smaller until GH release completely stopped. Increasing the value increased the height of GH peaks and slightly reduced the pulse length, but again maintained the regular pulse pattern. Changing these parameters affects the relation between the GH levels and the somatostatin store, and by extension, somatostatin release. With a lower threshold, or higher coefficient, the activation curve (the relation between the GH level and its effect) becomes steeper so that somatostatin release becomes closer to a square wave, giving very low levels between the high periods of somatostatin release, which creates the higher GH peaks. However the effect of these parameters on the regular pattern of release is constrained by there still being the absolute delay in GH feedback, in these experiments set at 60min. Part of this delay may be due to the mechanism by which GH triggers somatostatin release, after GH has reached the somatostatin neurons. This may be modulated in the female, but there is still likely to be some significant delay, and reducing the delay on its own shortens the pulse cycle length but still maintains regular pulses.

Attempting to reproduce the female release pattern by changing the parameters controlling the somatostatin store, s_{r1} and s_{r2}, is much more successful. Either reducing s_{r1} (the charge rate) or increasing s_{r2} (the discharge rate) reduces the levels which s_r charges to and in turn reduces somatostatin release to levels below the threshold required to block GHRH pulses. In combination with random GHRH input activity this creates a more random pattern of GH activity, still with some GH pulses but following a less regular cycle, and without the periods of very low GH release. Regular pulses are lost after s_{r1} is reduced to 0.2. Making it smaller makes the release pattern progressively less regular until release matches the pattern of GHRH input activity. Changing s_{r2} has a similar effect. Regular GH bursts are lost at 0.2 and with higher values, GH bursts disappear entirely, leaving just random pulses of GH release. Figure 4.3a shows an example pattern of release similar to the female rat, produced by reducing s_{r1} to 0.05.

Another way to achieve the same effect is to reduce $sr_{\max}$, the parameter controlling the maximum level for the somatostatin store. Reducing this to 0.5 (its normal value is 5) reduces the level of somatostatin release, producing a less regular pattern of GH release, with smaller GH pulses, tending to maintain a constant low level of somatostatin release (figure 4.3b). This last feature is in contrast to changing s_{r1} and s_{r2} which tends to maintain a more wave like pattern of somatostatin release, and has less of an effect on GH pulse heights. In real data, the difference between GH pulse heights in males and female varies between different papers. The consensus appears to be that GH pulses are usually smaller in females, but some data shows pulses which are as large as those in males, particularly during darkness. However, producing the female pattern by reducing s_{r1} does reduce also pulse height, although by a smaller proportion, and this isn't good enough evidence to choose between the two methods on the basis of which provides a better match to real data.

4.3.2 Varying Somatostatin - GHRH Inhibition

The two parameters tested here were n_1 and th_1, the coefficient and threshold for the Hill equation controlling somatostatin's inhibitory effect on GHRH release. Increasing n_1 increases the steepness of the switch between full inhibition and no inhibition of GHRH. Higher values increase the height of GH pulses and slightly reduce the GH pulse cycle length. Reducing n_1 to values below 0.7 breaks the regular pattern of GH release, but also greatly reduces the height of GH peaks with somatostatin release following a more random pattern but also still climbing to high levels.

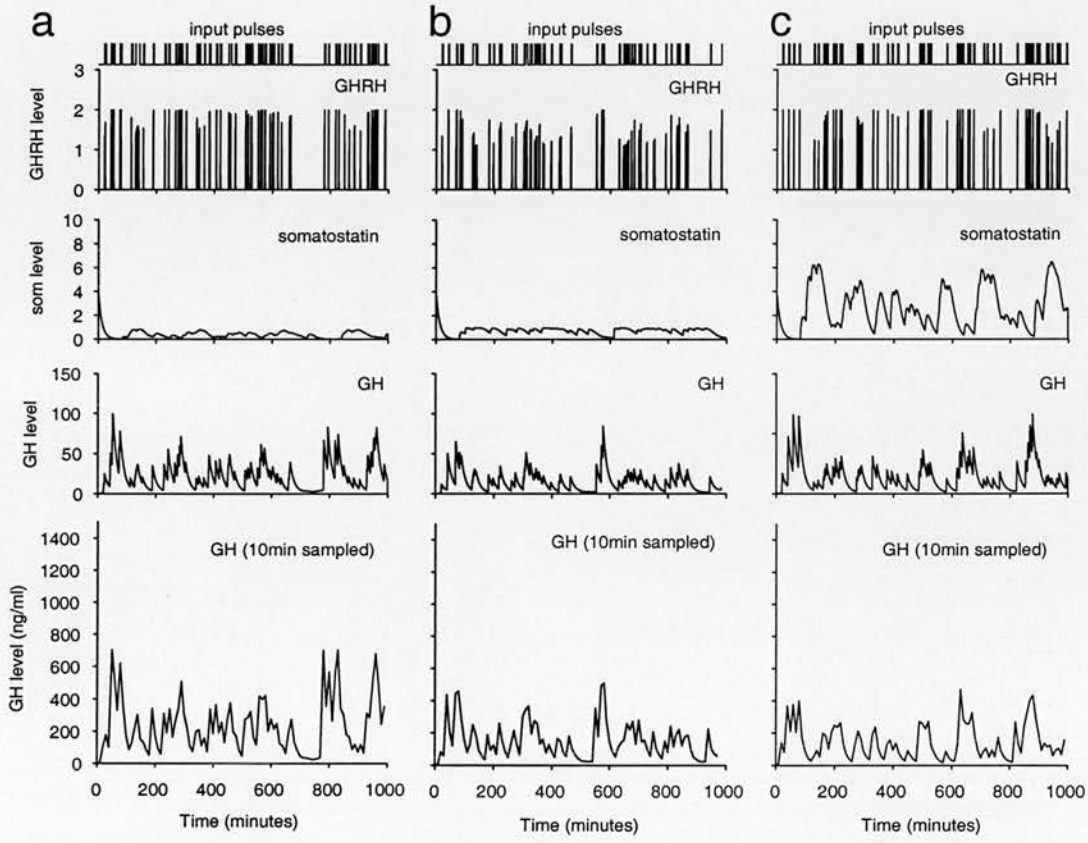

Figure 4.3 : Reproducing the female release pattern; **a**. s_{r1} reduced to 0.05, regular pulse activity lost, still some peaks similar in magnitude to males; **b**. $sr_{\max}$ reduced to 0.5, more level pattern of low somatostatin release, regular pulses lost, GH peaks smaller than in males; **c**. th_1 (som-GHRH inhibition threshold) increased to 0.7, regular pulses lost, GH peaks smaller than in males, high level somatostatin release continues but in a less regular pattern.

Reducing the threshold, th_1, initially increases GH pulse height and increases the pulse cycle length. However, after reducing th_1 to 0.2, the effect reverses and as th_1 is reduced further, GH pulse heights and the pulse cycle length are reduced until pulses become so small that they disappear. The regular pattern of release is maintained throughout. The cause of this is the minimum level of somatostatin release, between periods of high somatostatin, which is about 0.2 units. This is maintained by basal GH release having a small effect on s_r.

After increasing th_1 to values above 5, the regular pattern of GH bursts is lost, with GH peaks reduced in height. The effect progresses as th_1 is increased to higher values until the pattern of GH release matches the pattern of random GHRH input. GH pulses are reduced in height but less so than when the female release pattern is produced by reducing n_1. There are still occasional large peaks of GH release. Figure 4.3c shows an example pattern of release produced with $th_1 = 7$.

4.3.3 Conclusions

The experiments here have demonstrated that the model can easily be modulated to produce the female pattern of release. This an important validation of the model, on the basis that the GH systems in male and female rats are likely to be similar, with a sex hormone controlled modulation capable of switching between the two patterns of release. The model has also demonstrated two alternative methods of producing the female pattern, suggesting two possible sites of modulation in the real system. The main difference with the method of altering somatostatin's inhibitory effect on GHRH is that there is a larger reduction in GH pulse height along with the loss of the regular burst pattern. The variation between sets of real data is too great to use it as a basis to differentiate between the two. It may however be possible to test this further by simulating *in-vivo* experiments which show varied results between male and female rats, and this will be attempted later in this chapter.

4.4 Testing a Reciprocal GHRH-Somatostatin Connection

One of the apparent problems with the current model, from a design point of view, is the sensitivity of GHRH to the gradual changes in the somatostatin level, which are produced by the mechanisms which prolong somatostatin release. At the moment the model solves this problem by making the activation curve in the equation which defines the inhibitory effect, very steep, acting as a switch. This may be biologically feasible if the system combined several layers of non-linear relations, but is generally not an ideal solution and not very robust.

What is required is functional bistability in the GHRH neurons. This can be created by controlling the functional properties of the group of neurons on their own, or as part of a larger system. Reciprocal connections to another group of neurons can often produce such properties. There is circumstantial evidence that such connections between the somatostatin and GHRH may exist. Substances that are contained in the GHRH neurons have been found to act at the somatostatin neurons, with different results suggesting both excitatory and inhibitory effects. The model gives the opportunity to test what effect on the system such a connection might have. It is obvious within the current system that an excitatory connection from GHRH to somatostatin will not produce any useful or interesting behaviour. Any increase in the GHRH level would trigger somatostatin release which would then immediately suppress GHRH, so that GHRH would never be able to increase to a significant level. The behaviour of an inhibitory connection however is less predictable, and so this makes an interesting component to test with the model.

4.4.1 Implementing the Inhibitory GHRH-Somatostatin Connection

The new connection was implemented in a similar manner to the inhibitory somatostatin-GHRH connection, using a Hill equation to give a measure of activation due to the GHRH level. The new equation is called s_{act} and is given below:

$$s_{act} = 1 - \frac{r^{n_4}}{r^{n_4} + th_4{}^{n_4}}$$

The new parameters, th_4 and n_4, give the threshold and binding coefficient. This was integrated into the control of somatostatin, so that it can modulate release activity, using the following new equation :

$$\frac{ds}{dt} = s_{act} I_s s_r - k_7 s$$

The Hill coefficient, n_4, was set at an initial value of 2, similar to the GH feedback equation. The threshold parameter, th_4 was set at 1, a fairly low level of GHRH release. In the model software the new component was set up so that it could be switched on and off in order to easily to make a direct comparison of the model's behaviour with and without the new component.

4.4.2 Testing the New Component

The model was initially run with regular 20min GHRH pulse intervals. Its immediate effect was to increase the size of GHRH pulses and the corresponding GH peaks, particularly the smaller ones which had previously been partially inhibited by somatostatin (figure 4.4a). There was no effect on the overall pattern of GH bursts. Adding random pulse intervals to GHRH input, showed similar effects, with slightly larger GH pulses, and a few more single peaked pulses appearing in the sampled GH pulses (figure 4.4b).

The new component creates bistable behaviour in the GHRH neurons. When somatostatin partially inhibits GHRH, but GHRH is still above the threshold to inhibit somatostatin (th_4), then somatostatin is inhibited and the GHRH pulse becomes much larger. This results in either full size GHRH pulses or GHRH entirely inhibited by somatostatin. This makes the model more robust, with less variation in GH pulse size, but does not add anything functionally to the model. The resolution of real data and the rough scaling of the model's GH level to real GH release is not sufficient to judge such a subtle variation by comparing the effect with real data. The important test is whether this new component allows the inhibition of GHRH by

somatostatin to be made less steep. When the parameter controlling this activation curve, n_1, is reduced from 4 to 2 the pattern of GHRH release takes on a more wave like form, with smaller pulses at the start and end of the GH burst. Adding the new component allows n_1 to be reduced to 2, with larger pulses of GHRH maintained. In terms of comparing the sampled GH profile with real data, the GH pulses with the new connection tend to be taller with steeper sides (figure 4.4c), which appears to be a closer match to the real data.

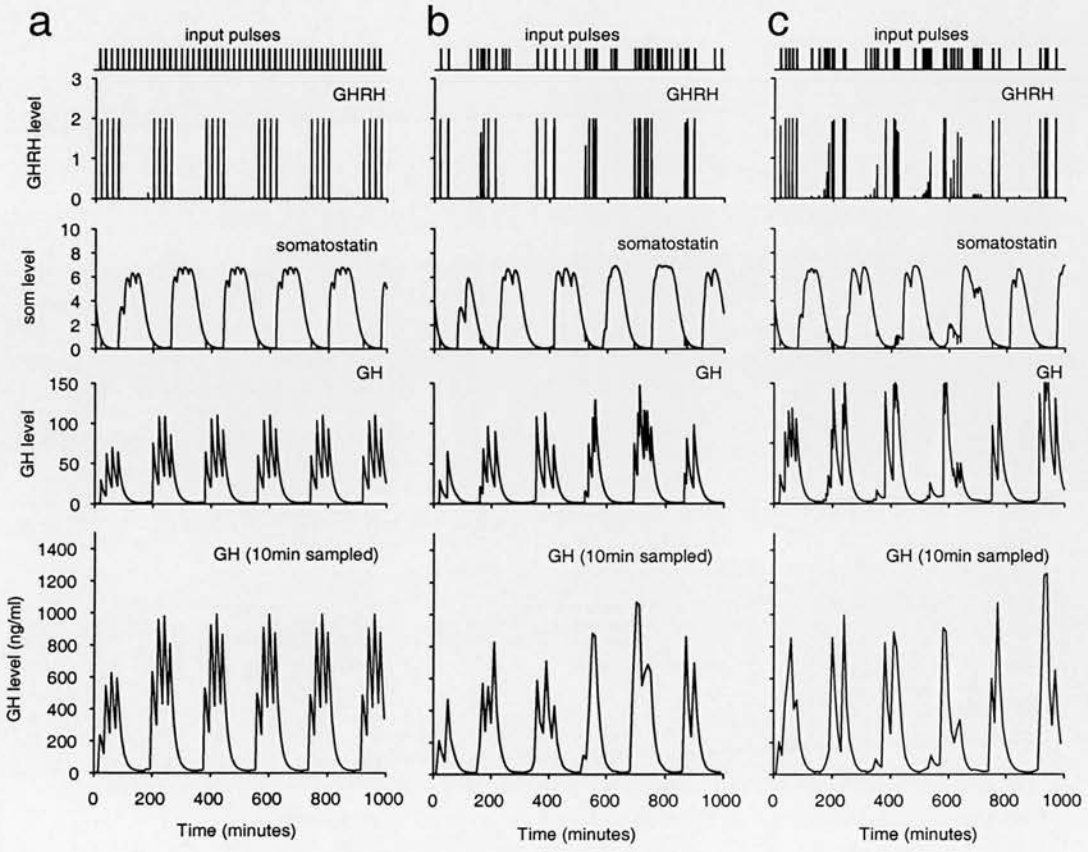

Figure 4.4 : GHRH-somatostatin inhibition; **a**. regular 20min interval GHRH pulse input, GHRH pulses over threshold inhibit somatostatin, removing their own inhibition, producing bistability in GHRH, GH pulses are taller and more regular; **b**. random 15min mean + 5min refractory period pulse input, GHRH pulse heights more regular, taller more regular peaks in GH pulses (cf figure 4.2c); **c**. as b. with n_1=2, similar GH release using less switch like somatostatin-GHRH inhibition.

4.4.3 Conclusion

The new component is based on evidence from real data, and added to the model it does play a useful role in the system, making GHRH activity robust and allowing a more biologically plausible relation in the inhibitory effect of somatostatin on GHRH, requiring a simpler biological mechanism. The new connection has no negative effect on the model's behaviour although at the same time, it doesn't add anything to the model functionally and if the main goal is to keep the model simple then this new connection should probably be left out. However, its role in making the system more robust and providing a use for some of the experimental evidence is strong enough to suggest possible experiments with the real system, looking for such a connection.

4.5 GH-GHRH Feedback

When it originally became apparent that GH feeds back to inhibit its own release, there were two possible ways in which it could do this, by inhibiting GHRH, or by exciting somatostatin release. Evidence for both of these connections exists at the anatomical level. Testing exogenous GH along with injections of GHRH and somatostatin also suggests that both of these connections exist, and probably vary between the sexes. The main reason for not including the GH-GHRH connection in the model this far was that it was not required to produce the basic pulsatile release pattern, for which the GH-somatostatin connection is essential. It is essential to have high somatostatin release as well as low GHRH between the pulses in order to get the periods of very low GH release. The motivation for adding the GH-GHRH connection at this stage is to find a more self contained method of producing the pattern of input required by the GHRH neurons. In order to match the appearance of real GH profiles, the model needs input pulses that are separated by much longer intervals then would normally be expected from a triggering input coming from another part of the brain. A possible candidate for producing this pulse interval might

be an inhibitory input triggered by GH. The interval between GH peaks appears to match their duration, determined mainly by the half life of GH in the bloodstream.

4.5.1 Implementing the GH-GHRH Feedback Component

The new component uses a similar form to the mechanism by which somatostatin inhibits GHRH. A new Hill equation, hr_{act}, gives a measure of the GHRH inhibition due to GH :

$$hr_{act} = 1 - \frac{h^{n_5}}{h^{n_5} + th_5{}^{n_5}}$$

The new parameters n_5 and th_5 give the Hill coefficient and threshold and were initially set to the same values as those used for GH feedback at the somatostatin neurons to give $n_5 = 2$ and $th_5 = 30$. The new equation is integrated into the GHRH equation so that it can directly modulate release activity :

$$\frac{dr}{dt} = r_{act} hr_{act} I_r - k_6 r$$

Similarly to the new GHRH-somatostatin connection, the new component was set up in the model software so that it could be switched on and off for comparison. The model was tested using the standard set of parameters, and without the GHRH-somatostatin connection.

4.5.2 Testing GH-GHRH Feedback

The goal for the new connection is to be able to replace the pulsed external input to GHRH. Even if it is capable of producing the required pattern of modulation, it is likely that there will still need to be a level of input activity, perhaps a constant high input similar to that used with the somatostatin neurons in the model. In the first

instance the new connection will be tested with the normal pattern of GHRH input to see how it can work with the current form of the model. The aim is that it should be able to override the external pattern of input pulses and change the form of the GH bursts.

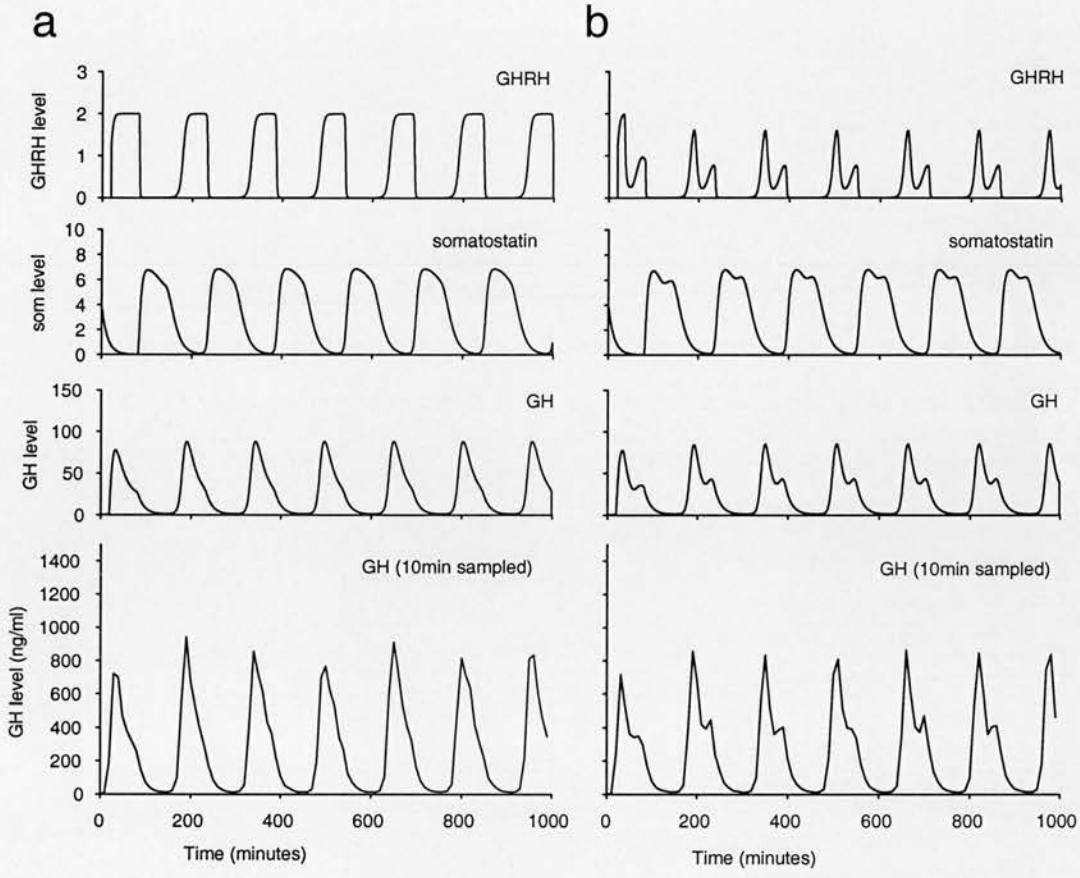

Figure 4.5 : **a**. GHRH input at constant level, pulsatile GH release continues with reduced cycle length (152min); **b**. first attempt at using GH-GHRH feedback, after delay GH peak inhibits GHRH producing two peaks within each GHRH pulse and corresponding GH release (n_5=2, th_5=30, delay2=15) (pulse cycle=158min)

For the first test the new component was set up with parameters as specified above, running the model with regular input pulses to GHRH. The only effect of adding the new connection was to reduce the size of the GH pulses. With an immediate feedback effect the individual pulses just work to inhibit themselves. Testing with a constant level of GHRH input, instead of regular pulses, still produces

the pattern of 3h pulses of GH release, but the pulses consist of one long period of sustained release with no individual peaks. The obvious problem is that there needs to be a delay in GH feedback, similar to the delay used for feedback at the somatostatin neurons. This makes sense biologically as a similar process that is responsible for at least part of the somatostatin delay is also likely to affect feedback to the GHRH neurons. However, if the GH-GHRH feedback effect is to be used to form the local structure of the GH pulses then the delay will need to shorter, probably in the same 15-30min range determined for the external input pulses. The equation for the new component was altered to give it the following new form :

$$hr_{act} = 1 - \frac{h_{delay2}{}^{n_5}}{h_{delay2}{}^{n_5} + th_5{}^{n_5}}$$

The new value, h_{delay2} gives the value for h (the GH level) at a previous time point, specified by the parameter delay2. This was initially set to 15min. In the first test with the delay, the model was given regular GHRH input pulses at matching 15min intervals. This produced a similar result to using no delay, with the delayed inhibition effect working on the following GH pulse, although it did have some effect on the relative heights of the individual peaks, tending to make the later ones in the burst smaller. It was clear at this stage that attempting to test the new component alongside the existing input pattern added too much extra complication and so the input pattern was set give a constant high input, the same as that used with somatostatin.

For a first control test, the model was run with constant GHRH input and no GH-GHRH connection. The model continued to produce a pulsatile pattern of GH release, but GH pulses consisted of just one large peak of GH release, with a shorter pulse cycle length of 152min (figure 4.5a). GHRH release corresponding to each pulse consisted of just a single period of constant high release, lasting for approximately 60min. For the next step, the GH-GHRH connection was added in, with parameters n_5=2, th_5=30 and delay2=15. This immediately had some success, producing a smaller second peak in GHRH release, and a corresponding small second peak in the GH pulse (figure 4.5b). The pulse cycle was slight increased to

158min. The change in GHRH inhibition was too gradual to produce sharp pulses of GHRH release and so the parameters for GH-GHRH feedback were adjusted to try and produce sharper inhibition of GHRH. Reducing th_5 to 20 and increasing n_5 to 4 produced two distinct pulses of GHRH for each pulse and a much more distinct second peak within the GH pulse. The cycle length was again slightly increased to 162min. This improved further by increasing n_5 to 8, producing a very switch like inhibition of GHRH and a larger second peak in the GH burst, though still smaller than the first. The cycle length increased to 164min. More changes to the parameters did not produce any significant change in the form of the GH pulse.

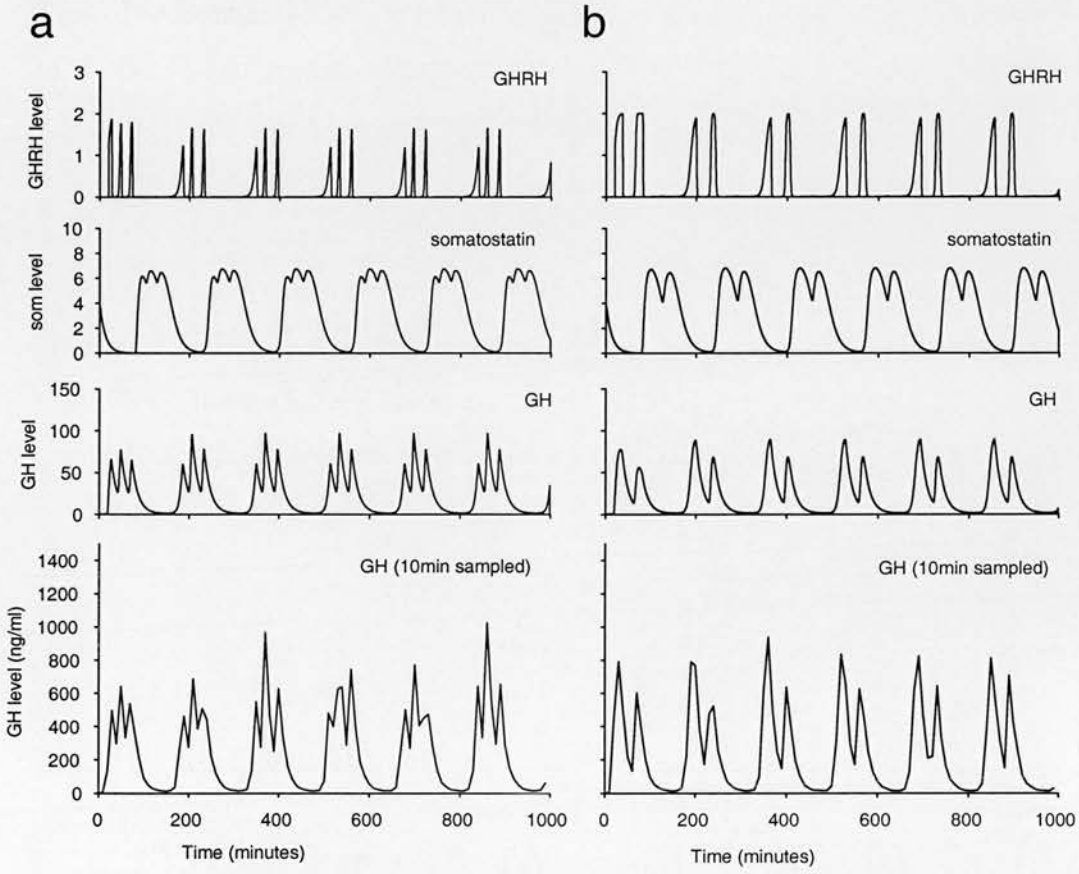

Figure 4.6 : **a**. steeper gradient on GH-GHRH inhibition produces sharper GHRH pulses, producing well defined individual peaks within each GH pulse (n_5=16, th_5=30, delay2=5); **b**. increasing GH-GHRH feedback delay reduces the number of peaks (n_5=16, th_5=30, delay2=15)

The next stage was to test the effect of changing the delay length, delay2. This began with parameters n_5=8 and th_5=20. Decreasing delay2 to 5 min produced 3 peak bursts of GH release, but the peaks were small and the pulse cycle length was reduced to 150min. Further increases in n_5 made the individual peaks much larger, with the second peak usually the largest in the un-sampled data, and also increased the cycle length. After increasing n_5 to 16, the middle peak began to dominate the pulse, with the third peak becoming smaller until it disappeared at n_4 =22. At the same time the reduction in the third peak reduced the effect on somatostatin feedback and reduced the pulse cycle length. At n_5=16, th_5 could be increased to 30 to produce larger to GH peaks and a longer pulse cycle (164min), but further increases in th5 moved the peaks closer together and reduced the pulse cycle length.

Increasing delay2 to 10min (n_5 = 8 and th_5 = 20) returned the pulse to two distinct peaks of GH release, although, unlike the 15min delay, the second peak tended to be the largest. Increasing n_5 and reducing th_5 produced a very large second peak and a corresponding long cycle length of over 170min. Increasing delay2 to 20min produced a GH pulse with only a very small second peak and shorter cycle length (148 min with n_5=8 and th_5=30).

For further testing, the two Hill equation parameters were fixed at n_5=16 and th_5 = 30 since these values produce GH pulses with a good resemblance to real data with each of the values for delay2. The model's GH output with these parameters and delay2=5 and delay2=15 is illustrated in figure 4.6. With both delay2=5 and 15min the pulse cycle length can be returned to over 180min by reducing s_{r2} to 0.004 or by increasing the GH-somatostatin feedback delay to 75min. The sampled model GH profiles with the GH-GHRH feedback connection using these parameters give a good match to real data, except for having too regular a form to the GH pulses, which in real data vary in the number and heights of GH peaks. One way to solve this problem is to replace the constant level of GHRH input with frequent randomly timed input pulses, such as a mean 5min interval with no refractory period. With no GH-GHRH feedback this produces correspondingly frequent GH pulses, which in the sampled data appear as a single long peak of GH, but the feedback component can act to enforce longer, fewer, more distinct pulses of GH, with GH bursts ranging from two

to four peaks in the data (delay2 = 5) processed through 10min sample intervals (figure 4.7). Using higher values for delay2 (10 or 15) produces GH bursts with usually two, and occasionally, three peaks.

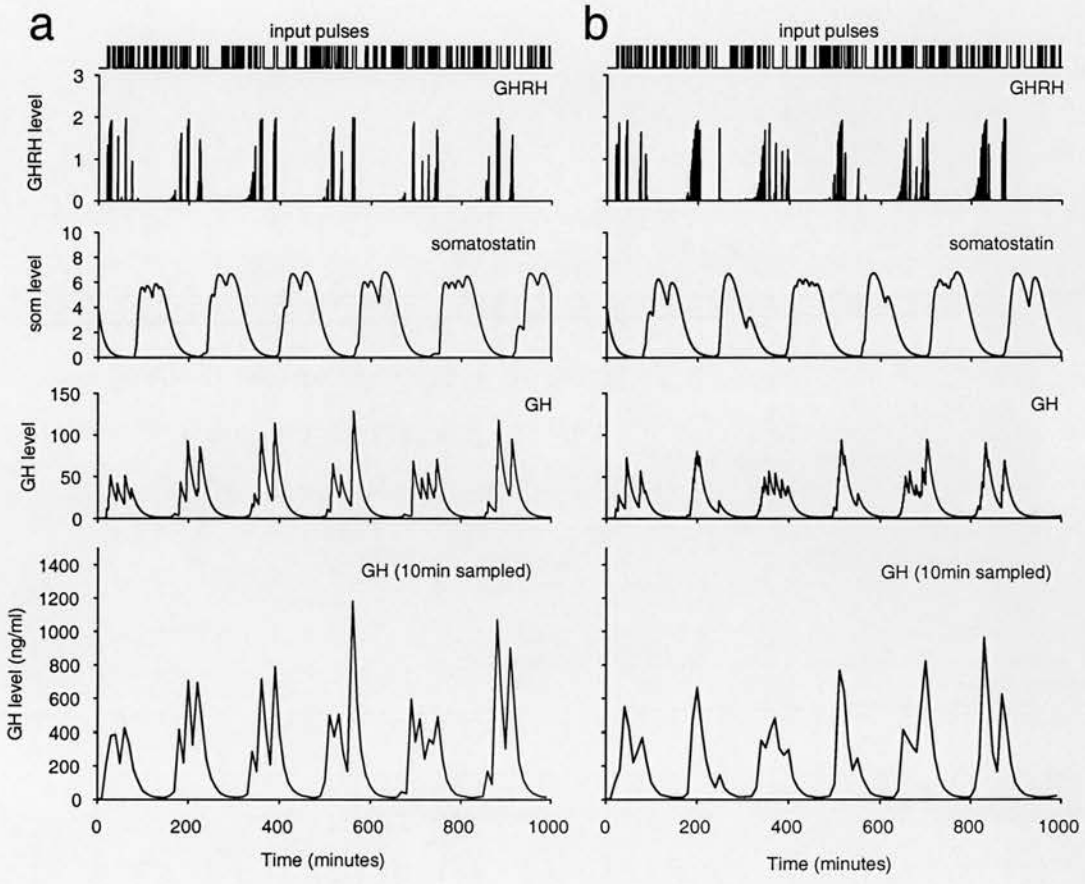

Figure 4.7 : Mixing short mean interval (5min) random GHRH pulses with GH-GHRH feedback; **a**. 5min feedback delay, produces 2 to 4 peaks within each pulse; **b**. 15min feedback delay, usually 2 and occasionally 3 peaks within each GH pulse

4.5.3 Conclusions

Given the useful role that the GH-GHRH feedback component plays in the model, and the physiological evidence for such a connection, it seems likely that this may be a part of the real system. Experimenting with the model's sampled output in comparison with real data indicates that there needs to be an average interval

between GHRH input pulses (or release triggering activity in general) of at least 15min. Even if the system does not rely on this input being regular, it is unlikely that there could be an external input that could fulfil this criteria without having a specific pulse generator. Adding the new feedback component to the model gives the system its own pattern generator for GHRH activity and makes it more self-contained, one of the original goals of the modelling. However, the irregularity of real GH release profiles still suggests that the model needs a random element in driving the GHRH pulses. The irregular pattern is evident even on a very long timescale and the relatively small errors in sampling are not sufficient to reproduce this pattern. Adding a high frequency randomly timed input to GHRH, which is regulated by the GH-GHRH feedback connection, allows the model the produce a more irregular pattern of GH release which gives a closer resemblance to real data.

The parameters used with the new connection use very high Hill coefficients, values which specify a much sharper change in the activation level than would normally be produced by a simple biological mechanism. The high values are required in order to reproduce the fairly sharp peaks observed in real GH release data. These require sharp pulses of GHRH, and a more gradual change in GH feedback inhibition cannot produce these.

4.6 Simulating Real Experiments

An important test of the model, after reproducing normal function in the system, is to be able to reproduce the results of *in-vivo* experiments where substances are administered. If the model is able to reproduce these results then it will provide more validation of the model and also help to interpret the real experiments. If the model does not match the results then the conclusion will depend on the particular instance, but it may suggest that the model's behaviour needs to be altered to better represent the real system. The experiments to be used here include those where the three substances, GHRH, somatostatin and GH itself, are manipulated, either by injection or infusion, or blocking endogenous content using antibodies. The first stage in doing

this is to alter the model so that the artificial addition or removal of these substances can be simulated.

4.6.1 Implementing Artificial Substance Control

For the purpose of simulating *in-vivo* experiments, the input protocol system was updated and extended. A separate GHRH input pulse protocol was added, to replace use of the general GHRH input protocol, and the original GHRH protocol was returned to a form where it can control the GHRH variable independently of other influences. The new GHRH equation is given below :

$$\frac{dr}{dt} = r_{act} hr_{act} I_r - k_6 r + I_{r2}$$

The input pulse protocol controls the value I_r and the general GHRH input protocol controls I_{r2}, with its own input rate parameter. Since development of the full hypothalamic model, somatostatin has been given a constant input and so this was replaced in the somatostatin equation by just a constant value, the somatostatin release rate parameter (here denoted s_p). It is uncertain whether exogenous somatostatin acts at the hypothalamus or just at the pituitary, and so the model was set up to allow testing of both alternatives. Simulating action at just the pituitary was more complex because the model needs to maintain separate levels for exogenous and endogenous somatostatin, summing the two for pituitary actions. To do this, a new variable was added to the model, s_e, using the same form as the somatostatin equation in the pituitary model. The input value I_s was left in the main somatostatin equation for simulating the alternative mechanism. The new equations are given below :

$$\frac{ds}{dt} = s_p s_r - k_7 s + I_s$$

$$\frac{ds_e}{dt} = I_{s2} - k_7 s_e$$

The final change was to add a similar general input protocol for GH, controlling the new value I_{gh}. This gave the following new GH equation :

$$\frac{dh}{dt} = [k_4 + k_5(1 - \Phi(s))][r + c]f - k_8 h + I_{gh}$$

The general input protocols use the same form as the original versions in the pituitary model, but because they are summed with other components, they no longer entirely control input to their variables. Instead, they add some quantity, specified by the input rate parameters to the variable at specified time points, defined by the input protocol. In this way they perform the same function as an artificial injection or infusion.

Experiments which add antibodies for a substance to the system can be simulated by increasing the substance's clearance rate (reducing half-life) in the model. This is fair way of simulating this effect in the model since this is essentially what the antibodies do, eliminating the substance after release, rather than blocking release in the first place.

4.6.2 Simulating GHRH Injections

For these experiments the model was set up using the standard set of parameters and tested using three different forms for GHRH input; regular GHRH input pulses, random input pulses and GH-GHRH feedback. In the real experiments where GHRH injections are given, the exogenous GHRH is usually at a concentration sufficient to produce a maximal GH response, and usually produces larger GH pulses than those normally observed. The GHRH input rate used for GHRH input pulses in the model is currently $I_r = 10$. This is sufficient to produce large GH pulses but is not maximal. According to the scaling experiments with the pituitary model, the large 1μg injection used in *in-vivo* experiments is equivalent to a 1000 unit input rate in the model. The GHRH-GH dose response curve follows a logarithmic scale and so 1000 units produces roughly five times as large a GH response as 10 units, without the

presence of somatostatin. During normal function of the model, with somatostatin in the system, giving an artificial pulse of GHRH and increasing I_{r2} from 10 to 1000 units only produces a 200% increase in GH pulse height. The effects of sampling further reduce the difference in pulse height. These differences in pulse height appear to match those observed in real data (Clark and Robinson 1985a) and so for experiments with the model GHRH input was kept fixed at 10 units, and injections use a rate of 1000 units.

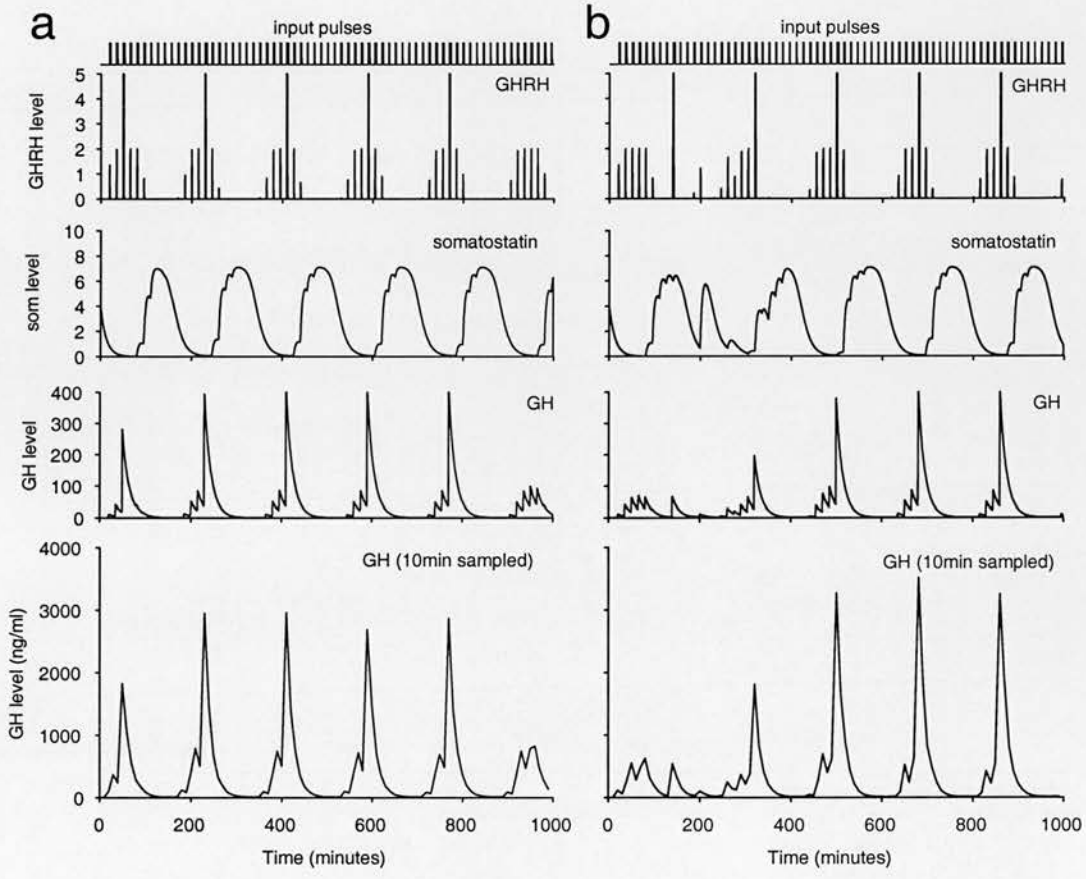

Figure 4.8: **a**. 180min interval GHRH injections (I_{r2}=1000), synchronised with exist GH pulses, produces large GH peak which dominates existing pulse; **b**. 180min injections 90min out of phase with existing GH pulses, release initially disrupted, then after two injections, release synchronises with injections

For the first test, the model was given 3h injections of GHRH, timed to either fall during normal GH pulses or during the low GH release periods. With regular GHRH

input pulses (15min interval), the injections during the GH bursts created a much larger pulse of GH release, dominating the pulse and appearing as a single peak in sampled data (figure 4.8a). Injections timed to fall between normal pulses initially produced irregular GH output but after the first two pulses there was a normal GH pulse and then all following pulses synchronised with a large GH peak in response to the injection and smaller pulses of GH release generated by normal GHRH activity (figure 4.8b). The effects using randomly timed GHRH input pulses were similar. Testing with constant GHRH input and GH-GHRH feedback also produced similar results, although with a smaller increase in GH peak height and retaining multiple GH peaks within the GH burst. The longer duration GHRH pulses produced by GH feedback control drain f (pituitary GHRH sensitivity) to a lower value so that there is less capacity to produce larger pulses of GH release. The lower ability to respond to GHRH is also why the pulses retain their multiple peaks, with the injection triggered peak unable to dominate. Replacing the constant GHRH input with frequent random input pulses produced similar results to those without GH-GHRH feedback, although still with more pulses showing multiple peaks.

These results are a good match to the equivalent real experiments (Clark *et al* 1986) where 3h injections of GHRH produce GH pulses with a large central peak and, if given out of synch with endogenous activity, cause the system to train to the new pattern. This was one of the most important pieces of evidence for feedback in the system, and the model's ability to reproduce this is an important validation for its design. In other experiments (Clark and Robinson 1985c) GHRH was injected at more frequent intervals and produced a more varied response, with the system continuing to follow the pattern of 3h responsiveness, although sometimes producing smaller responses to the injections falling between the dominant release periods.

For the next test the model was run with injections of GHRH at 90min intervals. Testing with no GH-GHRH feedback and regular GHRH input pulses produced a pattern of extended GH bursts, separated by a very short quiet period. The pulses continued to follow the three hourly pattern but the large extra pulse of GHRH, out of synch with the main pulse produced an extra peak of GH release, making the pulse much longer (figure 4.9a). The timing of the pulses entrained to peak with every

second injection. The peaks were also smaller than the large ones observed with the injections at 180min intervals. Somatostatin remained high during the second GHRH injection in each pulse cycle but the inhibition at the pituitary was insufficient to block release by the large dose GHRH injection. In real experiments there is a large GH response to every second injection, with the alternate ones producing only a very small pulse of GH. This difference could be due to the fitted somatostatin inhibition in the pituitary model being too weak compared to the real system and so the dose rate of the GHRH injections was reduced. This reduced the size of the second peak, but still did not produce the very small response observed in real data. Testing with random GHRH input pulses produced similar results. The same test was repeated after adding GH-GHRH feedback back into the model but this still produced the long pulses with a GH peak in response to both GHRH injections within the 180min cycle periods.

Adjusting the Pituitary Model

In the pituitary model the GH equation has a release component which is relative to the GHRH level but not modulated by somatostatin. This component is scaled to produce much lower levels of release than the somatostatin modulated component, but with the very high levels of GHRH the model is exposed to, simulating the injections, this component produces a large release of GH. Before the model was tested with injections of GHRH, all of the GHRH in the system was also inhibited by somatostatin in the hypothalamus. The injections are not subject to this inhibition and this is the first time that the model has had to be able to suppress GH release using just somatostatin inhibition at the pituitary. Inhibition at the pituitary was tested during the model's development, but not with such high doses of GHRH. The real results (Clark and Robinson 1985c) show the system producing almost no response to the large dose injections of GHRH, when they fall during the period of high somatostatin release, suggesting that high levels of somatostatin at the pituitary should be sufficient to almost entirely block GH release. On this basis it was decided

to experiment with the pituitary model's parameters which control GH release, particularly k_4, which gives the level of release which is not modulated by somatostatin.

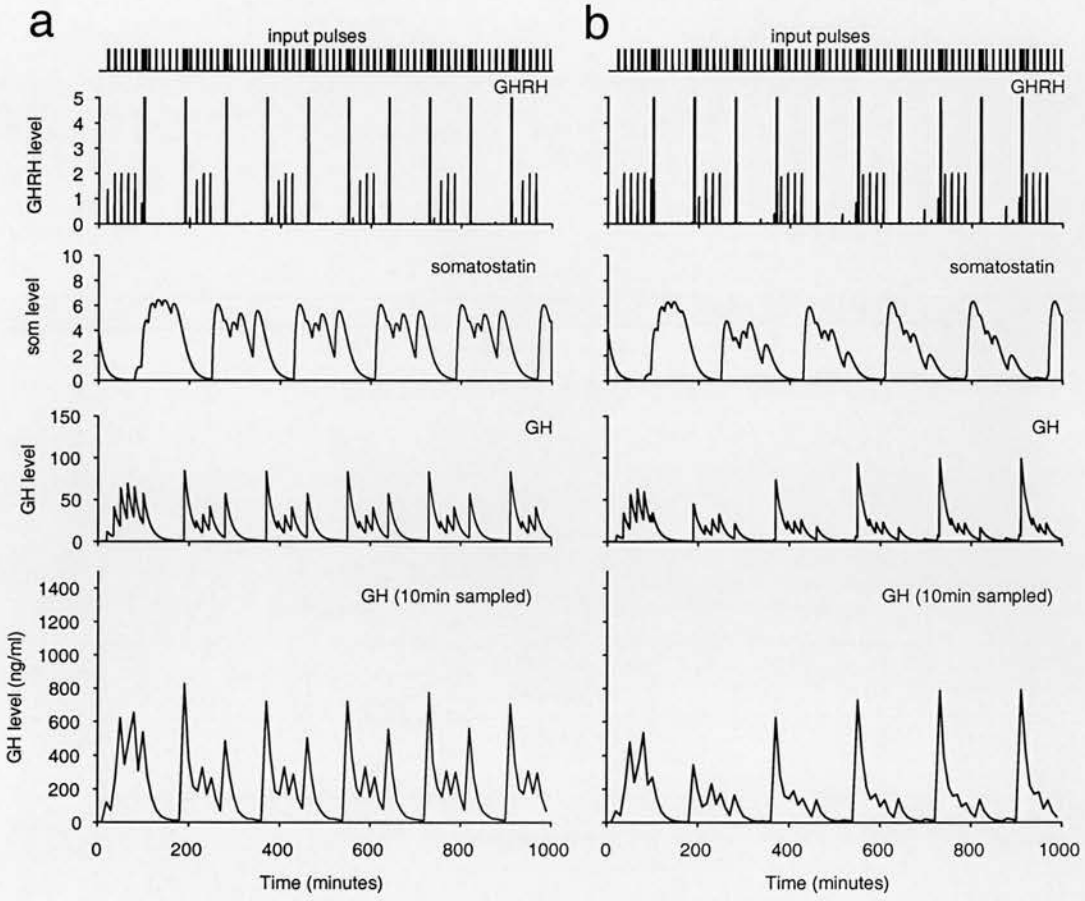

Figure 4.9 : **a**. 90min interval GHRH injections (I_{r2} = 1000). Some disruption before pulses synchronise with injections, then large response to both injections in each 180min pulse cycle, creating extended pulse with short low GH release period. Second injection in pair falls during high somatostatin, but insufficient inhibition at pituitary (k_4=9); **b**. non-somatostatin modulated GHRH-triggered GH release reduced (k_4=2), much smaller response to second injection in each pair, similar to result in real experiment, but smaller peak GH in pulse.

To test this, k_4 was reduced from 9 to 2 units and the model was tested first with no injections of GHRH. The heights of the GH peaks were slightly reduced, but the pattern of GH bursts and the peaks within them was not changed. GHRH injections

were then added and the model produced a pattern of release with a much closer resemblance to the real data. The GH response to the second injection in each pair was much smaller, making the response to the injection during the main pulse larger, with the reduced second peak no longer causing depletion of pituitary GHRH sensitivity and higher somatostatin levels (figure 4.9b). The model was tested further using injections of GHRH at 40min intervals. With the normal pituitary model parameters 3h GH pulses were lost, with the model producing regular single GH peaks in response to each injection (figure 4.10a). It was necessary to reduce k4 to 0.5 and also to strengthen somatostatin's inhibition of GH release at the pituitary by reducing delta1 from 0.3 to 0.2. This produced a good match to the real experimental results (figure 4.10b).

Conclusion

Overall the model worked well in reproducing these experiments but it has forced the pituitary model to be re-examined at a late stage. The current model is unable to reproduce the real system's ability to block the response to high dose injections of GHRH. The non-somatostatin modulated component in the pituitary model's GH release equation allows too high a rate of release, and it appears that this part of the pituitary model needs to be changed, in order to give a better simulation of the real system. Before this point in testing, where GHRH was also subject to central inhibition in the hypothalamus, the model did not require such strong inhibition at the pituitary and so if this change, reducing the value of parameter k_4, had been made earlier, it would not have had a significant effect on the previous results. Testing this here, with the model's normal behaviour showed only a small reduction in the height of GH peaks, with no change to the overall pattern of release. The case for blocking GHRH at both the hypothalamus and the pituitary remains, since the two levels of inhibition produce a more switch like change in GH release levels, and also block basal GH release due to constitutive activation in the GHRH-GH release pathway at the pituitary.

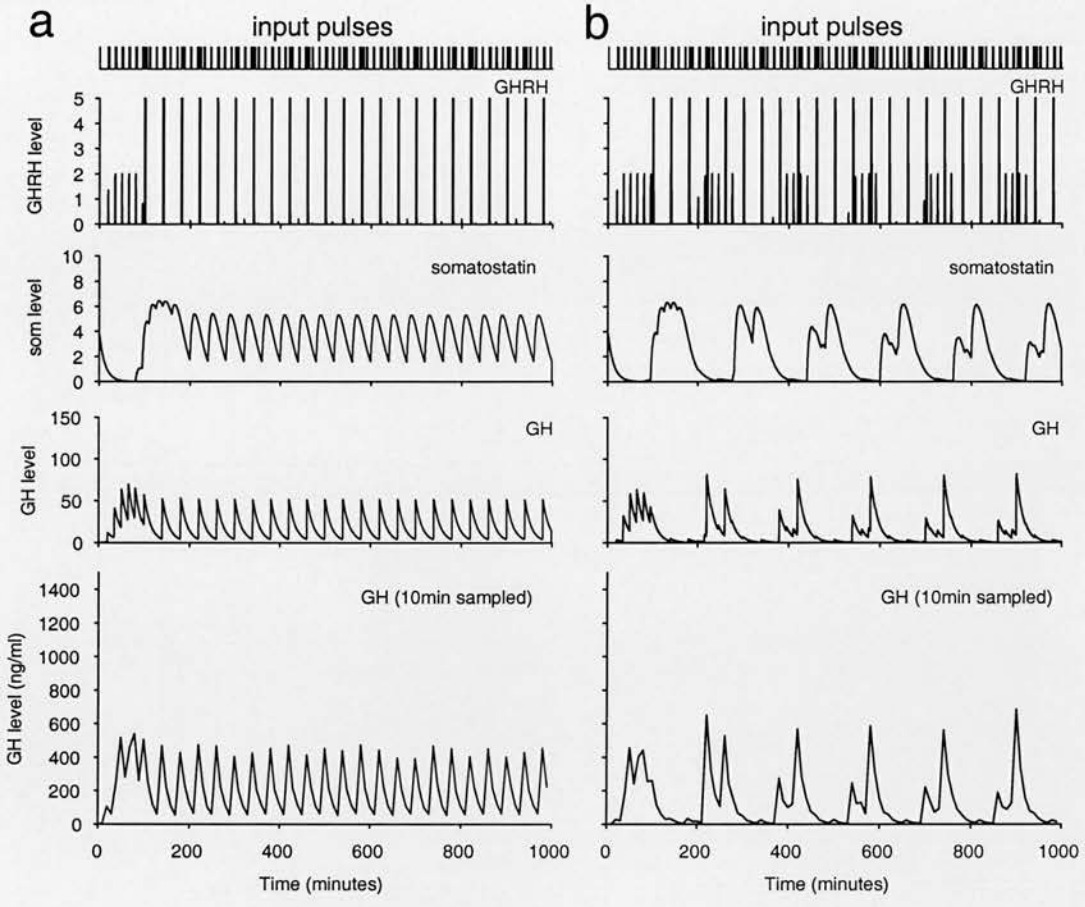

Figure 4.10 : **a**. 40min interval GHRH injections (I_{r2}=1000). Normal GH pulses lost, GH peak in response to each injection (k_4=9, δ_1= 0.3); **b**. pituitary model parameters adjusted to reduce non-somatostatin modulated GHRH triggered GH release (k_4=0.5) and increase somatostatin inhibition of GH release (δ_1= 0.2). Large GH response to only every fourth injection, smaller response to preceding injection, similar to result in real experiment

4.6.3 Simulating Somatostatin Infusions

Giving a high dose (50μg/h) infusion of somatostatin almost entirely blocks GH release in the male and female rat (Clark *et al* 1988a), with only occasional detectable levels of GH in blood samples. With a lower dose infusion (10μg/h), which is likely to be closer to endogenous levels of release, there is some response to high dose (1μg) injections of GHRH, but still producing very small pulses of GH

release, no higher than 100ng/ml. The lowest dose somatostatin infusion in the experimental results referenced here is 1μg/h, given to male rats (Clark *et al* 1988a). At this dose there is still GH release, although at reduced levels, and without the distinctive pulsatile pattern, almost resembling the female pattern of release.

Following the somatostatin infusion there is large rebound release of GH, producing a very high GH peak. This rebound is almost entirely knocked out when animals are given anti-GHRH serum and must be to be due to either an increased ability to respond to GHRH, or a large release of GHRH triggered by hypothalamic action of somatostatin. The latter was the basis for using the rebound to trigger release in the first version of the model, but it is probably the least likely of the two explanations. It would require that exogenous somatostatin is somehow transported into the hypothalamus, which although possible, is considered unlikely. But the best argument against this is that a large release of GHRH alone, such as the high dose injections of GHRH, is insufficient to produce the very large rebound. The sensitivity to GHRH at the pituitary and the ability of somatostatin the increase this factor makes this the more likely explanation.

The aim here is to attempt to reproduce these results with the model, and to use the model to further suggest which mechanisms are most likely to be responsible for these effects. Some of the experimental results are from female rats and this will provide a test of the different methods used to reproduce the female pattern of release with the model.

For the tests here the model was set up with GH-GHRH feedback switched on (delay2=5, n_4=16, th_4=30), with random input pulses (mean interval 5min, no refractory period). The first experimental data for comparison is figure 1 in (Clark et al 1988a). This shows the GH rebound in male rats given a 4h high dose (50μg) infusion of somatostatin. The model was set up to reproduce this experiment with I_{s2}=50, high enough to almost totally block GH release. For the first test the model was switched so that the exogenous somatostatin only acted at the pituitary (figure 4.11a). This immediately demonstrated the same problem with non-somatostatin controlled GH release, as seen with the GHRH injection experiments. Parameter k_4 was reduced to 1 and this solved the problem, producing very low levels of GH

release during the somatostatin infusion (figure 4.11b). However, there was no apparent rebound GH release following the somatostatin infusion. Although GH release is blocked during high somatostatin, pulses of GHRH continue to reduce sensitivity to GHRH. Switching the model to allow exogenous somatostatin to act at the hypothalamus and block GHRH release, as well as GH release at the pituitary, allows the sensitivity to GHRH to charge up at the pituitary.

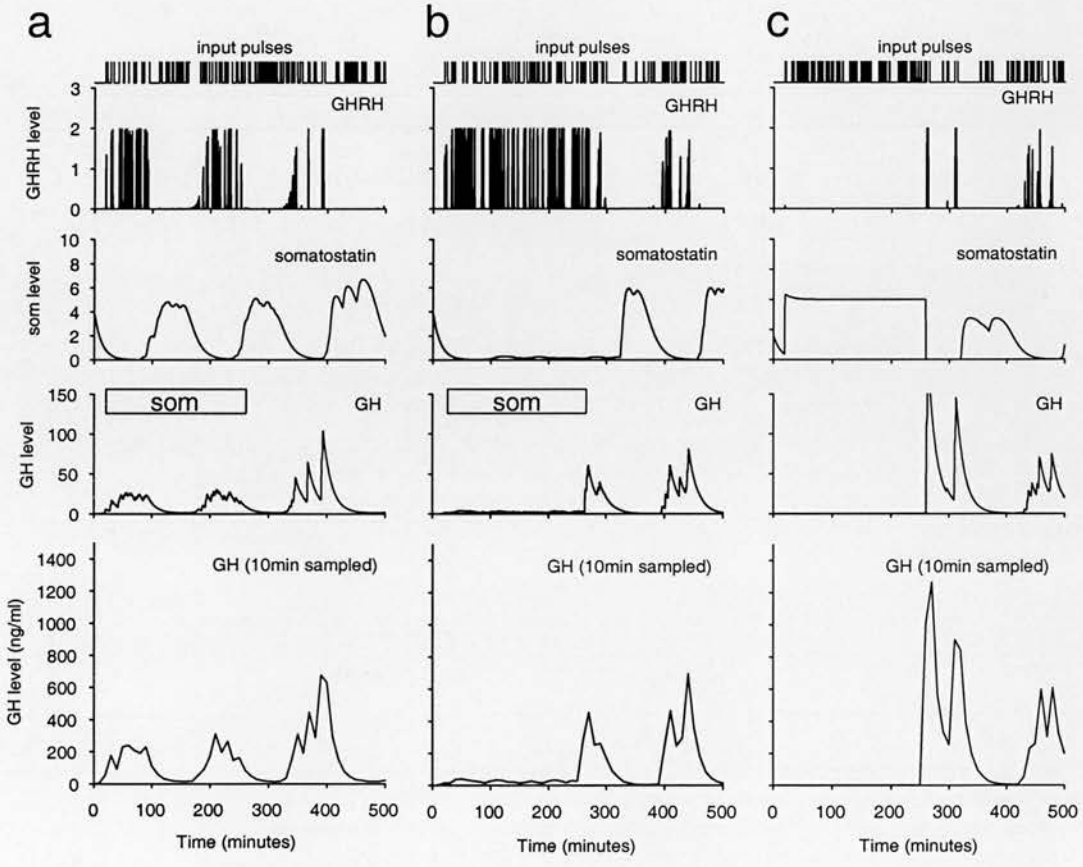

Figure 4.11 : **a**. somatostatin infusion only acting at pituitary, high dose unable to block GH release (k_4=9, I_{s2}=50); **b**. pituitary non-somatostatin modulated GHRH triggered GH release reduced (k_4=1, I_{s2}=50), now get almost total block of GH release during infusion, but no large GH rebound release after withdrawal; **c**. somatostatin infusion acting at pituitary and hypothalamus, GH release completely blocked during infusion, large rebound GH release following infusion.

This successfully produced a large rebound release of GH following the somatostatin infusion (figure 4.11c), with a good resemblance to the real experimental data.

The second real experiment to be simulated is figure 5 in (Clark *et al* 1988b). Here female rats were given a similar long infusion of somatostatin, but also with injections of GHRH. The results are similar, a GH peak in response to each injection, with the first injection following the infusion producing a much larger rebound GH pulse. The model was set up to produce female release behaviour by reducing s_{r1} to 0.07 and with exogenous somatostatin set to act at the hypothalamus. Figure 4.12a shows the model at this stage, producing a female release pattern. Parameter th4 was reduced to 20, to give more distinct pulses of GH with the lower levels of GH release. For the next test an infusion of somatostatin was added, timed to match the real experiment. This successfully produced a rebound release of GH following the infusion, similar to the model simulating the male rat (figure 4.12b). Finally, GHRH injections were added (at maximal dose, input rate = 1000) matching the real data's timing (9 injections at 45 minute intervals, with 2 injections before the somatostatin infusion). The model produced slightly larger responses to GHRH during the somatostatin infusion than the real experiment but the pattern of GH release was otherwise very similar, with a larger GH peak at the end of the infusion followed by two smaller responses to the following injections (figure 4.12c). The tests here were repeated with the alternative method of producing female behaviour by reducing srmax to 0.5, but the results were very similar.

These successful results further validate the model's ability to reproduce the behaviour of the real GH system. They also give evidence to suggest that artificially administered somatostatin acts at the hypothalamus, since the model is unable to reproduce the rebound otherwise. Without hypothalamic action, GHRH release continues to desensitise the pituitary's response and there is no priming effect from the prolonged high levels of somatostatin to produce the large GH rebound. It was attempted to use the model to test the alternative idea of the GH rebound being due to a GHRH rebound, but because the model was already producing a rebound effect with exogenous somatostatin allowed to act centrally, there was no way to test this properly. Disabling the components which allow the pituitary generated rebound

would change the model too much. The fact that the pituitary system is already capable of producing the rebound (in conjunction with hypothalamic GHRH release) is evidence against the need for a hypothalamic system.

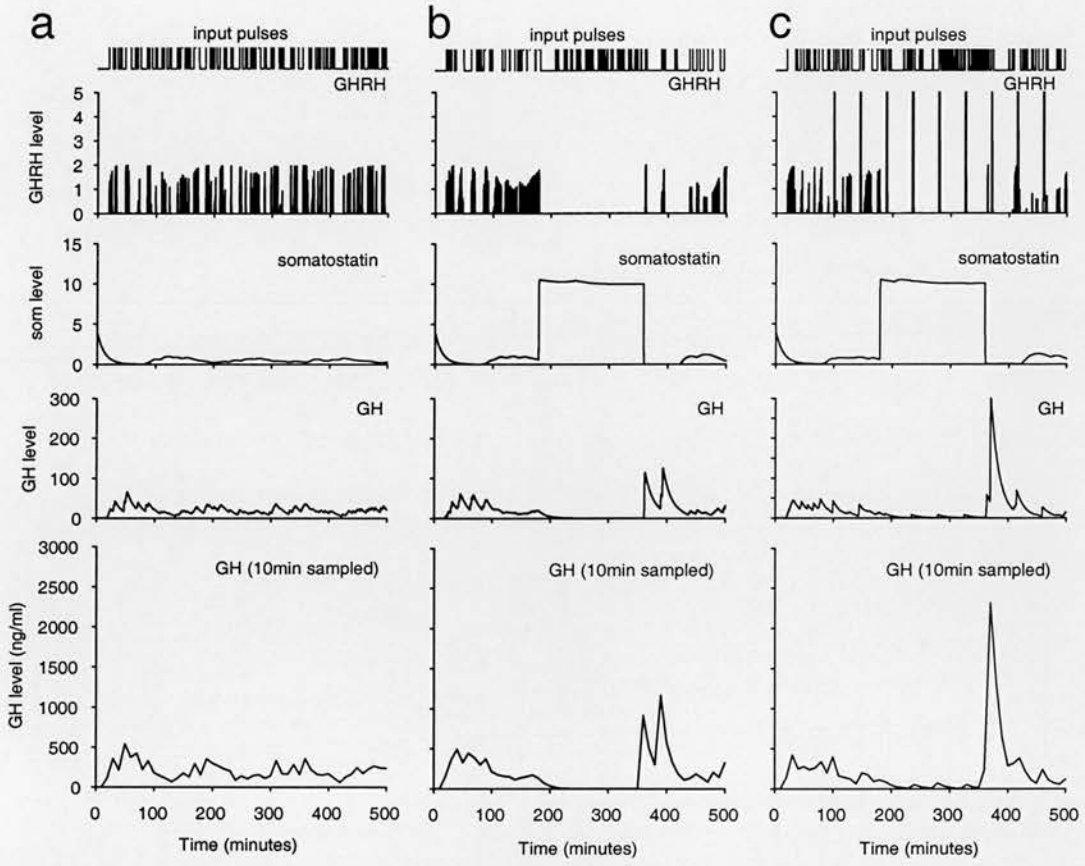

Figure 4.12 : **a**. female release pattern produced by reducing s_r charge rate (s_{r1} = 0.07); **b**. somatostatin infusion (with hypothalamic action) (I_s=50), all GH release blocked during infusion, period of very low somatostatin after infusion with rebound GH pulse; **c**. 45min interval GHRH injections (I_{r2}=1000), very small GH responses during infusion, period of low somatostatin and large GH rebound pulse in response to first injection after infusion, good match to real experiment (Clark et al 1988b figure 5); (k_4=1)

4.6.4 Simulating GH Infusion and Injections

Infusing human GH in the male rat produces an inhibition of GH release, with only very small responses to GHRH injections. There is however usually a delay on

the order of 1h before the rat stops responding to GHRH after the start of the infusion (Carlsson et al 1990 figure 2a). The model was used to attempt to reproduce this experiment. Pituitary model parameters were set up to allow somatostatin to almost fully block GH release (k_4=0.5, δ_1=0.2). GH-GHRH feedback was switched on with random 5min mean interval GHRH input pulses. The model was given 45min interval maximal dose injections of GHRH timed to match the real experimental data (figure 4.13a). GH pulses synchronised to the injections, producing large 2 peak GH pulses and only a very small response to injections during high somatostatin release.

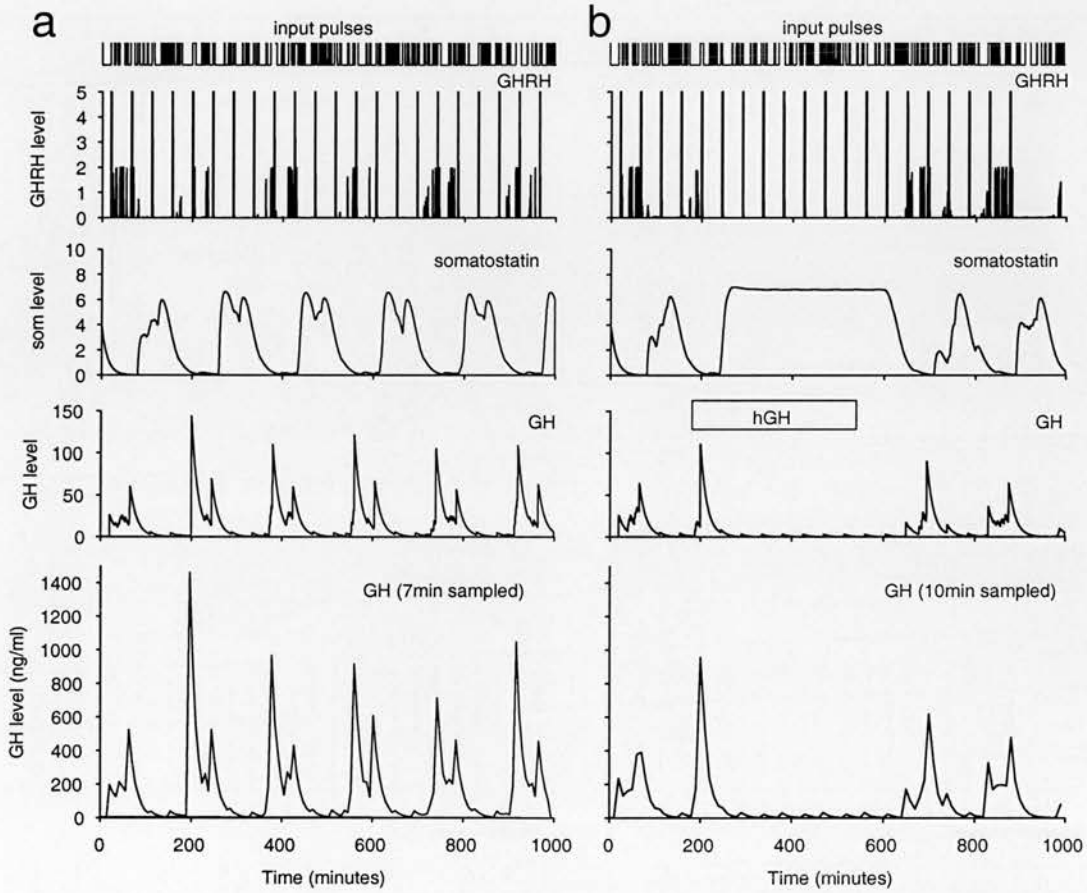

Figure 4.13 : Simulating GH infusion and GHRH injections in male rat; **a**. 45min interval GHRH injections, produces large 2 peak GH pulses; **b**. 6h GH infusion, timed to match real experiment, get 1 injection response during infusion and then only very small GH responses to each injection, normal response recovers after a delay following the end of the infusion; (GH-som feedback delay=60min) (k_4=0.5, δ_1=0.2)

Next, the 6h GH infusion was added, timed to match the real experiment. The first GHRH injection after the start of the infusion still produced a large GH response, due to the 60min GH-somatostatin feedback delay. For the rest of the infusion, and for a period afterwards, matching the delay, GH release was almost entirely blocked with only very small responses to each GHRH injection. After the delay at the end of the infusion, the injection response recovered (figure 4.13b).

The result with the model is a very good match to the real experiment and suggests the result is due to the infused GH inhibiting endogenous somatostatin release after a long delay. In the real experiment, the second GHRH injection after the start of the infusion (approximately 60min into the infusion) still produces a GH response, suggesting that the feedback delay in the real system is at least 60min.

The final experiment tested with the model, gives male rats injections of hGH, following varied time patterns (Carlsson and Jansson 1990). Injections give a closer approximation of endogenous GH release. They showed, that in a similar manner to GHRH injections, endogenous GH secretion, after 2 or 3 pulses, synchronises with the 3h injections. They also showed how the pattern could be disturbed by shifting the phase of the injections or doubling the frequency to 90min intervals. The model set up with the new pituitary parameters (k_4=0.5, δ_1=0.2), GH-GHRH feedback (5min delay) and random 5min mean interval GHRH input to test all three of these results. The GH injections in the model were simulated by short 3min infusions at input rate I_{gh}=10, set to give a comparable response to the real experiments. In the first test, the model was given 4 180min interval GH infusion. The first GH infusion was followed by a large GH peak after a slight delay. Following GH pulses gradually synchronised until the GH pulse was already rising slight before the GH infusion (figure 4.14a). This is a good match to the real experimental result (Carlsson and Jansson 1990 figure 2). The next test gave four infusions, with the second pair 90min out of phase with the first pair. The first two produced similar GH responses. There was no response to the third GH infusion and there was GH pulse already rising at the fourth infusion (figure 4.14b). The real data shows similar results, but a smaller response to the fourth infusion and then very little GH release for the rest of the experiment (approx 4h). The model in contrast produced a large GH pulse 3h after

the last infusion and then returned to the normal release pattern. In the final test the model was given 7 GH infusions at 90min intervals. The first infusion produced a fairly large GH pulse response. Following that, there was a small GH pulse following every second GH infusion, and no response to the others. The results in the real data are less clear, but show a similar pattern of GH pulses following every second infusion.

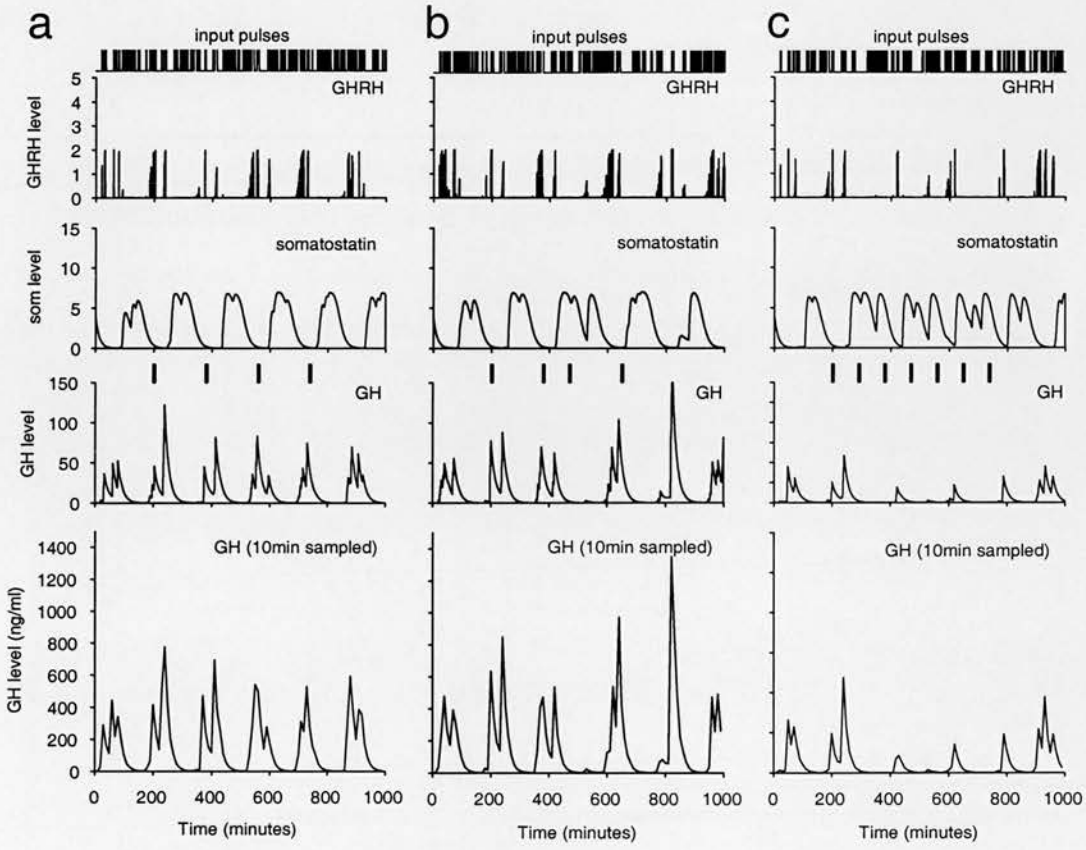

Figure 4.14 : **a**. 180min interval short (3min) GH infusions. GH pulses gradually synchronise with infusions, later pulses already rising before the infusion; **b**. second pair of GH infusions 90min out of phase, no response to third infusion, early response to fourth infusion, followed by another large GH pulse, not observed in the real data, probably random coincidence of two GHRH pulses in quick succession; **c**. 90min interval short GH infusions, GH response to first infusion, followed by small responses to every second infusion, following normal 180min responsiveness, eventual return to normal release pattern; (cf (Carlsson and Jansson 1990) figure 2, 3 and 4); GH infusions are indicated by short lines above the non-sampled GH profiles.

Based on the model, the effects of the infusions appear to be a combination of GH's feedback on GHRH and somatostatin. The inhibitory GH-GHRH feedback is probably responsible for the slightly delayed GH response to some of the infusions, temporarily inhibiting GHRH release. The GH pulses which are already rising during the infusion show a period of inhibition, with a fall between peaks within the pulse. The similar time frame here between the model and the real data supports the short 5min GH-GHRH feedback delay. The major effect, disturbing the GH pulse cycle, is due to GH feedback on somatostatin, triggering a refractory period following each GH infusion. The match with the real data is further evidence that the model is a good representation of the real system.

Chapter 5

Modelling Spike Firing in Oxytocin Cells

5.1 Introduction

This chapter moves away from the GH model to study a new modelling technique for the analysis of the spike firing patterns in neurons. The GH system eludes direct measurement while it is functioning, but it may be possible to find out more about the neurons by analysing what recordings we have and attempting to find general properties of their behaviour. However, in the first instance of this study, the firing patterns being studied are from oxytocin cells. These are large magnocellular neuroendocrine cells in the supraoptic nucleus of the hypothalamus that project to the posterior pituitary to release oxytocin into the bloodstream. These cells are relatively easy to record from and we already know a lot about their function and electrophysiological properties.

5.1.1 Previous Work

The new model is a development of previous work (Leng *et al* 2001) which produced a version of the classic integrate and fire model (Tuckwell 1988) for oxytocin and vasopressin neurons. The model was successfully used to explain the unusual linear increase in firing activity in response to increased input stimulation, demonstrating the apparently counter intuitive idea that this could be achieved by giving an equal amount of excitatory and inhibitory input pulses. It was able to predict and explain what had previously appeared to be contradictory experimental results. It was also successfully tested experimentally by blocking the inhibitory input transmitter GABA, the release of which had been detected in response to the osmotic stimulus that also increases excitatory input activity.

5.1.2 This Project

The main aim of the new work is to investigate a strange effect which can discovered by analysing long recordings from oxytocin neurons, looking particularly at the intervals between spikes. If the firing of each spike is independent from previous activity then there should be no relation between the length of a particular spike interval and those which come before. A plot of inter-spike intervals (ISIs) against the mean interval one spike before should be flat, indicating no relation. However, by progressively taking a large number of intervals of a particular length and plotting this interval length against the mean ISI previous to these intervals, a downward slope does emerge, indicating that a longer ISI is more likely to be followed by a shorter interval and vice-versa. This means that there must be some component of the oxytocin cell's behaviour which causes it to effectively remember previous firing activity. This would have to be an unusually long lasting electrophysiological effect, and the prime candidate for this was the after hyper-polarisation (AHP).

The AHP is a very small magnitude electrophysiological effect which is not normally detected when recording from oxytocin cells but can be observed by giving a very high frequency train of input pulses. The AHP then appears as a very long lasting (several seconds) hyper-polarisation which reduces the cell's ability to fire by lowering the membrane potential and increasing the amount of input activity required to reach firing threshold.

In order to test the ability of the AHP to produce the memory effect in oxytocin cells, the first stage of the new work was to reproduce the previous model and then add the AHP. This was then used to produce trains of artificial ISIs which could be analysed in the same way as the long oxytocin cells recordings. The artificial data with no AHP showed no relation between interval sizes, but by adding in the AHP the model's artificial data was able to replicate the interval relation discovered in real cells. The work has progressed to examine the effect in a more quantitative manner by attempting to fit the model to recordings from real oxytocin cells and produce values for the magnitude and time course of the AHP. The difficulty of detecting the

AHP and the relation between ISIs has meant that a new technique has had to be invented for measuring fit between sets of such data. Getting a sufficiently accurate measure of fit requires the model to be run for a very large number of spikes and many time intervals have to be compared between the generated and real sets of data, making this a very computationally intensive process. It has however been able to successfully produce values for the AHP parameters in comparison with real recordings and has been used to get a better understanding of how the AHP relates to the other properties of the cell. The model and the fitting process provide a powerful tool for analysing cell recordings and discovering behavioural properties which may not have been previously observed.

5.2 The Basic Oxytocin Firing Model

The previous model was a leaky integrate and fire model which simulates the firing response to a series of random input pulses, usually small exponentially decaying spikes. These represent the excitatory and inhibitory post-synaptic potentials (EPSPs and IPSPs) on the cell's dendrites. When these input spikes sum to a value above threshold the neuron fires an action potential, its timing is recorded and the following refractory period known as the hyper after-polarisation (HAP) is simulated by increasing the firing threshold value (measured in mV) and then allowing this increase to quickly decay away exponentially. In real cells this HAP (illustrated along with the AHP in figure 5.1) is the action of some ion channel (or channels) which hyperpolarizes the cell following an action potential, temporarily preventing firing and limiting the maximum firing rate. The HAP is of a large magnitude, effectively raising the firing threshold by the order of 60mV, but decays very quickly giving a refractory period of usually 10 to 20 ms. The model also includes the real resting potential, spike threshold, and excitatory and inhibitory input reversal potentials measured from oxytocin cells.

The first stage of the new work was to reproduce the previous model and its results and this is the work which is described immediately below. The reproduction of the

model is identical to the previous version except for a minor change to one of the equations which is described later.

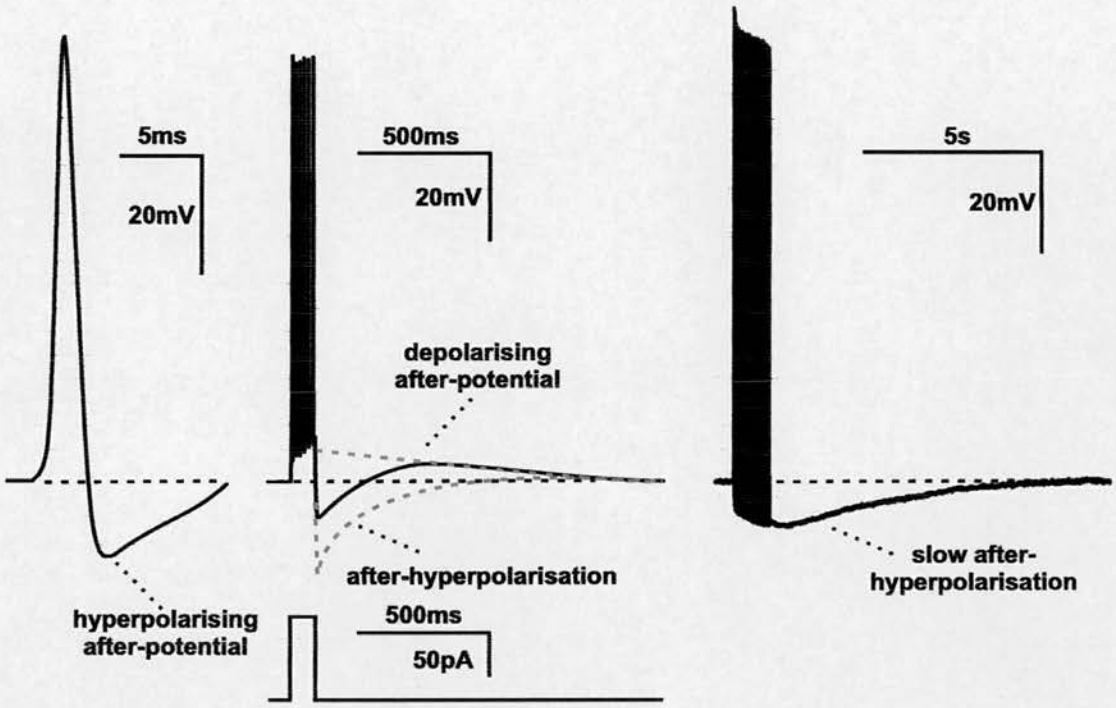

Figure 5.1 : The major post spike components in a supra-optic nucleus (oxytocin or vasopressin) cell. The AHP and the DAP are normally too small in magnitude compared to the HAP to be observed after a single spike, and so an artificial train of high frequency input pulses are given to make the AHP and DAP large enough to be visible. The model so far does not include the DAP, which is thought to be more dominant in vasopressin cells. The slow AHP is also not separately included. The upper and lower red lines show the respective effects of knocking out the AHP and DAP, which normally act against each other to make the AHP appear smaller and the DAP appear later. Figure by Dr. Colin Brown.

5.2.1 The Model Equations

The model uses two variables, *v*, representing the membrane potential and *ttime*, which measures the time since the last output spike. It runs over discrete 0.1 ms time steps. At each step the model generates EPSPs and IPSPs according to the input rate specified by the parameters *Ire*, which gives the EPSP frequency, and *Iratio* which

gives the ratio of IPSPs to EPSPs. Equal numbers of excitatory and inhibitory inputs, for example, would be *Iratio* = 1. The timing of individual input spikes is generated by a random Poisson process. Two equations give the time until the next input spike :

$$ept_{i+1} = \frac{-\log(1-rand)}{epf} + ept_i$$

$$ipt_{i+1} = \frac{-\log(1-rand)}{ipf} + ipt_i$$

Where ept_i is the current epsp time point, *rand* is a random number in the range 0 to 1, and *epf* = *Ire*/1000 to give the mean number of EPSPs per ms; ipt_i gives the current IPSP time point and *ipf* = *Ire* * *Iratio* / 1000 to give the mean number of IPSPs per ms.

At each time step these equations are run repeatedly generating time points for new input spikes until the next spike is due after the current time step. At each run through of the equations the model increments the number of spikes which fall in the current time step. Input pulse magnitude is calculated using the reversal potential and scaled by a parameter so that the spike magnitude at resting potential is 4mV. These scaling parameters are the values *a* and *b* for the EPSPs and IPSPs respectively in the two post-synaptic potential (PSP) height equations :

$$ep_h = a(v_e - v)$$

$$ip_h = b(v_i - v)$$

Where ep_h and ip_h are the epsp and ipsp magnitudes (mV) and v_e and v_i are the reversal potentials. The total input is calculated by summing the products of the number of spikes and spike magnitudes for the EPSPs and IPSPs using the equation :

$$input = ep_h ep_{count} - ip_h ip_{count}$$

Where ep_{count} and ip_{count} are the number of EPSPs and IPSPs for the current time step. The *input* value is then added to *v*. Instead of modelling the decay of each input spike

individually, a single decay component is added to v which makes it decay back to resting potential at a rate determined by the half life of the PSPs, *gamma*. The decay component is represented by the equation :

$$(v - v_{rest}) * hstep * gamma$$

Parameter *hstep* defines the time step size in ms. This gives the complete equation for v :

$$v = v - (v - v_{rest}) * hstep * gamma + input$$

The firing threshold (v_{thresh}) is modelled by an equation which combines the basic firing threshold (v_{thre}) with the effect of the HAP :

$$v_{thresh} = v_{thre} + HAP$$

The exponentially decaying HAP is modelled by the equation :

$$HAP = k * \exp(-\lambda * ttime)$$

The two parameters k and λ give the initial magnitude and decay rate respectively. If v is larger than v_{thresh} then an action potential spike is fired. The model records the time point of the spike, resets v back to the resting potential and generates a new HAP by setting *ttime* back to 0. The model then continues to run for a fixed number of time steps or until a fixed number of spikes have been generated.

The Matlab implementation of the model defined the firing threshold (v_{thresh}) as :

$$\begin{aligned} v_{thresh} &= v_{rest} + (v_{thre} - v_{rest}) * (1 + HAP) \\ &= v_{thre} + (v_{thre} - v_{rest}) * HAP \end{aligned}$$

making the size of the HAP dependent on the threshold and resting potentials. Whether this was intended is unknown, but here it was simplified to make the HAP magnitude depend just on parameter k. Otherwise, the basic model was left unaltered from the Matlab version.

5.2.2 Model Output

The model can display membrane potential against time by storing v at each time step, giving a trace which displays the input spikes (figure 5.2). It can also display a representation of the output action potential spikes by recording and displaying *vthresh* against time. On this trace each output spike appears as a sudden large increase in firing threshold followed by a steep decay back to the normal threshold, or interrupted by another spike. However, the normal output from the model, which is used for most results, is the record of spike timings, a series of time points at which the model fired an output spike. These are turned into a series of inter-spike intervals (ISIs) by calculating the time between each successive spike. This series of ISIs gives the most important output from the model, a form which can be analysed to determine the properties of the cell's firing pattern and can be compared to the equivalent data from real cells.

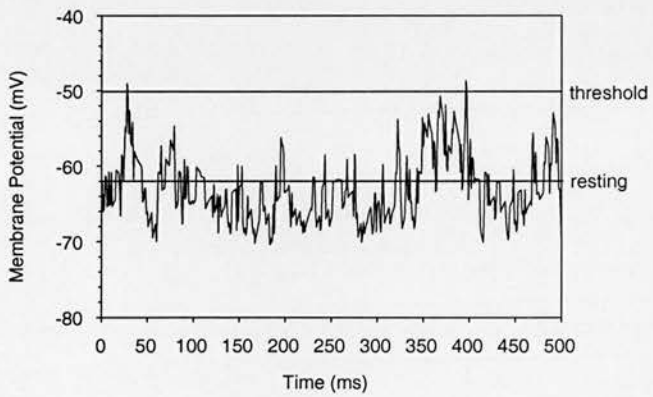

Figure 5.2 : Model cell input voltage with equal levels of excitatory and inhibitory input. Because of random timing, input pulses can still sum to a level high enough to cross firing threshold. In this trace, firing threshold is crossed twice to fire 2 spikes in the 500ms period. Lines mark threshold and resting potential.

The most common form for displaying the ISIs is the inter-spike interval histogram which counts up the number of ISIs within a series of short, usually uniform, time ranges (bins) and displays these as a graph showing the distribution of time intervals between spikes. This shows many features including the range over which the

intervals are spread, the most common size of interval and the minimum interval between spikes, indicating the refractory period.

5.2.3 Parameter Values

The parameter values (apart from the model step size obviously) are all based on electrophysiological data from real oxytocin cells. Some of them are fixed exact values that can be accurately derived from real experiments and others are rougher estimates.

EPSPs and IPSPs can be detected by intracellular recording from oxytocin cells. These input pulses have a magnitude in the range 2-5 mV and last for 5 to 10 ms. For the model we make the assumption that the excitatory and inhibitory potentials have equal and opposite magnitude and have a size in the same 2-5mV range with a half life of 3.5 to 20 ms. For all of the initial results here the magnitude and half life have been fixed at 4mV and 7.5ms. The resting and threshold potentials for oxytocin cells have been measured at approximately –62mV and -50mV (Bourque and Renaud 1990). The reversal potentials for EPSPs and IPSPs are set at –38mV and –72mV from estimates in (Randle *et al* 1986). The default parameter values for the HAP and the input pulse rates, *Ire* and Iratio, are rougher estimates mainly based on early experimentation with the model in order to produce a firing rate within the normal range for an oxytocin cell. These less well defined values are the main ones that are varied during experimentation with the model.

The table below summarises the set of parameters and their default values

Parameter Name	Description	Default Value
hstep	model step size	0.1
v_{rest}	resting potential	-62mV
v_{thre}	threshold potential	-50mV
a	EPSP height scaling	0.4
b	IPSP height scaling	0.04
v_e	EPSP reversal potential	-38mV
v_i	IPSP reversal potential	-72mV
k	HAP height	60mV
λ	HAP time constant	0.1

Ire	EPSP frequency	300Hz
Iratio	IPSP/EPSP ratio	100%

5.3 Results from Real Oxytocin Cells

As a preparation for working with the model we need to examine the real data which is to be reproduced and so here we follow previous analysis (Leng *et al* 2001). By taking long recordings from oxytocin cells which give the timing of individual action potentials we can construct an inter-spike interval histogram for the cell in order to examine the distribution of ISIs and fit functions so that the distribution can be described in formal mathematical terms. The histograms for each cell show a skew distribution with a mode in the range of 40 to 60ms and a long tail, indicating that the majority of spikes are fairly close together but can still fall over a large range of intervals. The tail of the histograms can be well fitted by a single exponential suggesting that after a certain interval, around 80ms, the timing of spike firing is essentially random. Extrapolating the exponential curve over the front end of the histogram shows a deficit of spikes in the 0 to 40ms range indicating a refractory period, likely to be caused by the hyperpolarizing after potential (the HAP). What the randomness indicates about the functional properties of the oxytocin cells is that activity is dominated by factors independent of previous activity, properties that are constant for the cell or activity within a time window that only affects a single spike such as resting potential and rate of synaptic input. The deficit of activity in the 40 to 80ms range indicates the time period where the HAP is decaying away and gives us an estimate of its half life. For the effect of the HAP to become negligible (well below 0.5mV) would take at least eight half lives giving a half life of no more than 10ms to fall within the 80ms range. The default value for λ in the model, 0.1, gives an HAP half life of approximately 7ms. In the paper the model is fitted to the data from one of the real cells with $\lambda = 0.08$, giving an 8.7ms half life.

5.3.1 Fitting the Model to Real Data

The first experiments with the model used it to fit the data from real cells by comparing the ISI histograms from the real cells with those produced by the model. For all the cells tested it was possible to fix the parameters for resting potential, threshold potential and PSP amplitude and half life to the default values in the table above. The model obtained a good fit to all the cells with HAP parameters $k = 60$ and λ in the range 0.08 to 0.15 and each cell could be fitted by varying just λ and *Ire*, the EPSP rate. These fits were not unique however; equally good matches could be produced with larger or smaller amplitude input pulses or a more depolarised resting potential by compensating with the input rate, and different values of k could be compensated by adjusting λ. These experiments to fit real data used only EPSPs, but adding in IPSPs has no effect on the overall shape of the histogram and can be compensated just by increasing the input rate (figure 5.6).

With a fixed value for k every oxytocin cell could be characterised by a unique value for λ and by values for v_{rest}, *Ire* and *Iratio*, which change the output rate but have little effect on the actual shape of the histogram, only shifting it to the left or right to match the cell's output rate. The paper goes on to test this by producing histograms for a real cell with varied amounts of input activity, controlled by increasing the level of osmotic stimulation. These were successfully fitted with the model by varying only the parameters controlling the input rate and membrane potential and keeping a the same value for λ.

5.3.2 First Experiments with the Model

The first stage of working with the new implementation of the model was to reproduce some of the results in the previous paper in order to validate the new version. For comparison with the previous paper experiments were chosen which examine the effect of varied input rates on the shape of the histogram and the output rate, since these test a range of values and give a suitably well defined target to

reproduce. The aim of these tests was to investigate what effect the parameters that had to be altered to fit the real cells are having on the model cell's behaviour, how they affect the output rate and the shape of the histogram and how this relates to the cell at a functional level.

Although not stated in the publication, the results in the paper use two different implementations of the model, an older version coded in C and a new Matlab version. These both implement the same integrate and fire model but use different representations for the cell's membrane potential and input pulses. Both models produce very similar results and qualitatively are identical, but the varied implementations mean that the scaling varies between the two versions and so they produce results which are slightly different quantitatively. The new version of the model being used here and the equations described above are based on the Matlab version of the model but the new version is re-implemented in C++. It does however produce results which are identical to the paper's Matlab version.

5.3.3 Pulse Input Rate

The model's input consists of a train of randomly timed excitatory and inhibitory post-synaptic potentials of uniform magnitude following a Poisson process governed by an average input rate. The rate for the EPSPs is defined by the parameter, *Ire* and the IPSP rate is defined proportionally to the EPSP rate by *Iratio*. The aim is here is to test the effect of input rate on the shape of the ISI histogram and measure how it affects the cell's output rate. We also want to examine how the two parameters for excitatory and inhibitory input interact and whether they can compensate for each other.

For these experiments all of the parameters except the ones being varied were set to the default values in the table above and the model was run for 50000 spikes. The ISI histograms were created using 5 ms bins. A range of values for *Ire* was chosen which produces spike output rates within a range comparable with the real cells. The results with varied *Ire* and *Iratio* = 0 (no inhibitory input) are as follows :

Ire	Output Freq	ISI Mode	Mode Height	Mean ISI
50	0.37	140	106	2709.2
75	1.58	100	412	634.3
100	3.81	60	990	262.4
125	6.75	45	1819	148.1
150	10.02	50	2782	99.8
175	13.18	40	3771	75.9
200	16.25	45	4949	61.6
225	19.13	35	5979	52.3
250	21.88	30	7324	45.7

The rate of increase in output rate initially climbs very quickly as the input activity increases (figure 5.3a). This highly non-linear relationship between input and output rate is observed in most neurons. The rate of increase in output rate only slows as the cell approaches the maximum firing rate governed by its refractory period. The table below shows the equivalent results with *Iratio* = 1.

Ire	Output Freq	ISI Mode	Mode Height	Mean ISI
50	0.16	275	54	6393.4
100	1.09	70	301	916.1
150	2.60	60	662	385.3
200	4.24	60	1064	235.8
250	5.84	50	1498	171.2
300	7.27	45	1892	137.6
350	8.51	45	2147	117.5
400	9.78	45	2604	102.2
450	10.88	40	2859	91.9
500	11.89	40	3127	84.1
600	13.74	40	3673	72.8
700	15.26	40	4185	65.5
800	16.75	40	4657	59.7
900	17.90	35	5118	55.9
1000	18.96	35	5437	52.7

Figure 5.3b shows the non-linear increase in output rate with increased input activity, the rate of increase slowing as *Ire* increases. The later part of the curve is very similar to that with *Iratio* = 0, however with inhibitory input the output rate increases with input activity in a much more linear form. This first part of the curve, with output rate in the range 0 to 10Hz best represents endogenous activity and this shows a much more linear response (compared to figure 5.3a) with mixed excitatory and

inhibitory input. This was one of the first major results for this model, explaining what had previously appeared to be a counter intuitive result when measured in real cells.

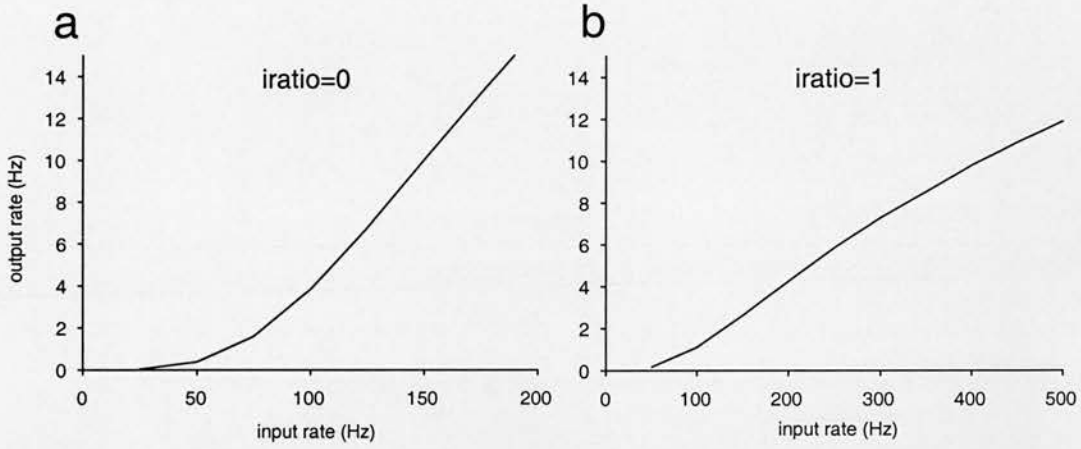

Figure 5.3: **a**. EPSPs only, non-linear increase in firing rate with increased input; **b**. EPSPs and IPSPs, slower, more linear increase in firing rate with increased input.

Figure 5.4a shows the histograms for some of the values for *Ire*. As *Ire* increases the histogram's mode increases in height and shifts to the left, indicating an increase in the number of short ISIs and an overall increase in firing rate which is also shown by the increase in output rate and reduction in mean ISI. With a smaller input rate the histogram's tail shows more longer intervals between pulses although the actual range of intervals doesn't change, with long intervals still occurring occasionally even with high levels of input. The slope can still be fitted by an exponential but becomes more linear with lower input rates.

The effect of reducing *Iratio* with a fixed value for *Ire* is very similar (figure 5.4b), more short intervals and an increased overall firing rate with the same effects on the shape of the histogram. Even with equal amounts of inhibitory and excitatory input the cell continues to fire, although with a reduced firing rate. The inhibitory input depresses the membrane potential but because of the exponentially decaying form of the input pulses and the random timing, the excitatory pulses are not entirely cancelled out and do eventually manage to push the cell above firing threshold.

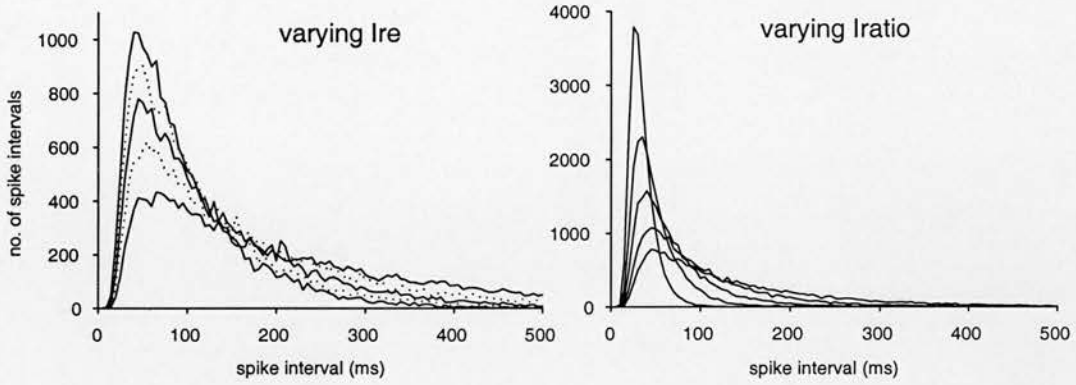

Figure 5.4 : **a**. ISI histograms with varied input frequency (*Ire*), range 200 to 400Hz, highest mode = highest *Ire*; **b**. ISI histograms with varied levels of inhibitory input (*Iratio*), range 0 to 1, highest mode = lowest Iratio; histograms generated from 50000 spikes

This is best illustrated by looking at a trace of membrane potential overlaid with the firing threshold in order to show where the cell is firing an output spike. The trace in figure 5.2 shows a run with equal amounts of excitatory and inhibitory input (*Iratio* = 1). With the inhibitory input the average membrane potential is much lower but because of the random nature of the pulse timings it does still occasionally pass the firing threshold and fire an output spike. The linearising effect of *Iratio* is demonstrated for a range of values of *Iratio* by figure 6D in the paper. This experiment was reproduced here (figure 5.5). The version in the paper uses the newer Matlab version of the model and so the data here matches it exactly. As *Iratio* increases the plot of output rate against input activity becomes progressively more linear. With lower levels of inhibitory input the curve is almost sigmoidal, initially curving up quickly before straightening out and then curving back towards a shallower climb as it approaches the maximum firing rate controlled by the HAP. Higher values of *Iratio* stretch out this curve to form a more steady, slower climb. This gives the cell the important property of producing uniform increases output in response to an increase in stimulation, independent of current activity. Without the inhibitory input the cell's response to a fixed level of added stimulation would depend very much on existing activity.

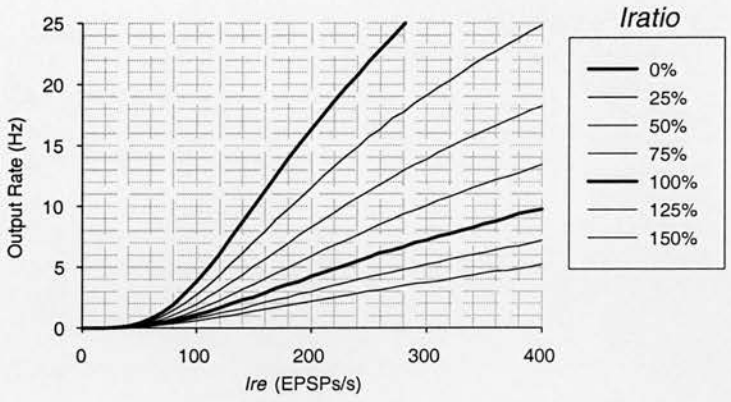

Figure 5.5 : Plots of output rate against input rate with varying *Iratio*, shows the increasingly linear response with increased inhibitory input.

To test whether the input rate could be increased to compensate for the effect of inhibitory input on the ISI histogram the model was tested over a range of values for *Iratio* with the output rate fixed at 10Hz (to within 0.05Hz) by varying *Ire*. The table below shows the values used :

Iratio	Ire	Output Freq	ISI Mode	Mode Height	Mean ISI
0.00	150	10.00	45	2795	100.0
0.25	183	10.01	50	2727	99.9
0.50	229	10.03	45	2664	99.7
0.75	299	10.00	40	2597	100.0
1.00	410	9.98	40	2596	100.2
1.25	586	10.00	45	2630	100.0
1.50	870	10.01	50	2584	99.9

Figure 5.6a shows the overlaid histograms for each value of *Iratio*. They are almost identical, except that the mode is slightly lower with the lower overall input rates. This indicates that *Ire* can be increased to compensate for the higher ratio of inhibitory input to get the same output rate without affecting other properties of the cell's behaviour. This simplifies further testing of the model since it shows that input rate can be treated as a single variable. For most experiments it will be sufficient to maintain *Iratio* at a fixed value.

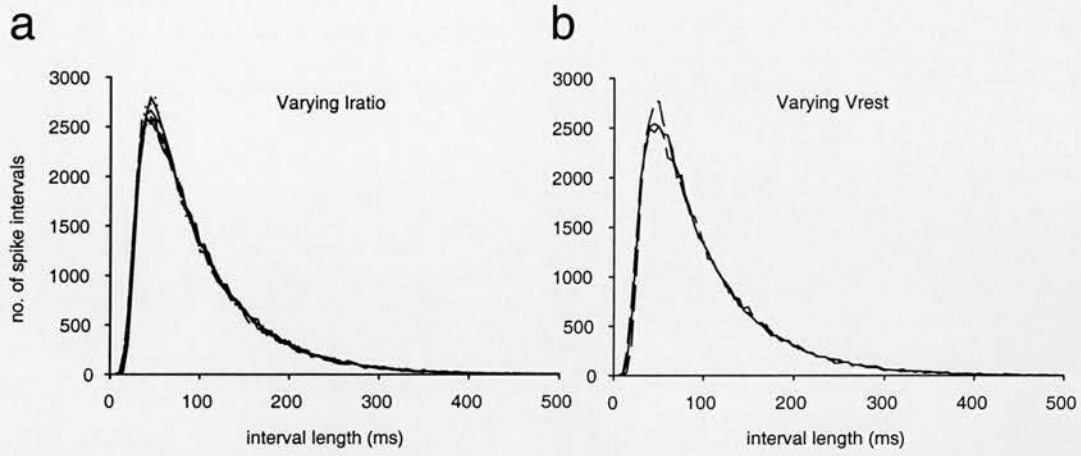

Figure 5.6: **a**. Overlaid ISI histograms varying *Iratio* (0 to 1.5) and compensating output frequency by adjusting *Ire*; **b**. Varying v_{rest} with frequency compensation.

The other parameter which directly affects the ability of input spikes to raise membrane potential above the firing threshold is the resting potential (v_{rest}). This defines the level of concurrent activity required to fire an action potential. A similar test was performed, varying *Ire* to compensate against v_{rest} as with *Iratio*. *Ire* was varied to fix the output rate at 10Hz and *Iratio* was fixed at 1. The results are presented in the table below and the overlaid histograms in figure 5.6b.

Vrest	Ire	Output Freq	ISI Mode	Mode Height	Mean ISI
-44	1275	10.01	50	2517	99.9
-46	880	10.00	40	2558	100.0
-48	605	10.04	50	2581	99.6
-50	410	10.02	45	2541	99.8
-52	270	9.99	45	2637	100.1
-54	169	9.99	45	2677	100.1
-56	96	10.02	50	2765	99.8

The result is very similar to the compensation of *Ire* against *Iratio*. With higher values for *Ire* the mode is slightly higher but otherwise the histograms are identical with no change in the slope or range of ISIs. The experiment also demonstrates a non-linear relationship between the change in v_{rest} and the value for *Ire* required to achieve the same output rate. A change of 12mV in v_{rest} (shifting the difference

between v_{rest} and v_{thresh} from 6mV to 18mV) requires a more than 10-fold increase in *Ire* with *Iratio* = 1.

The result here again allows us to conclude that we can investigate the effects of other parameters by varying only one of the excitation parameters, *Ire*, *Iratio* and *Vrest* since they can compensate against each other without affecting other properties of the cell's behaviour.

5.3.4 Mapping λ against Input Rate

The HAP is the only component of the basic model which is specific to the type of cells being studied, particularly oxytocin cells, and so this is the most important part of the model to understand for the purpose of fitting the model to real data and using the model as an accurate representation of real cells. Parameter λ controls the half life of the HAP and so will affect the time course of the refractory period following an action potential. The first experiment here tests the effect of varying λ on the shape of the ISI histogram and cell firing rate. A smaller value for λ produces a longer half life and so we would expect a longer refractory period, reducing the firing rate and pushing the mode of the histogram to the right. For the experiment, the model was run for 50000 spikes with the default parameters, *Ire* fixed at 300Hz and a set of values for λ which cover the realistic range. The table below gives the results, including the half-lives in ms :

λ	HAP half-life	Output Freq	ISI Mode	Mode Height
0.01	69.31	2.40	370	944
0.02	34.66	3.73	205	1219
0.04	17.33	5.32	110	1510
0.06	11.55	6.22	80	1657
0.08	8.66	6.85	65	1810
0.10	6.93	7.26	45	1924
0.12	5.78	7.61	45	1961
0.14	4.95	7.83	35	1942
0.16	4.33	7.99	35	2019
0.18	3.85	8.16	30	2154
0.20	3.47	8.32	25	2156
0.30	2.31	8.82	15	2170
0.40	1.73	8.92	10	2232
0.50	1.39	9.11	10	2365

The results show output frequency increasing non-linearly as the half life of the HAP is decreased, reducing its effect on the cell's firing rate. As the half life becomes very small the HAP has little effect on firing and the change in output rate flattens out (figure 5.7a). The mode also shifts to the left and increases in height as the as the area of histogram representing the refractory period is reduced. The effect on the shape of the histogram, showing this shift to the left, is illustrated in figure 5.7b.

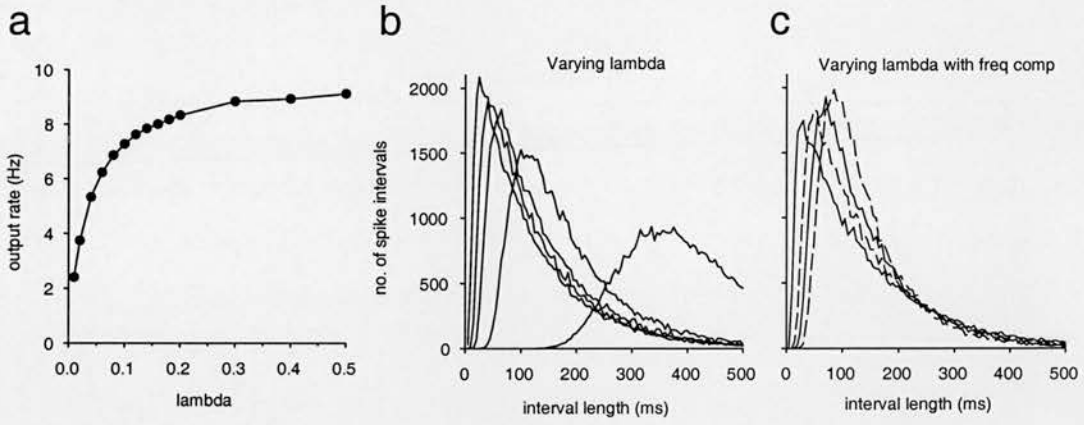

Figure 5.7: **a**. output rate varying with the HAP decay rate (λ); **b**. Overlaid ISI histograms with λ varying from 0.01 to 0.50. Highest mode = smallest λ.; **c**. Overlaid ISI histograms varying λ with *Ire* adjusted to match output frequency at 7Hz. Highest mode = smallest λ.

For the next experiment the effect of changing λ while maintaining a constant output rate is examined. The input rate (*Ire*) is shifted to get an output rate of 7Hz for each value of λ, in a similar manner to the experiments compensating *Ire* against *Iratio* and *Vrest*. This also compares with the experiment in figure 5A of the paper. The table below gives the values used for *Ire* to match the 7Hz output rate :

λ	Ire	Output Freq	ISI Mode	Mode Height
0.05	370	6.99	85	1985
0.07	320	7.00	70	1926
0.08	307	7.00	55	1876
0.10	292	6.98	50	1831
0.12	283	7.01	45	1779
0.15	273	7.00	40	1780
0.20	265	7.02	30	1747

The results are best observed by looking at the histograms in figure 5.7c. As λ increases the mode shifts to the right and falls in height, although slowly. However the tail end of the histogram does not vary between the different values of λ, where the HAP has decayed away and behaviour is entirely defined by the output rate.

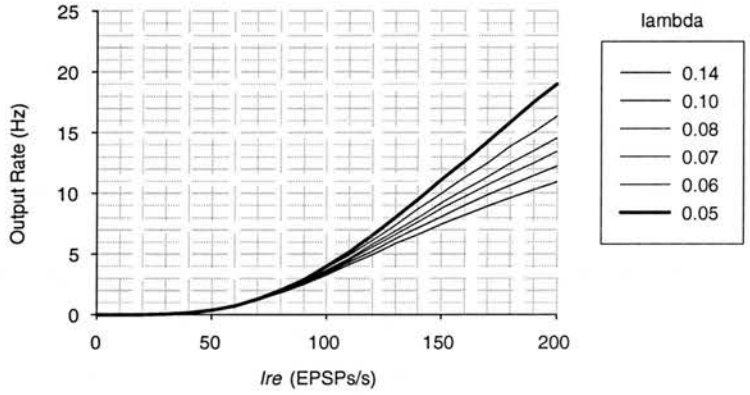

Figure 5.8: Plots of output rate against input rate with varying λ, non-linearity is reduced as λ is increased and the HAP has a greater influence over firing rate

The relation between output rate, *Ire* and λ is further studied in another experiment which reproduces data from the paper, figure 6B, which plots output rate against *Ire* for a range of values for λ, with no inhibitory input (*Iratio* = 0). The data created with the new version of the model is displayed in figure 5.8. The paper's version was generated with the newer Matlab version of the model and so new data here matches it perfectly, although the version here was generated with a larger number of spikes and shows smoother curves with smaller errors in the output rates.

The graph shows the familiar non-linear increase in output in response to increasing input activity but as λ is reduced, increasing the half-life, the HAP has a greater influence over the firing rate and the non-linearity is reduced, particularly when the input rate is higher and the cell's firing rate comes closer to the limit imposed by the refractory period. At lower output rates, when the HAP plays less of a role, the curves are very similar.

5.3.5 Fitting Against Real Data

The aim here is to attempt to reproduce the experiments in the paper fitting the model to ISI histograms produced from real data, recorded from oxytocin cells. The new version of the model should be able to get fits as good as in the paper but the parameter values will likely be slightly different due to the different implementations of the model. The fitting experiments in the paper were performed with the older version which differs from the version used here. The value for k is also going to be differently scaled because of the modification made to the HAP equation made for the new version of the model. The equivalent value in the new version of the model is equal to the old k multiplied by (v_{thre} - v_{rest}). In the fitting section of the paper this difference is fixed at 12mV and so k=5 in the paper is equivalent to k=60 in the new version. The new value for k gives the initial amplitude of the HAP in mV. The new version also uses reversal potentials which were not implemented in the older version of the model.

The first data from the paper to be fitted is figure 4, which gives an example of a single oxytocin cell fitted by the model. The parameters used are the same as the defaults specified above, except with $\lambda = 0.08$ and *Ire* = 380. The figure in the paper displays the histogram from the real cell overlaid with the histogram from the fitted model cell. The paper states that the cell's output rate is 6Hz, however reanalysing the same data here shows that it in fact 5Hz. The results which demonstrate how the excitation parameters can be compensated against each other to produce the same output rate indicate that it is only necessary to alter one of these to fit the model. The one which is normally used here is *Ire*, the overall input rate. A simple protocol for fitting was developed, of first adjusting *Ire* to match the output rate and then adjusting λ to match the shape of the histogram. Fit was assessed by eye with the two histograms graphically overlaid in the model software. Altering λ affects the output rate and so with each change in λ, *Ire* is shifted to match the output rate again. Using this process and the default parameters, which are based on those in the paper, it was only necessary to alter λ and *Ire* to get a good fit. The values using the new version of the model are different however, a good fit was obtained with $\lambda = 0.1$ and *Ire* =

230 (figure 5.9). The next set of data to be matched from the paper was figure 5B which fits the model against four sets of data from the same cell with varied levels of input activity, controlled by increasing the level of osmotic stimulation. Here there are also problems with apparent discrepancies between the values for output rate in the paper and those detected by the model, although unfortunately only the histograms from the real data were available and so the model's values for the output rate are approximated.

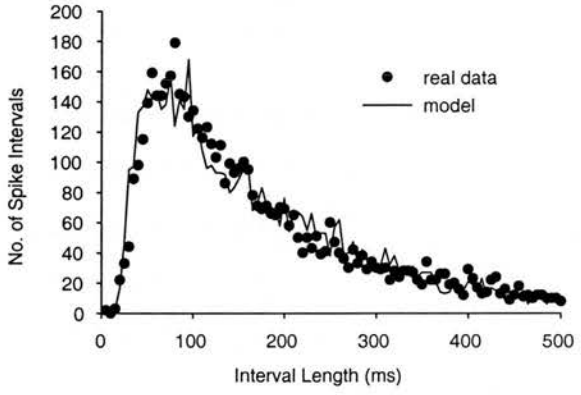

Figure 5.9 : a. oxytocin cell recording ISI histogram fitted with the model (λ=0.1, *Ire*=230).

However, there are also values for the output rates in a spreadsheet, from which the paper data is derived, which disagree with the paper. The fits here use the estimated values for output rate produced by the model. The 12.8Hz data in the paper is estimated at 12Hz by the model (agreeing with the spreadsheet), the 9.3Hz estimates at 9Hz (again matching the spreadsheet) and the 4.8Hz data estimates at 5.8Hz. Unfortunately this one doesn't have a figure in the spreadsheet to compare with. The final one is more problematic, the paper states 2.5Hz which almost matches the 2.6Hz marked in the spreadsheet, but the model estimates 5Hz. This particular recording only measures around 2000 spikes (compared to over 12000 on the highest output rate data) and so has the roughest histogram and output rate measure. The histogram data also only goes up to a 500 ms interval and it is likely to be missing some longer interval spikes from its tail, which will be making the model's

calculated output rate higher than the true rate. Although the model can produce quite a good fit, the fit looks better at the front end of the histogram with the higher output rate (5Hz) and better at the tail end of the histogram using 2.8Hz. Close examination of the original figure which is reproduced in the paper shows that the paper's model fit falls below the real data at the front of the histogram which would match the 2.8Hz figure given in the paper. The table below gives the figures for the fits using the new version of the model :

Real Data Set	Output Freq	Fitted λ	Fitted *Ire*
A	12.0	0.14	440
C	9.0	0.14	340
H	5.8	0.14	230
E	2.8	0.14	180

The 0.14 figure for λ differs from the paper's 0.08 figure which uses the older version of the model, but in common with the paper the new version of the model has fitted all of the real data, which comes from the same cell, with a single value for λ. The only parameter which varies between the four fits is the value for input activity, *Ire*. As stated in the paper, this demonstrates that the varied response to different levels of stimulation are due to increased levels in synaptic input and do not involve other changes to the cell's behavioural properties such as post-spike excitability governed by the HAP.

5.4 Modelling the AHP

The AHP behaves in a similar manner to the HAP, forming a hyper-polarisation after an action potential fires, with the difference that it is of much smaller magnitude (a shift of membrane potential in the range of less than 1mV compared to the 60mV HAP hyper-polarisation) and has a much longer time course, around 1 sec or more. The modelling of the HAP is relatively simple since the cell never fires another spike before most of the HAP has decayed away, meaning that there is only ever a single

HAP being modelled. With the longer time course and smaller magnitude of the AHP, the cell will be able to fire before the AHP has decayed away and so the effect of several successive AHPs must be maintained. However, because each AHP decays at the same rate, it is possible to sum the effect of successive AHPs and treat them as a single value, in a similar manner to the modelling of the input spikes. The AHP component adds a new equation to the model for the AHP and adds this AHP value to the equation representing the cell's current firing threshold. The equation below models the AHP with its decay during the current spike interval :

$$ahp_t = ahp_{t-1} * \exp(-\lambda 2 * ttime)$$

The variable *ttime* measures just the time during the current interval. When a spike is fired the current remaining AHP level is stored and then added to the new AHP generated by the new spike. The new value then decays with a reset time component. Intuitively it would seem necessary to maintain the two separately, keeping independent time counters but it is in fact mathematically equivalent to take the remaining level and then reset the decay timer so that the AHP from the previous interval can just be added to the new AHP and tracked with a single decay component. The new AHP is simply calculated as :

$$ahp_i = k2 + ahp_{i-1}$$

The parameters $k2$ and $\lambda 2$ are the AHP size and decay rate values, equivalent to the HAP's k and λ. The value for the current AHP level is simply summed with the equation for the current spike threshold :

$$v_{thresh} = v_{thre} + k * \exp(-\lambda * ttime) + ahp_i$$

The initial testing values for the two new parameters are rough estimates based on real data. The AHP's exact magnitude is very difficult to measure since it can only be detected by making a cell fire quickly enough for a number of successive AHPs to

overlap but it is likely to be smaller than 1 mV and so an initial value of 0.5 mV is used for $k2$. A further complication is that there more than one AHP or it may have two components. The normal AHP is thought to last around 1 second but there may also be an even smaller and longer lasting AHP of around 6 seconds duration. Here we only model a single AHP, based primarily on the larger 1 sec. duration version but hopefully capable of taking account of the AHP effect as a single component. The initial value for $\lambda 2$ is 0.002 which gives a half-life of 347 ms allowing the AHP to decay to 1/8 of its initial size in roughly 1 sec.

5.4.1 Initial Experiments with the AHP

The first experiments with the new version of the model incorporating the AHP test the effect on the previous results, how much the AHP affects spike response and the shape of the ISI histogram. These tests are all run for 50000 spikes with the default parameters and *Ire* set at 300 except where stated.

The first of these tests maps the effect of the new parameters, $\lambda 2$ and $k2$ on output rate and the histogram's mode and maximum height. Ranges of $k2$ and $\lambda 2$ were chosen that cover a realistic range of values. The results are presented in appendix table 1. Adding the AHP has what initially seems like a surprisingly strong effect on the output rate. As $k2$ increases, the output frequency is reduced, at a rate controlled by $\lambda 2$. The histogram's mode shifts to the right and its maximum height falls with more longer intervals between spikes and an increased refractory period. These effects are better observed by looking at pictures of this data. Figure 5.10a shows the ISI histograms for $k2$ ranging from 0 to 1 with $\lambda 2$ fixed at 0.002. Even with an AHP of 1mV, very small in comparison to the HAP, there is a large effect on firing rate and the distribution of spike intervals, producing a similar effect to a large change in input rate (figure 5.4a). In order to eliminate the effect on output rate, to examine the more subtle effects of the AHP, the same range of values for $k2$ were run with varied input rate in order to match the output frequencies. The results are in the table below :

k2	*Ire*	Output	Mode	Height
0	291	7.02	50	1783
0.2	332	6.98	55	1757
0.4	378	6.99	50	1698
0.6	430	7.02	50	1688
0.8	482	6.97	60	1638
1.0	544	6.98	50	1603

Figure 5.10b illustrates the ISI histograms. At a gross level the plots are very similar, but in comparison with other frequency matched plots such as figure 5.6a or 5.6b there are some variations, particularly towards the mode. At lower values for $k2$ the mode is slightly higher but more importantly the approach is also steeper suggesting that the AHP is having an effect on the number of short intervals even while the HAP still hasn't decayed away. This must indicate that the summing effect of the AHPs across several spike intervals is playing a large role in controlling firing. This was tested by repeating the experiment with a modified version of the model which does not carry on the AHP into the next interval. The results are below :

k2	Output	Mode	Height
0	7.24	50	1883
0.2	6.97	55	1775
0.4	6.74	55	1698
0.6	6.54	60	1661
0.8	6.26	50	1582
1.0	6.02	55	1540

Figure 5.10c shows the effect this has on the histograms, compared to figure 5.10a. There is still the variation in slope approaching the mean but the variation in height at the mode is much smaller and the effect on output rate is greatly reduced.

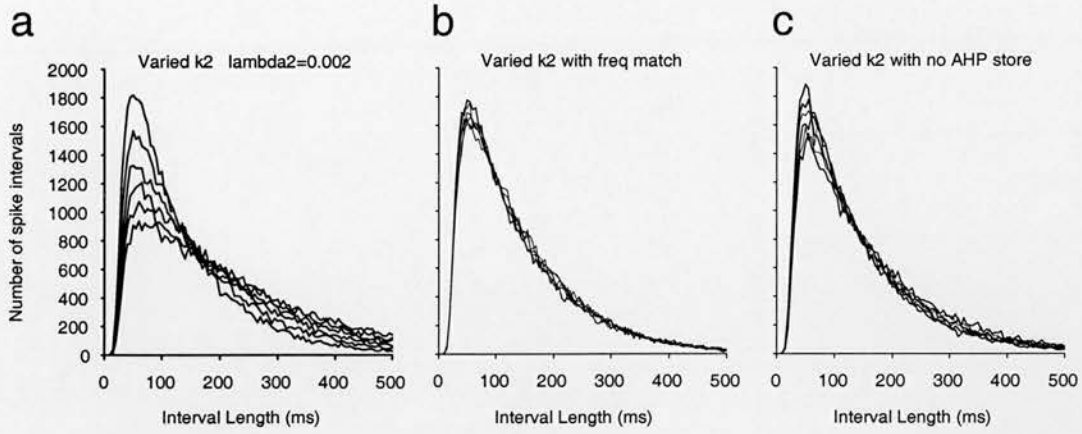

Figure 5.10: **a**. Overlaid ISI histograms with AHP magnitude ($k2$) varied from 0 to 1mV, highest mode = lowest $k2$; **b**. similar to a. with *Ire* adjusted to match output frequencies, lower $k2$ values have slightly higher mode and steeper mode approach; **c**. similar to a. with no AHP accumulation between spike intervals.

A similar set of experiments was carried out to compare the effect of varying the AHP's decay rate, $\lambda 2$. For these $k2$ was fixed at 0.5 mV and $\lambda 2$ was varied between 0.001 and 0.01. The pattern of results is similar to varying $k2$, with a slower decay rate producing a larger negative effect on the output rate, increasing the number of long spike intervals and reducing the height of the histogram's mode (figure 5.11a). When the output rates are matched the variation between the histograms (figure 5.11b) is eliminated, and the same effect is observed when there is no accumulation of the AHP (figure 5.11c). In the case of the AHP, output rate matching has a similar effect since this is also effectively eliminating the variation in the ability of the AHP's to overlap and accumulate. The variation in effect with longer time courses seems to be entirely due to the effect of accumulation, which is of course itself controlled by the length of time the AHP lasts. The AHP's magnitude is so small that even a much longer half life seems to make very little difference to its effect over the course of a single interval, a very different result to the large effects observed with changes in the HAP's decay rate.

A single AHP has little effect on firing rate but the long time course means that over the course of several spikes it can have a large effect on cell firing if the firing rate is fast enough for the AHP to accumulate. This means there is a complication to

interpreting the results of varying the AHP. While the individual AHP is of a larger magnitude, the output rate is lower, but this in turn reduces the cumulative effect with longer spike intervals increasing the firing rate, so there are two competing effects on the AHP's ability to influence firing. In this way it is somewhat self regulating and because it affects the firing rate, this may be passed on to make the cell's firing rate self-regulating. Faster firing produces a larger accumulation of the AHP which would reduce the firing rate. Slower firing would have the opposite effect and so make the output rate tend more towards a middle value, reducing the variation in firing rate.

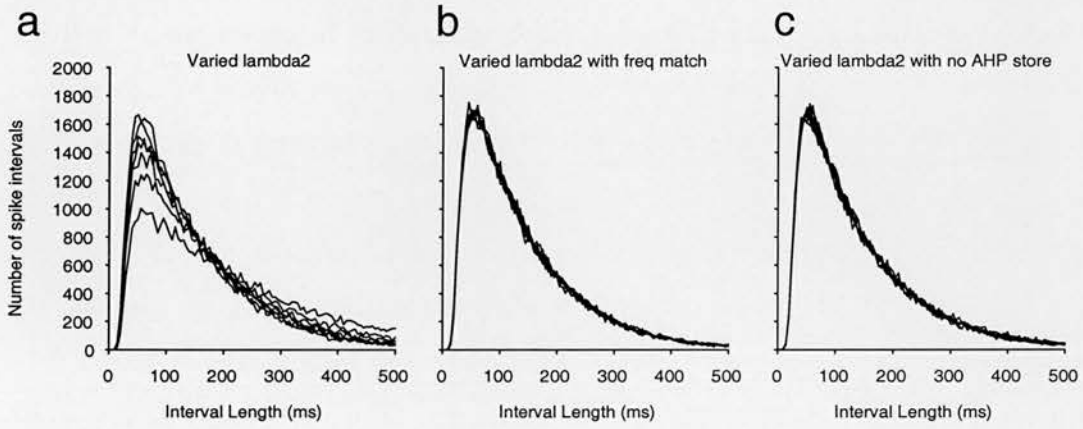

Figure 5.11: **a**. Overlaid ISI histograms with AHP decay rate (λ2) varied from 0.001 to 0.01, highest mode = highest λ2; **b**. similar to a. with *Ire* adjusted to match output frequencies, differences between histograms eliminated; **c**. similar to a. with no AHP accumulation between spike intervals.

In a final experiment for this section this was investigated by measuring the standard deviation of the spike intervals over a range of values for k2. The difficulty in making such a comparison is that the range of interval lengths is dominated by firing rate and so the standard deviations with varied k2 were compared with the same results for a range of values for *Ire* chosen to produce roughly the same output rates, but with no AHP. The results are below :

k2	Output Rate	ISI SD
0.0	7.25	105
0.2	6.29	121
0.4	5.59	136
0.6	5.05	148
0.8	4.66	159
1.0	4.32	169

Ire	Output Rate	ISI SD
300	7.27	106
265	6.24	126
244	5.63	143
227	5.11	160
214	4.71	177
203	4.30	198

These clearly show a smaller variation in spike interval size for the equivalent output rates suggesting that the AHP does work to reduce the randomness of spike firing. However, the other possible interpretation is that lower input rates increase variation and it is impossible to differentiate between the two without more sophisticated analysis.

5.5 Detecting the AHP in Spike Data

The AHP's small magnitude means that it has a fairly subtle effect on oxytocin cell firing rate, mostly dominated by the HAP and input activity. It does however have a small effect on the cell's chance of firing. While the AHP still has some size and the HAP has mostly decayed away it could make the difference between a border line level of input activity being able to trigger an action potential, a least delaying it by a small amount of time. When spikes are closer together such that a single AHP runs over several spike intervals, the AHPs get a chance to accumulate increasing the effect on the cell's ability to fire. The way to detect this effect is to examine the relation between the lengths of spike intervals and the immediately proceeding intervals. However, for a single interval the effect will be well within the noise level created by the random nature of the input activity, making it impossible to distinguish an AHP effect. What is required is to take all the intervals of a particular

length and then examine the average length of their respective proceeding intervals. This is repeated for increasing interval lengths and then each pair of values (interval length, average proceeding interval length) is plotted against each other. If there is no relation between the two then the average proceeding interval should always be roughly the same, producing a flat line. If there is a consistent relation between the two which relates to the interval length then there should be some sort of slope. This analysis can be extended by taking the average of a series of proceeding intervals instead of just one. This is called here spike train or AHP detection analysis.

5.5.1 Detecting the AHP in Real Data

The first test of this detection system is a newer set of real spike data, not used in the previous paper, recorded from an oxytocin cell in the female rat. Before calculating the values for detecting the AHP the data is subjected to some basic analysis for comparison with the basic experiments with the model. The results are presented below :

Dataset	mludw1
Number of spikes	5206
Recording time	15 min
Mean ISI	172.8 ms
Output Rate	5.79 Hz
ISI SD	137.47
Histogram Mode	55 ms
Mode Height	150 (1441 normalised)

The ISI histogram is presented in figure 5.11. The normalised value for the height of the mode is in comparison with the 50000 spike trains used for the previous model generated data. The values are all similar to those observed in the model data and it should be possible to reproduce this data with the model.

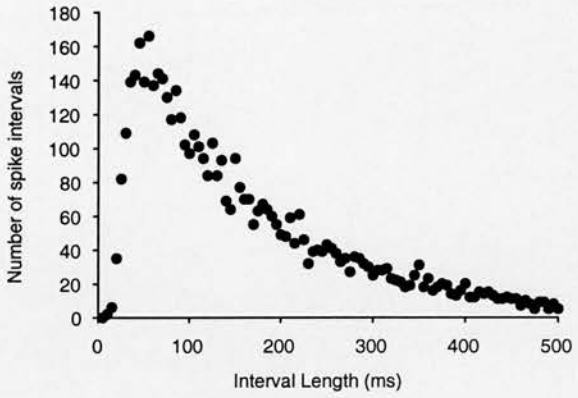

Figure 5.12 : ISI histogram for 5206 spike oxytocin cell recording mludw1, mean firing rate 5.79Hz

The next stage in the AHP detection process is to generate the average values for spike intervals and their proceeding intervals. Values are generated for progressively larger series of preceding intervals and the intervals are numbered in reverse time order, with the current interval known as T0 and the proceeding intervals T1, T2, T3, etc. Average values can be calculated for any number of proceeding intervals but the results displayed here show sets where the number of proceeding intervals is progressively doubled. In order to reduce the error and get a large enough variation to be observable and statistically significant, each of the averages is calculated from 200 spike intervals, taken in groups after sorting the spike intervals into order of length. So the first average is calculated from the shortest 200 intervals, the second from the 201st to 400th shortest and so on. The proceeding intervals (T1, T2, etc) remain indexed to their original corresponding T0 intervals and so these averages remain independent of the reordering of the T0 intervals. These values calculated for the real data are shown in appendix table 2.

The first plot of this data, in figure 5.13a, although noisy, clearly shows a downward correlation between T0 and T1 indicating that a longer interval is more likely to be proceeded by a shorter interval. As the plots progress over longer series of proceeding intervals the correlations at first become steeper before levelling out until the plot becomes flat, indicating no relation between the interval T0 and the average length of the proceeding series of intervals. Assuming that the AHP as

represented in the model is the cause of this correlation, this would suggest that the correlation becomes stronger until the series of proceeding intervals begins to include intervals which are too long before T0 for their AHP to have any effect. These intervals will have no correlation with T0 and so as more of these are included in the series the correlation will die away. The correlation with each successive (in a reverse time order) proceeding interval will be weaker as its AHP decays but because the correlations are being summed the total correlation becomes stronger over the first sets of intervals. This effect was measured by fitting straight lines to each of the plots for a range of series lengths and recording the gradient of the fitted line. Good fits can be achieved for plots which use up to 13 of the proceeding intervals. After this point the error in the fit becomes too great to achieve statistical significance but the fits have been measured for up to 32 proceeding intervals. The fitted line parameters are given in appendix table 3.

Figure 5.13b illustrates how the gradient changes with sums over longer series of intervals. It increases quite quickly and in a fairly linear fashion until using 8 intervals where it begins to decrease, again in a fairly linear form but less steeply. It is likely that the point at where the gradient begins to reduce depends on the decay rate of the AHP and the size of the spike intervals (determined by firing rate). Testing this is left for future work.

This method has successfully been used to detect a correlation between spike interval lengths which indicates some behavioural component which affects the chance of firing a spike based on previous activity. The properties of this effect so far detected are consistent with it being caused by the AHP. The next stage in testing this is to attempt to produce the same result with the model.

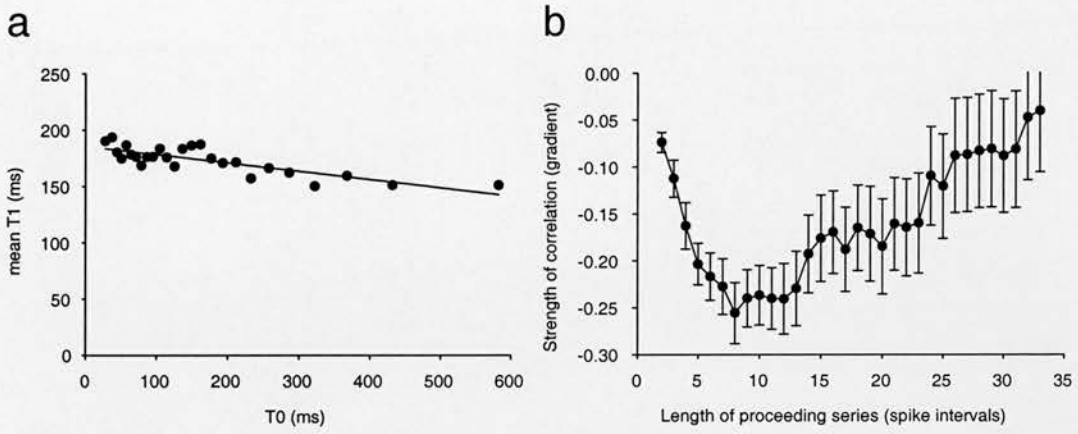

Figure 5.13: **a**. AHP detection in applied to oxytocin cell recording, binned spike interval lengths (T0) plotted against the mean previous interval length (T1), downward slope in fitted (non-linear regression) line indicates negative correlation between T0 and T1; **b**. plot of fitted gradients (with estimated fit error) for progressively longer spike trains (T1, T1+T2, etc.), shows an initial steep increase in correlation followed by gradual decay back to no correlation. The fit is only statistically significant up to 13 intervals in the spike train.

5.5.2 Detecting the AHP's Effect in Model Data

The aim here was to run the model with the AHP and perform the same analysis used to detect the AHP in real data by examining the relation between spike intervals and the length of those immediately proceeding. Assuming that the same type of correlation is found it would also be useful to compare the gradients of lines fitted to the plots of T0 against T1, T1+T2, etc. To generate the data the model was run for a matching 5206 spikes with the default parameters and an AHP generated using values $k2 = 0.5$ and $\lambda 2 = 0.002$. The spike intervals were run through the same type of analysis as that used with the real data above. The basic dataset analysis results are presented in the table below :

Dataset	modgen1
Number of spikes	5206
Mean ISI	189.3 ms
Output Rate	5.28 Hz

ISI SD	144.50
Histogram Mode	70 ms
Mode Height	150 (1441 normalised)

The data generated with the default model parameters has a slightly slower output rate (5.28Hz compared to 5.79Hz), with the mode slightly further to the right, but has a similar height at the mode. The model data also has a slightly larger variation in ISI length, but overall this data a quite a close match without doing proper fitting. This rather vague matching is deliberate in order to test the ability to detect the AHP independently of specific data parameters but still using model data which has a chance of producing a similar result to the real data. Appendix table 4 presents the equivalent analysis results.

The figures show a similar downward trend to the real data, suggesting that adding the AHP to the model produces a similar effect to that detected in the real data. The data is illustrated in figure 5.14, showing the noisy but consistent downward trend in the plot of T1 against T0. Each series ranging from T0 to T16 was plotted and fitted with a straight line to produce measures of these gradients. These values are in appendix table 5.

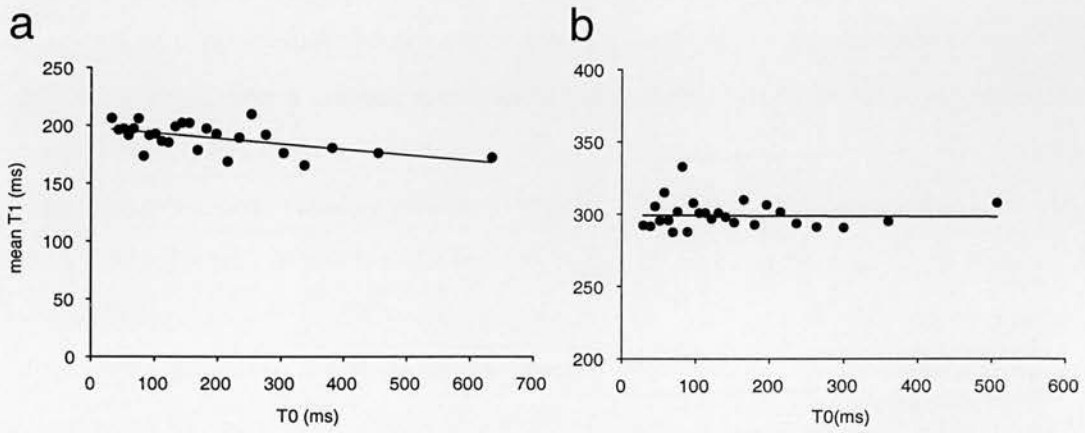

Figure 5.14: **a**. Spike train analysis applied to artificial data (modgen1) generated with AHP, fitted line shows negative correlation; **b**. model data generated without the AHP (modgen2) shows no negative correlation.

The gradients show an increase similar to the real data but they do not flatten out at the same rate. After 17 intervals the fit is no longer statistically significant and the trend in gradient becomes erratic sometimes decreasing and sometimes increasing again. However, within the range of series lengths which produces reliable results, the technique for detecting the AHP's effect on spike intervals has detected the same trend in model generated data. The control test of this is to compare the result with model data generated with no AHP. For this the model was properly fitted to the real data by adjusting λ and *Ire*, with *k*2 fixed at 0, to give no AHP. The basic analysis and fitted parameters are given below :

Dataset	modgen2
Number of spikes	5206
Mean ISI	171.2 ms
Output Rate	5.84 Hz
ISI SD	140.93
Histogram Mode	70 ms
Mode Height	163
λ	0.11
Ire	250

This model data has an output rate very close to the real data and the fitting process has given it an almost identical ISI histogram. Appendix table 6 gives the results of the interval length analysis.

The values immediately show the lack of any obvious trend against T0. Plotting T1 against T0 shows no significant downward gradient and the result is the same for each length of series. The fit gives a flat line indicating no relation between T0 and the proceeding intervals. This comparison of model data with and without the AHP proves that at least in the model data, the AHP is responsible for the correlation between spike interval lengths. The similarity with the results in real data is good evidence that the AHP is also responsible for this effect in real cells. This also casts doubt on the fitting results (including those published in the paper) which do not use the AHP. Although the model without any AHP can be made to accurately match the ISI histogram of real data, there are clearly properties of the cell's firing behaviour which are not adequately represented by the histogram alone, specifically those which affect firing at a level which involves activity beyond the time course of a

single spike. However, the AHP is the only major known electrophysiological property (except perhaps the DAP which is thought to be more significant in vasopressin cells, but more on which will come later) which is missing from the original model and so adding this should be sufficient to produce a good model of oxytocin cell firing. The next stage therefore is to reattempt the ISI histogram fitting with the addition of the AHP.

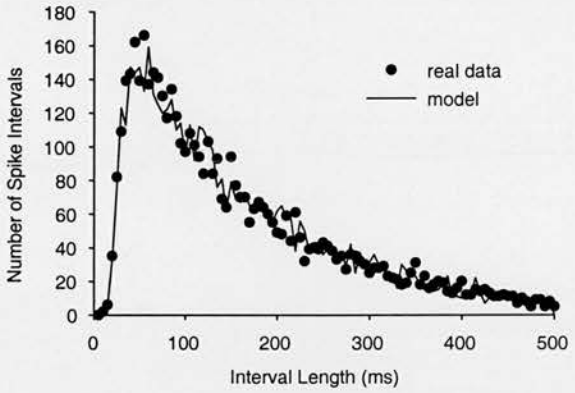

Figure 5.15: Real dataset mludw1 fitted with the model (dataset modgen3, parameters below)

5.5.3 Fitting the Model to Real Data With the AHP

The starting point for the fitting process is the fit without the AHP. The AHP does affect the front of the histogram but this is very dependent on output rate and it was hoped that this effect could be compensated by changing *Ire* without changing λ, the HAP's decay parameter. This in fact turned out to be the case; when the AHP was added with its default parameters, $k2 = 0.5$ and $\lambda 2 = 0.002$, the front of the histogram changed in gradient, with the mode shifting to the right. Readjusting the output rate to match the real cell by increasing *Ire* improved the fit again but still with a deficit of short spike intervals. To improve this, $k2$ was reduced and then *Ire* adjusted again to rematch the output rate and this produced a good visual fit between the two histograms, shown in figure 5.15. The process for adjusting $k2$ is similar to that for λ,

adjust $k2$ and then compensate the output rate with *Ire*. The final fit uses the parameters shown below with its basic analysis :

Dataset	modgen3
Number of spikes	5206
Mean ISI	174.2 ms
Output Rate	5.74 Hz
ISI SD	137.72
Histogram Mode	60 ms
Mode Height	159
λ	0.11
Ire	290
k2	0.3
λ2	0.002

All of the measured values are close to those for the real data, including the ISI standard deviation which is a closer fit than the model data (modgen2) that was fitted without the AHP and had a slightly higher value for the standard deviation. The output rate with modgen2 was slightly higher, but this would tend to make the ISI variance smaller rather than greater. This new model dataset was then tested by applying the AHP detection analysis (values presented in appendix table 7).

These new results immediately appear very similar to the equivalent figures from the real data. The plot of T1 against T0 shows a downward gradient similar to the real data which can be fitted with a statistically significant straight line. The fitted gradients for each of the series presented in the table above are given below, with the equivalent value from the real data for comparison :

Series	**Model Gradient**	**Real Data Gradient**
T1	-0.0785	-0.0739
T1+T2	-0.1245	-0.1125
T1+..+T4	-0.1480	-0.2037
T1+..+T8	-0.2008	-0.2400
T1+..+T16	-0.2009	-0.1881
T1+..+T32	-0.2867	-0.0406

Over the shorter series the model data produces a close match to the real data and the model data is definitely showing the same correlation between interval lengths, but in a similar manner to the earlier set of model data generated with the AHP, the plots against the longer series do not show the same decline in gradient as the real data.

This really needs to be tested by running the same analysis on more sets of real and model generated data to see whether this is a consistent result. If it is then the model must either be missing some behavioural element which exists in the real cells or there is a problem with model's implementation of the existing functional elements. The close match so far makes it appear likely that the AHP is responsible for the correlation between interval lengths in the real cell and given this assumption we can make some predictions about what results we would expect from the analysis. The effect of the AHP relative to a particular interval has to die out because of its decay. With the value for $\lambda 2$ used here the half life is 346.6 ms. At the output rate of 5.74Hz the start of the 32 spike series will on average be over 5.5 sec before the interval T0. With this half life, any significant remaining AHP is not likely to come from any longer than 2 sec before interval T0 and so the relation between T0 and the sum for the proceeding series of intervals should be reduced no later than when the series gets beyond this 2 sec point. Beyond this the average for the proceeding intervals should just level out and the gradient should gradually disappear. This is exactly the result which the real data produces but not what the analysis of the model data shows. The simplest explanation would be a difference in $\lambda 2$ between the two sets of data and the way to test this is to run the model data with a more quickly decaying AHP. Previous results have demonstrated that adjusting $\lambda 2$ and then changing *Ire* to match the match the output rate has no detectable effect on the histogram and so fitting the data by comparing ISI histograms does not necessarily fit $\lambda 2$. The results for the model data with $\lambda 2 = 0.003$ and *Ire* = 270 are given below :

Dataset	modgen4
Number of spikes	5206
Mean ISI	175.3 ms
Output Rate	5.71 Hz
ISI SD	138.13
Histogram Mode	40 ms
Mode Height	149
λ	0.11
Ire	270
k2	0.3
$\lambda 2$	0.003

This change in $\lambda 2$, which reduces the half life of the AHP to 230 ms, almost eliminates the detectable effect of the AHP. Fitted lines still produce a negative gradient, but much smaller than with the previous set of model data and not with a fit which satisfies statistical significance. This suggests that the previous match in gradients with the real data over shorter series already indicated a good fit with $\lambda 2$ and it appears unlikely that this parameter is the cause of the lack of gradient decay in the model data. The other simple explanation could just be error in the results. The effect of the AHP is of a very small magnitude compared to most of the model cell's behavioural components and so there is a large error in detection which requires the use of the large bins over interval lengths. The measure of gradient for long series of summed intervals is likely to carry a very large error. This was tested by re-running the model with identical parameters to the mode dataset modgen3, the best fit to the real data. The new results are below under model run 2 :

Series	Model Run 1	Model Run 2	Real Data Gradient
T1	-0.0785	-0.0678	-0.0739
T1+T2	-0.1245	-0.0896	-0.1125
T1+..+T4	-0.1480	-0.1395	-0.2037
T1+..+T8	-0.2008	-0.1819	-0.2400
T1+..+T16	-0.2009	-0.1676	-0.1881
T1+..+T32	-0.2867	-0.1121	-0.0406

This data shows similar values for the shorter series of intervals but very different results at the longer series which show a decrease in gradient in the same manner as the real data. The conclusion is that the current analysis technique has too great an error to properly detect the gradients of longer series. Improving the technique is left to later work, but although the current form is not good enough to accurately map the gradient as it falls back to a flat line, it has consistently detected the increasing gradient over shorter series of intervals where the AHP is still active relative to T0. Therefore it is sufficient to detect the effect of the AHP which it has successfully done in real and model generated data.

At this stage the data has been fitted as well as it can be by using just the ISI histogram to make a comparison. The form of the histogram is dominated by the output rate and what we now need is a more sensitive fitting mechanism which is

sensitive to the behavioural properties which are observed over a longer time course, particularly the relation between spike interval lengths. The next stage is to develop such a measure of fit, which can compare model data to a real data set by examining trains of individual spikes instead of just the histogram, which examines just the overall distribution of activity.

5.6 Measuring Fit Over Spike Trains

The idea here is to take a set of spike interval data and calculate the probability of each individual interval length based on the proceeding intervals being run through the model, i.e. present the model with the real spike timings and compare what would happen in the model with the real next spike.

A cut down version of the model takes the series of known spike firing times and simulates the AHP following each spike so that the model can produce a value for the summed AHP following the train of spikes. It is sufficient just to consider the AHP at this stage since this is the only value which is stored across spike intervals, and in fact it is this simplification that makes it a tractable problem to use the model to calculate fit based on spike interval lengths. This AHP value is then used to run the model for a single spike firing to match the one being examined in the real data. By repeatedly running the model for that single spike a histogram can be built up showing the probability distribution of spike intervals following the train of known intervals from the real data. This histogram is then used to get an approximate probability value for the actual interval length. The final measure which is used is the natural log of the probability value. This process is repeated for each spike interval in the real data so that the log probabilities of each spike interval can be summed to get a measure called the log likelihood. The set of model parameters which best match the real data should produce the highest value for the log likelihood. Likelihood in this context is defined as 'the hypothetical probability that an event which has already occurred would yield a specific outcome', in this case the set of proceeding spike intervals and the one being examined. The log likelihood gives a measure of

the likelihood of observing a whole set of data given a specific model. The assumption here is that the basic model is a good enough representation of the real system, and the set of varied specific models are based on just changes to the parameters.

5.6.1 Formalising and Implementing the Likelihood Measure

The likelihood of getting a predetermined series of spike intervals given the model with a specific set of parameters is represented by :

$$\begin{aligned} L(\Theta) &= P(\delta_1, \ldots\ldots, \delta_n \mid \Theta) \\ &= P(\delta_1 \mid \Theta)\ P(\delta_2 \mid \delta_1, \Theta) \ldots P(\delta_n \mid \delta_{n-1}, \ldots, \delta_1, \Theta) \end{aligned}$$

where Θ is the set of parameters and $\delta_1, \ldots, \delta_n$ are a series of n spike intervals with δ_1 representing the interval after the first spike fired by the cell. To calculate the exact value requires the product of the probabilities of each interval length given the model parameters and all those spikes which have come before. The log likelihood uses the sum of the logs of these probabilities instead of the product. Since we only have a limited record, of the cell's most recent activity, the simplification is made that the probability for each spike is conditional on a finite number of proceeding spikes, rather than all previous activity. This gives the form :

$$\log L(\Theta) = \sum_i \log(P(\delta_i \mid \delta_j, \Theta)) \qquad s.t.\ \ i > j > i - 20$$

where the likelihood is calculated from the last 20 spikes.

Each of these probabilities can then be calculated by using a cut down version of the model to generate the initial AHP for each spike, and then using a histogram to produce a probability distribution, as noted above. It is likely that similar values for the generated AHP levels will reoccur many times over the thousands of spikes being

examined and so the process is made more efficient by generating a table of histograms for all possible AHP values within the range that are found in the set of spike data.

The complete process is as follows :

1. For each spike use AHP portion of model to generate AHP level before that spike, store these
2. Analyse set of generated AHPs to find range of values and generate set of probability histograms to cover this range

To do this, for each AHP value the model is run thousands of times (usually 50000 runs) to produce a map of all possible spike intervals following the specified initial AHP level (the sum of AHPs from previous spikes). All of the generated spike intervals are then counted within short length ranges (bins) usually of 10ms. These bins are normally of uniform length over the whole range of spike intervals but they can also be sized on a logarithmic scale so that the front of the histogram where there are more spikes uses shorter bins and the tail where there are fewer spike uses longer bins. The size of the bins is a compromise between how finely the histogram can be indexed and the number of spikes which fall in each bin. More bins gives more accurate, finer indexing but too few spikes means that there will be too high an error in the count for that bin. The model in fact generates two versions of the histogram using uniform and logarithmically sized bins. These generate results which are slightly different by a small scaling factor and the result which is normally used is the one generated from the log binned histogram. A final issue with the bins of spike counts is that there is a small possibility of a long interval (at the tail of the histogram) occurring in the test data which does not occur during spike generation, giving a bin which has a zero count. This would return a 0 probability which can not used with the log function. To alleviate this, each bin is initialised with a count of 1. This has a small scaling effect on the final result but has no relative effect on the ordering of results from different tests.

The histogram forms an approximation of the probability distribution for the possible range of spike intervals. The probability for a specific spike interval is given by accessing the corresponding bin (which makes an approximation) and dividing the count for that bin by the total number of spikes. Generating a larger number of spikes for the histogram gives more accurate probability values but it is a very computationally expensive process and so is limited by the need to calculate a value within a reasonable time. The process is further approximated by binning values over the range of generated AHPs. The bin size is set so that approximately 100 histograms are generated for the AHP range. A typical range might be 0 to 5mV and so AHP values for indexing the histograms would be approximated to the nearest 0.05mV. This is still quite a fine measure and unlikely to compromise accuracy but it can be tested by repeatedly running to process to get a measure of the variation in the results.

3. For each spike interval in real data, access its initial AHP from previously generated values and then use this to index table of histograms
4. Index histogram using spike length to get probability value (count / total spikes in histogram)
5. Calculate log of probability and repeat for each spike summing log probabilities

The final value is the log likelihood, the measure of fit for the model and a specific parameter set, to the spike data being analysed. Because the log is being taken of values which are all below 1, the log values are negative and so the final total is negative number. A larger (or smaller if you take the absolute) value indicates that the probability scores were higher overall and so the fit is better. The log value is used to scale the probabilities which will usually be very small numbers.

This process generates a measure for just a single set of parameters. In order to fit the model it will be necessary to search over a range of values, over several parameters requiring many uses of the mechanism for measuring fit. The cost of this more sophisticated measure of fit is that it is a very slow process. Even on fast

modern computers searching the parameter space for a single set of real data can take days of run time. It is desirable to reduce the number of parameters which need to be varied to as few as possible. Some parameters can be fixed by using data from real cells which gives reliable values which apply across all cells of the specific type. The work here has also shown that it should be possible to fit some parameters, especially those which only effect behaviour over the course of a single spike interval, by matching the ISI histograms generated by the model and from the real data. These fits however are not unique and any of the parameters which may directly or indirectly affect behaviour beyond the range of a single interval (activity dependent behaviour) will still need to be searched with the more sophisticated interval analysis fitting system. A third way to reduce the parameter search space is by attempting to understand the dependencies between parameters. This can be used to simplify the search by replacing two parameters, treated independently, by a method where one is varied and the other is given a value calculated from the first. It is such dependencies which some of the earlier results in this chapter attempt to investigate but it can be an ambiguous and difficult process and only sometimes can the relations be well enough understood in order to eliminate a parameter from the search space. There can be middle ground however where knowledge can be used to at least limit a parameter's range.

5.6.2 Testing the Likelihood Measure

The first stage in using the new measure is to test that it does indeed return the best score for known best fits of parameters. To do this, instead of using real data, a dataset is artificially generated using the model. This gives a controlled set of data which definitely is represented by the model and has a known set of parameters. When the fitting mechanism is run with these parameters it should return the best fit value. The best value will vary between different datasets because they are calculated from spike interval distributions and so datasets with a higher output rate and

relatively taller columns in the histogram (larger numbers of short intervals) will be capable of returning higher log likelihoods.

The likelihood measure has been implemented in the model software so that the model can load a set of test data (either real or artificially generated by the model) and given a set of parameters, test the model with these values against the test dataset and produce a value for the log likelihood. The model software has also been adapted so that it can repeatedly generate fit measures for a range of parameter values, outputting the results to a text file.

A graph plotting the log likelihood against a single parameter being varied should show a peak at the true value for the parameter, the value which was used to generate the data. This graph is the form of the first tests of the fitting process. The first experiments test the two AHP parameters $k2$ and $\lambda 2$. These are likely to be two of the most important parameters in fitting data on the basis of spike intervals since it is appears to be the AHP which controls the relation between interval lengths.

The artificial data set was generated using the default model parameters with AHP parameters $k2 = 0.5$ and $\lambda 2 = 0.002$ and contains 10000 spikes. Its basic analysis is below :

Dataset	modgen5
Number of spikes	10000
Mean ISI	187.1 ms
Output Rate	5.34 Hz
ISI SD	141.20
Histogram Mode	50 ms
Mode Height	250
λ	0.1
Ire	300
k2	0.5
$\lambda 2$	0.002

When generating the fit scores (log likelihoods) the model was run with all the same parameters as the test data except for those being varied and 10000 spikes were used to generate each of the probability histograms.

In the first experiment the log likelihood was generated with a range of values for $\lambda 2$, varying from 0.0005 to 0.1. This more than covers all reasonable values for this parameter. Increments over this range were chosen to give enough values to accurately follow the resulting plot of log likelihood values, roughly varying the

change in the parameter value inversely with the rate of change in the fit score. The result is illustrated in figure 5.16a. The peak is at exactly 0.002, the value used to generate the test data and so the likelihood measure has correctly identified the true value for the data. The other important features are the slopes on either side of the best value. With lower values for λ2 the fit quickly degrades but higher values follow a much shallower slope, even if we plot λ2 over a logarithmic scale (figure 5.16b). It makes sense to plot λ2 on a logarithmic scale because its equation uses it in an exponential function. A similar plot to figure 5.16b is obtained by replacing λ2 in the plot with the AHP's half life (not shown).

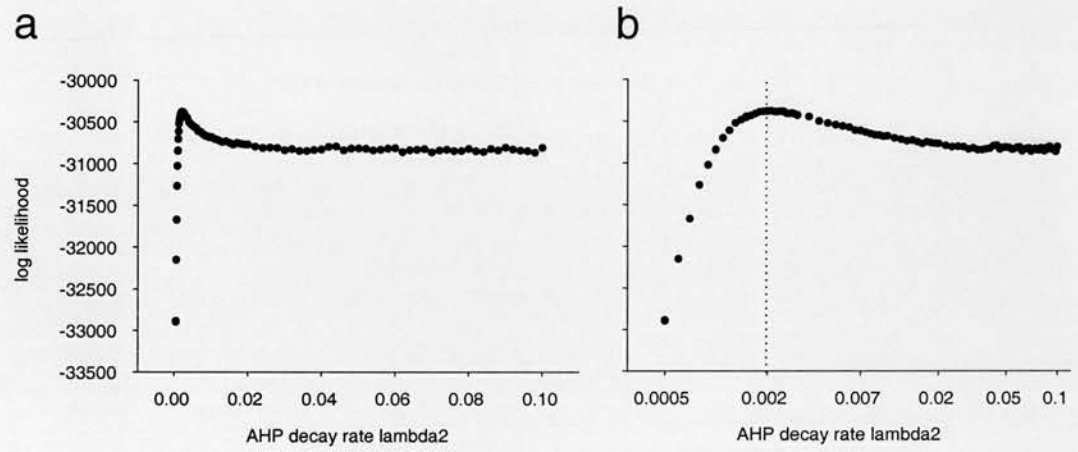

Figure 5.16: **a**. Measuring fit against model generated data (modgen5), varying λ2, true value is λ2=0.002; **b**. as a. with x-axis plotted on log scale, best fit measure at λ2=0.002, matching value used to generate data. Curve becomes less smooth, indicating larger error, at larger values for λ2.

The slope also gives some indication as to how difficult it will be to search for the correct value. A shallower slope will make the correct value harder to find with similar fit measures over a larger range of parameter values. A final feature to note is the less smooth curve for larger values of λ. This suggests a greater error in the log likelihood at larger values for λ2 and in fact the error becomes greater than any detectable slope. One of the problems with this method of measuring fit and the binning of data used to calculate values is that the amount of error will depend on parameters which determine the range of output values. If output values are over a greater range (for example a large range of spike interval lengths) then binning will

not have much effect on accuracy, being small relative to the range of values, but if bins are larger than ideal for the range of data values then they introduce a large error in the results.

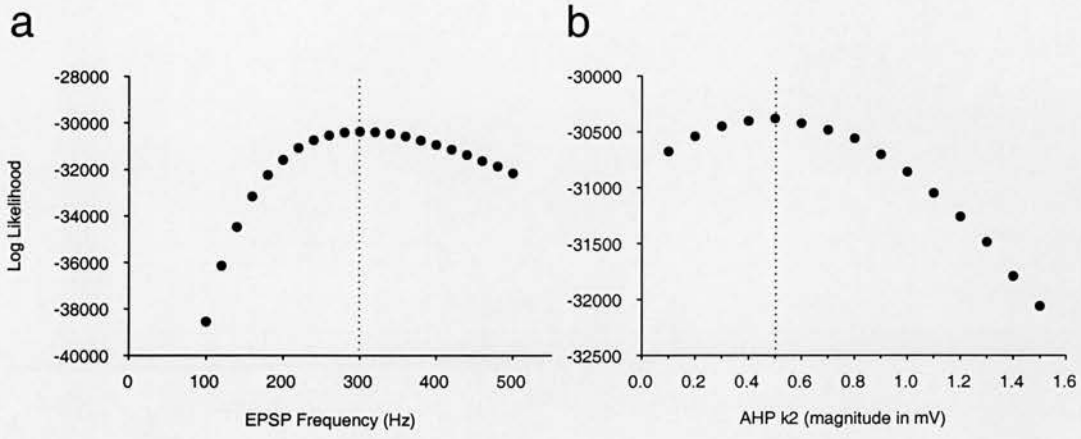

Figure 5.17: **a**. Measuring fit against generated data (modgen5), varying *Ire*, true value = 300; **b**. testing fit against *k*2, true value = 0.5; both plots show maximum fit score at the true value, plot gradients indicate how difficult finding true value might be in parameter searching, more gradual gradient makes searching harder

The second experiment repeats the same process for *k*2. This works as a more linear parameter and so we only need the single plot, figure 5.17a. Values for *k*2 were used covering a realistic range from 0.1 to 1.5 mV. The graph peaks at the true value for the dataset at 0.5mV with curved downward slopes on either side, of increasing gradient. This suggests that *k2* will be an easier parameter to search than λ2 with a well defined peak and reasonably steep slopes on either side giving lower fit scores for values which are too large or too small. The plot shows no obvious evidence of variation in error in the fit values.

The third experiment tests the log likelihood against variation in *Ire*. The true value for the test data was 300Hz and to generate fit values the parameter was varied over the range 100 to 500Hz. The plot (figure 5.17b) shows a clear peak at the correct value, sloping away to the left and right of the peak. With smaller values the log likelihood falls rapidly but not so quickly with larger values and with a more linear slope. Again there is no obvious variation in error in the data and the smooth slopes suggests that the error is small.

5.6.3 Error in the Log Likelihood Measure

To properly test the error in the log likelihood the fitting process was run repeatedly with the same set of parameters and a fixed number of spikes for the probability histogram on the test dataset. Ideally the error needs to be measured with different parameter values in order to show how the parameters affect error, but this is limited by the time taken to run the fitting process. The first plotted results (figure 5.16) with varied parameter values suggest that the error increases with larger values for $\lambda 2$ and so this is also tested by varying $\lambda 2$. However this initial test just measures the error with two different sizes of probability histogram, 10000 spikes and 50000 spikes and two values for $\lambda 2$. More thorough testing is left for later work.

A larger number of spikes should reduce the error but it is difficult to predict by how much since there are other factors which approximate the log likelihood such as the bins for indexing the AHP size to the probability histogram. Each test is based on 50 runs. The results are in the table below :

Histogram Spikes	10000	50000	10000	10000
Mean Log Likelihood	-30346.32	-30365.37	-30446.00	-30813.75
Maximum	-30333.22	-30359.43	-30433.34	-30799.87
Minimum	-30359.88	-30372.35	-30458.01	-30834.25
Range	26.66	12.93	24.67	34.38
Standard Deviation	6.11	3.11	6.50	6.71
Standard Error	0.87	0.44	0.93	0.96
$\lambda 2$	0.002	0.002	0.001	0.004

The results using 50000 spikes clearly show a reduced error in the log likelihood but it also produces a mean which is shifted to a lower (more negative) value. When the binned histogram is used to calculate probabilities the number of intervals falling within the bin's range is divided by the total number of spikes. This means that initialising the bins with a count of one has a greater biasing effect when the number of spikes is lower, resulting in a higher log likelihood. This effect probably explains the variation in mean log likelihood observed here. The alternative to using 1 unit initialised bins is returning a very small value, epsilon when the bin is empty but this can result in similar problems when fewer spikes leave more empty bins and epsilon

is used more often. The results here show no significant variation in error with $\lambda 2$, although the slightly larger error with $\lambda 2 = 0.004$ is still consistent with this idea. It would require to be tested with a larger number of spikes and a larger range of values for $\lambda 2$ to prove this properly. Unfortunately this takes a very long time to run and is left for future work.

Relative to the size of the log likelihood scores the error here is very small although whether it is small enough to be insignificant in searching for a best fit will depend on the gradients in the search space. If these gradients are very shallow with little variation in search score over a range of parameter values, as is suggested by the plot of fit against $\lambda 2$, then the error may play a role in making the search more difficult.

5.6.4 Varying Two Parameters

Fitting is very easy with only a single parameter to vary since the search space of possible parameter values is only a single dimension and so it is only necessary to search a reasonable range of values on this single line to find the peak fit and best parameter value. However with real data, even if the HAP parameters can be sufficiently uniquely and reliably fitted using just the ISI histogram, and other parameters which have remained fixed so far can stay so, it will be necessary to vary at least *Ire*, $k2$ and $\lambda 2$ to find the model's best fit to the data. This will give a three dimensional search space and it is likely to be much more complicated than just a single peak with simple continuous slopes leading to the best of parameter values. It is likely to have many peaks which may be close in height to the true peak and may have deep valleys nearby the true maximum making it difficult to find. More dimensions also mean a far greater number of parameter combinations (essentially vectors if each parameter is considered as an axis of the search space) to test, which grows exponentially with the number of parameters.

It is only possible to easily visualise a two dimensional search space since a third dimension is required for the measure of fit. The two parameters being investigated

here are $k2$ and $\lambda 2$ since these are likely to have a complex and important relationship to the model's fit to the data. Here the model is tested in a factorial manner, essentially a grid of values for these two parameters, varying one parameter over its full range, changing the second parameter by one unit and then repeating to test every pair of values over a range for each parameter. The log likelihood is plotted as a third dimension against the two parameter values. To show this in a two dimensional figure a contour plot is used, where the two parameters form the two dimensions of the surface and the third height dimension is represented by variation in colour or contour lines, similar to a map. This depicts the search space as a landscape with areas of low and high fit scores represented by peaks and valleys. The shape of the search space should give some indication of how best to go about searching the parameters for the best fit in real data, particularly suggesting how fine the increments in parameter values may need to be and how to relate changes in value between the two parameters. With dependent parameters such as these two it should be possible to find ways of changing them in a non-independent manner, i.e. changing one parameter only relative to the other, which will greatly cut down the search space.

5.6.5 The $k2$-$\lambda 2$ Search Space

To investigate this space, the model was run to generate log likelihoods for the test dataset modgen5 with $k2$ varying from 0.1 to 1.0mV in 0.1mV increments and $\lambda 2$ varying from 0.0005 to 0.03 in varied increments chosen to get a good idea of the search space's form. The model was run using 50000 spikes to generate the probability histograms. The fit scores were then plotted as a coloured contour plot of $k2$ against $\lambda 2$ with shade and contour lines indicating the log likelihood. Scores were also rescaled to give a more linear contour distribution. The plot with rescaled height values (figure 5.18) illustrates the shape of the search space. The highest point (in red) matches the true values for the parameters at $k2 = 0.5$ and $\lambda 2 = 0.002$ but there is a ridge of points with very similar fit scores, of a range within the error in the log likelihood.

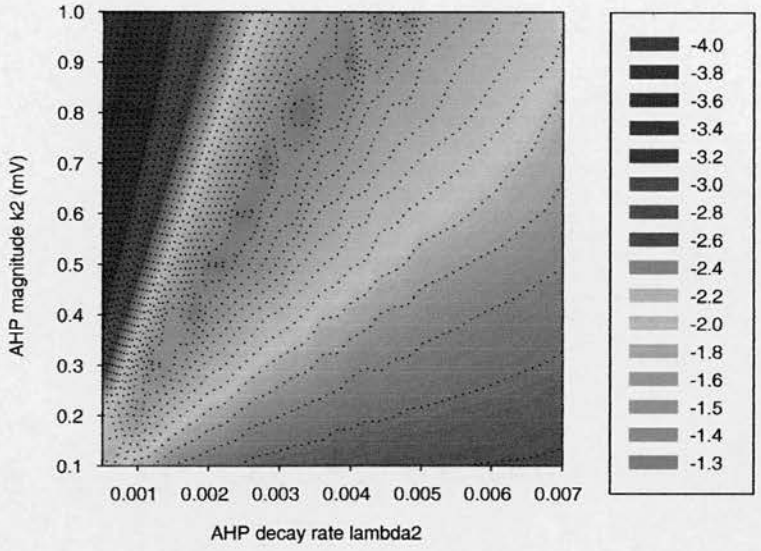

Figure 5.18: Contour plot of fit measure (indicated by colour, red=best fit) against $k2$ and $\lambda 2$; model generated dataset modgen5, k2=0.5, $\lambda 2$=0.002; log likelihood score rescaled, shows diagonal ridge indicating best fits, ridge becomes wider as $k2$ or $\lambda 2$ increases, low gradient along ridge makes finding exact maximum difficult. Local peaks on the ridge correspond to parameter resolution rather than the true form.

There is a slope in the ridge up towards and down from the point with the real parameter value but it is very shallow particularly in the direction towards higher values of $k2$ and $\lambda 2$. This ridge corresponds to pairs of $k2$ and $\lambda 2$ values which all generate good fits to the dataset, with $\lambda 2$ increasing as $k2$ increases in an almost linear relationship. The description of the linear form of the ridge is based on initial observation of the plot. It does also suggest that the ridge may curve to the left at higher values for $k2$ but at this point the ridge also becomes wider and less sharp and there may be a larger error in the fit values with the larger values for $\lambda 2$. The exact form needs to be traced by running the model with larger numbers of spikes to reduce the error and using finer increments in the parameter values. The fit values slope away steeply to the left of ridge and slope downwards at a more shallow gradient to the right, in a similar manner to the plot of $\lambda 2$ (figure 5.15) which dominates the form over $k2$, with its more extreme gradients. If the $\lambda 2$ axis is

replaced with the AHP half life, which essentially linearises the axis with respect to time, the ridge remains but curving upwards as $\lambda 2$ increases.

Ideally this plot would be repeated for at least varied values for the parameter *Ire* but unfortunately the amount of computation required to construct this plot using sufficient numbers of spikes to reasonably reduce the error restricts this so far. However it is unlikely that the basic form would change. It appears that there is a linear relationship between $k2$ and $\lambda 2$ with respect to the best fit value, and it should be possible to use this in searching by fixing one of the two parameters and then finding the best value for the other. The search routine would then restrict itself to searching along the ridge by using the relationship to calculate the value of the second parameter given the first. Assuming the linear form is reliable it should be possible to discover the relationship for any set of test data by finding the best score for two values of one parameter to find a line between the two (or more to reduce the error if finding reasonably exact values is difficult) and then using this to generate a formula for the relationship.

5.6.6 The $k2$–$\lambda 2$ Ridge

In this experiment the ridge in the $k2$-$\lambda 2$ search space was further investigated by plotting it with finer increments in the two parameters, searching, with values for $k2$ ranging from 0.1 to 2.0mV, to find the $\lambda 2$ value with the best fit score, in order to trace the ridge. The probability histograms were generated using 50000 spikes. The results are plotted in figure 5.19a. This clearly shows a linear relation between $k2$ and $\lambda 2$ and the log likelihood. A straight line can be fitted very closely to the points on the plot. The gradient for the fitted line is very close to the ratio between the true values for the two parameters indicating that the best value for $\lambda 2$ can be predicted using the formula $\lambda 2 = k2 / 250$. The plot also illustrates the increase in error at higher values for λ. A second figure (figure 5.19b) plots the log likelihoods at these points against $k2$. This shows a well defined peak, covering a fairly small range of values for $k2$. The best score is at a $k2$ value slightly higher than the true best fit at

0.5, but the difference in score is well within the error in the log likelihood. A difference of about 0.5 covers the range of $k2$ values within the error range of being the best value. This range extends mainly to the right of the true value, towards higher $k2$ values.

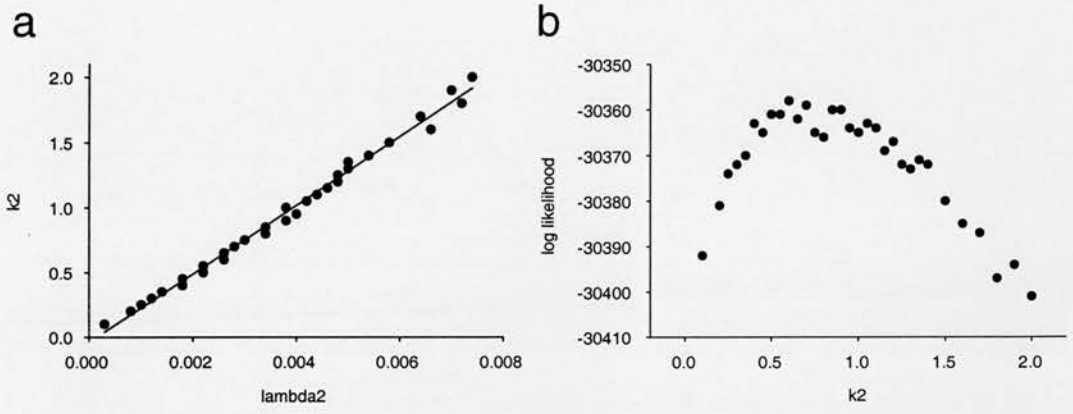

Figure 5.19: **a**. plot of λ2 values corresponding to best log likelihood scores over a range of k2 values, shows a distinct linear relationship between the two parameters, corresponding to the ridge observed in figure 5.18; **b**. plot of the corresponding best log likelihood scores over k2, showing the gradient along the ridge, does show a maximum but error in log likelihood scores mean this covers a range of k2 (and corresponding λ2) values.

The second plot shows that the linear relationship between $k2$ and λ2 cannot be used to reduce the two to a single parameter, but it does demonstrate that it should be possible to use this relationship to vastly reduce the search space by using the method described in the previous section. If the ridge can be found and accurately defined by a formula relating $k2$ and λ2 then the search between these two parameters will be reduced to a one dimensional space.

5.7 Searching the Parameter Space

The work here has suggested some ways of searching the parameters for the best fit but this is in the limited scope of just two parameters. The method may still work

with more parameters but it will not be so simple, and testing this properly is currently out of range of the time available. The third parameter to consider is *Ire* and with other parameters fixed it should be possible to fit this just on the basis of output rate, although this relies heavily on having good values for the other parameters.

The first search method which is to be tested is a standard method for finding the best fit in a multiple parameter search space called the *downhill simplex method* (Nelder and Mead 1965). This is a method for moving through the parameter space which attempts to go in a direction which leads to better fit scores eventually finding the best set of parameter values. A multiple parameter search space contains so many possible sets of parameter value that it is only ever possible to evaluate a small proportion of these sets of parameters, especially when, as is the case here, the evaluation function (running the model to get the log likelihood) is very expensive computationally. It is necessary to use some sort of rules to govern how to move through the search space. In simplex searching a set of parameter vectors is maintained which consists of a single apex point and then a set of points which each vary from the apex in just a single, unique, dimension, i.e. just one parameter value varies from the apex. The simplex has one more point than the number of parameters (dimensions). In three dimensions the simplex takes on the form of a triangular pyramid. The simplex moves through the search space by changing one of its points (parameter vectors) at a time using several different methods including stretching one point away from the others, reflecting itself, shrinking, or tilting onto another side. The simplex can use many more than just 3 parameters, in which case it becomes more difficult to follow a geometric interpretation. Its goal is to have all of its points (sets of parameter values) all within a specified range of the best fit score it has found. This type of method is classed as 'evolutionary' since it consists of a population of solutions (parameter sets) that it is gradually evolved towards an ideal based on some measure of fitness.

5.7.1 Implementing Simplex Search

The simplex search has been added in to the model software directly using the code from Numerical Recipes (Press *et al* 1992). A fitness function interfaces the simplex search procedure with the model's log likelihood generation by converting the parameter set into a form that can be passed to the model and also filtering parameter values which are beyond the accepted range (limits which go well beyond the range of biologically realistic values) by immediately returning a very low fitness score (a value lower than any that can be returned by the log likelihood). These accepted ranges are presented in the table below :

Parameter	Minimum	Maximum
Ire	100	none
*k*2	0	10
λ2	0.00005	0.2

The final output is a text file detailing each fitness evaluation made during the search, including each set of parameter values tested and the final set of parameter vectors which achieve the best fitness score. If the simplex search successfully converges and manages to get all the points (parameter vectors) within the specified range then this gives a final set of parameters fitted to the test data. This range is specified by a parameter, *ftol*, which defines the range relative to best score. The value currently used for this is 0.0001. With scores in the range of –30000 this means the scores for the final set of points must be within around 3 units. This is well within the error in the log likelihood but setting a larger range would risk the simplex converging before getting very close to the true parameter values and so choice of the range against which to test for convergence is based on a compromise between getting the fit scores for each point to eventually converge and not converging before each score is reasonably good. This can be tested empirically to find the best value and the initial value used here is already based on early testing. Even if it does not converge within a reasonable amount of time, the search can be halted and the current set of parameter vectors taken as the result. The simplex tends to reduce its step size to a very small value as it gets close to the best fitness score and it can

sometimes have effectively already converged without getting scores for the parameter sets that satisfy the range test. In this case the process is stopped and the current set of parameter sets taken as the result.

The simplex method is fairly economical in terms of the number of fitness evaluations (tests of a particular set of parameters) required to search the space, on the order of 100 when varying three parameters, but given the already computationally expensive fitness test, running the model around 200000 times to generate a probability histogram, the search takes a long time, around 24h when varying 3 parameters. This has limited the range of testing that has been done so far.

5.7.2 Initial Parameter Sets

The only major issue in using the simplex method, after selecting which parameters to vary, is the choice of initial parameter sets, of which with 3 parameters for example there need to be four. The problem of choosing the initial parameter sets is related to choice of step size for each parameter. The version of the simplex method used here varies step size for each parameter as it searches, so step size is not such an important factor in search but it does play a role in setting up the initial simplex, which will affect how well the search progresses. In fact, the current version of the method uses the distance of each parameter set from the apex to define the initial step size for the parameter which is being varied by that particular set (each initial parameter set varies from the apex set in just one parameter). An old paper, (Yarbro and Deming 1974) deals with this problem. The two options are either to start with a small simplex and step size and let it grow in the appropriate direction towards the best solution or to start with a larger simplex and step size and let the simplex shrink and refine itself down a set of ideal parameter sets. Which method is best will depend on the particular problem and so both of these methods will be tested. A small simplex would consist of an apex set either somewhere in the middle of the range of sensible parameter values or at the lower end of each range with other points spaced by a small step (sized relative to each parameter range) away from the

apex. A large initial simplex would use an apex with parameter values at the lower end of each range and other points which alter one parameter towards the upper end of its range.

5.7.3 Testing the Simplex Method With Artificial Data

The first stage in testing this search method is to test whether it can find the true parameter values for data which has been generated by the model. With such artificial data it is known for certain that the model is a perfect fit and the parameters not being varied are controlled. In order to give the simplex a more linear range for $\lambda 2$, it works with a logarithmic function of the parameter value. Where the simplex uses the value x, $\lambda 2$ is calculated using the formula below :

$$\lambda 2 = \exp(-x)$$

This reduces the non-linear variation in the effect on the fit score with parameter value steps of a similar size.

The first test varies just a single parameter. The simplex search was run on the test dataset modgen5 ($k2$=0.5, $\lambda 2$=0.002), using 10000 spikes for the histogram, varying $\lambda 2$ and using the following initial parameter sets :

Initial Set	$\lambda 2$ (mapped value)
1	0.00091 (7.0)
2	0.49700 (0.7)

The simplex search ran for 17 fitness evaluations (testing a set of parameters with the model) and finished with the following parameter sets :

Result Set	$\lambda 2$ (mapped value)
1	0.0019 (6.2617)
2	0.0020 (6.2125)

The search has successfully found two good parameter sets, one with the exact true value for λ2, 0.002 and another which is very close. The second test varies just the parameter *k*2, which already works on a linear scale and requires no re-mapping such as that used for λ2. The initial parameter sets were as follows :

Initial Set	*k*2
1	*0*
2	*5*

The simplex ran for 14 fitness evaluations and produced the following final parameter sets :

Result Set	*k*2
1	0.4688
2	0.5078

These results are both close to the true value at 0.5 and so the simplex has successfully found the true parameter value. Both of these initial tests use sets of initial parameters (just one in this case) which cover the range of normal values giving a large initial step size. In the case a single parameter this appears to work well. Future work should add a test with a smaller initial range.

The next experiment moves to varying two parameters, λ2 and *k*2. A range of values for *k*2 and λ2 along the ridge previously described produce very similar fitness scores, within the error in the log likelihood and the simplex is likely to have problems differentiating values which fall along this ridge. For this experiment the simplex was tested with three different sets of initial parameter sets, these and the respective result sets, including the ratio of *k*2 to λ2, are given below :

Initial Set	λ2 (mapped)	*k*2
1	0.00091 (7.0)	0.0
2	0.49700 (0.7)	0.0
3	0.00091 (7.0)	5.0

Result Set	λ2	*k*2	ratio	Fitness score
1	0.0037	0.9821	265.4	30343.09
2	0.0029	0.7475	257.8	30344.06
3	0.0028	0.6055	216.3	30344.01

Initial Set	λ2 (mapped)	$k2$
1	0.00248 (6.0)	0.1
2	0.01111 (4.5)	0.1
3	0.00248 (6.0)	2.0

No sufficient convergence in fit scores (although close)

Stop at $\lambda 2 = 0.0046$, $k2 = 1.04$ (ratio = 226.1)

Initial Set	λ2 (mapped)	$k2$
1	0.00091 (7.0)	0.1
2	0.01111 (4.5)	0.1
3	0.00091 (7.0)	2.0

Result Set	λ2	$k2$	ratio	Fitness score
1	0.0045	1.1910	264.7	30343.15
2	0.0034	0.8097	238.1	30344.62
3	0.0023	0.5750	250.0	30343.31

The first test uses a set of initial parameters which covers the range of normal values and finished searching after 20 fitness evaluations. Its results are close to the true values although all of them have values which are higher than the perfect $k2 = 0.5$ and $\lambda 2 = 0.002$. The ratio between the two appears to follow the ridge, which relates $k2$ and $\lambda 2$ by the exact value 250. The second test uses initial parameter values which cover a smaller range, although they still vary on either side of the known true value. This run failed to find three parameter sets with sufficiently close fitness scores and was stopped, with the simplex testing the values shown. These are again fairly close to the true values, following a similar ratio. The third test uses a mix of the first and second initial parameter sets and successfully converged after 16 fitness evaluations. The results are similar to the first test but one parameter set is very close to the true values with the exact 250 ratio. The final fitness scores for the two converged runs are very similar and are toward the lower end of the range of scores obtained testing the log likelihood with the true parameter values and 10000 spike histograms. On the basis of the log likelihood and the error in its calculation the simplex is fitting the parameters as well as it can. The varied initial parameter sets have had no effect on the quality of the final fit, at least on the basis of the scores.

5.7.4 Fitting Artificial Data with Three Parameters

The third parameter to be added to the simplex search is *Ire*, the PSP input rate. The work in earlier sections of this chapter suggests that a more intelligent way to fit this parameter would be to match the output rate of the test data but the trouble with this is that it assumes that the other fixed parameters, and the model itself, are a good fit to the test data. While this is known with the artificial test data, it will not be so certain with real data and since this is a very important parameter and one which is difficult to estimate a value for from general experimental data, it makes the ideal parameter to add to the search. The range of initial values for *Ire* had been chosen to vary on either side of the true value, 300.

The first test is detailed below :

Initial Set	λ2 (mapped)	*k*2	*Ire*
1	0.00091 (7.0)	0.0	100
2	0.01832 (4.0)	0.0	100
3	0.00091 (7.0)	5.0	100
4	0.00091 (7.0)	0.0	500

Result Set	λ2	*k*2	ratio	*Ire*	Fitness score
1	0.0013	0.2374	182.6	284.2	-30349.34
2	0.0012	0.2319	193.3	288.0	-30349.40
3	0.0013	0.2292	176.3	283.8	-30351.39
4	0.0012	0.2316	193.0	287.5	-30350.29

This run converged after 46 fitness evaluations. The final parameter sets are all very similar and fairly close to the true parameter values. The *k*2 values are all quite low however and should be slightly higher relative to this value for λ2, indicated by the low ratio which ideally should be 250. This is probably partly due to the slightly lower than true (300) *Ire* values which compensate against lower *k*2 values (see section 5.4.1). For the next experiment the same test was repeated using 20000 spikes to generate the probability histograms, it converged after 37 fitness evaluations :

Result Set	λ2	*k*2	ratio	*Ire*	Fitness score
1	0.003214	0.8570	266.6	297.8	-30352.90
2	0.004625	0.8889	192.2	285.2	-30349.96
3	0.004566	0.7218	158.1	273.0	-30357.24
4	0.003285	0.8823	268.6	304.9	-30350.21

These are better fits than those obtained with 10000 spikes. Although the fitness scores are similar it must be remembered that they tend to be more negative with a larger number of spikes and so these are actually better scores. The parameter set (number 3) with the worst $k2/\lambda2$ ratio and lowest *Ire* value has the worst fit score. The $k2$ values are all higher than the true 0.5 value but they have good matching $\lambda2$ values, particularly sets 1 and 4 which also have the best values for *Ire*, very close to the true 300. This is more evidence that there is a relation between the ratio and the value for *Ire*, with lower *Ire* values coinciding with a lower $k2/\lambda2$ ratio.

For the final testing (so far) of the simplex search with artificial data a new test data set was created with different parameter values for $k2$ and *Ire* :

Dataset	modgen6
Number of spikes	10000
Mean ISI	119.4 ms
Output Rate	8.38 Hz
ISI SD	84.89
Histogram Mode	45 ms
Mode Height	450
λ	0.1
Ire	400
k2	0.2
$\lambda2$	0.002

This new dataset has a smaller magnitude AHP and faster input rate, producing a higher output rate than the modgen5 dataset. Different datasets have a different range of log likelihood scores and so to find the ideal score for comparison with the simplex results the new dataset was first tested by running the model 5 times with 20000 spikes histograms to produce a range of fit scores with the true parameters. The results were as follows :

Histogram Spikes	20000
Mean Log Likelihood	-27823.04
Maximum	-27819.07
Minimum	-27825.93
Range	6.87
Standard Deviation	2.84
Standard Error	1.42

With a higher output rate and larger numbers of spikes in a smaller spread of intervals this dataset will tend to get higher probability scores, with fewer spike intervals falling in long interval bins with low numbers of spikes, and the final log likelihoods are correspondingly higher. The range of values is smaller but the number of trials here is too small to really compare with the earlier more thorough error analysis.

This new dataset was tested with the simplex using 20000 spike histograms and two different initial parameter sets :

Initial Set	λ2 (mapped)	*k*2	*Ire*
1	0.00091 (7.0)	0.0	100
2	0.01832 (4.0)	0.0	100
3	0.00091 (7.0)	5.0	100
4	0.00091 (7.0)	0.0	500

Result Set	λ2	*k*2	ratio	*Ire*	Fitness score
1	0.000819	0.2727	333.0	552.62	27812.52
2	0.000823	0.2698	327.8	548.85	27823.66
3	0.000811	0.2711	334.4	551.09	27823.48
4	0.000840	0.2720	323.8	545.63	27819.16

Initial Set	λ2 (mapped)	*k*2	*Ire*
1	0.00091 (7.0)	0.1	500
2	0.01832 (4.0)	0.1	500
3	0.00091 (7.0)	5.0	500
4	0.00091 (7.0)	0.1	200

Result Set	λ2	*k*2	ratio	*Ire*	Fitness score
1	0.002065	0.2719	131.7	422.37	27815.26
2	0.002064	0.2707	131.2	421.93	27815.07
3	0.002080	0.2704	130.0	421.69	27813.38
4	0.002060	0.2708	131.5	422.42	27808.87

The first test has found quite a poor fit with a small value for λ2 and a high value for *Ire*. The *k*2/λ2 ratio is much higher than the ideal score of 100 (0.2 / 0.002) for this dataset. It appears that the low value for λ2 and the high input rate have compensated against each other to create good fit scores. The second test run has found a much closer match to the true parameter values. The value for *k*2 is still slightly high but the λ2 and *Ire* values are much closer to the true parameter values at 0.002 and 400

respectively. The $k2/\lambda2$ ratio is correspondingly much closer to the true value, 100. The values for the ratio and *Ire* are consistent with the previous relationship observed with modgen5, with a higher $k2$ compensating against the higher input rate (*Ire*).

These experiments have demonstrated that the simplex search can find a close match to the real parameter values. As would be expected it becomes more difficult as the number of parameters increases, with the quality of the final set of parameters, in terms of their closeness to the true values, varying between runs and different sets of initial parameters. The search does however always find parameter sets which have a fitness close to the best which can be achieved. Unfortunately the error in the log likelihood means that there are a range of parameter values which can achieve very high fitness scores. Attempts so far have not been able to reduce this error without making the amount of time required to run the tests impractical. One of the most important results here is the ability to relate the variations in parameter values between each other. When just $k2$ and $\lambda2$ are varied, the fit which the search finds always lies close to the $k2$-$\lambda2$ ridge in the search space, and since this ridge is a straight line this can be measured by calculating the ratio between these two parameter values. With three parameters this ratio can in turn be compared with the value for *Ire*. As was demonstrated in the early experiments with the AHP, variations in $\lambda2$ and $k2$ can be compensated by varying *Ire*, at least to match the ISI histogram. These compensations can be related to the values found by the simplex, with a higher value for *Ire* corresponding to a lower $\lambda2$ or higher $k2$ value and a matching increase in the ratio between $k2$ and $\lambda2$. It may be possible to better prove and extend these relations with further testing of greater ranges of values but this is left for future work.

Whether these relations will hold with real data will depend on how well the model in general and the other, fixed parameters fit the real data. The earlier results comparing the model and real data with the ISI histograms suggest that the model is a good fit to the real data and these experiments also demonstrated how to fit some of the parameters before experimenting with the AHP. It should be possible to use these techniques to attempt to fit the real data with the simplex using a fairly small number of varied parameters. The major difficulty with real data compared to the artificial

data is assessing how good the resulting parameter sets are, without knowing the true parameters or the best possible fit scores. The only way to test the found parameters will be to run the model with them and then compare the ISI histogram and the fitted line gradients using the spike interval analysis AHP detection technique.

5.7.5 Testing the Simplex Method With Real Data

The first tests of the simplex with real data go directly to running the simplex search with the current default parameters and just allowing $\lambda 2$, $k2$ and *Ire* to vary. The purpose of this is to compare the results with later experiments, yet to be run, which allow the simplex method to vary a larger number of parameters, and attempts to fit some of the other parameters such as λ before fitting with the simplex. The aim of this is to test how consistent the results with real data are and to find out more about how the parameter fits which are found might be affected by varying more parameters or using different values for the fixed parameters. The overall goal is to be able to produce a consistent and confident fit to real data with parameter values that relate directly to real neuronal components, or failing that identify how the model needs to be changed to achieve this. This is ambitious but if it could be achieved then the model would provide a powerful tool for measuring otherwise inaccessible properties of neurons and their firing patterns.

The first experiment tests the simplex with the real dataset mludw1 and was run using 20000 spike histograms. The initial parameter sets are similar to those used with the artificial data. The results show two identical runs which both failed to converge but did end with fairly consistent final parameter sets :

Initial Set	**$\lambda 2$ (mapped)**	***k2***	***Ire***
1	0.00091 (7.0)	0.0	100
2	0.01832 (4.0)	0.0	100
3	0.00091 (7.0)	5.0	100
4	0.00091 (7.0)	0.0	500

The first run was ended with the parameter set :

Result Set	λ2	*k*2	ratio	*Ire*	Fitness score
1	0.0078	0.18	23.1	258	-30071

The second run ended with :

Result Set	λ2	*k*2	ratio	*Ire*	Fitness score
1	0.0056	0.193	34.5	259.6	-30067

All of the four parameter vectors in each set were very similar, identical to 3 significant digits, and so just a single parameter set is shown for each run. The two sets are similar with very close values for *Ire* and a slightly higher *k*2 and lower λ2 giving a higher ratio on the second run. The parameter values all fall within the normal range of values used with the model data although the *k*2/λ2 ratio is smaller than with the artificial data. In earlier work this real dataset was fitted using the ISI histogram and also by comparing the fitted line gradients in the spike train analysis. The values for the fitted AHP parameters were $k2 = 0.3$ and $\lambda 2 = 0.002$ and *Ire* was fitted at 290Hz. The only fixed parameter which varied with the previous fitting was the HAP λ at 0.11 compared to the 0.10 used with the simplex search. The next experiments here should be to run the simplex search with $\lambda = 0.11$ and to produce a set of model data using the parameter values found with the varied values for λ for comparison with the real data's ISI histogram and spike train analysis, but these are yet to be run.

The final experiment tests a second real dataset, mludw2, with the simplex using two different initial parameter sets. The basic analysis for this real dataset is presented below :

Dataset	mludw2
Number of spikes	13000
Recording time	45 min
Mean ISI	208.1 ms
Output Rate	4.81 Hz
ISI SD	139.88
Histogram Mode	95 ms
Mode Height	350

This is a longer recording than mludw1 and has a lower average firing rate (compared with 5.74Hz) with a slightly higher ISI standard deviation. The simplex search was run using the default fixed parameters and 20000 spike histograms. The results for the two runs are shown below :

Initial Set	λ2 (mapped)	*k*2	*Ire*
1	0.00091 (7.0)	0.0	100
2	0.01832 (4.0)	0.0	100
3	0.00091 (7.0)	5.0	100
4	0.00091 (7.0)	0.0	500

Stopped at :

Result Set	λ2	*k*2	ratio	*Ire*	Fitness score
1	0.0043	1.55	360	300.9	-30565

Initial Set	λ2 (mapped)	*k*2	*Ire*
1	0.00091 (7.0)	0.1	500
2	0.01832 (4.0)	0.1	500
3	0.00091 (7.0)	5.0	500
4	0.00091 (7.0)	0.1	200

Stopped at :

Result Set	λ2	*k*2	ratio	*Ire*	Fitness score
1	0.0073	2.88	394	299.1	-30545

These two runs use the same initial parameter sets as the final experiment with the artificial data. The first initial set is the same as the test run with mludw1.

Both runs produced almost identical values for *Ire* but the second run fitted a much higher value for *k*2. However this is matched by a higher value for λ2 and the *k*2/λ2 ratios are quite a close match. The fitness scores for the second run are slightly better. The fitted parameter values are all still within the range of values considered to be realistic although the higher value for *k*2 is beyond what has previously been tested with the model. The fits with both of these real datasets have close values for the *k*2/λ2 ratio suggesting that there may be a similar ridge in the search space to the

artificial data. The way to proceed with this dataset is to attempt the same type of fitting with the ISI histogram used with mludw1 to get estimated values for the HAP and AHP parameters and then use these to run the simplex search again. These fits can then used to be used to generate artificial datasets which can compared with the real data using spike train analysis. It may also be worth testing the simplex with more varied sets of initial parameters, to test how consistent the fits are, and to better define the relations between the different sets of fitted parameters.

5.8 The First Future Work

Many of the experiments presented can themselves be extended, and this has already been outlined. The main limitation has been the computational load of calculating the log likelihood. It will be important to extend the number of real datasets tested, to test the consistency of results, and also to further develop the parameter relations with respect to the search space in order to make search for the best fit more efficient and accurate. There may be better search algorithms to use. The search space is very gradient sensitive and there are other multi-parameter search algorithms which are specifically designed to take gradient into account. A further way of exploring the behaviour of the AHP will be to detect how much it summates between spikes. When it climbs to a higher level it slows down firing rate, limiting its own accumulation. It is therefore likely to have some form of equilibrium level. It will be possible to compare the value detected with the model to equivalent measures in electrophysiological experiments.

Another direction will be to expand the model by including the DAP. This is more dominant in vasopressin cells, but it is also thought to be present in oxytocin neurons. Its effect is usually masked by the AHP. An important test will be whether adding this has a significant effect on the existing results. It will also allow the model to be tested with recordings from vasopressin cells.

Chapter 6

Discussion and Conclusions

6.1 Introduction

The aim of the GH project was to examine the experimental evidence and use this to build a model of the GH release system. Modelling provides a structure in which to formalise existing knowledge and test theories on how the system might function as a whole. The goal was also to keep the model as simple as possible, in order to understand the system in its barest functional form. A model was successfully built which is able to reproduce the behaviour and functional properties of the real system. This was used to go on and test more complex versions, incorporating more system components, suggested from experiments, testing what role these might play in the system. The final version of the model produces output which closely resembles the qualitative and quantitative properties of the real data, in both male and female rats. Matching the system's behaviour using components suggested from experimental data is good evidence that the model is an accurate representation of the real system. On this basis, the model is able to predict and aid the interpretation of experimental data and should provide a powerful tool for further studies of the system, as well as suggesting general techniques for modelling other brain systems.

The first part of the chapter summarises the GH system modelling before moving on to discuss the work within the more general context of research into the system. The final section discusses the oxytocin cell spike firing model.

6.2 Modelling the GH Release System

It's well established that GH release is controlled by the two hypothalamic peptides, GHRH and somatostatin. Somatostatin controls the overall pulsatile pattern of release by exerting permissive control over the ability of GHRH to trigger GH release at the pituitary. The form of individual GH pulses is controlled by the pattern of GHRH release. Experiments with the complete system, and tests with the pituitary model, suggest a fairly square wave pattern of somatostatin release, matching the periods of low GH release in the male rat. GHRH release must correspond to the

individual peaks of GH, suggesting an irregular pattern of pulses at roughly 15min intervals. GH feeds back to regulate its own release by stimulating somatostatin and inhibiting GHRH release. The cross-gender variation in the release pattern appears to due to modulation of GH-somatostatin feedback by gonadal steroids. The GH-somatostatin feedback in particular seems to act with a long delay, indicated by experiments administering GH to the system, measuring GH release and also measuring the Fos response at the periventicular nucleus. This inhibitory feedback combined with the delay produces a cycle which creates the pulsatile release pattern.

GHRH and somatostatin are controlled by the GHRH neurons in the arcuate nucleus and the somatostatin neurons in the periventricular nucleus of the hypothalamus. GH appears to feedback directly to the somatostatin neurons, and also through the NPY neurons in the arcuate nucleus. GH-GHRH feedback also appears to be mediated by the NPY neurons and also the group of somatostatin neurons in the arcuate nucleus, acting on the sst2 receptors on the GHRH neurons. The sst1 receptors of the GHRH neurons probably mediate an inhibitory signal from the periventicular somatostatin neurons. The best evidence for this connection is the electrophysiological experiments which demonstrated suppressed electrical activity at the GHRH neurons in response to periventicular stimulation. More circumstantial evidence also suggests an reciprocal inhibitory connection from the GHRH to somatostatin neurons, mediated by galanin. The main excitatory input to the GHRH neurons appears to come from another part of the brain, probably an adrenergic driving input.

6.2.1 Designing the Model

This evidence formed a sufficient base from which to build the model, starting out with as few components as possible in order to generate pulsatile release. The pituitary model had been established as a reliable starting point, producing GH release from GHRH and somatostatin and accurately representing the dynamics of the real system. The first two additions were the delayed GH-somatostatin feedback

and the inhibitory somatostatin-GHRH connection. This was sufficient to produce the pulsatile GH pattern, but the multiple peaks within each GH pulse also required a pulsed input to the GHRH neurons. Although somatostatin already inhibits the release triggering action of GHRH at the pituitary, this isn't strong enough alone to produce the almost undetectable levels of GH release observed inter-pulse in the male rat. Later work with the model, attempting to reproduce the GH rebound following a somatostatin infusion, also suggested that the central somatostatin-GHRH block is required to increase GHRH sensitivity at the pituitary. On the basis of the pituitary model (and also probably in the real system given the matching results between real experiments and the model) even when somatostatin blocks GH release, GHRH continues to desensitise its receptors. Blocking central release prevents this and allows the high inter-pulse somatostatin levels to recharge pituitary GHRH sensitivity.

The first version of the model implemented these connections as crude switch-like sigmoidal curves. The second version improved on this by replacing these with Hill equations and also by using a more sophisticated GH-somatostatin feedback mechanism. The first version of the model originally used a central somatostatin-GHRH rebound mechanism to trigger GHRH release for each GH pulse. This became redundant once an external pulse input was added but designing it developed a new modelling form, a releasability variable, allowing a substance to increase a readily releasable pool of another substance rather than directly triggering its release. Release is then generated as the product of the releasable pool and electrical activity. This gives the system a form of memory, recording the effect of a signal, rather than immediately responding. In the model this allowed GH to charge the releasable pool of somatostatin so that the period of high somatostatin release would not depend directly on delayed GH activity, allowing a longer period of high somatostatin release with a shorter feedback delay. The real mechanism by which GH triggers the long period of somatostatin release is still unknown and the model's form gives a mechanism to test in the real system. The dynamics of this mechanism, the charge and discharge rate, were set by matching the model's output with the magnitude and timing of real GH release. It would be better if these could be measured more

directly at the somatostatin neurons, assuming such a functional mechanism exists. Releasability in the model is a deliberately vague term. In the real system it would relate to some mechanism such as vesicle mobilisation creating a readily releasable pool at the cell membrane or increased synthesis.

Sampled Release Profiles

The model built from these components was able to reproduce the qualitative behaviour of the real system. The important step in going on to reproduce the quantitative details was to introduce the simulation of the sampling involved in measuring real GH profiles. This has a dramatic effect on the appearance of the GH output, reducing the apparent height of GH peaks, and also reducing the number of visible peaks and changing their height order. Testing the pituitary model, and later the full model in combination with a sample rate matching real data allowed a better guess at the real pattern of GHRH release, suggesting that a 15-30min pulse interval is required to produce the observed form of the GH pulses. More frequent pulses actually produce fewer GH peaks in the sampled data.

Random GHRH Pulse Input

The other important step in reproducing the form of real GH release was to make the GHRH input pulse intervals random. This did not disturb the overall pattern of GH pulses but did produce the irregular pattern of GH peaks, and slightly varied inter-pulse intervals observed in real data. This was first tested with the pituitary model and later added into the full system model. Function with the random input pattern was also an important validation, that model wasn't relying on a patterned external input.

6.2.2 Extending the Model

After successfully reproducing the male rat's pattern of GH release, the next aim for the model was to reproduce the female release pattern with the goal that this should be possible just by parameter modulation. The female release pattern is thought to be due to a more constant low level release of somatostatin, caused by varied GH feedback on somatostatin. Developing the model had identified another way to modulate the system to produce the female release pattern, by modulating the inhibitory effect of somatostatin on GHRH release, increasing the threshold for somatostatin to trigger inhibition of GHRH release. Both of these methods were able to reproduce the female release pattern. However, modulation of GH-somatostatin feedback is the method best supported by experimental evidence. This could be reproduced in the model either by reducing the charge rate for somatostatin releasability or by reducing the maximum level for somatostatin releasability. Attempt to use *in-vitro* preparations test the variations in the periventricular somatostatin release mechanism have so far produced results which contradict *in-vivo* behaviour (Murray *et al* 1999b). Stimulation in an explant preparation from a female rat produces higher levels of release than from a male preparation, despite a higher somatostatin content in the male. It has been shown that levels of somatostatin mRNA are higher in the male and this is consistent with the model result suggesting a larger store of releasable somatostatin, or a larger effect of GH on charging the store.

GHRH-Somatostatin Inhibition

This was added to model in order to test what functional role such a connection might play in the system. What it did was to produce bistability in GHRH activity. Smaller GHRH pulses, below threshold to inhibit somatostatin were blocked by the somatostatin-GHRH inhibitory connection. Medium size GHRH pulses however, remove their own inhibition by inhibiting somatostatin, becoming larger GHRH

pulses. This had the effect of making GH pulse size more regular and reducing the number of small GH peaks at the start of pulses observed in the model. This made the model more robust and allowed the steepness of somatostatin-GHRH inhibition to be reduced. However it did not make any major functional contribution to the model, and in order to maintain simplicity, this was not permanently added to the model at this stage.

GH-GHRH Feedback

The final major development of the model was to add in GH feedback at the GHRH neurons in an attempt to generate the pattern of GHRH input activity without such a defined external input. This was successfully implemented and was able to generate the required pattern of pulsed GHRH input to produce individual peaks within the GH pulses. The best results were achieved using a very steep inhibitory curve in the relation between the GH level and GHRH activity, in order to form the sharp GHRH pulses required to get the corresponding sharp peaks within the GH pulse. This steep activation is plausible in the real system, particularly given that GH-GHRH feedback appears to be mediated through arcuate NPY and somatostatin neurons. Several layers of non-linear relations is one way to produce a very steep non-linear relation. GH-GHRH feedback also required a delay in the range of 5-15min in order to produce more than 2 peaks within the GH pulse. This matches experimental data that shows activation of arcuate neurons in response to GH occurring without the long delay observed with periventricular neurons.

Although this new component was able to replace the need for the external input to produce distinct peaks within the GH pulse, it still produced GH output which was more regular than observed in the real system. This was fixed by adding a higher frequency external input with mean 5min interval pulses.

6.2.3 Reproducing Real Experiments

The model was now able to produce a good match to normal GH profiles in male and female rats. The next important test was to attempt to reproduce the effects of injections and infusions of GHRH, somatostatin or GH itself. This would further validate the model and help to interpret the results of these experiments. The first of these was injections of GHRH at varied intervals. The real experiments were important results because they were one of the best demonstrations of feedback in the system, with the endogenous pulse pattern becoming entrained into the artificial input. The model easily reproduced the results with injections at 180min intervals but had problems with the more frequent injections. The pituitary model had not previously been tested with maximal dose injections of GHRH and produced a much higher GH response during high levels of somatostatin than in the real system. To reproduce the real results the non-somatostatin modulated GHRH triggered release component was reduced in size and the steepness of the somatostatin controlled inhibition was also increased. This may have knock on effects for other parameters in the pituitary model and future work will involve rechecking the parameter fitting with these new adjustments.

With these changes the model was also able to reproduce the effects of somatostatin and GH infusions, producing very good matches to the real experimental results. Results with the model suggest that exogenous somatostatin must be able to act on the hypothalamus in order to produce the observed rebound release. In the model the rebound is produced by charging pituitary GHRH sensitivity to a high level and this requires GHRH release to be blocked. Because the model is already able to produce the rebound effect, a hypothalamic rebound mechanism cannot be tested without changing the pituitary model. This change would likely make the model less representative of the real system. The model suggests that the hypothalamic involvement is the requirement for a pulse of GHRH release to trigger the large GH release. Testing the model against experiments infusing short pulses of GH provided evidence in support of the short GH-GHRH feedback delay on the basis of matching the delayed GH response to GH infusions.

The response to longer infusions supports a GH-somatostatin feedback delay of approximately 1h.

It was actually surprisingly easy to get the model to reproduce the real results, requiring no changes to the model equations or parameters that were used to produce the normal release pattern, apart from the adjustments to the pituitary model, which had no significant effect on the previous results with the final version of the model.

6.3 GH Model Discussion

Discussed below are some particular issues which developed during the design and testing of the GH model. These are mainly to do with the model components which had to be hypothesised rather than directly based on experimental data. When adding such components the most important final aspect is that they produce something that can be tested in the real system. In this way modelling forms a circular process of basing components on real data, designing a more complete version, filling in uncertainties and then testing the result of this back in the real system.

Effect of the Pituitary Model

One of the major influences at the beginning, and throughout the modelling work, was the fact that it had started with, and continued to use as a major component, the existing pituitary model. Treating this model as sufficiently well tested to be considered 'correct' and fixed meant that the hypothalamic components had to satisfy extra demands that may not have been there if the new modelling work had started from scratch. For the most part this was probably a good thing, having to deal with a realistic representation of the pituitary dynamics instead of some simplified representation, with the risk of it being tailored to make the hypothalamic components easier to design. The problem is that the pituitary model was tested against, and designed to reproduce, results from *in-vitro* experiments. The features

identified at this level will almost certainly still manifest in the natural, *in-vivo*, system, but possibly with varying emphasis. An example of this is the rebound effect observed *in-vitro*. At this level it presents as a major feature of the pituitary systems' functional description, and likely provides good clues to the mechanisms behind the pituitary components. However, considering the whole system, the rebound involving the hypothalamic systems is of a much larger magnitude, and more significant to the whole system's behaviour. The later work with the model, reproducing the experiments designed to trigger the rebound, suggested that the larger rebound also uses the pituitary mechanism, but attempting to produce the rebound with just the pituitary model may have resulted in an unnaturally high weighting to the non-GHRH and non-somatostatin controlled GH release components in the pituitary model.

It is these components, particularly the non-somatostatin controlled GHRH triggered GH release component (*k4*) that have formed the problems with the pituitary model which became apparent when testing the model's response to simulated GHRH injections. Component *k4* is an odd, counter-intuitive feature which came to exist as an artefact of the pituitary model's development path rather than as a designed feature. It was always given a much smaller weighting than the somatostatin inhibited GH release component, but was still left with a fairly large (approx 10% of the normal somatostatin controlled component) parameter value following fitting of the model to *in-vitro* data. How this final value was derived is not clear unfortunately. For the fitting process, a simplified version of the model with fewer parameters was produced, but there is no record of how the fitted values for the reduced model were translated back into the full version.

The other pituitary model parameter which had to be altered is the strength of somatostatin's inhibitory effect on GH release. The required increase in inhibition only became apparent when challenging the system with very high doses of GHRH, comparable to the maximal dose injections. The pituitary model was fitted against dose response curves but was likely never directly tested against a maximal dose of GHRH, which may also vary in magnitude between the in-vitro and in-vivo system.

The effect of the weakened somatostatin controlled inhibition during the development of the hypothalamic components was to place more importance on the inhibition of GHRH release at the hypothalamus than was necessary. High somatostatin levels at the pituitary were not sufficient to generate the periods of very low inter-pulse GH release, and so GHRH had to also be blocked at the hypothalamus by the inhibitory somatostatin connection. Whether the model, with the adjusted pituitary parameters can function with the hypothalamic somatostatin-GHRH inhibition reduced in strength (weaker inhibition) remains to be tested. The later work with the model suggests that hypothalamic inhibition of GHRH is required, not to block GH release, but to maintain sensitivity to GHRH at the pituitary. This assumes that the pituitary model's interpretation that desensitisation to GHRH takes place at the receptor and early second messenger level is correct, which on the basis of the lack of cross-desensitisation between GHRH and GHRP seems likely to be the case.

Fortunately the model's structure and its dependence on individual elements was kept sufficiently flexible that the pituitary model could be altered at the later stages in chapter 4 without having a large effect on the results.

The GHRH Input Pulses

Of the model's elements this is the part which was most purely hypothesised rather than being based on experimental evidence. Evidence for an essential adrenergic input to the GHRH neurons does exist, but not on what form it might take. Adding inhibitory GH-GHRH feedback demonstrated that even constant, non-pulsatile input to the GHRH neurons could still produce multiple peaked GH pulses, but these still lacked the form of the sharp GH peaks observed in real GH profiles. The final version of the model in chapter 4 uses randomly timed input pulses overlaid with the GH feedback control to produce the sharper, more randomly spaced GH peaks that more closely resemble the real data. The justification for this defined input is that it is a specification of the final release triggering activity at the GHRH neurons rather

than an actual input. The input could be a more variable form of activity that is processed through a threshold to produce the on-off pattern of input pulses. One experimental method for testing this might be to stimulate GHRH neurons with patterns of activity varying between distinct pulses to continuous activity, measuring the resultant GH release, similar to the experiments in (Dickson *et al* 1993).

GH-Somatostatin Feedback

The most distinct feature of this component is the absolute delay required by the model, usually set to 60min. The only direct evidence for such a delay in the literature reviewed by this thesis is (Minami *et al* 1992) where stimulation of NPY neurons produces a delayed response (of a similar time magnitude) at somatostatin compared to GHRH. However, this would not account for the delayed response to GH acting directly at the somatostatin neurons. It may be that the delay is due to the process by which GH is transported from pituitary release to the periventricular nucleus. This will require some special method of transporting the large GH molecules past the blood brain barrier, either by some special cross-membrane transport mechanism or following a reverse route up the neuronal projections to the median eminence. Alternatively, the delay may be part of the process by which GH triggers increased somatostatin release. The model suggests that GH charges the level of somatostatin ready for release, and this process may take time, for something such as vesicle transportation. Actual increased somatostatin synthesis would be on too long a timescale. One manner of experimentation might be to use an explant type *in-vitro* preparation to measure somatostatin release from the periventricular neurons in response to electrical stimulation, first to establish measurable release in response to stimulation, and then to test the effect of pre-treatment with GH, over varied time courses.

6.4 Previous and Contemporary Modelling Work

The first published attempt at modelling the GH release system [Chen et al 1995.] produced a model with a similar set of components to this one but with a very homogenous structure including all possible connections, and using standard highly parameterised relations between components. The model was able to reproduce the qualitative properties of basic GH release but contained a very large number of parameters (~80) and such an abstract structure that it could not be properly analysed or related back to the biological system.

The second published attempt (Wagner *et al* 1998) was much simpler, incorporating just GH-somatostatin feedback and somatostatin-GHRH inhibition represented by Hill equations, with a very basic representation of GH release in response to GHRH and somatostatin. This model successfully reproduced the basic pattern of GH release but relied upon a regular 1h interval input to GHRH to drive the system.

The most recent attempt (Farhy *et al* 2001) produced a model very similar to the one presented in this thesis, incorporating GH feedback to somatostatin and GHRH, and somatostatin-GHRH inhibition, also represented by Hill equations. It uses no external GHRH input and instead generates the pattern of individual GH peaks within each pulse using GH-GHRH feedback, with a 7min delay. GH-somatostatin uses a 60min feedback delay. Giving the current model a constant level of GHRH input and adjusting the GH-GHRH feedback parameters produces very similar output to the model presented in the paper. A second paper (Farhy *et al* 2002) also goes on investigate reproducing the female release pattern using a very similar method of reducing the feedback effect of GH and somatostatin. The random element is release is produced by adding Gaussian noise to the pattern of somatostatin release, based on unpublished evidence from endogenous somatostatin release measured in ewes. The paper also adds the simulation of sampling.

The main difference from the current work is the more abstract forms for the relations between substances, particularly GH-somatostatin feedback, although this is likely to have similar functional properties to the construction in the current model. It

also lacks the more sophisticated model of pituitary action. The only unique component presented in the current model is the inhibitory GHRH-somatostatin connection.

For the most part the work is remarkably similar and serves to confirm the approach and results of the current model. The main overall advantage of the work here is that it maintains a closer connection to the biology, which makes it a better system for maintaining a relationship with experimental work with the real system. The enhanced representation of the pituitary makes this model better at explaining many of the experimental results, particularly the GH rebound in response to somatostatin withdrawal, and also in justifying the nature of the hypothalamic components, rather than just demonstrating that they work. The careful construction of this model has demonstrated the 'necessary' as well as the 'sufficient' quality of the model's components. An example is the need for distinct GHRH pulses to produce the individual GH peaks observed in real release data. This is a feature missing from the published material on the Farhy model. It is never as strictly compared with real release patterns as this model, basing it's comparison purely on the basic characteristics of endogenous release patterns rather than a direct detailed comparison of the forms. Despite varying amplitude, the Farhy model maintains regular spacing between GH peaks, each pulse consisting of two peaks when simulating normal activity in the male rat. Timing of each GHRH pulse is entirely controlled by inhibitory GH feedback, which is itself determined by the GH-GHRH feedback delay of 7.5 min. In the most advanced version of the current model, GH peaks are determined not only by GH feedback, but also the background of random GHRH input pulses. The Farhy model effectively uses a constant input to drive GHRH, similar to the continuous input to somatostatin used in the current model. The current model can also function with just a constant background input to GHRH, and, doing this, produces a similar output to the Farhy model.

The Farhy model creates the variation in GH pulses by adding a random component to somatostatin release. This produces variation in the amplitude, but not timing of GH peaks. Unfortunately the determination of how regular these peaks really are in real data is limited by sampling, but it seems unlikely that release is so

regular in the real system. The varied substrates for randomness in the system leaves an interesting variation between the two models which makes predictions which are, at least theoretically, open to experimental investigation.

6.5 Future Work

The model makes many predictions for the function of the real system and the way forward is for these to be tested experimentally, particularly the dynamics of GH's feedback effect on somatostatin and somatostatin's inhibition of GHRH. This would work well in combination with the recent advances in detecting and specific blocking of somatostatin receptor subtypes. The model's predictions for the endogenous patterns of GHRH and somatostatin release are not currently testable at sufficient temporal resolution. An advance to the model might be to add in GHRP and use the model of a tool for finding the best method for treating GH deficiency. The model's accurate reproduction of real GH release suggests that it is sufficiently reliable for such a task. Another approach is to use the form of analysis developed with firing patterns in oxytocin cells to examine the firing properties of GHRH neurons in response to stimulation.

Treating the Model as a Theory

To take a more general view, the approach from this point is test the model to destruction, place the assumption that the model is a correct representation of the real system, and work to show why this isn't true. The model can be attacked from two sides, reflecting the combined bottom-up (basing the model on known components) and top-down (aiming at a known output) approach that was used to build it in the first place. The first of these is to keep testing it against real experimental data, in a similar manner to the later part of chapter 4. This should go on until the model fails, is unable to reproduce the real experiment. At this point, the model, maintaining the

rigours of biological plausibility and the essentials that had made it successful thus far, should be altered to try and match the offending experiment. Failing this, the model fails and has to be rejected. The further the model gets (and indeed it is arguably already at this stage) the less likely this occurrence should be. This process will continue to validate the model, and also further explain experimental results.

The second manner of attack, and perhaps also the most important manner of advance, is to test the basis of the model. Some of the model's components and based on well established knowledge of the real system, but other parts are more postulated and require to be searched for, and found, in the real system before they can be established as true representations of the real system. This is the form of the experiments suggested earlier in this chapter. The model should also be checked to be sure that it's abstract forms do represent established knowledge. A thorough version of this process would involve carefully formalising the properties of the real components and then comparing these with the model counterparts.

More Detailed Modelling

In order to establish some of the model's more abstract components, such as the GH-somatostatin feedback mechanism it may be necessary to produce more detailed models, focussing on these mechanisms, when there is sufficient experimental evidence to do so. This can test how such a component might work and properly establish its functional properties. This however should be seen as a temporary step, a manner of properly justifying and determining the functional properties of a component before returning to the more minimal model of the system. Following a reductionist path of adding more and more complexity to explain behaviour will result, not in explaining or understanding a system, but merely achieve a replication of the complexity, albeit a more controlled and accessible one. The brain, for all its complexity, includes much homogeneity, and the only way to make understanding it a tractable problem is to derive general principles and more abstract understandings of its goings on.

A final conclusion is that this project has demonstrated the usefulness of modelling as a technique. Many investigations within neuroscience would benefit from tandem efforts combining modelling and experimental work.

6.6 The Oxytocin Cell Firing Model

In relation to the GH modelling project, the aim of this work was to investigate how electrophysiological properties of a particular type of neuron might be detected by analysing recordings from the cells. The eventual aim would be to apply this technique to cells such as the GHRH neurons in which normal activity is difficult to detect, in this case due to its blocking by anaesthesia. The oxytocin neurons are already relatively well understood and accessible to recording, under a range of conditions, making them an ideal system in which to begin developing such a method.

The Limitations of ISI Histograms

The previous work, which developed the oxytocin cell version of the integrate and fire model did all of its comparisons with real data on the basis of the ISI (inter-spike interval) histograms. The first part of the new work recreated this and looked at how the histogram forms related to the model parameters, and how much information they preserved. The main conclusion was that the histogram was dominated by firing rate, and could not be used to distinguish between different parameters that can affect firing rate, such as the inhibitory to excitatory PSP ratio (*Iratio*) and the overall PSP rate (*Ire*), with it being possible to use these to compensate against each other to produce identical histograms. However, this result also produced the ability to mask the firing rate effects of parameter changes which also had more subtle effects on the ISI distribution, such as the HAP parameters. This was able to isolate the effects of the HAP on the front end of the histogram, and produce a technique for fitting the

model to real data by matching firing rate in combination with matching the front end of the histogram.

The limits of using histogram matching to fit the model to real data were really revealed when using spike train analysis to look for a relation between adjacent ISIs. The model without the AHP can match a real recording on the basis of the histogram without being able to reproduce the negative gradient revealed by spike train analysis.

Log Likelihood and Simplex Search

The version of log likelihood used here gives a measure of fit that preserves the relations between individual ISIs, allowing it to take account of properties such as the correlation detected by spike train analysis. The main limitation with this measure is that the practical manner of calculation is an approximation, and creates error in the final value. This means that only a range of parameter values where the best fit lies can be determined, rather than exact values. Examining the search space with model generated data varying the two AHP parameters shows an almost flat, straight, ridge of the best fit values, with AHP magnitude and decay rate increasing, compensating against each other. A peak can be detected at the true values used to generate the data, but the gradient along the ridge is very shallow, giving a range of pairs of values falling within the error in the fit measure. One way to proceed here will be to test how the size of this range varies with the AHP magnitude, the idea being that a larger AHP may have a less well distributed (over following spike intervals) effect, making it more distinguishable from a smaller AHP with longer duration. The linear relation between the two parameters and the best fit can be defined by a single ratio value. The results presented here have also begun to indicate a relation between this value and the PSP input rate. Further work may be able to determine a precise relation.

How well this will all apply to real data is difficult to predict. These precise relations are in model generated data where the parameters are all known and

controlled. The basis for believing that similar relations may apply to real data, if less precisely, is the early fitting work with the ISI histogram which was able to get good fits to real recordings from different cells without varying many parameters. However, this of course is qualified by the limitations of fitting with the histograms. If a similar linear relation between parameters can be found in real data then this will allow the search to be reduced to just one parameter for the AHP, finding the ratio, and then searching along the ridge.

Simplex search is a method of moving through a multiple parameter search space which alters all of the parameters in parallel, rather than fitting each parameter in turn, in the manner of some other multiple parameter search methods. Considering the interaction between parameters, this is likely to be the best type of method for the search space here. It makes a good job of finding the best fit with one or two varied parameters, but results are more variable with three parameters, depending partly on the initial parameter set. Results here vary between using initial parameters which cover the range of expected values (i.e. k = 0 and k = 5) or defining a smaller initial simplex with values all in the range of those normally used with the model (i.e. k = 0.1 to k = 1). Unfortunately the time required for a simplex run has limited the range of initial parameters tested so far, and there is so far not enough data to find a relation between the result parameter sets and the initial parameters, assuming a regular pattern is to be found.

Simplex search does always manage to find a result set which gets the best possible fit score for a spike dataset, and the varied results from different initial parameter sets can be related by the AHP magnitude-decay rate ratio and also to the input rate, although the later relation is less well defined. Additional tests (not shown) have established that repeated runs with the same initial parameter set produce the same result set. The way to proceed with this is, in the first place, more results, testing more varied parameters with model generated datasets, and more varied initial parameter sets. It will also be necessary to test with a larger number of varied parameters, such as input spike magnitude, or the HAP parameters. The ultimate aim is to be able to take a real recording and then use the search mechanism to analyse the data, producing reliable parameter values that can be directly

translated back to electrophysiological properties that could not otherwise be detected.

The AHP

Adding the AHP to the model allowed it to reproduce the ISI correlation detected by spike train analysis in real cell recordings. Combined with the knowledge that the AHP exists in the real cells, this suggests that it is the AHP that is responsible for this correlation in real data. Since it is a fairly intuitive process to understand the AHP having this effect, in combination, it seems like a reasonably safe conclusion. The question from here is 'What's it for ?'.

Functionally, the AHP works in one direction; more rapid firing increases the size of the AHP and effectively increases the firing threshold, reducing the firing rate, assuming that the input rate isn't also increasing. As the firing rate slows, the AHP decays away, restoring the firing threshold, eventually allowing the firing rate to increase again. This is what creates the correlation observed by spike train analysis, the slight bias towards longer ISIs after short ISIs and shorter ISIs after longer ISIs. This acts to reduce the variation in the ISIs. Results show this effect, showing a smaller ISI standard deviation in model generated spike trains using the AHP, although more work is required to conclusively separate this effect from being caused purely by the reduced firing rate. So, in a single cell, the AHP forms a short term memory for previous firing activity, acting to reduce firing in response to high activity, modulating the firing rate, limiting the maximum firing rate, and also increasing (although in effect reducing, because it's working against a stronger non-linearity in the opposite direction) the non-linearity of the relation between the input rate and spike firing. Conceivably the AHP ion channels could also activate other mechanisms, beyond its effect on membrane potential, perhaps more directly using the AHP as a form of memory.

In oxytocin cells, the AHP is likely to play a role in the varied firing modes, which occur to trigger different forms of oxytocin release, which varies between slow gradual release and very large discrete pulses, such as during parturition and milk

ejaculation. These pulses correspond to a rapid increase in firing rate which may normally be switched off partly by the existence of the AHP. The tentative prediction here is that the AHP detected in recordings during these phases of intense firing should have a smaller magnitude or faster decay rate, reducing its effect.

Within a network with several output neurons competing to respond to a shared set of inputs, the AHP could work to reduce the dominance of cells which fire very often, (assuming a mechanism that limits the number of responding cells, such as inhibitory interneurons) giving a chance back to other cells, so that particularly common input pattern doesn't preclude the learning of other patterns by dominating the feedback that strengthens synaptic connections to the output cells. It would be interesting future work to test this in some network (perhaps for pattern recognition) using a more sophisticated representation of the individual neurons, such as the integrate and fire model.

To Conclude

Beyond the AHP, there may be a lot that can be done with the new analysis and fitting techniques, detecting neuronal properties from cell recordings. The next step will be to continue development to a point where reliable parameter estimates can be produced, for a limited number of parameters. At the current stage, testing has only just begun attempting to fit real data, but, as noted above, it does seem hopeful that the fitting process can be used to get accurate parameter values, perhaps by getting values defined relative to another parameter (such as the magnitude / decay rate ratios) and then converting them to absolute values by using another source to determine one of them. One of the current limitations is that a constant mean input rate is assumed. The limits the type of cell activity that can be used for fitting, but if a cell's properties can be well defined then it may be possible to use the model and fitting process to test possible input patterns against measured output activity. The work here could potentially create an important new tool for exploring neuronal activity and understanding brain systems.

Appendix

Table 1 : Varied AHP parameters

k2	λ2	Half-life	Output Rate	Mode	Height
0.0	0.001	693.1	7.26	45	1927
0.2	0.001	693.1	5.54	60	1368
0.4	0.001	693.1	4.59	55	1112
0.6	0.001	693.1	3.97	65	931
0.8	0.001	693.1	3.53	55	805
1.0	0.001	693.1	3.18	70	713
0.0	0.002	346.6	7.27	45	1865
0.2	0.002	346.6	6.28	50	1520
0.4	0.002	346.6	5.59	60	1338
0.6	0.002	346.6	5.09	55	1185
0.8	0.002	346.6	4.67	70	1038
1.0	0.002	346.6	4.31	60	963
0.0	0.003	231.0	7.28	55	1893
0.2	0.003	231.0	6.61	55	1642
0.4	0.003	231.0	6.03	65	1449
0.6	0.003	231.0	5.64	65	1302
0.8	0.003	231.0	5.29	55	1221
1.0	0.003	231.0	4.96	70	1092
0.0	0.004	173.3	7.28	45	1847
0.2	0.004	173.3	6.75	55	1665
0.4	0.004	173.3	6.36	50	1548
0.6	0.004	173.3	5.96	65	1386
0.8	0.004	173.3	5.70	45	1331
1.0	0.004	173.3	5.41	65	1201
0.0	0.005	138.6	7.23	45	1860
0.2	0.005	138.6	6.85	50	1770
0.4	0.005	138.6	6.51	60	1555
0.6	0.005	138.6	6.24	50	1466
0.8	0.005	138.6	5.94	60	1415
1.0	0.005	138.6	5.71	55	1318

Table 2 : Real data spike train analysis

T0	T1	T1+T2	T1+..+T4	T1+..+T8	T1+..+T16	T1+..+T32
27.85	190.15	382.29	733.01	1422.86	2781.42	5542.90
37.33	193.39	381.48	739.05	1447.03	2828.10	5592.91
44.35	180.01	342.20	709.06	1429.34	2801.09	5597.57
50.72	174.48	342.20	684.57	1380.79	2767.48	5477.98
57.39	186.43	364.36	709.45	1395.37	2810.72	5546.69
64.11	177.99	346.62	708.52	1374.39	2763.23	5452.84
71.22	176.00	363.94	716.57	1422.65	2772.64	5567.47
78.54	168.34	333.96	703.59	1392.69	2789.43	5565.77
86.62	175.96	347.54	697.08	1369.20	2708.22	5449.63
94.82	176.07	353.12	711.98	1401.46	2787.03	5513.45
104.60	183.25	367.65	727.94	1387.18	2752.33	5515.01
114.22	175.44	366.57	701.45	1415.10	2783.83	5513.50
125.16	167.57	332.18	676.33	1401.88	2771.25	5540.28
136.25	183.07	361.11	710.72	1393.90	2764.46	5506.70
149.10	186.12	365.56	695.17	1411.72	2770.66	5530.20
161.80	187.05	356.27	702.74	1407.43	2823.32	5608.76
176.99	174.54	332.57	680.70	1375.01	2742.66	5481.82
193.07	170.61	347.53	704.12	1388.21	2787.90	5532.19
211.85	171.20	334.45	686.12	1347.83	2714.68	5513.24
232.65	156.96	335.79	682.83	1350.21	2744.56	5495.58
257.52	165.93	320.86	664.18	1378.02	2785.20	5591.60
286.46	161.99	333.85	658.92	1349.61	2774.46	5558.68
322.23	149.95	318.69	650.69	1355.90	2709.92	5487.46
367.40	159.13	327.95	679.11	1372.71	2778.48	5565.34
432.01	150.88	332.37	656.22	1320.36	2708.65	5496.38
582.49	150.76	296.25	586.41	1258.97	2656.42	5499.82

Table 3 : Real data spike train analysis gradients

Series	Gradient
T1	-0.0739
T1+T2	-0.1125
T1+T2+T3	-0.1629
T1+..+T4	-0.2037
T1+..+T5	-0.2169
T1+..+T6	-0.2276
T1+..+T7	-0.2558
T1+..+T8	-0.2400
T1+..+T9	-0.2368
T1+..+T10	-0.2402
T1+..+T12	-0.2297
T1+..+T14	-0.1762
T1+..+T16	-0.1881
T1+..+T18	-0.1715
T1+..+T20	-0.1609
T1+..+T24	-0.1209
T1+..+T28	-0.0813
T1+..+T32	-0.0406

Table 4 : Model generated data spike train analysis

T0	T1	T1+T2	T1+..+T4	T1+..+T8	T1+..+T16	T1+..+T32
32.32	206.16	399.17	802.92	1550.73	3074.18	6133.705
43.24	196.00	422.49	794.70	1558.99	3073.05	6157.59
51.45	196.93	391.44	774.32	1540.93	3074.24	6113.57
58.93	191.33	396.82	791.60	1556.29	3067.21	6102.43
66.89	197.08	381.85	768.24	1538.62	3064.22	6078.78
74.45	205.87	386.09	766.30	1510.95	3027.38	6009.26
82.85	173.46	370.04	764.78	1511.33	3016.79	6038.46
91.64	191.38	399.36	761.96	1537.58	3005.47	6039.82
101.18	192.51	380.54	752.56	1532.38	3099.55	6155.58
111.14	186.32	398.37	779.93	1538.18	3061.91	6050.85
121.84	185.18	378.88	741.72	1515.30	3027.61	6054.81
132.59	198.78	370.48	780.21	1551.61	3036.07	6002.12
143.33	202.03	375.74	765.44	1558.04	3021.60	6025.99
154.95	201.90	381.90	758.53	1527.24	3038.44	6103.20
168.14	178.43	374.97	743.23	1525.80	3036.75	6050.79
181.70	197.01	385.40	774.68	1526.38	3088.16	6070.09
197.49	192.45	375.80	737.48	1483.73	3017.50	6098.62
215.24	168.72	349.45	742.26	1484.04	2987.29	6020.40
233.27	189.27	378.83	745.14	1490.85	3068.19	6062.64
252.79	209.48	369.26	753.18	1508.27	3049.06	6064.19
275.61	191.61	363.96	755.59	1475.76	2975.18	6058.89
303.51	176.00	382.82	754.89	1484.05	2981.66	6014.77
337.07	165.37	356.59	740.30	1498.20	2960.53	5974.67
381.54	180.41	362.56	726.73	1477.37	2993.53	6030.63
454.34	175.97	360.82	694.37	1440.07	2922.57	5933.97
635.01	172.14	350.80	717.76	1449.10	2959.16	5983.46

Table 5 : Model generated data spike train analysis gradients

Series	Gradient
T1	-0.0478
T1+T2	-0.0840
T1+T2+T3	-0.1145
T1+..+T4	-0.1357
T1+..+T5	-0.1709
T1+..+T6	-0.1784
T1+..+T7	-0.1809
T1+..+T8	-0.1991
T1+..+T9	-0.2200
T1+..+T10	-0.2235
T1+..+T12	-0.2015
T1+..+T14	-0.2175
T1+..+T16	-0.2337
T1+..+T18	-0.2367
T1+..+T20	-0.2316
T1+..+T24	-0.2188
T1+..+T28	-0.2045
T1+..+T32	-0.2470

Table 6 : Model generated data spike train analysis (no AHP)

T0	T1	T1+T2	T1+..+T4	T1+..+T8	T1+..+T16	T1+..+T32
28.55	171.04	337.72	656.99	1320.95	2708.72	5404.61
37.67	161.86	340.02	691.89	1339.70	2666.89	5354.49
45.16	171.14	341.53	704.60	1341.90	2700.85	5490.44
51.72	170.84	336.42	696.64	1385.71	2733.81	5418.82
58.77	180.91	361.99	698.31	1398.64	2720.09	5514.65
65.78	157.81	313.79	664.29	1342.12	2711.77	5433.26
72.37	173.16	354.86	693.69	1378.13	2720.79	5417.23
79.59	173.29	354.54	700.83	1384.43	2760.72	5458.85
87.39	164.63	331.93	673.67	1380.40	2756.04	5492.72
94.91	171.16	331.47	679.82	1337.56	2693.76	5455.77
102.95	195.91	348.48	699.78	1393.94	2810.49	5553.08
112.27	162.17	334.73	656.71	1365.95	2758.05	5445.49
121.80	185.87	365.95	714.43	1402.31	2803.70	5501.90
132.77	186.99	366.48	713.25	1436.26	2822.23	5555.54
144.04	157.91	325.66	664.07	1351.78	2693.43	5491.14
157.44	169.76	328.83	677.54	1387.66	2778.01	5526.80
172.02	169.61	336.35	678.02	1364.01	2763.98	5493.15
187.38	175.14	350.67	708.95	1408.26	2756.30	5506.91
204.51	189.04	362.74	704.36	1365.52	2752.20	5506.72
224.16	153.04	319.49	673.73	1336.77	2710.11	5420.78
247.38	158.21	343.86	679.96	1378.04	2746.28	5507.52
276.20	160.98	336.28	701.59	1355.86	2691.46	5478.09
314.63	176.50	349.35	679.89	1374.83	2736.44	5443.63
358.78	187.49	343.00	660.52	1357.64	2733.89	5522.24
434.56	158.30	334.87	640.45	1325.38	2668.04	5402.31
607.76	166.69	345.00	679.86	1379.00	2775.49	5568.22

Table 7 : Fitted model generated data spike train analysis

T0	T1	T1+T2	T1+..+T4	T1+..+T8	T1+..+T16	T1+..+T32
28.48	180.43	355.21	705.26	1433.50	2841.41	5576.77
37.84	178.28	357.32	711.57	1408.73	2849.14	5605.36
45.10	187.65	375.10	724.74	1437.21	2825.75	5645.02
52.15	180.05	345.28	695.88	1394.77	2743.40	5538.87
59.10	185.46	361.17	718.55	1416.76	2807.75	5643.75
65.77	186.40	371.25	722.18	1426.27	2806.56	5602.33
73.57	185.54	366.97	701.99	1405.94	2786.69	5577.17
81.76	197.36	372.17	719.43	1421.29	2801.64	5600.86
89.97	178.11	357.77	719.34	1396.72	2784.08	5554.07
98.61	184.05	372.57	738.23	1466.02	2872.72	5686.59
108.31	169.00	350.97	707.34	1420.65	2850.59	5637.59
117.95	167.44	357.04	710.11	1396.49	2791.11	5612.34
127.36	181.77	361.05	715.06	1392.51	2798.59	5567.45
137.95	168.48	349.77	686.75	1388.81	2794.01	5589.59
151.64	181.08	355.09	707.65	1389.24	2792.19	5603.37
165.72	168.26	335.84	686.79	1401.82	2762.94	5557.29
180.65	158.37	342.88	689.60	1360.71	2762.31	5566.43
196.75	175.24	329.49	663.55	1392.36	2754.94	5513.01
213.27	193.59	357.96	695.13	1386.12	2769.81	5532.99
233.30	181.90	352.75	691.13	1406.19	2805.67	5632.10
257.14	166.78	336.22	668.01	1321.07	2735.22	5504.23
284.92	156.77	331.66	669.21	1356.23	2751.03	5561.44
317.37	161.27	323.66	685.54	1377.87	2758.44	5575.72
360.58	165.36	326.03	683.51	1360.93	2736.46	5480.65
426.16	143.75	307.94	663.76	1357.31	2758.34	5492.39
592.85	143.29	302.53	632.30	1313.61	2717.05	5455.95

References

Alpert, L. C., J. R. Brawer, Y. C. Patel and S. Reichlin (1976). Somatostatinergic neurons in anterior hypothalamus: immunohistochemical localization. Endocrinology. **98**(1): 255-8.

Argente, J., J. A. Chowenbreed, R. A. Steiner and D. K. Clifton (1990). Somatostatin Messenger-Rna in Hypothalamic Neurons Is Increased by Testosterone through Activation of Androgen Receptors and Not by Aromatization to Estradiol. Neuroendocrinology **52**(4): 342-349.

Arnold, M. A. and J. D. Fernstrom (1980). Administration of antisomatostatin serum to rats reverses the inhibition of pulsatile growth hormone secretion produced by injection of metergoline but not yohimbine. Neuroendocrinology. **31**(3): 194-9.

Barinaga, M., G. Yamonoto, C. Rivier, W. Vale, R. Evans and M. G. Rosenfeld (1983). Transcriptional Regulation of Growth-Hormone Gene-Expression By Growth Hormone-Releasing Factor. Nature **306**(5938): 84-85.

Blondel, O., G. I. Bell and S. Seino (1995). Inositol 1,4,5-Trisphosphate Receptors, Secretory Granules and Secretion in Endocrine and Neuroendocrine Cells. Trends in Neurosciences **18**(4): 157-161.

Bourque, C. W. and L. P. Renaud (1990). Electrophysiology of Mammalian Magnocellular Vasopressin and Oxytocin Neurosecretory Neurons. Frontiers in Neuroendocrinology **11**(3): 183-212.

Brown, D., A. E. Herbison, J. E. Robinson, R. W. Marrs and G. Leng (1994). Modelling the luteinizing hormone-releasing hormone pulse generator. Neuroscience. **63**(3): 869-79.

Brownstein, M., A. Arimura, H. Sato, A. V. Schally and J. S. Kizer (1975). The regional distribution of somatostatin in the rat brain. Endocrinology. **96**(6): 1456-61.

Carlsson, L. and J. O. Jansson (1990). Endogenous Growth-Hormone (Gh) Secretion in Male-Rats Is Synchronized to Pulsatile Gh Infusions Given At 3-Hour Intervals. Endocrinology **126**(1): 6-10.

Carlsson, L. M. S., R. G. Clark and I. Robinson (1990). Sex Difference in Growth-Hormone Feedback in the Rat. Journal of Endocrinology **126**(1): 27-35.

Ceda, G. P. and A. R. Hoffman (1985). Growth Hormone-Releasing Factor Desensitization in Rat Anterior-Pituitary Cells-Invitro. Endocrinology **116**(4): 1334-1340.

Chan, Y. Y., E. GrafsteinDunn, H. A. DelemarreVandeWaal, K. A. Burton, D. K. Clifton and R. A. Steiner (1996). The role of galanin and its receptor in the feedback regulation of growth hormone secretion. Endocrinology **137**(12): 5303-5310.

Chihara, K., A. Arimura, C. Kubli-Garfias and A. V. Schally (1979). Enhancement of immunoreactive somatostatin release into hypophysial portal blood by electrical stimulation of the preoptic area in the rat. Endocrinology. **105**(6): 1416-8.

Chihara, K., N. Minamitani, H. Kaji, A. Arimura and T. Fujita (1981). Intraventricularly Injected Growth-Hormone Stimulates Somatostatin Release into Rat Hypophyseal Portal Blood. Endocrinology **109**(6): 2279-2281.

Chowenbreed, J. A., R. A. Steiner and D. K. Clifton (1989). Sexual Dimorphism and Testosterone-Dependent Regulation of Somatostatin Gene-Expression in the Periventricular Nucleus of the Rat-Brain. Endocrinology **125**(1): 357-362.

Clark, R. G., L. M. S. Carlsson, B. Rafferty and I. Robinson (1988a). The Rebound Release of Growth-Hormone (Gh) Following Somatostatin Infusion in Rats Involves Hypothalamic Gh-Releasing Factor Release. Journal of Endocrinology **119**(3): 397-404.

Clark, R. G., L. M. S. Carlsson and I. Robinson (1988b). Growth-Hormone (Gh) Secretion in the Conscious Rat - Negative Feedback of Gh On Its Own Release. Journal of Endocrinology **119**(2): 201-209.

Clark, R. G., L. M. S. Carlsson and I. C. A. F. Robinson (1987). Growth-Hormone Secretory Profiles in Conscious Female Rats. Journal of Endocrinology **114**(3): 399-407.

Clark, R. G., G. Chambers, J. Lewin and I. Robinson (1986). Automated Repetitive Microsampling of Blood - Growth-Hormone Profiles in Conscious Male-Rats. Journal of Endocrinology **111**(1): 27-35.

Clark, R. G., J. O. Jansson, O. Isaksson and I. Robinson (1985). Intravenous Growth-Hormone - Growth-Responses to Patterned Infusions in Hypophysectomized Rats. Journal of Endocrinology **104**(1): 53-61.

Clark, R. G. and I. Robinson (1985a). Effects of a Fragment of Human Growth Hormone-Releasing Factor in Normal and Little Mice. Journal of Endocrinology **106**(1): 1-5.

Clark, R. G. and I. Robinson (1985b). Growth Induced By Pulsatile Infusion of an Amidated Fragment of Human Growth-Hormone Releasing-Factor in Normal and Ghrf-Deficient Rats. Nature **314**(6008): 281-283.

Clark, R. G. and I. Robinson (1985c). Growth-Hormone Responses to Multiple Injections of a Fragment of Human Growth Hormone-Releasing Factor in Conscious Male and Female Rats. Journal of Endocrinology **106**(3): 281-289.

Clark, R. G. and I. Robinson (1987). Growth-Hormone (Gh) and Body-Growth Responses to Intermittent Somatostatin (Ss) Infusions in the Rat. Journal of Physiology-London **382**: 33.

Critchlow, V., K. Abe, S. Urman and W. Vale (1981). Effects of Lesions in the Periventricular Nucleus of the Preoptic-Anterior Hypothalamus on Growth-Hormone and Thyrotropin Secretion and Brain Somatostatin. Brain Research **222**(2): 267-276.

Daikoku, S., S. Hisano, H. Kawano, M. Chikamoriaoyama, Y. Kagotani, R. Zhang and K. Chihara (1988). Ultrastructural Evidence for Neuronal Regulation of Growth-Hormone Secretion. Neuroendocrinology **47**(5): 405-415.

Daikoku, S., H. Kawano, M. Noguchi, J. Nakanishi, M. Tokuzen, K. Chihara and I. Nagatsu (1986). Grf Neurons in the Rat Hypothalamus. Brain Research **399**(2): 250-261.

Day, T. A. and J. O. Willoughby (1980). Noradrenergic afferents to median eminence: inhibitory role in rhythmic growth hormone secretion. Brain Research. **202**(2): 335-45.

Dickerman, Z., H. Guyda and G. S. Tannenbaum (1993). Pretreatment with Somatostatin Analog Sms 201-995 Potentiates Growth-Hormone (Gh) Responsiveness to Gh-Releasing Factor in Short Children. Journal of Clinical Endocrinology and Metabolism **77**(3): 652-657.

Dickson, S. I., G. Leng and I. Robinson (1994). Electrical-Stimulation of the Rat Periventricular Nucleus Influences the Activity of Hypothalamic Arcuate Neurons. Journal of Neuroendocrinology **6**(4): 359-367.

Dickson, S. L., G. Leng and I. Robinson (1993). Growth-Hormone Release Evoked By Electrical-Stimulation of the Arcuate Nucleus in Anesthetized Male-Rats. Brain Research **623**(1): 95-100.

Durand, D., J. B. Martin and P. Brazeau (1977). Evidence for a role of alpha-adrenergic mechanisms in regulation of episodic growth hormone secretion in the rat. Endocrinology. **100**(3): 722-8.

Eden, S. (1979). Age- and sex-related differences in episodic growth hormone secretion in the rat. Endocrinology **105**(2): 555-60.

Epelbaum, J., E. Moyse, G. S. Tannenbaum, C. Kordon and A. Beaudet (1989). Combined Autoradiographic and Immunohistochemical Evidence for an Association of Somatostatin Binding-Sites with Growth Hormone-Releasing Factor-Containing Nerve-Cell Bodies in the Rat Arcuate Nucleus. Journal of Neuroendocrinology **1**(2): 109-115.

Farhy, L. S., M. Straume, M. L. Johnson, B. Kovatchev and J. D. Veldhuis (2001). A construct of interactive feedback control of the GH axis in the male. American Journal of Physiology-Regulatory Integrative and Comparative Physiology **281**(1): R38-R51.

Farhy, L. S., M. Straume, M. L. Johnson, B. Kovatchev and J. D. Veldhuis (2002). Unequal autonegative feedback by GH models the sexual dimorphism in GH secretory dynamics. American Journal of Physiology-Regulatory Integrative and Comparative Physiology **282**(3): R753-R764.

Ferland, L., F. Labrie, M. Jobin, A. Arimura and A. V. Schally (1976). Physiological role of somatostatin in the control of growth hormone and thyrotropin secretion. Biochemical & Biophysical Research Communications **68**(1): 149-56.

Fodor, M., Z. Csaba, C. Kordon and J. Epelbaum (1994). Growth hormone-releasing hormone, somatostatin, galanin and beta-endorphin afferents to the hypothalamic periventricular nucleus. Journal of Chemical Neuroanatomy. **8**(1): 61-73.

Giustina, A., M. Licini, A. R. Bussi, A. Girelli, G. Pizzocolo, M. Schettino and A. Negrovilar (1993). Effects of Sex and Age on the Growth-Hormone Response to Galanin in Healthy-Human Subjects. Journal of Clinical Endocrinology and Metabolism **76**(5): 1369-1372.

Guillemin, R., P. Brazeau, P. Bohlen, F. Esch, N. Ling and W. B. Wehrenberg (1982). Growth-Hormone Releasing-Factor From a Human Pancreatic Tumor That Caused Acromegaly. Science **218**(4572): 585-587.

Hartman, M. L., A. C. S. Faria, M. L. Vance, M. L. Johnson, M. O. Thorner and J. D. Veldhuis (1991). Temporal Structure of Invivo Growth-Hormone Secretory Events in Humans. American Journal of Physiology **260**(1): E101-E110.

Helboe, L., C. E. Stidsen and M. Moller (1998). Immunohistochemical and cytochemical localization of the somatostatin receptor subtype sst(1) in the somatostatinergic parvocellular neuronal system of the rat hypothalamus. Journal of Neuroscience **18**(13): 4938-4945.

Herbison, A. E. (1995). Sexually Dimorphic Expression of Androgen Receptor Immunoreactivity by Somatostatin Neurons in Rat Hypothalamic Periventricular Nucleus and Bed Nucleus of the Stria Terminalis. Journal of Neuroendocrinology **7**(7): 543-553.

Herbison, A. E. and D. T. Theodosis (1993). Absence of Estrogen-Receptor Immunoreactivity in Somatostatin (Srif) Neurons of the Periventricular Nucleus but Sexually Dimorphic Colocalization of Estrogen-Receptor and Srif Immunoreactivities in Neurons of the Bed Nucleus of the Stria Terminalis. Endocrinology **132**(4): 1707-1714.

Hisano, S., Y. Tsuruo, Y. Kagotani, S. Daikoku and K. Chihara (1990). Immunohistochemical Evidence for Synaptic Connections between Neuropeptide Y-Containing Axons and Periventricular Somatostatin Neurons in the Anterior Hypothalamus in Rats. Brain Research **520**(1-2): 170-177.

Jacobowitz, D. M., H. Schulte, G. P. Chrousos and D. L. Loriaux (1983). Localization of Grf-Like Immunoreactive Neurons in the Rat- Brain. Peptides **4**(4): 521-524.

Kamegai, J., S. Minami, H. Sugihara, O. Hasegawa, H. Higuchi and I. Wakabayashi (1996). Growth hormone receptor gene is expressed in neuropeptide Y neurons in hypothalamic arcuate nucleus of rats. Endocrinology **137**(5): 2109-2112.

Kamegai, J., S. Minami, H. Sugihara, H. Higuchi and I. Wakabayashi (1994). Growth-Hormone Induces Expression of the C-Fos Gene on Hypothalamic Neuropeptide-Y and Somatostatin Neurons in Hypophysectomized Rats. Endocrinology **135**(6): 2765-2771.

Kawano, H., S. Daikoku and S. Saito (1982). Immunohistochemical Studies of Intrahypothalamic Somatostatin- Containing Neurons in Rat. Brain Research **242**(2): 227-232.

Krulich, L., M. A. Mayfield, M. K. Steele, B. A. McMillen, S. M. McCann and J. I. Koenig (1982). Differential effects of pharmacological manipulations of central alpha 1- and alpha 2-adrenergic receptors on the secretion of thyrotropin and growth hormone in male rats. Endocrinology. **110**(3): 796-804.

Krulich, L. and S. M. McCann (1966). Influence of growth hormone (GH) on content of GH in the pituitaries of normal rats. Proceedings of the Society for Experimental Biology & Medicine **121**(4): 1114-7.

Lanneau, C., M. T. Bluet-Pajot, P. Zizzari, Z. Csaba, P. Dournaud, L. Helboe, D. Hoyer, E. Pellegrini, G. S. Tannenbaum, J. Epelbaum and R. Gardette (2000). Involvement of the sst1 somatostatin receptor subtype in the intrahypothalamic neuronal network regulating growth hormone secretion: An in vitro and in vivo antisense study. Endocrinology **141**(3): 967-979.

Leng, G., C. H. Brown, P. M. Bull, D. Brown, S. Scullion, J. Currie, R. E. Blackburn-Munro, J. F. Feng, T. Onaka, J. G. Verbalis, J. A. Russell and M. Ludwig (2001). Responses of magnocellular neurons to osmotic stimulation involves coactivation of excitatory and inhibitory input: An experimental and theoretical analysis. Journal of Neuroscience **21**(17): 6967-6977.

Loche, S., N. Vista, E. Ghigo, S. Vannelli, E. Arvat, L. Benso, R. Corda, S. G. Cella, E. E. Muller and C. Pintor (1990). Evidence for Involvement of Endogenous Somatostatin in the Galanin-Induced Growth-Hormone Secretion in Children. Pediatric Research **27**(4): 405-407.

Lumpkin, M. D., A. Gegro-Vilar and S. M. McCann (1981). Paradoxical elevation of growth hormone by intraventricular somatostatin: possible ultrashort-loop feedback. Science **211**(4486): 1072-4.

Maiter, D., J. I. Koenig and L. M. Kaplan (1991). Sexually Dimorphic Expression of the Growth Hormone-Releasing Hormone Gene Is Not Mediated by Circulating Gonadal-Hormones in the Adult-Rat. Endocrinology **128**(4): 1709-1716.

Maiter, D. M., S. C. Hooi, J. I. Koenig and J. B. Martin (1990). Galanin Is a Physiological Regulator of Spontaneous Pulsatile Secretion of Growth-Hormone in the Male-Rat. Endocrinology **126**(2): 1216-1222.

McCarthy, G. F., A. Beaudet and G. S. Tannenbaum (1992). Colocalization of Somatostatin Receptors and Growth Hormone- Releasing Factor Immunoreactivity in Neurons of the Rat Arcuate Nucleus. Neuroendocrinology **56**(1): 18-24.

Miki, N., M. Ono and K. Shizume (1984). Evidence that opiatergic and alpha-adrenergic mechanisms stimulate rat growth hormone release via growth hormone-releasing factor (GRF). Endocrinology. **114**(5): 1950-2.

Minami, S., J. Kamegai, O. Hasegawa, H. Sugihara, K. Okada and I. Wakabayashi (1993). Expression of growth hormone receptor gene in rat hypothalamus. Journal of Neuroendocrinology. **5**(6): 691-6.

Minami, S., J. Kamegai, H. Sugihara, O. Hasegawa and I. Wakabayashi (1992). Systemic Administration of Recombinant Human Growth-Hormone Induces Expression of the C-Fos Gene in the Hypothalamic Arcuate and Periventricular Nuclei in Hypophysectomized Rats. Endocrinology **131**(1): 247-253.

Murray, H. E., S. X. Simonian, A. E. Herbison and G. E. Gillies (1999a). Correlation of hypothalamic somatostatin mRNA expression and peptide content with secretion: Sexual dimorphism and differential regulation by gonadal factors. Journal of Neuroendocrinology **11**(1): 27-33.

Murray, H. E., S. X. Simonian, A. E. Herbison and G. E. Gillies (1999b). Ontogeny and sexual differentiation of somatostatin biosynthesis and secretion in the hypothalamic periventricular- median eminence pathway. Journal of Neuroendocrinology **11**(1): 35-42.

Nelder, J. A. and R. Mead (1965). A simplex method for function minimization. Computer Journal **7**(4): 308-313.

Niimi, M., J. Takahara, M. Sato and K. Kawanishi (1990). Immunohistochemical identification of galanin and growth hormone-releasing factor-containing neurons projecting to the median eminence of the rat. Neuroendocrinology. **51**(5): 572-5.

Okada, K., I. Wakabayashi, H. Sugihara, S. Minami, T. Kitamura and J. Yamada (1991). Electrical stimulation of hypothalamic periventricular nucleus is followed by a large rebound secretion of growth hormone in unanesthetized rats. Neuroendocrinology **53**(3): 306-12.

Painson, J. C., M. O. Thorner, R. J. Krieg and G. S. Tannenbaum (1992). Short-Term Adult Exposure to Estradiol Feminizes the Male Pattern of Spontaneous and Growth Hormone-Releasing Factor- Stimulated Growth-Hormone Secretion in the Rat. Endocrinology **130**(1): 511-519.

Pelletier, G., F. Labrie, A. Arimura and A. V. Schally (1974). Electron microscopic immunohistochemical localization of growth hormone-release inhibiting hormone (somatostatin) in the rat median eminence. American Journal of Anatomy. **140**(3): 445-50.

Peterfreund, R. A. and W. W. Vale (1984). Somatostatin analogs inhibit somatostatin secretion from cultured hypothalamus cells. Neuroendocrinology **39**(5): 397-402.

Plotsky, P. M. and W. Vale (1985). Patterns of Growth-Hormone Releasing-Factor and Somatostatin Secretion Into the Hypophysial-Portal Circulation of the Rat. Science **230**(4724): 461-463.

Press, W. H., S. A. Teukolsky, W. T. Vettering and B. P. Flannery (1992). Numerical Recipes in C, 2nd Ed. Vol, Cambridge University Press.

Randle, J. C. R., C. W. Bourque and L. P. Renaud (1986). Characterization of Spontaneous and Evoked Inhibitory Postsynaptic Potentials in Rat Supraoptic Neurosecretory Neurons Invitro. Journal of Neurophysiology **56**(6): 1703-1717.

Rettori, V., L. Milenkovic, M. C. Aguila and S. M. McCann (1990). Physiologically Significant Effect of Neuropeptide-Y to Suppress Growth-Hormone Release by Stimulating Somatostatin Discharge. Endocrinology **126**(5): 2296-2301.

Richman, R. A., J. P. Weiss, Z. Hochberg and J. R. Florini (1981). Regulation of growth hormone release: evidence against negative feedback in rat pituitary cells. Endocrinology **108**(6): 2287-92.

Robinson, I. (1991). The Growth-Hormone Secretory Pattern - a Response to Neuroendocrine Signals. Acta Paediatrica Scandinavica(S372): 70-78.

Sawchenko, P. E., L. W. Swanson, J. Rivier and W. W. Vale (1985). The Distribution of Growth-Hormone-Releasing Factor (Grf) Immunoreactivity in the Central Nervous-System of the Rat - an Immunohistochemical Study Using Antisera Directed Against Rat Hypothalamic Grf. Journal of Comparative Neurology **237**(1): 100-115.

Schoemaker, R. C., J. Burggraaf and A. F. Cohen (1998). Assessment of hepatic blood flow using continuous infusion of high clearance drugs. British Journal of Clinical Pharmacology. **45**(5): 463-9.

Tannenbaum, G. S. (1980). Evidence for autoregulation of growth hormone secretion via the central nervous system. Endocrinology **107**(6): 2117-20.

Tannenbaum, G. S. and J. B. Martin (1976). Evidence for an endogenous ultradian rhythm governing growth hormone secretion in the rat. Endocrinology **98**(3): 562-70.

Tannenbaum, G. S., W. H. Zhang, M. Lapointe, P. Zeitler and A. Beaudet (1998). Growth hormone-releasing hormone neurons in the arcuate nucleus express both sst1 and sst2 somatostatin receptor genes. Endocrinology **139**(3): 1450-1453.

Terry, L. C., W. R. Crowley and M. D. Johnson (1982). Regulation of episodic growth hormone secretion by the central epinephrine system. Studies in the chronically cannulated rat. Journal of Clinical Investigation. **69**(1): 104-12.

Toth, Z. E. and M. Palkovits (1998). Distributions of periventricular projections of the paraventricular nucleus to the median eminence and arcuate nucleus. Brain Research **802**(1-2): 294-297.

Tuckwell, H. C. (1988). Introduction to theoretical neurobiology. Vol 2, Cambridge University Press.

Wagner, C., S. R. Caplan and G. S. Tannenbaum (1998). Genesis of the ultradian rhythm of GH secretion: a new model unifying experimental observations in rats. American Journal of Physiology-Endocrinology and Metabolism **38**(6): E1046-E1054.

Wehrenberg, W. B., P. Brazeau, R. Luben, P. Bohlen and R. Guillemin (1982). Inhibition of the Pulsatile Secretion of Growth-Hormone By Monoclonal-Antibodies to the Hypothalamic Growth-Hormone Releasing- Factor (Grf). Endocrinology **111**(6): 2147-2148.

Wehrenberg, W. B., P. Brazeau, R. Luben, N. Ling and R. Guillemin (1983). A Non-Invasive Functional Lesion of the Hypothalamo-Pituitary Axis For the Study of Growth Hormone-Releasing Factor. Neuroendocrinology **36**(6): 489-491.

Wehrenberg, W. B., H. Seifert, L. M. Bilezikjian and W. Vale (1986). Down-Regulation of Growth-Hormone Releasing-Factor Receptors Following Continuous Infusion of Growth-Hormone Releasing-Factor Invivo. Neuroendocrinology **43**(2): 266-268.

Wiegand, S. J. and J. L. Price (1980). The cells of origin of the afferent fibres to the median eminence of the rat. J. Comp. Neurol. **192**: 1-19.

Yarbro, L. A. and S. N. Deming (1974). Selection and preprocessing of factors for simplex optimization. Analytica Chimica Acta **73**(2): 391-398.

Zhang, W. H., A. Beaudet and G. S. Tannenbaum (1999). Sexually dimorphic expression of sst1 and sst2 somatostatin receptor subtypes in the arcuate nucleus and anterior pituitary of adult rats. Journal of Neuroendocrinology **11**(2): 129-136.

Zheng, H., A. Bailey, M. H. Jiang, K. Honda, H. Y. Chen, M. E. Trumbauer, L. H. T. VanderPloeg, J. M. Schaeffer, G. Leng and R. G. Smith (1997). Somatostatin receptor subtype 2 knockout mice are refractory to growth hormone-negative feedback on arcuate neurons. Molecular Endocrinology **11**(11): 1709-1717.